THE ROLE OF SPHINGOSINE-1-PHOSPHATE IN MACROPHAGE RECRUITMENT AND FUNCTION IN DIFFUSE LARGE B-CELL LYMPHOMA

by TRACEY ADAMS PERRY

A thesis submitted to the

University of Birmingham

for the degree of

DOCTOR OF PHILOSOPHY

Institute of Cancer and Genomic Sciences

College of Medical and Dental Sciences

University of Birmingham

April 2019

ABSTRACT

Diffuse large B cell lymphoma (DLBCL) is the most common non-Hodgkin lymphoma. Currently, approximately 40% of DLBCL patients treated with standard of care therapies, which include a combination of immunotherapy (Rituximab; R) and chemotherapy (CHOP), will have disease that is refractory or will relapse. Tumour-associated macrophages can phagocytose opsonised DLBCL tumour cells and are therefore centrally important in determining therapeutic outcomes for patients treated with R-CHOP. Recent data from our lab and from others suggests that the modulation of sphingosine-1-phosphate (S1P) signalling may therapeutically benefit some patients with this tumour.

In this study, the effects of S1P on macrophage functions relevant to DLBCL were investigated. Using *in vitro* phagocytosis assays, S1P signalling through the major receptor, S1PR1, suppressed the phagocytosis of rituximab-opsonised DLBCL cells. However, chemotherapy potently induced monocyte recruitment to DLBCL tumours *in vivo* and S1PR1 is a primary mediator of monocyte migration both *in vitro* and *in vivo*. This work suggests that S1PR1 signalling inhibitors could improve the therapeutic efficacy of rituximab-based therapies for DLBCL patients. However, these drugs should be given only after chemotherapy and before rituximab administration so as to maximise the S1P-mediated recruitment of therapeutic macrophages to the tumour site.

ACKNOWLEDGEMENTS

Achieving my PhD would not have been possible without the generosity of Professor Paul Murray. I am so grateful to Paul for allowing me to do this project, for giving me the independence to pursue my ideas and assuaging my frustrations, and for making work full of fun and laughter.

I cannot begin to express my thanks to Professor Pam Kearns who has been my mentor, supervisor, and friend for ~15 years. Pam has allowed me to grow into an independent researcher by giving me opportunities to achieve this milestone. It has been life-changing. Pam has been my biggest supporter and I am forever grateful.

I have had the privilege of working with amazing people at LCCTP, Avalon, POET, and at the University of Birmingham. I thank them for sharing their knowledge and for the many wonderful memories. Special thanks to Dr Navta Masand for helping me through long evenings in the lab; Dr Kate Vrzalikova and Dr Carmela De Santo for their guidance and advice; Dr Matt Pugh for his help with the pathology; Dr Robert Hollows for providing bioinformatics analysis; and special thanks to Professor Tanja Stankovic for her encouragement and support.

Finally, I must acknowledge Dr Stuart Yuspa—my "science dad". I learned so much during my time at the National Cancer Institute which has made me the scientist I am today. Stu lifted as he climbed teaching us perseverance, integrity, and to respect and value each other. The environment of collaboration, community, and discovery at LCCTP forged friendships and strong bonds beyond the lab. My heartfelt thanks to Stu and everyone from the Yuspa Lab.

This work is dedicated to my mom, Brenda, my sisters, Mary and Nettie,
my late grandparents, Dorothy and Johnnie Adams
and to my beloved, Simon, Isak and Iris.

Table of Contents

List of Figures

Chapter 1

Chapter 3

Chapter 4

Chapter 5

List of Tables

Chapter 1

Chapter 2

Chapter 3

Chapter 5

List of Abbreviations

ABC-type	activated B cell type diffuse large B cell lymphoma
ADCC	antibody dependent cellular cytotoxicity
ADCP	antibody dependent cellular phagocytosis
AID	activation-induced cytidine deaminase
AKT	protein kinase B
ANOVA	analysis of variance
ATP	adenosine tri-phosphate
BAF312	siponimod
BALB/c	inbred strain albino wild type mice
BCR	B cell receptor
BSA	bovine serum albumin
CAR-T cells	chimeric antigen receptor T cells
CDC	complement dependent cytotoxicity
CFSE	carboxyfluorescein succinimidyl ester
CHOP	cyclophosphamide, doxorubicin, oncovin (vincristine), prednisolone
CM	conditioned medium
COO	cell of origin
CSR	class switch recombination
DLBCL	diffuse large B cell lymphoma
DLBCL, NOS	diffuse large B cell lymphoma, not otherwise specified
EBV	Epstein-Barr virus
EC50	effective concentration 50
EC80	effective concentration 80
ECL	enhanced chemiluminescence
EDA	experimental design assistant
ER	endoplasmic reticulum
ERK	extracellular signal-regulated kinases
ETOH	ethanol
FBS	foetal bovine serum
FDC	follicular dendritic cells
FDR	false discovery rate = $q < .01$
FFPE	formalin fixed paraffin embedded
GC	germinal centre
GCB-type	germinal centre B cell type diffuse large B cell lymphoma
GEP	gene expression profiling
GM-CSF	granulocyte-macrophage colony-stimulating factor
GO	gene ontology

HDL	high-density lipoprotein
HPF	high-power field
HRP	horse radish peroxidase
HSC	haematopoietic stem cell
IC50	inhibitory concentration 50
IgG	immunoglobulin G
IHC	immunohistochemistry
IMDM	Isocove's modified Dulbecco's medium
IMS	industrial methylated spirits
IP	intraperitoneal
ISH	*in situ* hybridisation
ITAM	immunoreceptor tyrosine-based activation motif
IV	intravenous
LPS	lipopolysaccharide
M1	GM-CSF polarised macrophages
M2	M-CSF polarised macrophages
MACS buffer	magnetic activated cell sorting buffer
MAPK	mitogen-activated protein kinases
MCP-1	monocyte chemoattractant protein 1
M-CSF	macrophage colony-stimulating factor
MNC/MON	monocytes (CD14+)
MZ	mantle and marginal zone
NBF	10% neutral buffered formalin
NC3Rs	National Centre for the Replacement, Refinement, & Reduction of animals in research
NFκB	nuclear factor kappa-light-chain enhancer of activated B cells
NHL	non-Hodgkin lymphoma
NSG	NOD-*scid* IL2Rgamma^{null}
OS	overall survival
p	p value < .05
PBS	phosphate buffered saline
PBS-T	phosphate buffered saline + tween 20
PCR	polymerase chain reaction
PD-1/PDL-1	programmed cell death-1/ programmed cell death ligand-1
PFS	progression free survival
P13K	phosphatidylinositol 3-kinase
PMSF	phenylmethane sulfonyl fluoride
PO	oral gavage
q-PCR	quantitative or real-time PCR

R-CHOP	rituximab, cyclophosphamide, doxorubicin, vincristine, prednisolone
RPMI 1640	Roswell Park Memorial Institute medium 1640
S1P	sphingosine-1-phosphate
S1PR	sphingosine-1-phosphate receptor
SC	subcutaneous
SMH	somatic hypermutation
SOV	sodium orthovanadate
SPHK1	sphingosine kinase 1
SPHK2	sphingosine kinase 2
TAM	tumour associated macrophages
TBS	tris buffered saline
TBS-T	tris buffered saline + tween 20
TGFβ	transforming growth factor beta
TGI	tumour growth inhibition
TME	tumour microenvironment
WHO	World Health Organisation
ΔCT	change in cycle threshold

CHAPTER 1

Introduction

Chapter 1

Non-Hodgkin lymphoma

The majority (90%) of all lymphomas are classed as non-Hodgkin lymphoma (NHL) and are distinguished from Hodgkin lymphoma by the absence of large multi-nucleated tumour cells known as Hodgkin and Reed/Sternberg cells (HRS cells) (Kuppers, 2005). NHL is the fifth most common cancer in the United Kingdom (UK) and is comprised of a broad range of malignancies that include both fast growing aggressive tumours such as diffuse large B cell lymphoma (DLBCL) and Burkitt lymphoma as well as more indolent neoplasms such as follicular lymphoma (Figure 1.1) (CRUK, 2015). Most NHL are B cell malignancies (85-90%) but a small portion are derived from T cells or natural killer (NK) cells (Shankland et al., 2012).

1.1 Diffuse large B cell lymphoma

1.1.1 Epidemiology of DLBCL

DLBCL is the most common NHL subtype making up 36% of NHL cases (Figure 1.1) (Quintanilla-Martinez, 2015, Scott and Gascoyne, 2014). In the UK, there are about 5000 new cases of DLBCL per year with a slight gender bias towards males and an overall median age of 65 years old (NICE, 2016, Ruhl JL, 2018). DLBCL is a highly aggressive disease with a 5-year overall survival (OS) of 60% and those patients who are >65 years old have decreased 5-year survival rate compared to DLBCL patients under 55 years old

(Gisselbrecht and Van Den Neste, 2018). The frequency of relapse among DLBCL patients is approximately 30% with an additional 10% who are refractory (Gisselbrecht and Van Den Neste, 2018, Ruhl JL, 2018).

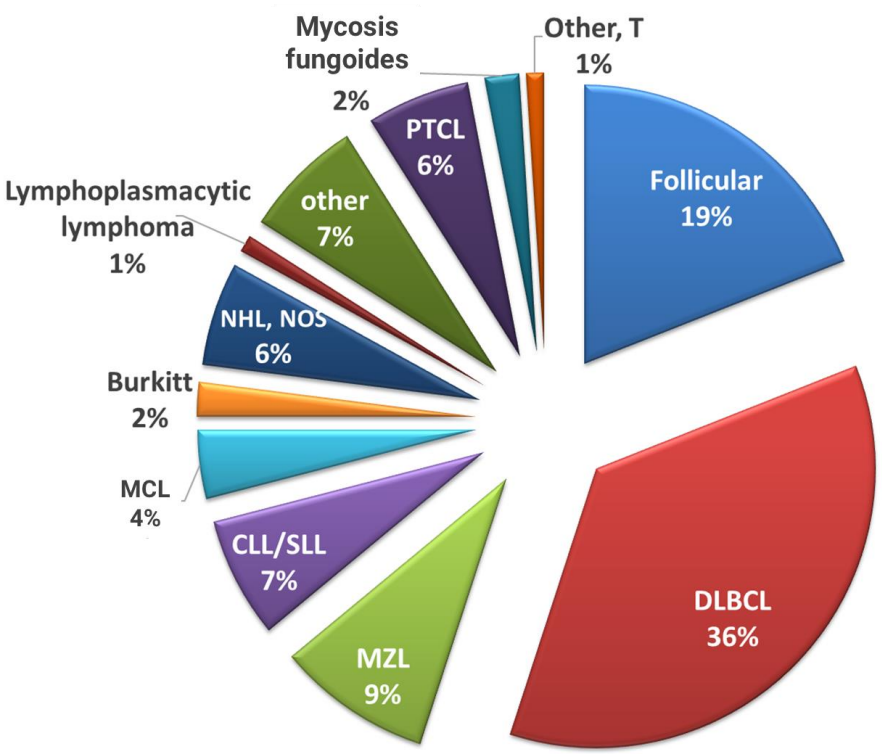

Cancer statistics taken from SEER 2000-2015

Figure 1.1 Frequency of various types of non-Hodgkin lymphoma (NHL). Diffuse large B cell lymphoma (DLBCL) is the most common NHL making up 36% of all cases and is highly aggressive. Follicular lymphoma, marginal zone lymphoma (MZL), and CLL/SLL (chronic lymphocytic leukaemia/small lymphocytic lymphoma) make up the next most common indolent lymphomas. PTCL (peripheral T cell lymphoma) and MCL (mantle cell lymphoma) are less common but highly aggressive forms of NHL. Burkitt lymphoma is a high-grade highly proliferative and aggressive lymphoma which can be associated with Epstein-Barr virus.

DLBCL patients commonly present with enlarged lymph nodes in the neck, groin or abdomen but extra-nodal presentation of DLBCL is not uncommon, most often presenting in the stomach or gastrointestinal tract (Tilly et al., 2015). More than half the patients are diagnosed with DLBCL are at later stages (Stage III and Stage IV) of disease (Table 1.1). DLBCL patients at these advanced stages are treated with a combination of chemotherapy (CHOP; cyclophosphamide, doxorubicin, vincristine and prednisolone) and immunotherapy (R; rituximab). Those with more localised disease at (Stage I and Stage II; Table 1.1) are also treated with R-CHOP but supplemented with radiation therapy. (Tilly et al., 2015)

Table 1.1 Disease stages of DLBCL adapted from Tilly *et al*, 2015

STAGE	
I	Single lymph node or a group of adjacent nodes involved
II	Multiple lymph node regions on the same side of the diaphragm involved
III	Groups of lymph nodes found on both sides of the diaphragm involved (i.e. neck, chest or abdomen)
IV	Lymph nodes on both sides of the diaphragm with or without involvement of extra lymphatic organs (i.e. spleen, liver, lungs, bones or bone marrow)

The addition of rituximab to CHOP therapy in 2000, resulted in increased survival from 40% to the current 5-year overall survival rate of 60% (Kunkel et al., 2000, Chapuy et al., 2018). Nearly 20 years since the addition of rituximab, all DLBCL patients are still uniformly treated with R-CHOP or R-CHOP plus radiation regardless of clinical presentation, phenotype or genetic disparities. There has been no further improvement to overall survival since the introduction of rituximab to DLBCL treatment (Coiffier and Sarkozy, 2016). For those patients who relapse or are refractory, there are few alternative treatment options and are currently given salvage therapy which include rituximab plus combinations of other chemotherapeutic agents with little improvement in survival (Gisselbrecht and Van Den Neste, 2018).

1.1.2 Classification of DLBCL

The complexity and heterogeneity of DLBCL has made stratification and classification challenging. Alizadeh *et al* was the first to demonstrate and stratify DLBCL into disease subtypes (Alizadeh et al., 2000). They hypothesised that DLBCL could be stratified by cell of origin (COO) at different stages of normal B cell differentiation (reviewed in section 1.1.4) which they demonstrated by gene expression profiling (GEP). Using normal germinal centre B cells isolated from tonsil and a range of *in vitro* activated B cells isolated from peripheral blood, Alizadeh *et al* derived specific gene signatures for these B cells at the various stages of differentiation. Then the gene expression profiles of untreated patient samples diagnosed with DLBCL (N=42), follicular lymphoma (N=9), or CLL (N=11), as well as a selection of

lymphoma and leukaemia cell lines were compared with the gene signatures derived from the range of normal B cells (Alizadeh et al., 2000).

Alizadeh *et al* found that the DLBCL cases clustered into two distinct groups by gene expression: 1) germinal centre B cell type (GCB) DLBCL that clustered with normal germinal centre B cells and 2) the rest that clustered outside of this group they called the activated B cell type (ABC) (Alizadeh et al., 2000). They also found some DLBCL cell lines that clustered with DLBCL patient samples by COO: SUDHL6 which clustered with patient GCB-DLBCL and OCI-Ly3 and OCI-Ly10 which clustered with patient ABC-DLBCL (Alizadeh et al., 2000). Rosenwald *et al* took this work further and analysed a cohort of 240 DLBCL cases at presentation with clinical follow-up after treatment with CHOP (Rosenwald et al., 2002).

Using DNA microarray analysis, Rosenwald *et al* began by subtyping their cohort of DLBCL according to the GEP signatures derived by Alizadeh *et al* and found that their samples clustered into ABC, GCB, or into a third unclassifiable group, Type 3 (Rosenwald et al., 2002). By histology, Rosenwald *et al* found that there were no histologic features specific to any of the three DLBCL subtypes. Evaluating survival after CHOP between the GCB, ABC and Type 3 subtypes, they found that the GCB type had 60% OS survival while the ABC and Type 3 had 35% and 39% OS survival respectively in accordance with the survival results reported by Alizadeh *et al* (Rosenwald et al., 2002, Alizadeh et al., 2000). But Rosenwald *et al* also recognised the diverse survival rates *within* each subtype with some GCB-type patients having 35%

3-year survival while some ABC-type patients with complete response to CHOP (Rosenwald et al., 2002). This observation suggested that DLBCL stratification required further exploration.

Oncogenic pathways that typified GCB-DLBCL and ABC-DLBCL subtypes were garnered from the gene expression profiling data from Alizadeh *et al* and Rosenwald *et al*. Amongst the oncogenic pathways that are characteristic of GCB-DLBCL, are the deletion or loss of *PTEN*, and *MYC* and/or *BCL2* translocations (Figure 1.2). Oncogenic pathways considered hallmarks of ABC-DLBCL include mutations in *NF-κB* and *BCR* signalling as well as *BCL6* translocations (Figure 1.2) (Sehn and Gascoyne, 2015).

Due to the high cost and low availability of GEP in the decade following COO classification of DLBCL, immunohistochemistry (IHC) algorithms were developed as an alternative. IHC was rapid and more cost-effective compared to GEP therefore, several different IHC algorithms have been developed (Hans et al., 2004, Choi et al., 2009, Muris et al., 2006, Nyman et al., 2009, Meyer et al., 2011, Visco et al., 2012). The Hans algorithm is the most commonly used; GCB-type DLBCL is positive for CD10 and BCL6 and negative for MUM1 while ABC/non-GC-type DLBCL is characterised by CD10-negative BCL6-negative or CD10-negative BCL6-positive MUM1-positive (Figure 1.3). Another common algorithm used is the Choi algorithm which added GCET (germinal centre expressed transcript) and FOXP1 to the classification tree in order to further refine classification of DLBCL by IHC (Figure 1.3). Unfortunately, the different types of IHC algorithms do not always correlate

with prognosis and lack reproducibility perhaps due to the differences in methodology and reagents (Swerdlow et al., 2016). While GEP is considered the most accurate way of classifying DLBCL, it still leaves 10-15% of DLBCL cases as unclassifiable which cannot be resolved by IHC methods (Swerdlow et al., 2016).

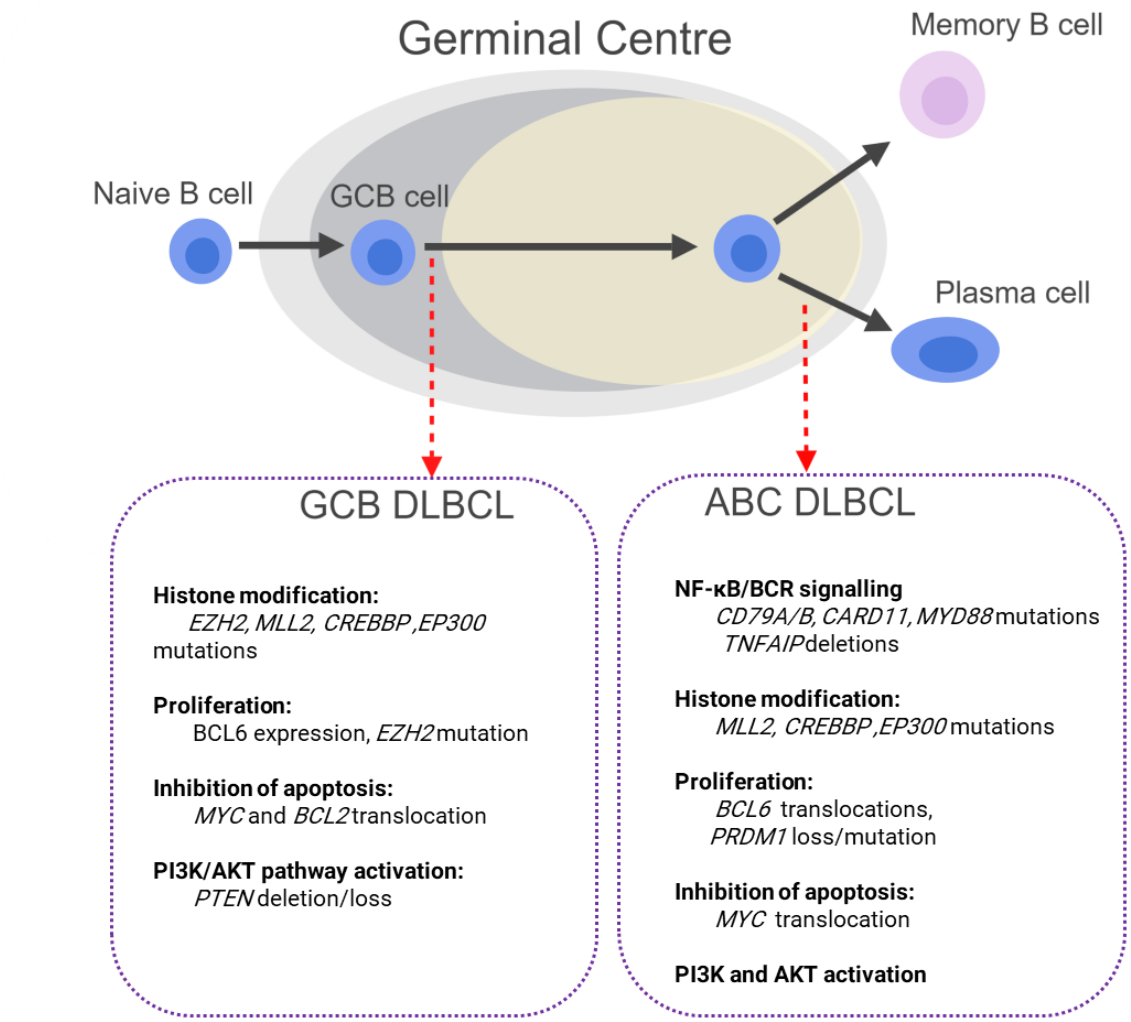

Figure 1.2 Oncogenic pathways in DLBCL subtypes. ABC and GCB-types are characterised by specific molecular subtypes. ABC-DLBCL is characterised by mutations in NF-κB/BCR signalling and *BCL6* translocations. GCB-DLBCL is characterised by the loss or deletion of *PTEN*. High-grade lymphomas have been shown to be a subtype of GCB-DLBCL that have poor prognosis with R-CHOP (Sha *et al*, 2019 and Ennishi *et al,* 2019). (Figure adapted from Sehn, L. H. and Gascoyne, R. D., 2015).

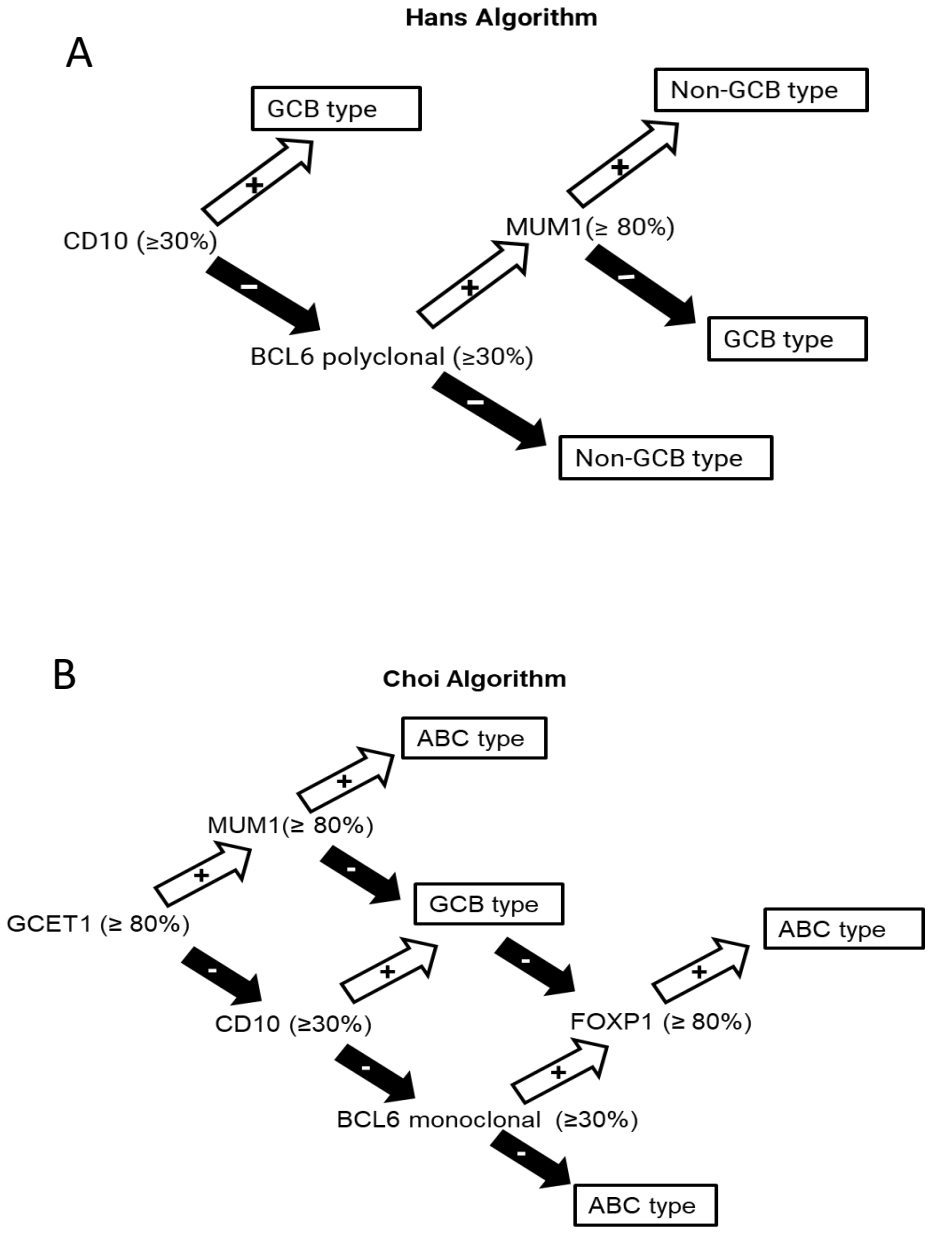

Figure 1.3 Hans and Choi algorithm for immunohistochemical classification of DLBCL. (A) Hans (2004) and (B) Choi (2009) were two examples of IHC algorithms developed for DLBCL classification. They differ in that Choi added GCET and FOXP1 to the original Hans algorithm. There are other IHC algorithms available but Hans remains the most commonly used. It is recognised that there are limitations to the IHC method of DLBCL classification and that gene expression profiling or RNA analysis for specific transcripts are more accurate though still not adequate in classifying all patients.

In 2016, the World Health Organisation (WHO) made changes to the 2008 DLBCL classification which requires DLBCL, NOS to be designated as GCB-type or ABC/non-GC type by either IHC or GEP (Swerdlow et al., 2016, Campo et al., 2011) (Table 1.2). Other changes added to the 2016 classification of DLBCL include separate classifications for Epstein-Barr Virus (EBV) and Herpes Simplex Virus 8 (HHV8) associated DLBCL as well as the addition of a separate classification for high-grade lymphomas, NOS and high-grade lymphomas with *BCL2* and/or *BCL6* plus *MYC* rearrangements ("double-hit" and "triple-hit" lymphomas) (Swerdlow et al., 2016).

Barrans *et al* showed that DLBCL patients that harbour *MYC* plus *BCL2* and/or *BLC6* mutations and/or rearrangements were a separate subgroup of DLBCL that showed poor response to R-CHOP indicating that further stratification of GCB and ABC subtypes were needed (Barrans et al., 2010). Reported to occur in <10% of DLBCL cases, "double-hit" or "triple-hit" lymphomas are currently underdiagnosed as shown by the recent work from Sha *et al* and Ennishi *et al* published simultaneously in the Journal of Clinical Oncology (Friedberg, 2017, Barrans et al., 2010, Sha et al., 2019, Ennishi et al., 2019). They used gene expression profiling of DLBCL patients to reveal a molecularly distinct subgroup amongst the GCB types (Sha et al., 2019, Ennishi et al., 2019). Sha *et al* defined a subgroup they call the molecular high-grade lymphoma (MHG) group which was more likely to be of GCB-type and found that the "double-hit" lymphomas actually only made up half of all the MHG lymphomas in their cohort (Sha et al., 2019). Ennishi *et al* developed

Table 1.2 2016 WHO classification for DLBCL (Swerdlow, 2016)

***Different from the 2008 classification. DLBCL, NOS must be classified as GCB or ABC by immunohistochemistry or gene expression; addition of virus (EBV+ and HHV8+) associated DLBCL; recognition of high-grade lymphomas as separate disease types from GCB type DLBCL.*

- Diffuse large B-cell lymphoma (DLBCL), NOS
  - Germinal centre B-cell type*
  - Activated B-cell type*
- T-cell/histiocyte-rich large B-cell lymphoma
- Primary DLBCL of the central nervous system (CNS)
- Primary cutaneous DLBCL, leg type
- EBV+ DLBCL, NOS*
- DLBCL associated with chronic inflammation
- Primary mediastinal (thymic) large B-cell lymphoma
- Intravascular large B-cell lymphoma
- ALK1 large B-cell lymphoma
- Plasmablastic lymphoma
- HHV8+ DLBCL, NOS*
- High-grade B-cell lymphoma, with MYC and BCL2 and/or BCL6 rearrangements*
- High-grade B-cell lymphoma, NOS*
- B-cell lymphoma, unclassifiable, with features intermediate between DLBCL and classical Hodgkin lymphoma

a “double-hit” gene signature in order to distinguish these tumours from the other GCB-types. They found that within their cohort of GCB patients, 27% were positive for the “double-hit” gene signature (Ennishi et al., 2019). These studies taken together demonstrate that “double-hit” lymphomas are only part

of a larger distinct subgroup of molecular high-grade lymphomas found within the GCB subtype that have poor response to R-CHOP further adding valuable nuances to the newly defined genetic subgroups of DLBCL published in 2018.

In 2018, Schmitz *et al* aimed to classify DLBCL by shared genomic abnormalities using a combination of exome and transcriptome sequencing and DNA copy number analysis (Schmitz et al., 2018). They obtained a cohort of fresh frozen DLBCL biopsies (N=574) mostly at presentation and enriched for ABC and unclassified DLBCL (Schmitz et al., 2018). In order to do the DNA copy number analysis for samples where matched normal DNA was not available, they used the sequencing data from a cohort of 48 matched samples to developed multiple decision trees which allowed them to determine somatic mutations accurately (Schmitz et al., 2018).

Using these genetic algorithms for calling somatic mutations, Schmitz *et al* defined four types of genetic aberrations that stratified nearly half of the DLBCL samples in their cohort (Figure 1.4). They called these four genetic groups 1) MCD (*MYD88*^{L265P} and *CD79B* mutation), 2) BN2 (*BCL6* fusion and *NOTCH2* mutation), 3) N1 (*NOTCH1* mutation), and 4) EZB (*EZH2* mutation and *BCL2* translocation) (Schmitz et al., 2018). They found patients from the three COO of subtypes (ABC, GCB, and unclassified) were present in each of their genetic subgroups. MCD and N1 groups were mainly comprised of ABC-DLBCL while the EZB group was largely made up of GCB-DLBCL (Schmitz et al., 2018).

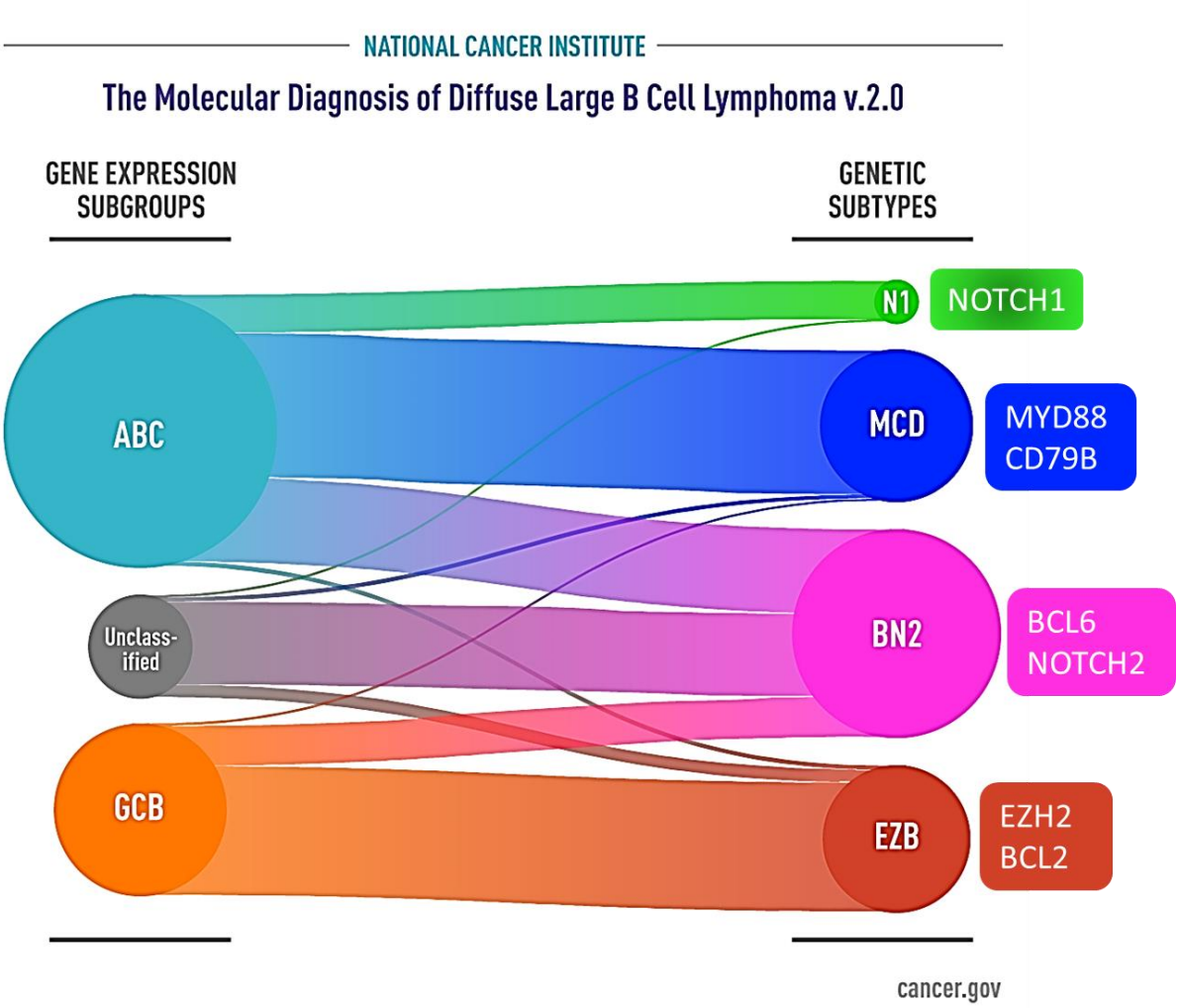

Figure 1.4 Newly defined genetic subtypes of DLBCL Schmitz *et al* (2018). Four genetic subtypes were found using a combination of exome and transcriptome sequencing and DNA copy number analysis. The groups were called: MCD (*MYD88*^{L265P} and *CD79B* mutation), BN2 (*BCL6* fusion and *NOTCH2* mutation), N1 (*NOTCH1* mutation), and EZB (*EZH2* mutation and *BCL2* translocation). Each group contained tumours from the ABC, GCB or unclassified subtypes reflecting the heterogeneity within each COO subtype. Still more than half of the cohort evaluated by Schmitz *et al* could not be classified into one of the four new genetic subtypes they defined. (Image credit: National Cancer Institute)

More importantly, about half of the unclassified DLBCL in their cohort could be classified into the BN2 group. ABC, GCB and unclassified DLBCL was spread across all of the newly identified genetic subtypes except for the N1 group where GCB-DLBCL was notably absent (Schmitz et al., 2018).

Despite the identification of the new molecular groups, 53.5% of their DLBCL patients could not be classified into any of the four genetic subgroups highlighting the heterogenous genetic landscape of DLBCL (Schmitz et al., 2018). Schmitz *et al* also examined the survival data of the patients within the four genetic subtypes and found that N1 and MCD subtypes had a worse progression-free survival and overall survival than the EZB and BN2 subtypes regardless of COO. For example, ABC-BN2 patients and the "other ABC" (56.5% of the ABC cohort that could not be classified into any genetic subgroup) had better OS than patients classified as ABC-MCD and ABC-N1 patients. The group they termed as "other GCB" (51.1% of GCB cohort that could not be classified into any genetic subgroups) had a better survival than the patients that were classified as GCB-EZB (Schmitz et al., 2018).

In the same year, Chapuy *et al* published whole exome sequencing of 304 DLBCL samples in which there were 135 matched normal samples. While Schmitz *et al* used fresh frozen biopsies, 55% of the samples used by Chapuy *et al* were obtained from formalin-fixed paraffin embedded samples (FFPE). Chapuy *et al* found six clusters they designated as C0 – C5 which were similar to the genetic subgroups described by Schmitz *et al.* Cluster 1 (C1) includes *BCL6* and *NOTCH2* mutations and was mostly made up of ABC-DLBCL

tumours which corresponds to the BN2 group from Schmitz; Cluster 2 (C2) had biallelic inactivation of *TP53* which was found in both ABC and GCB subtypes; Cluster 3 (C3), mostly of the GCB subtype and could also be found in follicular lymphoma, had *BCL2* mutations but also frequently had mutations in *EZH2* and *PTEN* which corresponds to the EZB group from Schmitz; Cluster 4 (C4) had mutations in the *NF-κB* and *RAS/JAK/STAT1* pathways as well as in *BCR/PI3K* signalling and mutations in *CD83, CD58, CD70* important in immune evasion; Cluster 5 (C5) was characterised by consistent gain in *18q* and mutations in *MYD88* and *CD79B* found mostly in ABC DLBCL corresponding to the MCD group described by Schmitz. Finally, there was a small group termed by Chapuy *et al* as cluster 0 (C0), which had no defining genetic drivers. (Chapuy et al., 2018)

Since Alizadeh's seminal publication in 2000, COO has dominated the classification of DLBCL. Whether or not the concept of COO of DLBCL will continue to be relevant in light of the new genetic subtypes uncovered remains to be seen. There are at least four newly defined genetic subgroups in DLBCL and along with COO could result in better treatment stratification for patients. To contextualise COO, B cell development is reviewed in the following section.

1.1.3 Normal B cell development

Normal B cell development begins in the bone marrow (a primary lymphoid organ) with haematopoietic stem cells (HSCs) and proceeds to multipotent/oligopotent progenitors where lineage fate is determined and pro-

B cells emerge (Figure 1.4) (Seita and Weissman, 2010). When cells acquire the pre-B cell receptor (pre-BCR), an important checkpoint in B cell development, rapid proliferation occurs (Martensson et al., 2010). During this rapid proliferation, extensive rearrangements of the variable (V), joining (J) and diversity (D) gene segments occur on the heavy chain of the BCR and is initiated by *RAG-1* and *RAG-2* (recombinant activating genes 1 and 2) occurs (Bassing et al., 2002).

When immature B cells exit the bone marrow and encounter an antigen, they enter the dark zone of a germinal centre where B cells, now called centroblasts, undergo clonal expansion (LeBien and Tedder, 2008). Centroblasts then exit the dark zone and differentiate into centrocytes in the light zone where they undergo somatic hypermutation (SMH), point mutations of the V-regions in the heavy and light chains of the BCR, in order to produce B cells with high affinity for the specific antigen encountered (Figure 1.5) (Bassing et al., 2002). Two types of selection then occurs when centrocytes bind antigen: negative selection, where B cells bind antigen and will undergo apoptosis; or positive selection, where centrocytes exit the germinal centre and undergo class switch recombination (CSR) on the heavy chain, switching μ (IgM) to γ, ε, or α (IgG, IgE, IgA) (Fast, 2013, Zhang et al., 2016b). Activation-induced cytidine deaminase (AID) mediates SMH and CSR (Fast, 2013). As B cells exit the germinal centre, they can differentiate into memory B cells or plasma B cells which are long-lived and form the long-term humoral immunity to a particular antigen (Fast, 2013).

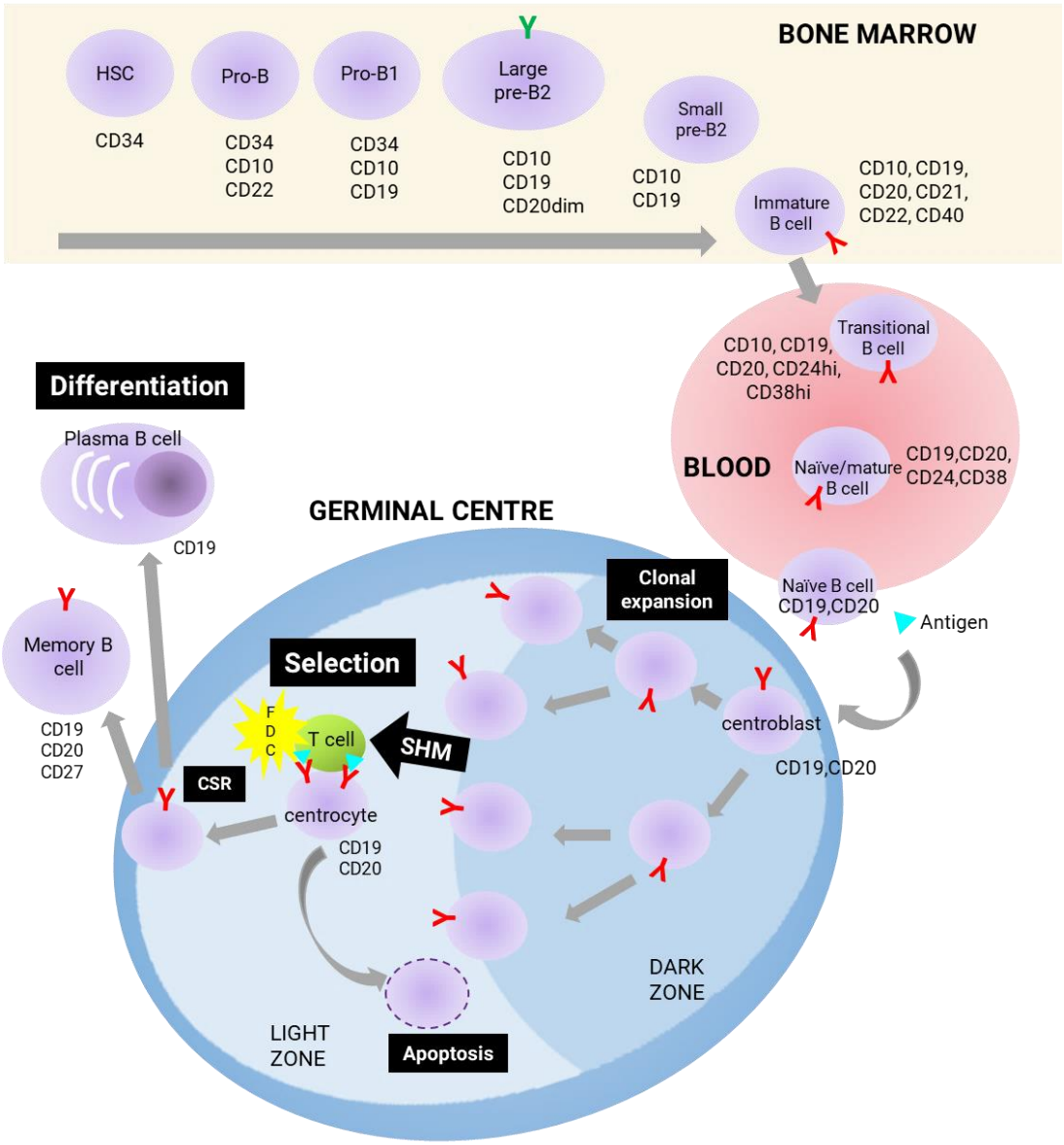

Figure 1.5 Stages of B cell development. Normal B cell development begins in the bone marrow with haematopoietic stem cells (HSC). As B cells differentiate in the bone marrow, they lose CD34, a marker of stemness and gain CD19, a pan B cell marker. Pre-B cell receptor (pre-BCR, green) is expressed leading to proliferation or differentiation into small pre-B cells. Upon further rearrangements of the transiently expressed pre-BCR, naïve B cells with BCR (red) will enter the blood stream and circulate between the bone marrow and lymphoid organs. When naïve B cells encounter antigen (blue triangle), they become activated resulting in clonal expansion in the dark zone of the germinal centre. Germinal centre B cells or centroblasts, undergo somatic hypermutations (SHM) which increases affinity for the antigen. B cells will then move through the light zone, where centroblasts differentiate into centrocytes. Centrocytes are committed and along with the antigen presentation by follicular dendritic cells (FDC) and T helper cells, leads to further differentiation. Through negative selection, centrocytes may undergo apoptosis if the affinity for the antigen is low. Those that do not apoptose, will undergo class switch recombination (CSR) which leads to activation of transcription factors. Activation leads to migration out of the germinal centre where centrocytes will then differentiate into plasma B cells or memory B cells.

1.1.4 Molecular pathogenesis of DLBCL

Our current understanding of the pathogenesis of B cell lymphomas has largely arisen from the study of normal B cell biology (Shaffer et al., 2012). The theory of COO dictates that GCB-DLBCL and Burkitt lymphoma originate from germinal centre B cells while ABC-DLBCL originates from post-germinal centre plasmablasts (Shaffer et al., 2012, Alizadeh et al., 2000). Most malignant B cells hijack normal B cell signalling pathways either by mutation gain/loss of function or activation of autocrine receptors in order to grow and survive (Shaffer et al., 2012). Multiple signalling pathways are not only activated at the same time in lymphoma, but these pathways are interconnected creating a therapeutic challenge (Shaffer et al., 2012).

B Cell Receptor signalling

As already discussed, in normal cells, the B cell receptor (BCR) is used to bind antigen. IgH and IgL chains are bound to CD79A and CD79B subunits that regulate *BCR* expression and internalisation. Unlike in normal cells, malignant B cells constitutively express *BCR* on the cell surface. When the malignant B cell encounters antigen and is bound to *BCR*, CD79A and *CD79B* transmit downstream signals. Immune-receptor tyrosine-based activation motifs (ITAMs) on *CD79A* and *CD79B* recruit *SYK*, which in turn initiates a signalling cascade involving *NF-κB, PI3K*, and other signalling pathways to promote survival and proliferation. (Shaffer et al., 2012) *BCR* signalling does not always require antigen. This is known as tonic *BCR* signalling. Conditional knockout of different components of BCR signalling

revealed those genes that are vital for B cell maturation. For example, *IgM* or *CD79B* ablation in mice resulted in a lack of mature B cells in spleen or lymph nodes after 2 weeks. This phenotype was rescued in the case of *IgM* ablation where there was constitutively active *p110α* of *PI3K*. But in mice with *CD79A* but without *ITAM*, their B cells were able to express *BCR* on their cell surface which resulted in no surviving mature B cells. Also, constitutive *NF-κB* signalling mediated by *IKKβ* did not result in B cells after *BCR* loss of function. (Shaffer et al., 2012, LeBien and Tedder, 2008).

BCR signalling in DLBCL involves somatic hypermutation of the IgV region. In GCB-DLBCL, there is continuous mutation of the IgV regions. This results in GCB types to express IgG BCR eliciting *ERK, MAPK* and calcium responses known to promote B cell differentiation into marginal zone B cells and plasma cells (Shaffer et al., 2012). While in ABC-DLBCL, there is a static set of IgV mutations resulting in ABC types to express IgM BCR. This is known to promote proliferation and suppress differentiation. (Shaffer et al., 2012)

NF-κB

The pathogenesis of lymphoma includes the NF- κB signalling pathway. The NF-κB family of proteins is made up of several subunits that form heterodimers mediating their entry or exit from the nucleus (Heckman et al., 2002). NF-κB is used for survival by both normal and malignant B cells with activation occurring downstream of several receptors including B cell receptor (BCR) and CD40 (Shaffer et al., 2012).

The classical *NF-κB* pathway in B cells is activated by cytokine stimulation such as IL-1, TNF-α, or pathogens that bind to BCR or CD40. This results in phosphorylation of *IKKβ*, which is part of the IKK complex (IkB kinase made up of α, ß, ɣ (NEMO) subunits, and ubiquitination of IKKɣ which in turn allows for recognition of the proteasome leading to IKKß degradation. Subunits of NF-κB in the cytoplasm can then translocate to the nucleus where gene transcription is activated (Shaffer et al., 2012, Jost and Ruland, 2007). Activation of the IKKß requires the CBM (CARD11, BCL10, and MALT1) complex. CARD11 is in the cytosol until it is phosphorylated and able to translocate to the plasma membrane where it can bind *BCL10* and *MALT1* (Shaffer et al., 2012). Constitutively activated *NF-κB* signalling by the classical pathway is a hallmark of ABC-DLBCL which promotes survival by acting as an antagonist to chemotherapy resulting in refractory disease (Shaffer et al., 2012).

BCL-2

NF-κB can transcriptionally regulate another pro-survival gene, *BCL-2,* in lymphoma (Heckman et al., 2002). *BCL-2* was first described in Follicular lymphoma where the t(14;18) translocation is a hallmark of this disease but is also found in many DLBCL patients (Barrans et al., 2003). In both normal and malignant cells, *BCL-2* plays a role in the mitochondrial apoptotic pathway (Czabotar et al., 2014). In GCB subtype of DLBCL and Follicular lymphoma, the t(14;18) translocation is commonly active in pre-B cells rather than in mature B cells (Shaffer et al., 2012). Interestingly, healthy adults also

have circulating B cells with this translocation residing in their memory B cells which indicates that *BCL-2* expression is not sufficient to transform B cells nor does the presence of this translocation mean that *BCL2* is expressed (Shaffer et al., 2012). But several groups have shown the presence of the t(14;18) translocation does not alter the expression of *BCL-2* and that patients with both the translocation and *BCL2* expression have the most adverse prognosis (Huang et al., 2002, Barrans et al., 2003).

MYC

MYC expression in lymphoma confers poor prognosis and is expressed by a small subset of germinal centre B cells although contradictorily not in the highly proliferating B cells (Ott et al., 2010, Perry et al., 2014). During germinal centre formation, *MYC* is up regulated in these B cells just before BCL6 is activated which then represses *MYC* as they enter the dark zone (Ott et al., 2010). This *BCL6-MYC* switch is associated with the formation of the dark zone of germinal centres and expansion of the centroblasts. Then *MYC* is re-expressed in the light zone after *NF-κB* up-regulation which then re-enters the dark zone for more rounds of proliferation. *MYC* negative cells in the light zone exit as memory cells or early plasmablasts. *BLIMP1* is then induced which promotes plasma cell differentiation and represses *MYC*. (Ott et al., 2010)

In DLBCL, 10% of cases will have *MYC* translocations and only 2% will have amplification of *MYC* (Ott et al., 2010). Most cases of *MYC* rearrangement in DLBCL, occur in conjunction with t(14;18) (q32;q21)

translocation/*BCL2* rearrangement (Ott et al., 2010). *MYC* and *BCL2* expressing lymphomas or 'double-hit' lymphomas are particularly aggressive and difficult to treat. Barrans *et al*. evaluated a large cohort of DLBCL cases and found 12% of DLBCL cases were a double or triple hit *MYC/BCL2/BCL6* subtypes (Barrans et al., 2003). While Foot *et al*. looked at aggressive high-grade B cell lymphomas regardless of histology/morphology and found an even larger proportion had *MYC* rearrangements as well as *BLC2* and *BCL6* indicating that 'double-hit' lymphomas may be under diagnosed (Foot et al., 2011).

Determining the biological and genetic differences in DLBCL can lead to more effective individualised therapy. Several genetic aberrations in DLBCL, including *BCL2* and *IRF4*, are more easily exploited by targeted therapy while some such as *MYC* cannot (Ott et al., 2010). *MYC* is not considered a druggable target because of its encompassing role in gene activation so focus has been on downstream indirect effects on *MYC*. Inhibitors of *BRD4* which regulates *MYC* transcription have shown therapeutic efficacy in mouse models as well as in clinical trials (Ott et al., 2010).

1.1.5 Standard and emerging treatments for DLBCL

Standard treatment for lymphoma prior to 1997 was a combination of chemotherapies known as CHOP (cyclophosphamide, doxorubicin, vincristine, and prednisolone) where overall survival was only 35-40% (Sehn, 2010). With

the addition of rituximab, a monoclonal antibody to CD20, survival rates increased significantly to near 60% (Sehn, 2010). The clinical trial as reported by Coiffier *et al* provided evidence of the increased survival in patients treated with R-CHOP compared to CHOP (Figure 1.6A) (Coiffier et al., 2002). Yet the differences in overall survival of the ABC and GCB-type DLBCL have still not been resolved with ABC patients having a worse prognosis than GCB type. Lenz *et al* also did a prospective study of ABC and GCB patients treated with R-CHOP and found that GCB-type DLBCL had significantly higher overall survival than ABC-type DLBCL (Figure 1.6B) (Lenz et al., 2008). In order to further improve survival for the 40% of DLBCL patients who do not have complete response, new therapeutic strategies are being explored.

There are a number of emerging treatments for DLBCL in clinical trials which are listed on www.clinicaltrials.gov accessed on January 2019 from the National Institutes of Health (NIH). There were >200 clinical trials for DLBCL. About 30% of the trials were for interventions using biologics, a class of drugs isolated from natural sources such as human, animal or microorganisms. Biologics are more complex than conventional small molecule therapies where the structure is known, and may be effective for diseases that currently have no other treatments available. (CBER, 2018)

A

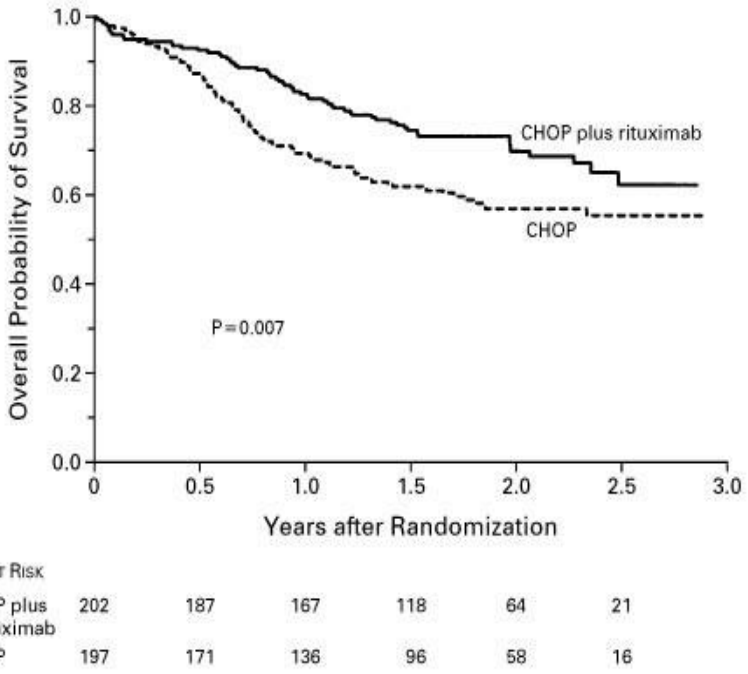

B

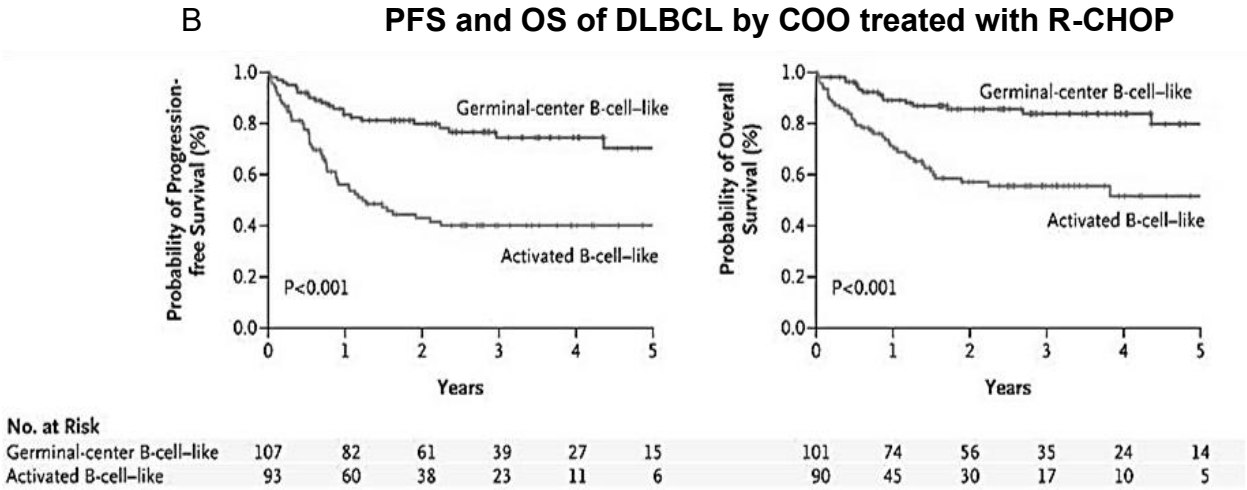

Figure 1.6 DLBC patients treated with R-CHOP had increased survival. (A) The addition of rituximab to standard of care in this study by Coiffier *et al*, resulted in an increased in OS to 70% in patients treated with R-CHOP compared to 63% in DLBCL patients treated with CHOP alone. (B) Lenz *et al* demonstrated that ABC-DLBCL had inferior survival compared to GCB-DLBCL after treatment with R-CHOP.

Highlighted in Table 1.3 are some of the clinical trials for DLBCL that are currently active (as of January 2019). They include several rituximab-similar monoclonal antibodies, anti-CD19 monoclonal antibodies (CD19 is a pan marker for B cells) as well as checkpoint inhibitors for PDL-1 and CTLA4, and recombinant IL-12. (Table 1.2) (Mueller et al., 2017). Besides antibody therapy, CD19 can now also be targeted using CAR-T cells or chimeric antigen recombinant T cell therapy. CAR-T cells involve engineering and clonal enhancement of autologous or allogeneic T cells to a specific target (Mueller et al., 2017). These CAR-T cells are injected into a patient and they work by binding to the target antigen on a cancer cell to induce apoptosis. CAR-T cell therapy can have adverse effects such cytokine release syndrome (an increase of over 150 inflammatory cytokines in the body leading to organ damage and even death), or graft vs host reaction (GVH), or neurological events such as encephalopathy (Mueller et al., 2017).

CTL019 from Novartis, the first approved CAR-T cell therapy by the FDA (Federal Drug Administration), is engineered to recognise CD19 found on B cells for the treatment of acute lymphoblastic leukaemia but is also being trialled in DLBCL (Mueller et al., 2017). They have found CTL019 beneficial in the majority of patients tested with many showing complete response/ remission (Schuster et al., 2017, Mueller et al., 2017). While CTL019 has shown to be therapeutically effective as a single agent, Novartis is also currently trialling CTL019 in combination with pembrolizumab which blocks PD-1. Combining treatments that target malignant B cells as well as

modulation of the tumour microenvironment could provide a more comprehensive treatment strategy. As it stands, standard treatment for DLBCL with R-CHOP remains unchanged for over two decades.

Table 1.3 Emerging treatments for DLBCL in clinical trials, January 2019

Drug name	Target	Phase	Company
CAR011	anti-CD19	Phase 1	Cellular Biomedical Group LTD
Blinatumomab	anti-CD19	Phase 1	Washington School of Medicine
Ofatumumab	anti-CD20	Phase 2	GSK
Obinatuzumab	anti-CD20	Phase 3	Nanjing Yoko Biomedical
JHL1101	anti-CD20	Phase 3	JHL Biotech
Atezolizumab	anti-PDL1	Phase 2	Genentech
Avelumab	anti-PDL1	Phase 3	Pfizer
Ipilimumab	CTLA-4 inhibitor	Phase 1/Phase 2	Bristol Meyers Squibb
Tremelimumab	CTLA-4 inhibitor	Phase 1	Medimmune/Astra Zeneca
CTL019	CAR-T cells	Phase 1/Phase 2	Novartis
Ibrutinib	BTK inhibitor	Phase1	Janssen R&D
Acalabrutinib	BTK inhibitor	Phase 1	Acerta
Chidamide	HDAC inhibitor	Phase 2	Zhejiang University
Panobinostat	HDAC inhibitor	Phase 2	Fondazione Italiana Linfomi
CUDC-907	PI3K/HDAC inhibitor	Phase 2	Curis
Bortezomib	proteosome inhibitor	Phase 2	Janssen R&D
NM-IL-12	recombinant IL-12	Phase 2	Neumedicines
L19-IL-12	recombinant IL-12	Phase 1/Phase 2	Philogen

Information from National Institutes of Health, www.Clinicaltrials.gov

1.1.6 Mechanisms of action of rituximab

Rituximab, a monoclonal antibody targeting CD20 on B cells, was the first immunotherapy to be approved for cancer. Several mechanisms of action (MOA) of rituximab have been reported (Figure 1.7) (Jaglowski et al., 2010, Herbrand, 2016).

Rituximab can induce apoptosis in the absence of effector cells by causing the reorganisation of CD20 into lipid rafts as well as through the inhibition or downregulation of survival signals such as AKT, ERK1/2, or NF-κB (Weiner, 2010). In synergy with chemotherapy, apoptosis induced by rituximab can lead to chemosensitivity (Weiner, 2010). Complement dependent cytotoxicity (CDC) is another mechanism of action for rituximab (Golay and Introna, 2012). Complement protein, C1q binds to rituximab which initiates the complement cascade. This results in the formation of a membrane attack complex (MAC) creating pores in the membrane leading to cell death (Jaglowski et al., 2010). Complement can also result in phagocytosis if the complement receptor on macrophages bind to rituximab (Jaglowski et al., 2010).

Other mechanisms of action require interaction with effector cells either NK cells or macrophages. ADCC (antibody dependent cellular cytotoxicity) can occur when NK cells bind to the Fc region on rituximab. This induces NK cells to release perforin and granzymes which cause cell death (Gul and van Egmond, 2015). Macrophages also can exert an antibody mediated response to rituximab-opsonised B cells. Antibody dependent cellular phagocytosis (ADCP) is initiated when Fc receptors on macrophages bind to the Fc region on rituximab-bound B cells leading to engulfment (Church et al., 2016).

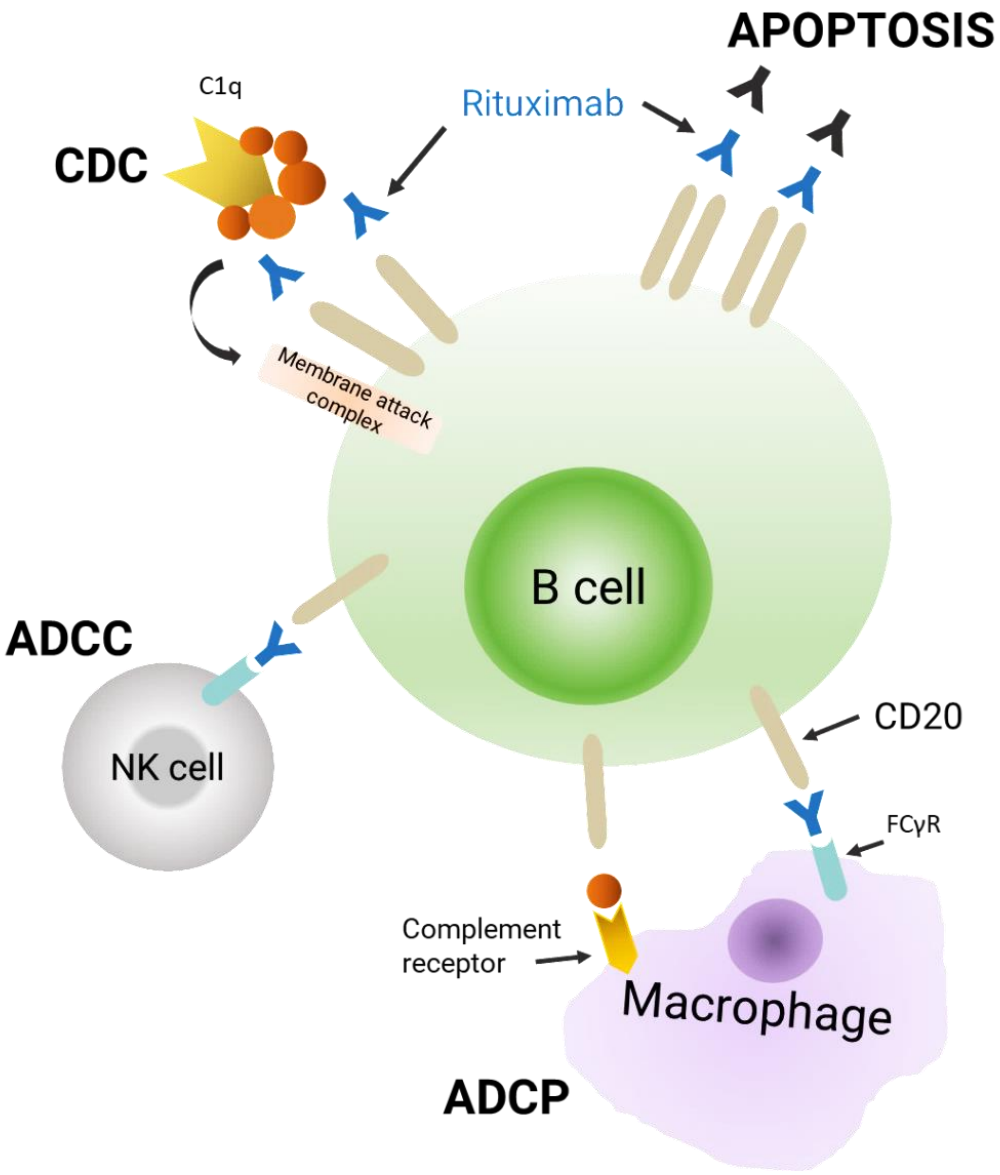

Figure 1.7 Mechanisms of action of rituximab. Rituximab is a monoclonal antibody binding to CD20. (1) Apoptosis can be induced through binding of rituximab to CD20 and the reorganization of CD20 into lipid rafts. (2) Complement dependent cytotoxicity (CDC) can be induced by the binding of rituximab to FC receptors leading to the activation of complement through complement receptor and further binding to membrane attack complex (MAC). (3) Antibody dependent cellular cytotoxicity (ADCC) can occur when NK cells bind to rituximab attached to CD20 on B cells. This induces NK cells to lyse the antibody-bound cell. (4) Antibody dependent cellular phagocytosis (ADCP) can be induced when macrophages bind to Fc region on rituximab bound to B cells which induces the macrophage to engulf the tumour cell. Complement may also induce phagocytosis by macrophages through activation of the complement receptor on macrophages. (Figure adapted from Jaglowski et al, 2010).

It is not known which mechanism of action is predominant but increasing evidence in murine models show that ADCP may be the primary mechanism of action for rituximab *in vivo* (Golay and Introna, 2012, Gul and van Egmond, 2015).

Murine studies pointed to ADCP as the main mechanism of action of rituximab through studies using the A20 murine lymphoma cell line in immune competent mice. A20 was determined to be sensitive *in vitro* to rituximab but when engrafted in BALB/c mice, rituximab showed no efficacy *in vivo* (Minard-Colin et al., 2008). Therefore, they developed a cell line using primary lymphoma cells from B6 c-Myc TG mice with C57BL/6 background known as BL3750 showed *in vivo* sensitivity to rituximab (Minard-Colin et al., 2008). Moreover, monocyte depletion of C57BL/6 mice engrafted with BL3750 reduced the therapeutic effect of rituximab in line with Riihijarvi's observations in DLBCL patients that those with high CD68 had favourable prognosis with R-CHOP (Minard-Colin et al., 2008, Riihijarvi et al., 2015). This work highlighted the utility of modulating the microenvironment as part of the treatment strategy for DLBCL.

1.2 Tumour microenvironment

The study of cancer had long been focussed on the study of malignant cells and how they differ from normal cells. Currently, the contribution of non-malignant components to tumourigenesis have recently become the focus of cancer research (Kenny et al., 2007). In lymphoma, the tumour

microenvironment (TME) is composed of residing lymphoid cells, inflammatory response cells, blood vessels, and collagen (Scott and Gascoyne, 2014). The expression of chemokines by different subtypes of lymphoma allows malignant cells to home to their preferential microenvironment where resident non-malignant cells are induced to cultivate that microenvironment (Scott and Gascoyne, 2014).

While biological and genetic abnormalities determine the phenotype of lymphoma cells, malignant cells themselves exert their influence on the location of lymphoma involvement and the make-up of the TME (Scott and Gascoyne, 2014). In short, malignant cells do not act in isolation but work in concert with their environment to enable progression, immune evasion and resistance to therapy (Scott and Gascoyne, 2014).

1.2.1 Gene expression profiling of DLBCL tumour microenvironment

The tumour stroma of DLBCL is made up of the extracellular matrix (ECM), fibroblasts of diverse phenotypes, blood vessels, immune and inflammatory cells (Mbeunkui and Johann, 2009). Gene expression profiling confirmed that the non-malignant components of lymphomas play a vital role in disease progression and treatment response (Lenz et al., 2008). Several groups have profiled large cohorts of DLBCL confirming that GCB and ABC as distinct subtypes and also investigated the nature of the TME in DLBCL (Lenz et al., 2008, Alizadeh et al., 2000, Reddy et al., 2017). Specifically, Lenz *et al.*, not only profiled the CD19-positive tumour cells but also the CD19-negative

stromal cells and defined distinct gene signatures based on the stromal component of DLBCL (Lenz et al., 2008). They assumed all CD19-positive cells were malignant and all CD19-negative cells were not. This excluded the contribution of non-malignant B cell (i.e. regulatory B cells) and ignores CD19-negative malignant B cells (Delage et al., 2019).

Lenz *et al* found that the gene signature from GEP of the non-malignant cells (CD19-negative) clustered into two clusters designated as stromal-1 and stromal-2 (Lenz et al., 2008). From multivariate analysis and combination of the expression of stromal-1 and stromal-2 gene signatures into a "stromal score" was predictive of survival: the higher the stromal score, the poorer the prognosis (Lenz et al., 2008). The stromal score was variably distributed amongst ABC and GCB DLBCL samples (Figure 1.8) (Lenz et al., 2008).

The genes in the stromal-1 signature include genes of the extracellular matrix (ECM) and collagen synthesis, MMPs, TIMP2, and genes representing tumour associated macrophages (TAMs), myeloid derived suppressor cells and Tie2 expressing monocytes (Lenz et al., 2008). Stromal-2 signature genes include angiogenesis-promoting genes, vascular endothelial growth factor (VEGF) and endothelial markers such as PECAM1 and SPARCL1 (Lenz et al., 2008). Lenz *et al* assert that stromal-1 genes tend to be genes involved at initiation of the tumourigenesis (Lenz et al., 2008). When the tumour undergoes an angiogenic switch, the genes of stromal-2 are expressed and the tumour becomes more aggressive (Lenz et al., 2008). They found tumours enriched with stromal-2 genes to have poor survival (Lenz et al., 2008).

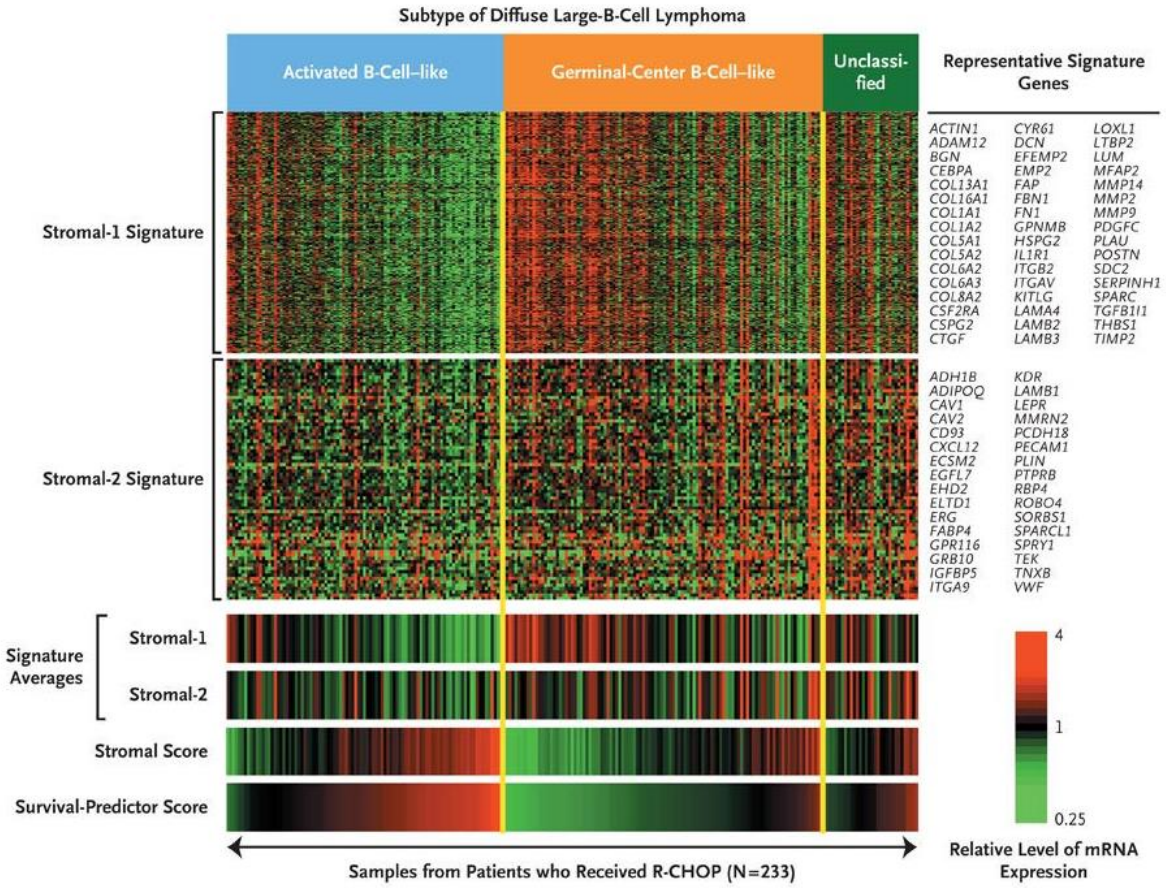

Figure 1.8 Gene expression profiling of the DLBCL microenvironment reveals two stromal gene signatures. Stromal-1 and Stromal-2 gene signatures were derived from the CD19-negative gene signatures of DLBCL. Stromal-1 includes genes of the extra cellular matrix and macrophages and stromal-2 is rich in vascular genes. Lenz *et al* classified DLBCL by COO and then clustered them by stromal-1 and stromal-2. ABC and GCB subtypes had genes from both stromal-1 and stromal-2 signatures and found that ABC had lower expression of stromal-1 genes. Stromal-2 genes were variably distributed among ABC and GCB but Lenz *et al* found that those tumours with higher proportion of stromal-2 genes had a worse survival.

1.2.2 Tumour microenvironment contributes to lymphomagenesis

The TME contributes to lymphomagenesis in several ways. First, the TME contributes to drug resistance by protecting B cell malignancies from the initial effects of therapy and that cytokines, chemokines, growth factors, and the interaction of malignant B cells with components of the TME are essential for this to occur (Shain et al., 2015). Therapy may kill some tumour subpopulations but the TME can shield a few tumour cells allowing them to survive treatment resulting in minimal residual disease (MRD) (Shain et al., 2015). These remaining tumour cells that survive through the stress of therapy along with its surrounding TME can begin a cascade of development and proliferation (Shain et al., 2015). The result is an even more complex, genetically altered, resistant phenotype that cause patients to relapse (Shain et al., 2015).

In early stages of tumour development, translocations in cell proliferation and survival genes together with epigenetic and genetic anomalies result in constitutive activation of oncogenes and inactivation of tumour suppressor genes that lead to malignant transformation (Shain et al., 2015). Along with these, tumour cells can manipulate and usurp survival signals from the surrounding microenvironment for their own purpose (Shain et al., 2015). As such, tumour cells do not act in isolation but are supported by the TME in cell homing and invasion, in resistance to cell death, proliferation, immunosuppression, self-renewal, and angiogenesis (Shain et al., 2015). As seen by tumour engraftment studies, the tumour cells influence

the biological makeup of the stroma. The TME evolves with the malignancy and demonstrate sustained gene expression changes that support critical aspects of tumour growth (Shain et al., 2015). Little is known about the "normality" of the tumour-associated stromal cells such as immune cells, macrophages, fibroblasts and endothelial cells (Shain et al., 2015). *In vitro* experiments can only provide limited information as tumour associated cells *in vitro* do not accurately mimic all components of the *in vivo* TME such as hypoxia, inflammatory cells, chemokines and cytokines (Dvorak, 1986). Preclinical models are useful for studying the tumour and its associated stroma in situ from early through to late stages of development.

1.2.3 Tumour microenvironment contributes to hallmarks of cancer

The experiments published by Lenz *et al*., draw attention to a field that began in 1889 when Stephen Paget published his hypothesis of "seed and soil" to explain the non-random pattern of metastasis (Witz, 2009, Paget, 1989). Paget's work has since continued by others such as Isaiah Fidler who found that metastatic cells homed to different sites based not only on the characteristics of the tumour cells but also by the host microenvironment (Fidler, 2003). Fidler demonstrated that within 24hrs of intravenous injection of cells in mice, that less than 0.1% of tumour cells were still viable in circulation and that less than 0.01% of these surviving cells were capable of metastasis which demonstrates the aggressive selection occurring during engraftment (Fidler, 2003). When tumour cells are injected intravenously in mice, they immediately go to the heart then disseminate to the lungs where

they arrest (Fidler, 2003). Once the cells eventually pass through the lungs they migrate to specific organs such as the liver and spleen (Fidler, 2003). This suggests that subpopulations exist in the primary tumour which, when injected, home to a preferential microenvironment to propagate (Fidler, 2003). Extending from the work of scientists such as Paget and Fidler, the tumour microenvironment has been shown to be as important to cancer pathogenesis as the tumour cells themselves contributing to many of the hallmarks of cancer (Hanahan and Coussens, 2012).

For the initiation and maintenance of each hallmark of cancer, many genetic factors, for example MYC, are contributed by the tumour cell (Gabay et al., 2014). But it is the host which provides the processes that impact MYC's ability to initiate tumourigenesis (Gabay et al., 2014). *In vivo* models have identified mechanisms of how host-dependent mechanisms influence MYC's ability to initiate tumourigenesis (Pelengaris et al., 2004). It has been shown that the suppression of MYC to endogenous levels in the mice could reverse tumourigenesis in a variety of cancers even in clonally and genetically heterogeneous tumours (Shroff et al., 2015, Lawlor et al., 2006).

1.3 Monocytes and macrophages

The immune cells of the microenvironment are recruited to the tumour site using signals similar to an inflammatory response (Coutinho et al., 2015). As part of the innate immunity, monocytes will migrate to sites of inflammation and polarise to different macrophage types based on the

cytokines present. The current paradigm of macrophage polarisation and their role in inflammation and how they contribute to cancer progression is described in the following section.

1.3.1 M1 and M2 paradigm

The first to label classically and alternatively activated macrophages as M1 and M2 was Mills *et al* (Mills et al., 2000). Studying immune responses in mice, Mills discovered that C57BL6 and BALB/c mice had different T cell responses. When C57BL6 mice were challenged with *Leishmania major*, he found their T cells produced INFγ, which activated their macrophages to produced nitric oxide (NO) and killed the parasite. In contrast, T cells from BALB/c mice challenged with *Leishmania major* produced more IL-4 that suppressed macrophage activation and NO secretion leaving BALB/c mice were sensitive to parasitic infection.

These observations led Mills to consider that perhaps macrophages and not T cells were directing immune responses. He termed the macrophages that mediated these responses as M1 and M2 to reflect the Th1 and Th2 responses associated with their activation (Mills et al., 2000, Mills, 2015). Mills found that macrophages do not merely respond to T cells but can control their own fate by secreting cytokines such as TGFβ1 to inhibit NO and increase IL-10 and ornithine (Mills et al., 2000). Metabolism of arginine by inducible nitrous oxide synthase (iNOS) is characteristic of M1-type macrophages where the result is release of nitrous oxide (NO). When macrophages produce NO, they

kill indiscriminately (Mills, 2015). In contrast, M2-type macrophages will metabolise arginine using arginase resulting in urea and ornithine which promotes proliferation and wound-healing (Mills et al., 2000). This concept has interesting applications in cancer and arginase inhibitors have been shown to inhibit proliferation of breast cancer and non-small lung cancer cells *in vitro* (Wang et al., 2018, Kotamraju et al., 2007).

These terms M1 and M2 have been taken further to include a multitude of macrophage phenotypes; M1, M2a, M2b, M2c, and M2d which are achieved through activation with different cytokines (Roszer, 2015, Mantovani et al., 2002). This goes beyond Mill's intention who acknowledged that terms M1 and M2 were an oversimplification and that macrophages phenotypes are not clonal populations but a continuum of phenotypes (Mills et al., 2000). It is likely that in any tissue either normal or neoplastic, there will be a range of macrophages in different phenotypic states co-existing (Figure 1.9).

1.3.2 Tissue resident macrophages

There are macrophages that do not circulate but remain in tissues i.e. Kupffer cells in the liver and alveolar macrophages in the lung (Italiani and Boraschi, 2014). Where the tissue resident macrophages come from is still unresolved (Hashimoto et al., 2013, Italiani and Boraschi, 2014). Since the "mononuclear phagocyte system" proposed in 1969 by van Furth and Cohn, it is widely accepted that all macrophages in blood and tissue are derived from precursor cells based on morphology and function (van Furth et al., 1972).

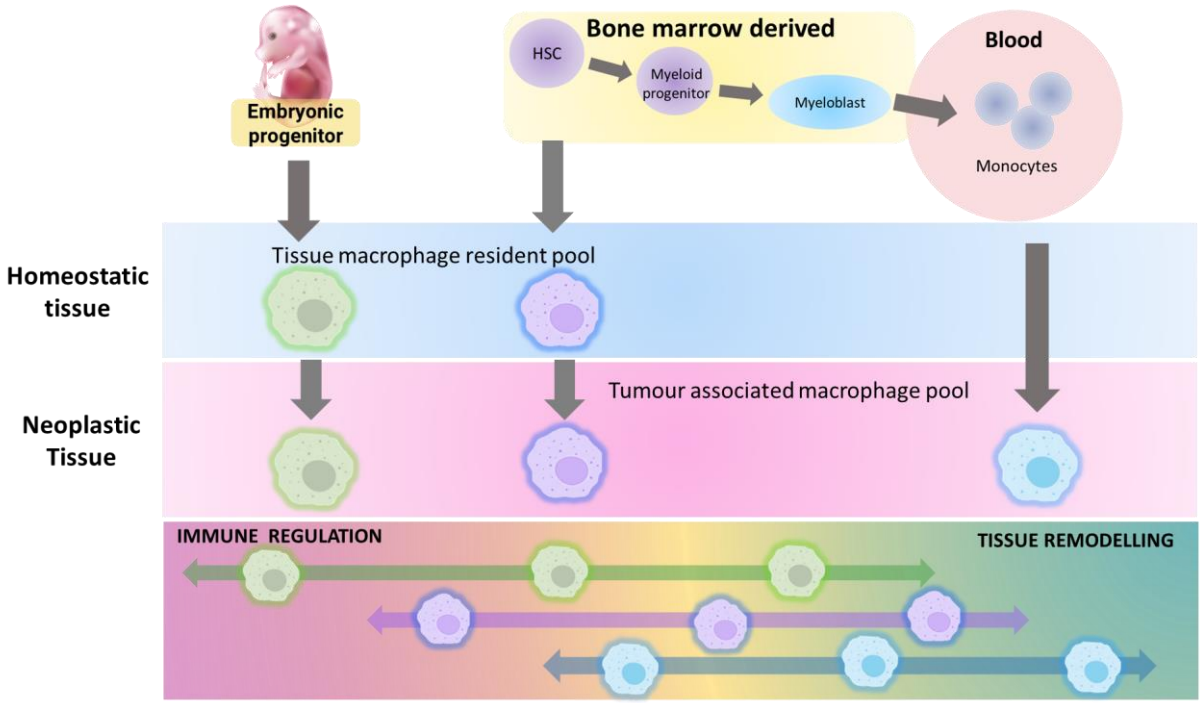

Figure 1.9. Origin of macrophages in homeostatic vs. neoplastic tissue.
Tissue resident macrophages are said to be of yolk-sac embryonic origin and may also come from adult bone marrow. These tissue resident macrophages are thought to be self-renewing. Tumour associated macrophages (TAMs) found in neoplastic tissue are said to include not only the tissue resident macrophages but also from a pool of monocyte derived macrophages. Differentiating between the tissue resident and monocyte derived macrophages is not clear but the recruited monocyte derived macrophages are the main pool of TAMs focussed on in this thesis.

Hashimoto *et al* determined that tissue resident macrophages were able to divide and proliferate and that their depletion was not replenished by infiltrating macrophages (Hashimoto et al., 2013). Tissue resident macrophages were instead replenished *in situ* which required GM-CSF and M-CSF in order to repopulate (Hashimoto et al., 2013). This is supported by reports that tissue resident macrophages (Kupffer, splenic, microglia) are formed at the embryonic stage and infiltrating macrophages which appear after infection are derived from classical monocytes (Murray and Wynn, 2011, Qian et al., 2011). Contradictorily, it was also shown that tissue resident macrophages cleared by irradiation were repopulated by monocyte derived macrophages (Hashimoto et al., 2013). It is likely that tissues will have various proportions of embryonically-derived tissue resident macrophages, bone marrow-derived macrophges and monocyte-derived macrophages (Figure 1.9) (Italiani and Boraschi, 2014).

1.3.3 Tumour associated macrophages

In the tumour, it is likely that tumour associated macrophages (TAMs) are made up both tissue resident and monocyte derived macrophages. The work published by Lenz et al. highlighted the stromal component of the tumour as predictive of a patient's response to therapy yet a microenvironment-derived biomarker remains elusive (Lenz et al., 2008, Kridel et al., 2015). Within the tumour microenvironment, innate immune cells such as macrophages are present (Hanahan and Coussens, 2012). TAMs

have been shown to play a role in tumour progression and may be potential targets for therapy (Qian and Pollard, 2010).

Macrophages are involved in promoting angiogenesis, invasion and migration of tumour cells, and immune suppression but also have roles in the early stages of tumour initiation (Pham et al., 2018, Mantovani et al., 2017). It has been suggested that specific subpopulations of macrophages promote tumour growth and progression (Qian and Pollard, 2010) but it is difficult to definitively distinguish these subsets from each other. Monocyte derived cells *in vivo* do not exist as distinct subpopulations but in stages along a continuum that change with environmental signals (Murray and Wynn, 2011, Mantovani and Locati, 2013).

Conditions that permit monocyte differentiation into macrophage subsets have been extensively studied *in vitro* (Mantovani et al., 2002, Lacey et al., 2012). Two subsets have been identified: M1 are classically activated in the presence of GM-CSF, INFγ, or TNFα and M2 are alternatively activated by M-CSF, IL-4, and IL-10 (Lacey et al., 2012, Italiani and Boraschi, 2014). M1 has been shown to have pro-inflammatory and anti-tumour properties while M2 macrophages have anti-inflammatory and pro-angiogenic properties (Mills et al., 2000, Minutti et al., 2017, Van Overmeire et al., 2016). Many groups report various cell markers to distinguish M1 from M2 as well as diverse *in vitro* conditions for differentiation into these subsets (Lacey et al., 2012, Van Overmeire et al., 2016, Italiani and Boraschi, 2014). In cancer, TAMs have been reported to exhibit properties of M2 type macrophages yet others have

also seen TAMs with both M1 and M2 type markers in cancer xenografts and by immunohistochemistry of patient tumours (Komohara et al., 2014, Mantovani et al., 2017, Shain et al., 2015). It is accepted that GM-CSF and M-CSF are cytokines which can polarise monocytes to M1-like and M2-like phenotypes respectively that the resulting phenotypes have opposing inflammatory reactions (Lacey et al., 2012, Hashimoto et al., 2013). For example, it has been shown that M1-GMCSF produced higher TNF and IL-12 and lower levels of IL-10 than M2-MCSF (Lacey et al., 2012, Verreck et al., 2004, Kamada et al., 2005). While a variety of different cytokines will result in varying degrees of M1 and M2 polarisation *in vitro,* the work described in the following chapters in this thesis will use M1 to describe GM-CSF polarised monocytes and M2 as M-CSF polarised monocytes.

A study by Riihijarvi *et al* that the frequency of CD68 positive cells was associated with favourable prognosis in DLBCL patients treated with rituximab + CHOP and associated with poor outcome in patients given CHOP only (Kridel et al., 2015, Riihijarvi et al., 2015). While CD68 expression did not correlate with either GCB or ABC distinction by immunohistological method of diagnosis (Kridel et al., 2015, Riihijarvi et al., 2015), Riihijarvi *et al* did correlate mRNA and protein levels of CD68 with CD163, a marker for M2 alternatively activated macrophages and suggested that the effect of rituximab could be attributed to binding of Fc receptor of rituximab (Riihijarvi et al., 2015, Kridel et al., 2015). .

1.3.4 Macrophage chemotaxis

Chemotaxis of monocytes and macrophages to sites of infection is part of the innate immunity (Jones, 2000). Macrophage migration is mediated by attractants that bind to serpentine receptors (i.e. S1P receptors) which then couple to G protein receptors that lead to activation of *PI3K* and other pathways (Jones, 2000). Surface receptor tyrosine kinases signalling through colony-stimulating factor-1 receptor (*CSF-1R*) which activate *PI3K* and *JAK/STAT* pathways will also mediate macrophage migration (Hamilton, 1997). Other chemokines that induce migration of classically activated (M1) and alternatively activated (M2) macrophages include: CXCL12 which mediates leukocyte trafficking during embryonic development and enhances the macrophage expression of CD14 and CD163; MCP-1 (CCL-2) which is highly expressed in rheumatoid arthritis and atherosclerosis; and CXCL10 (IP-10) which is elevated in pancreatic cancers (Lunardi et al., 2014, Chen et al., 2015, Durr et al., 2010, Deshmane et al., 2009, Xuan et al., 2015).

The cytokines and chemoattractants that mobilise macrophages are well known, but the drivers for the physical changes that need to occur for the macrophages to move are only recently being published. The actin skeleton of macrophages allow for migration towards a stimulus which can happen stochastically but can also occur in response to a chemoattractant (Mattila and Lappalainen, 2008). Actin filaments support filopodia which protrude and extend outwards then the rest of the cell is propelled forward (Jones, 2000, Mattila and Lappalainen, 2008). Recent studies have revealed that formins,

FMNL2 and *FMNL3*, drive the protrusion of filopodia by interacting with *Rac/Cdc42* which in turn activates the *PI3K* pathway (Kage et al., 2017).

1.3.5 Macrophages are professional phagocytes

Named from the Greek for 'big eaters', macrophages have long been known as professional phagocytes. In homeostasis, phagocytosis is required for the removal of dead cells which begins with the release of 'find me' signals such as S1P, CX3CL1, ATP, and UTP from apoptotic cells to recruit remote phagocytes (Arandjelovic and Ravichandran, 2015). In the case of S1P, it will bind to S1PR1 on macrophages and lead them towards the apoptotic cell where 'eat me' signals present on dead cells to initiate the process of engulfment (Figure 1.10) (Arandjelovic and Ravichandran, 2015).

Receptors on macrophages that recognise apoptotic cell ligands (i.e. phosphatidylserine, MFGE8 (milk fat globule-EGF factor 8 protein), and TSP1 (thrombospondin)) also have a role in inflammation and homeostasis (Arandjelovic and Ravichandran, 2015). The reason for multiple "find me" signals is not yet known. Despite the various receptors, it is known that the *PI3K/AKT* pathway is essential for actin filament reorganisation which allow macrophages to migrate and to phagocytose (Qian et al., 2004, Schlam et al., 2015, Zhang et al., 2009, Vergadi et al., 2017).

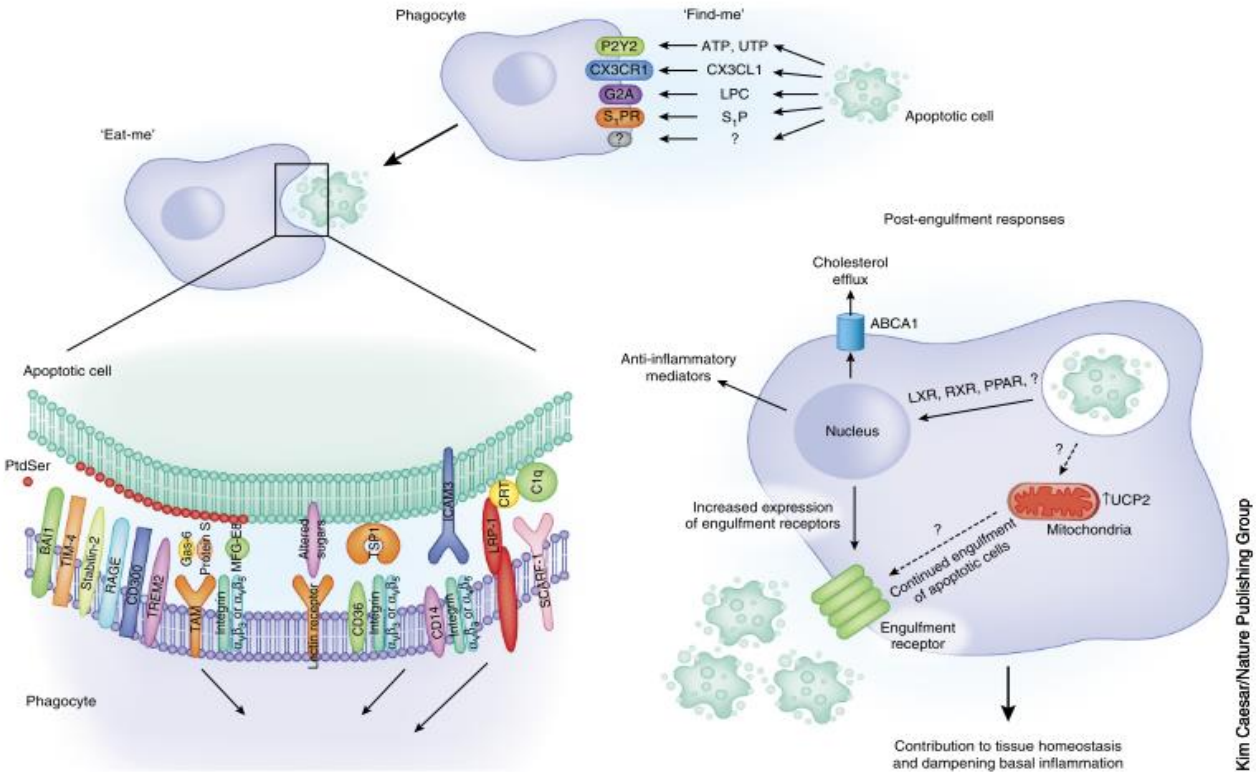

Reproduced with permission from (Arandjelovic & Ravichandran, Nature Immunology, 2015) Nature Publishing Group

Figure 1.10 Phagocytosis of apoptotic cells in homeostasis. Apoptotic cells release 'find me' signals such as S1P which bind to receptors on apoptotic cells i.e. S1PR1 thereby recruiting phagocytes such as macrophages. Macrophages express several phagocytic receptors which bind to apoptotic cells leading to engulfment.

1.4 Sphingosine-1-phosphate

Sphifngosine-1-phosphate (S1P) is a bioactive lipid vital for leukocyte trafficking, vascular formation, and regulation of apoptosis and exploring its role in cancer has led to the classification of S1P as an onco-lipid (Spiegel and Milstien, 2003, Pyne et al., 2018). Sphingosine-1-phosphate (S1P) is a component of the tumour microenvironments upon which malignant cells may be dependent. A potent regulator of a diverse repertoire of biological functions, S1P impacts homeostasis and disease (Tsai and Han, 2016). Erythrocytes and high-density lipoproteins (HDL) are the major source of S1P in the body (Spiegel and Milstien, 2003). The higher concentration of S1P in the blood creates a gradient to the lower concentration of S1P found in tissues which allows for leukocyte migration (Aoki et al., 2016).

S1P is formed within the cell and transported out where extracellular S1P can then bind to G-coupled protein receptors S1PR1, S1PR2, S1PR3, S1PR4, and S1PR5 (Hait and Maiti, 2017, Spiegel and Milstien, 2003, Blaho and Hla, 2014). Because of its varied effects on proliferation and migration, S1P signalling has been targeted therapeutically in autoimmune diseases and being explored in cancer such as breast, colon and lymphoma (Chimen et al., 2015, Kunkel et al., 2013, Ogretmen, 2018).

1.4.1 S1P formation

Sphingosine-1-phosphate (S1P) is formed by the ATP-dependent phosphorylation of sphingosine by SPHK1/SPHK2 (Spiegel and Milstien,

2003). This is reversible with SGPP1/SGPP2 or S1P can be permanently degraded with sphingosine-1-phosphate lyase (SPL) (Spiegel and Milstien, 2011). S1P concentrations are tightly controlled by its constant formation and degradation.

SPHK1 is located in the cytosol and is responsible for the formation of extracellular S1P (Spiegel and Milstien, 2003). The translocation of *SPHK1* to the plasma membrane occurs in response to growth factors and agonists, and *SPHK1* can regulate itself by inducing its own intracellular translocation back to the cytosol (Nishino et al., 2019). Its translocation and phosphorylation is fundamental to the activity of *SPHK1* (Nishino et al., 2019). SPHK1 phosphorylates sphingosine to form S1P which is then transported out of the cell through ATP-binding cassette type transporters (ABCC1, ABCA1, and ABCG1) or SPNS2 (Takabe and Spiegel, 2014). Transported extracellular S1P formed primarily by *SPHK1* is induced by the growth factor, PDGF, and/or inflammatory cytokines such as TNF-α and interleukins (Spiegel and Milstien, 2011). Signalling through G-coupled protein receptors, S1PR1-5, S1P then activates cellular pathways such as JNK, ERK, AKT, and Rho in order to mediate migration, proliferation, and angiogenesis (Figure 1.11) (Takabe and Spiegel, 2014, Kwong et al., 2015).

SPHK2 is located in the nuclear membrane, endoplasmic reticulum and mitochondria has a contrasting role to *SPHK1* (Maceyka et al., 2005, Ogretmen, 2018). Intracellular S1P produced by *SPHK2* inhibits histone deacetylases (HDACs) which suppresses cell growth and survival (Figure 1.12)

(Maceyka et al., 2005, Chen et al., 2016). Though *SPHK1* and *SPHK2* are said to produce functionally distinct S1P, studies with knockout mice show that they can compensate for the loss of the other thereby maintaining homeostasis (Xiong et al., 2016).

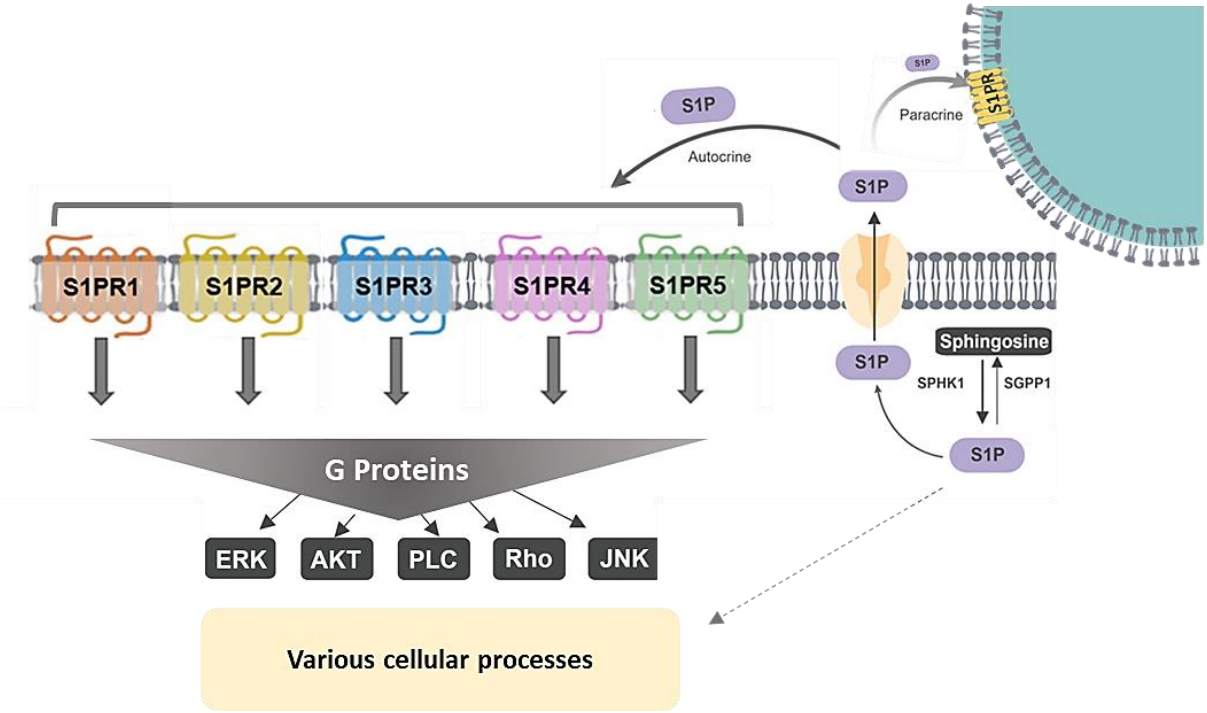

Figure 1.11 Inside-out signalling of S1P. S1P formed by SPHK1 is transported out of the cell where it can signal in either a paracrine or autocrine fashion. Binding to S1P receptors can increase or inhibit activation of *ERK, AKT*, *PLC, Rho, JNK* pathways depending on the receptor and cell type leading to various biological effects such as migration, apoptosis and

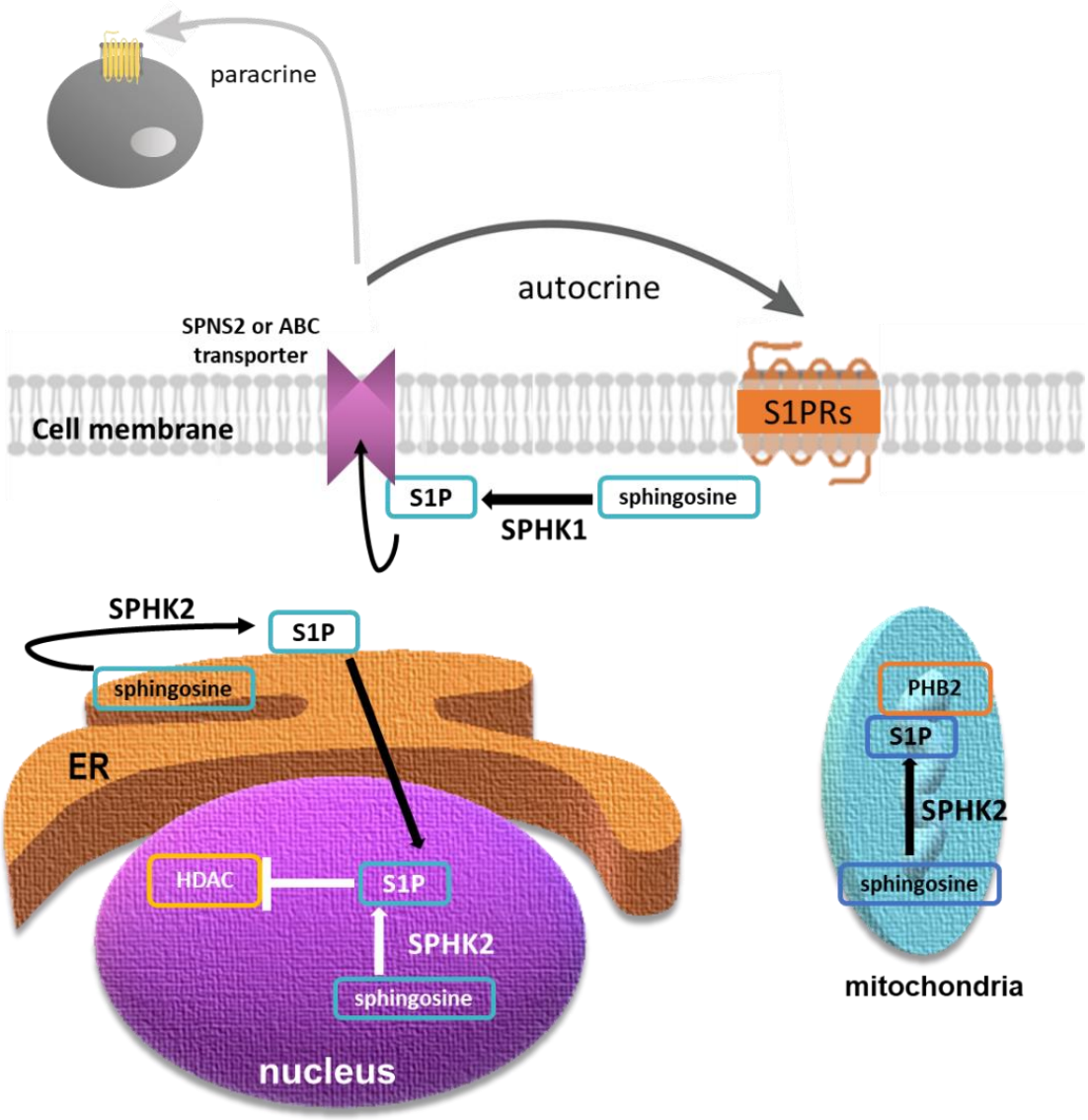

Figure 1.12 Formation of S1P. S1P is formed by phosphorylation by SPHK1 or SPHK2. SPHK2 is the main source of intracellular S1P where synthesis can occur in the nucleus and endoplasmic reticulum (ER). S1P produced here can inhibit HDACs. SPHK2 can also form S1P in the mitochondria where S1P can bind PHB2. SPHK1 can translocate to the cell membrane and form S1P that will be transported out of the and is transported out of the cell by ABC or SPNS2 transporters where it can signal.

S1P transport out of the cell is said to occur through several transporters. The ATP-binding cassette (ABC) type transporters (ABCC1, ABCA1, and ABCG1) were the first to be identified, followed by Spns2 and ApoM which showed to be highly specific transporters for S1P out of the cell (Takabe and Spiegel, 2014, Mitra et al., 2006, Aoki et al., 2016).

1.4.2 Sphingolipid rheostat

The formation of sphingosine/ceramide or conversely of S1P is known as the sphingolipid rheostat which illustrates the controlled responses of the cell to stress (Figure 1.13) (Newton et al., 2015). This model of S1P-ceramide signalling emphasises the contrasting biological functions mediated by S1P and ceramide (Hatoum et al., 2017, Newton et al., 2015). S1P formation by SPHK1 is in response to TNF-α which leads to activation of PI3K/AKT, ERK, and NF-κB pathways to promote proliferation and inhibit apoptosis (Osawa et al., 2001, Rutherford et al., 2013). Conversely, cytokines such as TNF-α and Fas ligand induces ceramide production which leads to apoptosis and senescence (Spiegel and Milstien, 2011). When S1P is transported out of the cell, it can bind to S1PR1 resulting in transport back into the cell creating a loop of "inside-out" signalling (Newton et al., 2015, Spiegel and Milstien, 2011).

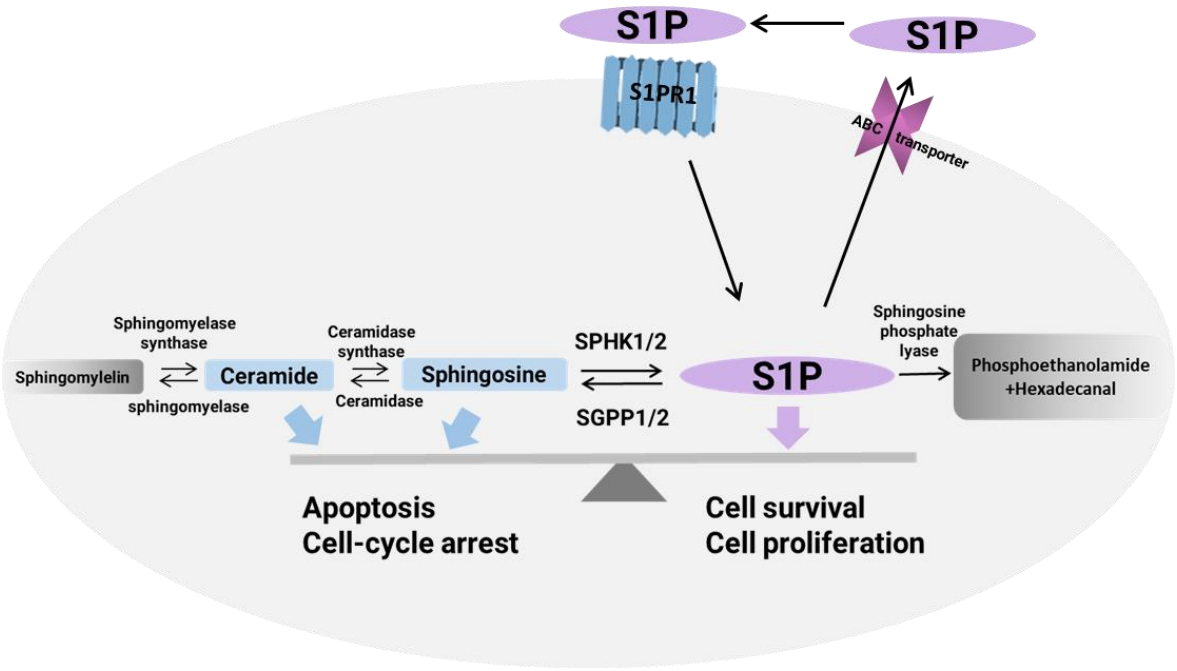

Figure 1.13 Sphingolipid rheostat. The balance between ceramide/ sphingosine and S1P maintains homeostasis in vivo. Increased ceramide leads to increased apoptosis and cell cycle arrest while increased S1P confers survival and proliferations. This diagram also reflects the "inside-out" signalling of S1P is transported out of the cell and signals the same cell through S1PR1 and transported back into the cell in a loop.

1.4.3 S1P receptors

S1P can bind to five receptors; S1PR1 (EDG1), S1PR2 (EDG5), S1PR3 (EDG3), S1PR4 (EDG6), and S1PR5 (EDG8) which couple to G-proteins that activate transcriptional pathways that lead to many different cellular processes (Pyne and Pyne, 2000). Originally named endothelial differentiation genes (EDG) due to the discovery of S1PR1 (EDG1) was Hla and Maciag set out to determine possible molecular mechanisms involved in angiogenesis (Hla and Maciag, 1990). They used human umbilical vein endothelial cells (HUVECs) treated with a known tumour promoter phorbol 12-myristate 13-acetate (PMA) and isolated a cDNA clone that was induced, edg-1. They noted that edg-1 had similar structure to G-coupled protein receptor although at this time its ligand was yet unknown (Hla and Maciag, 1990). Discovery of the other S1P receptors quickly followed It wasn't until 1998, when the ligand for edg-1 was determined to be S1P (Lee et al., 1998).

Cells can have different patterns of expression of S1P receptors that may alter depending on maturation or activation state (Blaho and Hla, 2014). The functional roles of S1P receptor signalling can vary depending on cell type as well as on the cytokines in the environment and there is considerable interest in the targeting of these receptors therapeutically (Figure 1.14).

There have been antagonists and agonists have been developed to target S1P receptors. Fingolimod was the first S1PR agonist targeting S1PR1, S1PR3, S1PR4 and S1PR5 but was also able to antagonise S1PR1

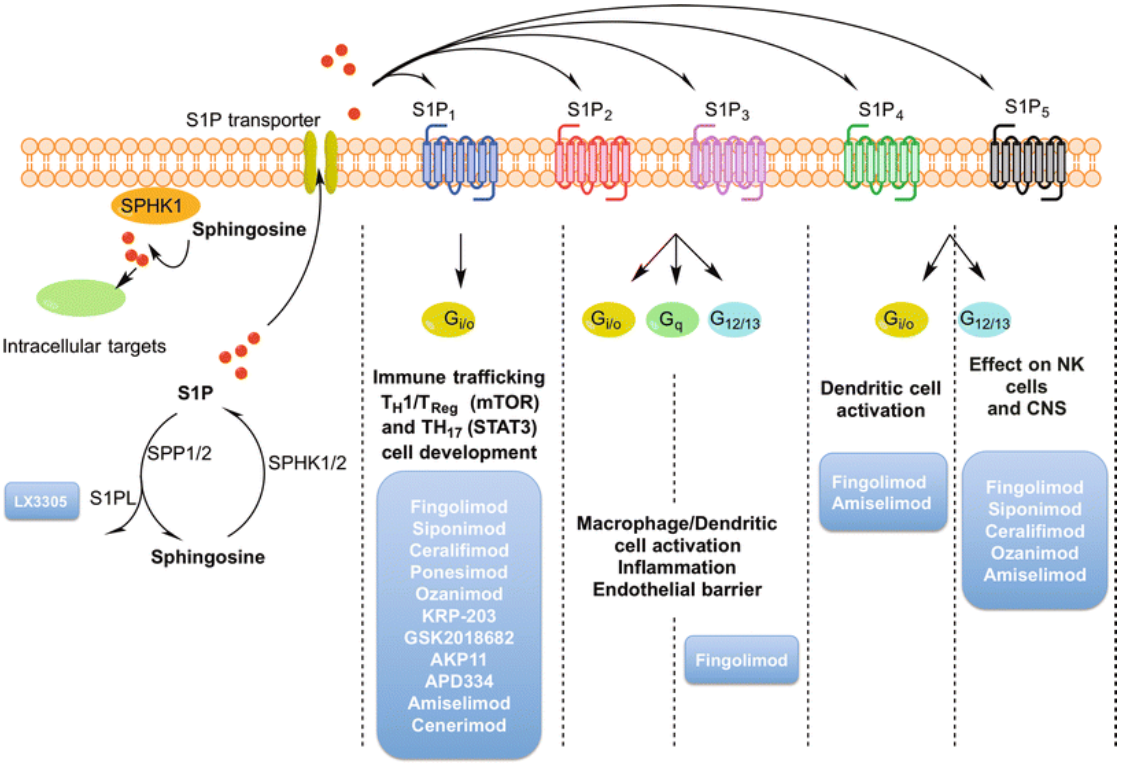

Figure 1.14 Drugs that target S1P signalling. S1P signals through five G coupled protein receptors which activates transcription pathways to regulate immune cell trafficking and activation. There are a number of drugs currently available that selectively target these receptors. There is an antagonist for S1PR2, JTE013, and an agonist, CYM5220 which were not included in this figure for unknown reasons.

(Blaho and Hla, 2014, Bolli et al., 2010). Siponimod (BAF312) is currently approved by the FDA for the treatment of multiple sclerosis and is specific for S1PR1 and S1PR5 (Kappos et al., 2018). A single S1PR2 antagonist has been developed, JTE013, but was found to target S1PR1 *in vitro* while an agonist to S1PR2, CYM5220, has shown to have superior specificity (Pyne and Pyne, 2011, Satsu et al., 2013). Targeting these receptors in cancer will require an understanding of the effect of the particular receptor in tissue of interest.

S1PR1

S1PR1 has the highest affinity for S1P compared to other receptors (O'Sullivan and Dev, 2013). Immune cells including macrophages, B and T cells, dendritic cells, and NK cells express S1PR1 which can mediate migration, proliferation, anti-apoptosis, and cytoskeletal assembly (O'Sullivan and Dev, 2013). Binding with S1P leads to coupling of S1PR1 to G_1 which results in the activation of ERK and PLC (phospholipase C) (Spiegel and Milstien, 2011).

In homeostasis, S1PR1 mediates egress of patrolling immune cells from primary and secondary lymphoid organs and migration through the blood (Spiegel and Milstien, 2011, Wang et al., 1999). S1PR1 is vital for the formation of vasculature as shown through S1PR1-/- mice which have impaired vasculature (O'Sullivan and Dev, 2013, Lee et al., 1999). Disruption of S1PR1 signalling using antagonists has been known to have therapeutic benefits for patients with multiple sclerosis (MS). FTY720 or fingolimod was approved for MS patients but due to its off-target effects more specific antagonists were

developed. Siponimod, a specific S1PR1/S1PR5 antagonist, has been recently approved by the FDA for the treatment of MS (Kappos et al., 2018).

S1PR2

Unlike S1PR1, S1PR2 has been shown to reduce migration. Cells that express high levels of S1PR2 will result in retention in the primary or secondary lymphoid organs. Binding of S1PR2 to S1P which leads to coupling G_1, G_q, and $G_{12/13}$ resulting in upregulation of Rho and downregulation of Rac and AKT/PTEN (Sanchez and Hla, 2004). It was also shown that binding of S1P to S1PR2 antagonises S1PR1-G_1-PI3K. S1PR2 has been shown to be critical in the formation of vasculature, where S1PR2 signalling results increased permeability which can be blocked by S1PR2 antagonist, JTE013. S1PR2 has been implicated in DLBCL, where S1PR2-/- mice were shown to develop DLBCL as they age (Aoki et al., 2016, Cattoretti et al., 2009).

S1PR3

S1PR3 coupled with G_1, G_q, and $G_{12/13}$ activates ERK, and Rho/Rac inducing proliferation and migration (Sanchez and Hla, 2004). Mediation of inflammatory responses and regulation of cardiac functions such as vasoconstriction and vasodilation are proposed roles for S1PR3 (Sanchez and Hla, 2004). Intracellular signalling of S1PR3 is reported to have vital role in immune responses to bacteria mobilising monocytes to enhance bactericidal activity and increase survival in sepsis (Hou et al., 2017).

S1PR4

Less is known about S1PR4 but some researchers report that dendritic cells and neutrophils are regulated by S1PR4 (Olesch et al., 2017, Sanchez and Hla, 2004). It was also shown that S1PR4 may regulate development of peripheral immune blood cells(Sanchez and Hla, 2004). S1PR4 couples with G_i and $G_{12/13}$ leading to activation of ERK and PLC pathways as well as inducing MAPK and RhoA pathways which can affect actin filament assembly (Olesch et al., 2017, Xiong et al., 2019).

S1PR5

S1PR5 couples with G_i and $G_{12/13}$ and is important in the trafficking of NK cells from the bone marrow and shown to be highly expressed in patrolling monocytes and by cells of the central nervous system (Debien et al., 2013, Tsai and Han, 2016). It was also shown that S1PR5 mediated cell survival in mature oligodendrocytes and to induce protective effect of autophagy in PC-3 (prostate cancer) cell line (Chang et al., 2009).

1.4.4 S1P and macrophage recruitment and function

Migration mediated by S1PR1, S1PR2 and S1PR3 were shown through experiments by Kon *et al.* They stably transfected Chinese hamster ovary (CHO) cells with *S1PR1*, *S1PR2* and *S1PR3* then examined the migration of these cells along an S1P gradient (Kon et al., 1999). They found that the *S1PR1* and *S1PR3* transfected cells migrated but *S1PR2* transfected CHO cells did not (Kon et al., 1999). There are a few studies on the effects of S1P on

phagocytosis. It has been shown that alveolar macrophages from chronic obstructive pulmonary disease (COPD) patients were found to be less phagocytic compared to macrophages from healthy donors mediated by *S1PR2* expression (McQuiston et al., 2011). Another study a similar result has shown that low expression of S1P2 led to better bacterial clearance and survival in patients with sepsis (Hou et al., 2015). These results point to a role of S1P in macrophage recruitment and function in inflammation. There are many studies which focus on the effects of S1P on migration and retention of macrophages in inflammation and in cancer (Yang et al., 2018, Weichand et al., 2017, Muller et al., 2017, Nagahashi et al., 2018a, Hait and Maiti, 2017).

1.4.5 S1P in inflammation and cancer

Evidence of the oncogenic potential of *SPHK1* and S1P came through experiments that demonstrated that the overexpression of *SPHK1* transformed NIH3T3 cells to fibrosarcoma (Pyne et al., 2018). While non-malignant cells contribute to S1P in the microenvironment, the neoplastic cells were the main source of *SPHK1* expression and that S1P produced by SPHK1 was responsible for the "inside-out" signalling (Nagahashi et al., 2018b, Pyne et al., 2018). S1P is controlled by constant formation and degradation with lyases and phosphatases. The expression of these lyases and phosphatases (*SGPP1* and *SPL*) were found to be under expressed in tumours compared to normal in gastric and breast cancers (Nakajima et al., 2017) In addition, the malignant and non-malignant cells within the tumour have different patterns of S1P receptor expression which can be stimulated by extracellular S1P in

the TME to maintain proliferation, foster an anti-apoptotic environment, and induce alternatively activate macrophages to secrete anti-inflammatory cytokines (Nakajima et al., 2017).

Tumours have been shown to rely on angiogenesis for trafficking, metastasis, and for their supply of essential nutrients (Nucera et al., 2011, Shen et al., 2016). S1P is shown to be involved in the recruitment of endothelial cells via S1PR1 to the tumour site and to enhance vascular formation (Zhang et al., 2013, Eklund et al., 2013). S1P not only mobilises and recruits immune and endothelial cells to the microenvironment, but will also facilitate metastasis of tumour cells through the vasculature in tumours such as melanoma, breast, thyroid cancer cells (Zhao et al., 2018, Nagahashi et al., 2018b, Rodriguez et al., 2016, Wang et al., 2019). S1P can foster an immune suppressive environment by alternatively activating macrophages and mediating the release of cytokines such as IL-10 and inhibition of IL-12 (Weigert et al., 2007, Guillermet-Guibert et al., 2009, Maiti et al., 2017).

In homeostasis, S1P released from apoptotic cells protects macrophages from apoptosis and tumour cells have co-opted this in order to protect itself from chemotherapy-induced apoptosis (Guillermet-Guibert et al., 2009). Apoptosis is important for the resolution of inflammation as neutrophils are induced to apoptosis by the inhibition of S1P signalling (Perez et al., 2019). S1P can also have contradictory effects by inducing apoptotic effects as well as proliferative anti-apoptotic effects on the same cell depending on certain *in vitro* conditions such as cell density in the case of mesangial cells of the kidney

(Gennero et al., 2002); ovarian cells in culture, if they are in suspension S1P induces apoptosis but induces survival if they are attached (Hong et al., 1999); and in hepatic myofibroblasts, which are important in the development of liver fibrosis, the balance of apoptosis and survival in hepatic myofibroblasts is mediated by S1PR1, S1PR2 and S1PR3 (Davaille et al., 2002).

The effect of S1P on DLBCL pathogenesis has largely come from the observation that *S1PR2* KO mice developed DLBCL as they aged (Cattoretti et al., 2009). This observation has been further cemented by work of Stelling et al and Vockerodt *et al* which demonstrated that *S1PR2* is a tumour suppressor in DLBCL absent mainly in the ABC subtypes. Stelling et al found that *S1PR2* expression in ABC-DLBCL was linked to a decrease in *SMAD1/TGFβ1* and an increase in *FOXP1* expression (Stelling et al., 2018). Interestingly, *SMAD1* embryonic knockout mice do not form mature macrophages suggesting a link between *S1PR2* and mature macrophages (McReynolds et al., 2007). Vockerodt *et al* further showed that in EBV+ DBCL, an increase in LMP1/AKT expression led to low expression of S1PR2 and that S1PR2 expression inhibited phospho-AKT (Vockerodt et al., 2019).

There was one study which indicated that increased *S1PR1* expression was associated with poor survival in DLBCL (Paik et al., 2014). Paik et al found that *S1PR1* as an independent prognostic indicator of OS in both GCB and non-GCB patients treated with R-CHOP. S1PR1 and *STAT3* expression was linked to poorer OS mainly in ABC-DLBCL (Paik et al., 2014). Our group has shown that angiogenesis in DLBCL was driven by S1PR1 signalling

(Lupino et al., 2019). Further exploration of *S1PR1* signalling in the pathogenesis of DLBCL has yet to be done but these findings suggest that therapeutically targeting *S1PR1* in DLBCL may be beneficial.

1.5 Hypothesis and aims

The combination of rituximab and chemotherapy make up the standard of care for all patients with DLBCL regardless of subtype. Currently about 40% of these patients do not respond or will relapse leaving them with few treatment options. Because of the role S1P in macrophage recruitment and evidence of its involvement in the pathogenesis of DLBCL, studying the effects of S1P in the context of macrophage recruitment in DLBCL is worthwhile. Especially as ADCP is the primary cytotoxic mechanism of rituximab (part of the standard of care of DLBCL) which is exerted by macrophages (VanDerMeid et al., 2018). It has been shown that S1P can exert contradictory functions on the same cell depending on certain conditions which may include macrophages. Therefore, it is important to evaluate the conditions in which S1P effects recruitment and function of macrophages in the context of DLBCL.

Therapeutic modulation of S1PRs on macrophages could be an alternative treatment strategy for DLBCL. But our current knowledge of the pattern of expression of the five S1P receptors on macrophages is limited to mouse macrophages (Muller et al., 2017). It would be advantageous to study the S1PR expression and its modulation using a model of human macrophages.

The expression of S1PR1 on primary human macrophages has been reported but the expression of the other S1P receptors has not been fully explored (Weichand et al., 2013a). The effect of S1P on macrophages has focussed mainly on its role in recruitment and retention. S1PR1 has also been implicated in the formation and recruitment of endothelial cells, and but up to now, its effect on macrophage function in DLBCL has not been fully explored.

This project will determine if S1P contributes to the recruitment of macrophages in DLBCL and the increased S1P concentration in the microenvironment could affect macrophage function. The specific aims of this study are:

1. Confirm the overexpression of SPHK1 in DLBCL and survey genes associated with macrophage recruitment and function for their differential expression in primary DLBCL datasets and correlation with SPHK1 expression;
2. Evaluate the expression of S1P receptors in polarised macrophages from healthy donors;
3. Determine if macrophages migrate to DLBCL in an S1P-dependent manner *in vitro* and in mouse models of DLBCL;
4. Examine the effect of S1P on the phagocytosis of rituximab-treated DLBCL cell lines and determine which S1P receptor(s) are involved;
5. Test the effect an S1P receptor antagonist on tumours from DLBCL engrafted mice treated with rituximab/chemotherapy.

CHAPTER 2

Materials and Methods

Chapter 2

Materials and Methods

2.1 Cell line cultivation and cryopreservation

Human DLBCL cell lines were obtained from ATCC (American Type Culture Collection). The FBS used in all experiments was heat inactivated. All cell lines were maintained in RPMI-1640 (GIBCO, Life Technologies) supplemented with 10% FBS (heat-inactivated foetal bovine serum, Invitrogen) except for OCI-LY1 which was maintained in IMDM (GIBCO, Life Technologies) + 20% FBS. A20 mouse lymphoma cell line was a gift from M. Hoogenkamp and THP-1 (ATCC) were maintained in RPMI-1640 + 10% FBS + Glutamax + 10mM HEPES + 1mM Na Pyruvate + 0.05mM 2-mercaptoethanol (all from GIBCO, Life Technologies) See Table 2.1 for summary of cell lines. Cells were incubated in a humidified incubator (RS, Biotech) set at 37°C 5% CO_2 and cultured according to ATCC guidelines.

Cells were counted first by doing a 1:10 or 1:100 dilution in trypan blue (Sigma Aldrich) then 10 µl was added to a Neubauer haemocytometer (BLAUBRAND, Sigma Aldrich). Cells were observed through an inverted microscope (Olympus CK30) and live cells were counted (those that did not take up trypan blue dye) within the four large corners. The number of cells were divided by 4 and then multiplied by the dilution factor of 10 or 100 and then multiplied by 10^4 to determine cells/ml.

To cryopreserve cell lines, they were washed in PBS and resuspended in 10% Dimethyl sulfoxide Hybri-max (DMSO, Sigma-Aldrich) + 90% FBS (GIBCO, Life Technologies) at approximately $1x10^7$/ml per cryovial (NUNC). They were stored in a Mr Frosty (Nalgene) cryogenic container at -80°C for up to one week then stored in liquid nitrogen long term. To thaw, cells were briefly warmed in a 37°C water bath until just melting and immediately transferred to 9mls of cold RPMI-1640 (GIBCO, Life Technologies). They were then centrifuged at 1000 RPM for 10 minutes in an Eppendorf 5810R centrifuge. Supernatant was aspirated and cells were resuspended in 10 ml of complete growth medium (Table 2.1).

2.2 Patient and donor samples

2.2.1 Ethical approval for research with human tissue

Patient DLBCL sections were obtained with ethical approval from the Human Biomaterials Resource Centre (HBRC, Birmingham) and Birmingham Women's and Children's Hospital (BWCH) (HBRC_10_022). Frozen DLBCL single cell suspensions were obtained with ethical approval from NHS GG&C Biorepository (NHS Glasgow Application/approval number 234). Tonsils were obtained with consent from adult patients from Queen Elizabeth Hospital (QE, Birmingham) and fixed in 10% neutral buffered saline and embedded in paraffin or made into single cell suspensions (HBRC_12_071). Leukocyte cones were obtained with consent through the National Blood Service and used for preparation of monocytes and polarised macrophages (RG_15_165). Cord

blood and reactive lymph nodes were obtained with consent through HBRC from BWCH and QE (HBRC_15_217).

2.2.2 Preparation of patient tissue for *in vitro* experiments

Patient lymphoma, reactive lymph nodes and tonsils were divided for (A) single cell suspensions and (B) for paraffin embedding.

(A) To prepare single cell suspensions, a portion of the tissue was briefly immersed in 70% ethanol and then in sterile PBS. Tissue was then placed in 70μM cell strainer which was placed over 60mm tissue culture dish with 3 ml sterile serum free RPMI (SF-RPMI). The tissue was chopped to a mush with sterile scissors then mashed through the strainer with the rubber end of a syringe plunger. The cells in single cell suspension were transferred to a 50 ml conical tube and brought up to 20 ml with SF-RPMI. Then 10ml of lymphoprep (Axis Shield) was placed into a fresh 50 ml conical tube and the cell suspension was carefully layered over the top. The tubes were centrifuged at 1400 RPM for 30 minutes without brake at room temperature in an Eppendorf bench top centrifuge. The buffy coat layer was removed into a fresh tube and topped up to 20 ml with SF-RPMI and counted as described in the previous section. Cells were then spun and resuspended to no more than $1x10^8$ cells/ml with 10% DMSO + 90% FBS. One ml of cells was added to each cryovial (Nunc) and then placed in a Mr Frosty filled with 2-propanol (Fisher). The Mr Frosty was kept in -80°C overnight to 1 week and then transferred to liquid nitrogen for long term storage.

(B) For paraffin embedding, tissue was fixed in 10% neutral buffered saline (Surgipath, Leica) for at least 48hrs. Tissue was embedded in paraffin and cut and mounted on slides by the Royal Orthopaedic Hospital Pathology Department, Birmingham.

Table 2.1 Summary of DLBCL cell lines used

Name	Cell type	Origin	Growth medium
A20*	Reticulum cell sarcoma	Spontaneous reticulum tumour from aging BALB/c mouse	RPM1 1640 + 10%FBS + 2mM L-glutamine+ 1mM HEPES, 1mM Na Pyruvate + hi L-glucose + 0.05mM 2-mercaptoethanol
BJAB	GCB-DLBCL	From inguinal tumour from 5yr female. Reclassified from Burkitt lymphoma	RPMI 1640 + 10% FBS
Farage	GCB-DLBCL	From lymph node EBV+ 70yr female	RPMI 1640 + 10% FBS
HT	GCB-DLBCL	From ascites of 70yr male	RPMI 1640 + 10% FBS
KARPAS 422	GCB-DLBCL	From a pleural effusion from 73yr female	RPMI 1640 + 20% FBS
OCI-Ly1	GCB-DLBCL	From bone marrow of 44yr male	IMDM + 20% FBS
OCI-Ly3	ABC-DLBCL	From bone marrow of 52yr male	RPMI 1640 + 10% FBS
OCI-Ly7	GCB-DLBCL	From peripheral blood of 48yr male	IMDM + 20% FBS
SUDHL4	GCB-DLBCL	From peritoneal effusion of 38yr male	RPMI 1640 + 10% FBS
SUDHL5	GCB-DLBCL	From peritoneal effusion of 17yr female	RPMI 1640 + 10% FBS
SUDHL6	GCB-DLBCL	From peritoneal effusion of 43yr male	RPMI 1640 + 10% FBS
U-2932	ABC-DLBCL	From ascites of 29yr female previously with HL	RPMI 1640 + 10% FBS

***** *Mouse lymphoma cell line*

Abbreviations: RPMI1640 – Roswell Park Memorial Institute 1640 medium; FBS – foetal bovine serum (heat inactivated); IMDM – Isocove's modified Dulbecco's medium; GCB-DLBCL – germinal centre B cell like diffuse large B cell lymphoma; ABC-DLBCL – activated B cell like diffuse large B cell lymphoma; EBV – Epstein Barr Virus; HL – Hodgkin lymphoma.

2.3 *In vitro* monocyte/macrophage experiments

2.3.1 Human monocyte isolation and macrophage polarisation

Peripheral blood monocytes were isolated from leukocyte cones. Blood was diluted with RPMI 1640 to 20 ml and layered over 10ml of lymphoprep (Axis Shield) then centrifuged at 1400rpm for 30 minutes without brake. Buffy coat layer was removed and washed in RPMI1640. Cells were counted by trypan exclusion and resuspended in 800µl of mini macs buffer (Table 2.2 for recipe). Then CD14-positive cells were isolated using Miltenyi human CD14+ magnetic beads according to manufacturer's protocol.

CD14+ cells were resuspended to $2x10^7$ cells/ml in macrophage medium (RPMI1640 + GLUTAMAX + 10% FBS all from GIBCO, Life Technologies). 0.5-1 ml of cell suspension was added to 9 cm petri dishes (uncoated) and 9 ml of macrophage medium (mac medium, see Table 2.2) supplemented with 5ng/ml human GMCSF (Peprotech) to polarise to M1 and 25 ng/ml human MCSF (Peprotech) to polarise to M2. Cells were incubated for 7-10 days with a medium change on day 5. Cells were harvested and counted using trypan blue exclusion.

Table 2.2 Recipes for buffers and reagents

Buffer	Recipe
Mini Macs Buffer	50ml 10x d-PBS (GIBCO, Life Technologies) 2ml 0.5mM EDTA pH 8.0 (Fisher) 2.5g BSA (Sigma) 38ml distilled water Heat to dissolve BSA then bring up to 500ml with distilled water and filter sterilise.
Mac Medium	500ml RPMI-1640 (GIBCO, Life Technologies) 50ml heat inactivated FBS (GIBCO, Life Technologies) 5ml 100x Glutamax (GIBCO, Life Technologies)
Citrate buffer	0.25g citric acid (Fisher) 1.26g sodium citrate (Fisher) 800ml distilled water pH to 6 Bring to 1L with distilled water
TBS-T	1.21g TRIS (Sigma Aldrich) 8.77g NaCl (Sigma Aldrich) 0.5ml Tween-20 (Thermo Scientific) 1L distilled water
PBS-T	100 tablets phosphate buffered saline (Sigma Aldrich) 10ml Tween-20 10L water

2.3.2 Flow cytometry of human monocytes and macrophages

CD14 monocytes from day of isolation and M1 and M2 polarised macrophages were analysed by flow cytometry using a panel of antibodies (Table 2.3). Cell surface staining was done with CD14 and CD206 by adding antibodies at 1:100 dilution and incubating 20 min in the dark at 4°C. The cells were then permeabilised using BD Cytofix/ Cytoperm according to manufacturer's instructions prior to adding CD163 and CD68 at 1:100 dilution for 30 min and washing and resuspending in 1% FBS/PBS. Samples were analysed on a BD LSRII flow cytometer and data analysed using BD FACS DIVA v8. BD CompBead anti-mouse (BD Biosciences) was used for single stained compensation samples.

Table 2.3 List of antibodies for flow cytometry

Antibody	Clone	Isotype	Fluorophore	Company
Mouse anti-human				
CD3	SK7	IgG1 kappa	FITC	Thermo Fisher 47-0036-42
CD10	CALLA	IgG2b kappa	FITC	Thermo Fisher 11-0106-42
CD11b	ICRF44	IgG1 kappa	PerCP-eFluor710	Thermo Fisher 46-01120-82
CD14	61D3	IgG1 kappa	FITC	Thermo Fisher 11-0149-42
CD19	H1B19	IgG1 kappa	PE-Cy7	Thermo Fisher 25-0199-42
CD20	2H7	IgG2b kappa	PerCP/cy5.5	Thermo Fisher 47-0209-41
CD31	WM-59	IgG1 kappa	PE	Thermo Fisher 12-0319-41
CD34	4H11	IgG1 kappa	APC	Thermo Fisher 17-0349-42
CD45	2D1	IgG1 kappa	Efluor-450	Thermo Fisher 48-9459-42
CD68*	Y1/82A	IgG2b kappa	PE-Texas red	Thermo Fisher 61-0689-42
CD163	GH/61	IgG1 kappa	APC	Thermo Fisher 17-1639-41
CD206*	19.2	IgG1 kappa	PE-Cy7	Thermo Fisher 25-2069-42
S1PR1	218713	IgG2b kappa	APC	R & D Systems FAB2016A
Rat anti-mouse				
B220	RA-6B2	IgG2a kappa	Pacific blue	Thermo Fisher 48-0452-80
CD3	17A2	IgG2b kappa	FITC	Thermo Fisher 11-0032-82
CD11b	M1/70	IgG2b kappa	PE-Cy7	Thermo Fisher 25-0112-82
CD19	MB19.1	IgA kappa	FITC	Thermo Fisher 11-0191-82
CD31	390	IgG2a kappa	PerCP/Cy5.5	Biolegend 102419
CD45	30-F11	IgG2b kappa	Alexa Fluor 700	Thermo Fisher 56-0451-82
F4/80	BM8	IgG2a kappa	PE	Thermo Fisher 12-4801-82
LY6 G	RB6-8C5	IgG2b kappa	PerCP/Cy5.5	Biolegend 108428

**intracellular staining*

2.3.3 ELISA for IL-10/IL-12 and Human Cytokine Array

M1 and M2 macrophages were plated at $1x10^5$ cells/well in 24-well low-attachment plates (Corning). 50ng/ml of LPS, vehicle (4% fatty-acid free BSA in PBS), 1μM S1P or 50ng/ml LPS+1μM S1P was added to appropriate wells (all from Sigma Aldrich Aldrich). The cells were incubated 18-24hrs, and then cell culture supernatant was harvested and stored in -20°C. Human IL-10 and IL-12 ELISAs (Biolegend) were performed as set out in the manufacturer's protocol with the exception that assays were plated in 96-well plates with ¼ well volumes (Corning). ELISAs were analysed on a Bio-Rad microplate reader spectrophotometer at wavelength 495nm and analysed using GraphPad Prism v8 software.

Thirty-five cytokines were also examined in the M1 and M2 macrophage conditioned medium from day 7 cultures. Proteome Profiler Human Cytokine array kit (ARY005B) from R&D Systems was used according to manufacturer's instructions. ChemiDoc MP imaging system (BioRad) was used to acquire images until saturation of the positive controls were reached. The images were analysed using ImageLab software v4.1.

2.4 Xenograft/syngeneic grafts of DLBCL

2.4.1 Application of NC3Rs and experimental design

All experiments involving animals for this thesis were done according to ARRIVE (Animal Research: Reporting of *In Vivo* Experiments) guidelines

published by the National Centre for the Replacement Refinement & Reduction of Animals in Research (NC3Rs) (Kilkenny et al., 2010). The Experimental Design Assistant (EDA) was available on-line at https://www.nc3rs.org.uk/experimental-design-assistant-eda which was used to design and determine sample sizes for each experiment. A power calculation at 80% power with 95% confidence was used to determine sample sizes.

2.4.2 Measuring tumours and calculating tumour volume

Once tumours were palpable, measurements were recorded at least 2x/week. Tumours were measured in two-dimensions (width and length) using calipers in millimetres (mm). Tumour volumes were calculated using the formula (Blumenthal, 2005):

$$tumour\ volume\ mm^3 = ((width)^2\ x\ (length))\ /\ 2$$

where width was considered the smaller of the two measurements.

For treatment experiments, tumour volumes at initiation of treatment was considered initial tumour volume. Tumour volumes at experimental endpoint was considered final tumour volume. The change in tumour volume for each mouse was calculated using the formula:

$$\Delta\ tumour\ volume\ (mm^3) = tumour\ volume_{\ final} - tumour\ volume_{\ initial}$$

and to calculate the % change in tumour volume the following formula was used:

$$\% \Delta \text{ in tumour volume} = (\Delta \text{ tumour volume} / \text{ tumour volume}_{initial}) / \times 100$$

As described in Chemosensitivity edited by Blumenthal and in accordance with the guidance written by Jackson Laboratory (Blumenthal, 2005, *Measuring treatment response in Patient Derived Xenograft (PDX) models at The Jackson Laboratory*, 2017).

2.4.3 Syngeneic A20 model

A20 cells were injected at $3x10^6$ cells/mouse in the tail vein or subcutaneously in the flank of BALB/c mice (female 6-9 weeks old, Charles River). A20 injected mice were monitored for engraftment using calipers to measure tumours. Intravenously injected mice are monitored by palpation of the abdomen to assess for enlarged spleen or liver. Mice were culled by Schedule 1 at experimental endpoint or at humane endpoints i.e. maximum tumour size 1.1cm or >18% weight loss.

2.4.4 Xenografts using DLBCL cell lines

OCI-Ly1, OCI-Ly3, and SUDHL6 were used for *in vivo* experiments. A total of $3x10^6$ cells/mouse was injected subcutaneously in the flank of NSG (female 6-8weeks, Charles River) mice. Mice were monitored for engraftment by palpation of flank and when tumours were palpable, calipers were used to measure tumours. Mice were culled by Schedule 1 at the experimental endpoint or at humane endpoints i.e. maximum tumour size 1.1cm or >18% weight loss.

2.4.5 Preparation of stock compounds used *in vivo* for treatments

Compounds and vehicles used for *in vivo* experiments are summarised in Table 2.4. The stock concentration of vincristine (Sigma) was 10mg/ml in water for injection and stored in aliquots in -20°C. Stock doxorubicin (Sigma) was diluted to 5mg/ml in water for injection and stored in aliquots in -20°C. BAF312 (siponimod, SelleckChem) was diluted to 100mg/ml in DMSO-Hybrimax (Sigma-Aldrich) to a milky white consistency and stored in aliquots at -20°C. BAF312 was further diluted for oral administration in vehicle; 10% 2-Hydroxypropyl-ß-cyclodextrin (Cayman Chemicals) in sterile distilled water.

2.4.6 *In vivo* efficacy experiments and statistical analysis

For the A20 model injected SC in the flank, solid tumours appeared around day 7-10. IV injected mice were randomised and treated on day 4 and culled on day 30 as previously determined by an engraftment pilot study. For the DLBCL cell line model, solid tumours appeared on day 14-21 post injection then randomised. For all experiments, mice were randomised into treatment groups using a random number generator from GraphPad QuickCalcs free website (https://www.graphpad.com/quickcalcs/). Mice with subcutaneous tumours were randomised when 75% of experimental mice had measurable tumours. After randomisation, the average initial tumour volumes for each group was calculated. Then using a method of stratified randomisation, each group was allocated an even distribution of the large, medium, and small tumour volumes. Using student's t-test, the p-values for the comparison of the

average tumour volumes for each group on the initial day of treatment was as close to 1 as possible and therefore, as equal as possible.

Treatments used *in vivo* are as follows:

The maximum tolerated dose of vincristine in mice is 1mg/kg IV once a week and for doxorubicin 5mg/kg IP twice a week (both Sigma-Aldrich) in vehicle, water for injection, confirmed in previous pilot experiments and in accordance with published work (Thompson et al., 1999, Mayer et al., 1990). Combination treatments *in vivo* were given by the following schedule and dose: single dose of vincristine at 0.5 mg/kg IV and 24hrs later rituximab 1mg/kg (MabThera, Roche) was given IV twice a week. These doses were confirmed in previous pilot experiments. BAF312 (siponimod, Selleck Chem) at 3mg/kg oral gavage was given three times a week as a single agent in accordance with published work (Gergely et al., 2012). See table 2.4 for treatment dosing and schedule. Blinding was employed at analysis stage where samples are coded during processing for flow cytometry, IHC, and further *ex vivo* analyses.

From previous work, I have found the *in vitro* IC50 does not correlate with *in vivo* efficacy. This may be due to the complex mechanisms of action of some drugs *in vivo* as well as the ability of the mouse to clear and metabolise the drug. For *in vivo* efficacy experiments, I would begin with 5 to 10 times the *in vitro* IC50 using the appropriate route of administration and scaling up dose as required. All doses are first tested by performing a dose escalation study to ensure that doses, schedule and route of administration we aim to use

in order to monitor any adverse effects or safety issues. Initial dosing schedule is based on pharmacokinetic data obtained from collaborator or drug manufacturer. Pilot studies were then performed to determine efficacy of tolerated/safe doses from the dose escalation studies.

Pilot studies to evaluate *in vivo* growth kinetics were completed in order to determine the appropriate window for treatment. These pilot studies also allowed us to estimate the standard deviation of tumour engraftment of future experiments. Using this estimated standard deviation, I then used the UCSF Sample Size calculator (http://www.sample-size.net/) or EDA from the NC3Rs to calculate the appropriate sample size at 80% power to detect a difference of ≥ 20% with 95% confidence.

Table 2.4 Drugs used for *in vitro* and *in vivo* experiments

DRUG	Vehicle	Company and catalogue #	Dose and schedule
BAF312 (siponimod)	0.1% DMSO in 10% HP-β-CD/PBS	Selleck Chem S7179	3mg/kg PO 3x/week
doxorubicin (hydroxydaunorubicin)	water for injection	Sigma-Aldrich D1515	5mg/kg IP 2x/week
human IgG isotype	water for injection	Invitrogen 02-7102	1mg/kg IV 3x/week
rituximab (MabThera)	ready to use	ROCHE IV infusion	1mg/kg IV 3x/week
vincristine (oncovin)	water for injection	Sigma-Aldrich V8879	1mg/kg IV once a week
	Vehicle	**Company and catalogue #**	
	2-hydroxypropyl-β-cyclodextrin	Cayman Chemicals 16169	
	water for injection	Norbrook 02000/4122	

Abbreviations: PBS – phosphate buffered saline; DMSO – dimethyl sulfoxide; PO – oral gavage; HP-β-CD – 2-hydroxypropyl-β-cyclodextrin; IP – intraperitoneal; IV – intravenous.

2.5 IC50 determination

Appropriate seeding density for each cell line was calculated by using doubling time information from ATCC and DSMZ websites such that the maximum density would be reached in 96hrs: A20 ($1x10^5$ cells/ml); OCI-Ly1 ($1x10^6$ cells/ml); OCI-Ly3 and SUDHL6 ($2.5x10^5$ cells/ml). Cells were then plated at this seeding density into 96-well white bottom plates (Corning) in 80µl per well with complete medium. Then compounds were serially diluted into 8 concentrations including a vehicle treatment and no cell controls at 5x the final concentration. Appropriate vehicle or drug concentrations were added in 1:5 dilution (20µl per well) in sextuplicate treatments to the 80µl of cells for a total volume of 100µl. The perimeter wells of the 96-well plate were filled with PBS to prevent evaporation and edge effects from incubation. Plates were incubated at 37°C for 96hrs and then Cell Titre Glo solution from Promega was prepared and added to wells according to manufacturer's instructions. Plates were analysed on a VICTOR plate reader to measure luminosity. Percent death of treated samples compared to control was calculated and the IC50 determined using GraphPad Prism v8 software.

2.6 Sphingosine-1-phosphate for *in vitro* use

2.6.1 Preparation of sphingosine-1-phosphate stock solution

A 95:5 ratio of methanol (Sigma Aldrich 676780) to diH_2O solution was prepared. The methanol: water solution was filtered through a 0.22µM syringe filter before 2 ml was added to vial of 1 mg of sphingosine-1-phosphate (S9666,

Sigma Aldrich) for a final concentration of 0.5mg/ml. To dissolve S1P, the vial was gently vortexed and then heated to approximately 65°C in a water bath for 10 minutes. After incubation, the glass vial was placed in an ultrasonic water bath briefly until fully dissolved. Low retention pipette tips (Corning) were used when pipetting S1P for all experiments. The stock of dissolved S1P was stored in -20°C for up to 1 year.

To prepare S1P for experimental use, 50µl of stock S1P was aliquoted into glass vials and allowed to evaporate in a biosafety cabinet for 3hrs or until a dried film was observed. Dried aliquots of S1P were stored in -20°C for up to 1 year. To prepare working concentration of 125 µM S1P, 520µl of sterile 4mg/ml fatty-acid free BSA (Sigma Aldrich) was added to the vial and incubated for 20 minutes at room temperature on a rolling platform. The S1P: BSA solution was never vortexed as this caused bubbles resulting in lost volume. Diluted S1P: BSA was stored in -20°C for up to 3 months.

2.6.2 Neutralising sphingosine-1-phosphate with Sphingomab

Sphingomab LT002 (12.1 mg/ml) and isotype control LT0015 (12.7mg/ml) (gift from Roger Sabaddini) were stored at -20°C. 1µM S1P was neutralised with 1µg/ml of Sphingomab or incubated with isotype control for 1 hr at 37°C according to communication from Dr Sabaddini.

2.7 Preparation of DLBCL cell line conditioned medium

To prepare conditioned medium from DLBCL cell lines, cells were diluted to $1x10^6$ cells/ml in fresh complete medium. Cells were incubated 24hrs in a humidified incubator set to 37°C and 5% CO_2. After 24hrs, the conditioned medium was collected, centrifuged at 1500 RPM for 5 minutes, filtered through a 0.22μM syringe filter and used immediately or stored at -20°C.

2.8 *In vitro* migration assay

Migration assays were performed in 24-well plates low-attachment plates (Corning) with 3 μM pore size cell culture inserts with high density PET membrane (Corning 353492). M1 and M2 macrophages were harvested and suspended to $1x10^6$ cells/ml in complete mac medium. To the bottom of the 24-well plate, 600 μl of conditioned medium was added then the cell culture insert was placed into the well. Into the cell culture insert, 100 μl of M1 and M2 cell suspension was added then incubated for 4 hrs at 37°C. Migrated cells were harvested into 5 ml Falcon polystyrene round-bottom tubes (Corning 352052) and washed with 1 ml PBS. After centrifugation at 1500 RPM for 3 minutes, the supernatant was aspirated and the cells were resuspended in 300 μl of PBS then counted using BD LSRII flow cytometer. Acquisition was set to 40 seconds per sample. The volume of sample taken up by the flow cytometer within 40 seconds was calculated by measuring the remaining volume. This was used to calculate events (cells) per μL.

2.9 Phagocytosis assay

2.9.1 Phagocytosis assay with FITC + latex beads

M1 and M2 macrophages were stained with eFluor450 dye (Thermofisher) according to manufacturer's instructions. Then macrophages were washed and then pre-treated with 1μM S1P or vehicle for 1 hr at 37°C in 1% FBS-mac medium. After pre-treatment, M1 and M2 macrophages were divided into the appropriate number of tubes at $1x10^5$ cells/100 μl per tube. FITC positive rabbit IgG coated latex beads (Cayman Chemical) were spiked into each tube in a 1:100 dilution of and incubated for a further 1.5hrs at 37°C. The protocol was followed according to the manufacturer's instructions. Diluted trypan blue included with the kit was added to quench signal from un-engulfed FITC+ beads. Then samples were kept cold during washes with assay buffer until analysis with the BD LSRII flow cytometer. BD FACs DIVA v8, EXCEL v10, and Graph Pad Prism v8 were used for analysis of phagocytosis. Student's t-test was used to calculate p-values.

2.9.2 Phagocytosis assay with DLBCL cell lines

Dead cells from DLBCL cell line cultures were removed by lymphoprep (Axis Shield) the day before phagocytosis assay. On the day of the assay, DLBCL cell lines and macrophages were harvested and counted. M1 and M2 macrophages were stained with CFSE cell tracking dye (Becton Dickinson) and DLBCL cell lines were stained with eFluor-450 cell tracking dye (eBioscience, Thermo Fisher) according to manufacturer's instructions. Then CFSE-positive

macrophages were resuspended to $1x10^6$ cells/ml in 1% FBS-mac medium and pre-treated with vehicle or 1μM S1P for 1 hr at 37°C. EFluor-450 positive DLBCL cell lines were resuspended to $1x10^6$ cells/ml in 1% FBS-RPMI1640 and pre-treated with isotype control (human IgG, Thermo Fisher), rituximab 10 μg/ml or ofatumumab 10 μg/ml, an alternative anti-CD20 monoclonal antibody (gift from Professor Stankovic) for 2-4hr at 37°C.

Pre-treated DLBCL and M1 or M2 macrophages were then co-cultured by adding 100 μl of each into polystyrene round bottom FACs tubes or 8-well chamber slides at 37°C for 1.5hrs in the following combinations: single, vehicle + isotype, vehicle + rituximab, S1P + isotype (IgG, Invitrogen), and S1P + rituximab or ofatumumab (both at 10μg/ml). Each sample was then washed in cold 0.9% NaCl + 0.1% EDTA and then resuspended in cold PBS. Samples were then analysed on BD LSRII for CFSE positive / eFluor 450 positive cells. At least 10,000 events were acquired and the total number of cells phagocytosed was calculated by total FITC+ macs/all macs counted. Analysis was done using BD FACS DIVA v8, EXCEL v10, and Graph Pad v8 and student's t-test was used to calculate p-values. Stained CFSE macrophages +/- S1P with stained eFluor45 DLBCL cell lines were plated in triplicate on 8-well chamber slides. After 1.5hr incubation, slides were fixed in formal saline for 30 minutes, dried, then stained with DAPI and mounted with Prolong Gold.

2.10 Annexin V/PI assay

DLBCL cell lines were plated at $1x10^6$ / ml and treated with vehicle or drug at various concentrations for 24 hrs. Samples were harvested and stained using BD Annexin V FITC kit I (Becton Dickinson) according to manufacturer's instructions. Samples were analysed on BD LSRII flow cytometer and BD FACS Diva 8 software within 1hr of addition of Annexin V/PI.

2.11 Protein extraction and determination of concentration

Cell pellets were lysed using 1x RIPA buffer (Cell Signaling) + 1µM PMSF (Sigma Aldrich) and passed through 19G syringe (Terumo). For lysates to be used to examine phosphorylated proteins, 1mM sodium orthovanadate (SOV) in PBS was added to cell pellets before lysing in RIPA buffer. Lysates were centrifuged at 4°C max speed for 10 min and placed into fresh protease free microfuge tubes. Lysates were stored long term at -80°C.

Concentration of protein was determined using protein assay reagent (BioRad) according to manufacturer's instructions. Stock 1mg/ml of bovine serum albumin (BSA, Sigma Aldrich) was used to prepare serial dilutions at 0, 0.1, 0.2, 0.3, 0.4, 0.5 mg/ml for standard curve. BSA standards and proteins of unknown concentration (neat or diluted 1:10) was loaded in triplicate in 96 well flat bottom plate. A 1:5 dilution of BioRad protein assay reagent in water was prepared immediately prior to adding 200µl to each well. A BioRad

microplate reader was used to measure absorbance at 595nm. Plotting of standard curve and interpolation of unknowns were done using GraphPad Prism v8 software.

2.12 Western blot analysis

Protein previously isolated was diluted with 2x Laemmli Sample Buffer (BioRad) to the same concentration in all samples (usually 50 µg). Samples were boiled at 95°C for 10 minutes and then immediately loaded into pre-cast 10% SDS-page gel (BioRad). Gels were run in 1x tris-glycine running buffer (Geneflow, Ltd.) at 120v for 1.5-2hr.

Proteins were transferred from gel onto nitrocellulose membrane (Bio Rad) using ready to use Trans-Blot Turbo Mini transfer packs along with the Trans-Blot Turbo Transfer System from Bio Rad at 25V for 7 min.

After transfer, membranes were incubated in blocking solution: 5% BSA in TBST-T or in 5% non-fat dried milk powder in TBST-T for 1hr to overnight. Primary antibody diluted to appropriate concentration in blocking solution was added to membranes and incubated on rocking platform overnight at 4°C. The next day, the membranes were washed with TBS-T on rocking platform. The TBS-T was changed every 10 minutes 3x. Secondary antibody in appropriate species conjugated to horse radish peroxidase (HRP, DAKO) was diluted in blocking solution. Membranes were incubated in diluted secondary antibody for 1hr at room temperature. Membranes were then washed 3x in TBS-T for 10 minutes each.

Membranes were then incubated with enhanced chemiluminescence (ECL) reagent mixture (Amersham) for 1 minute and then immediately imaged using ChemiDoc MP imaging system (BioRad). The images were analysed using the ImageLab software v4.1.

Membranes were then stripped with 1x mild stripping solution (Millipore) according to manufacturer's instructions then blocked and probed with appropriate house-keeping antibody conjugated to HRP (Cell Signaling) for 30 minutes at room temperature. No secondary was required. After 3x washing with TBS-T at 10 minutes each, the membrane was then incubated with ECL and analysed as described above.

2.13 RNA extraction and cDNA synthesis

At least $5x10^5$ cells was pelleted and RNA was isolated using Qiagen Micro/Mini RNEASY kit according to manufacturer's protocol. RNA concentration was determined using nanodrop (Thermo Fisher) and then stored at -80°C prior to cDNA synthesis. To prepare cDNA, 400ng or 200ng of RNA was added to rnase/dnase free PCR tubes along with 4µL Quanta Supermix and nuclease-free water to a total volume of 20µL. Tubes were placed in PCR machine with following program; 25°C, 5 min; 42°C, 30min; 85°C, 5 min; then 4°C, until the cDNA could be stored at -20°C.

2.14 Quantitative PCR (Real-Time PCR)

Quantitative PCR analysis for S1PR1, S1PR2, S1PR3, S1PR4, S1PR5, SPHK1, and SGPP1 (Thermo Fisher) was performed with cDNA diluted 1:10 or 1:20 in water (Table 2.5)(Vockerodt et al., 2019). GAPDH from Cell Signaling was used as housekeeping gene and diluted as for all probes. Fast Start qPCR mix from R&D Systems was used according to manufacturer's protocol and added to master mix. Probes were used in 1:20 dilution for a total volume of 20 µl. The samples, probes, and qPCR mix are added into 96 well PCR plate including a water control and centrifuged briefly. Plate was placed in ABI 7500 qPCR machine using standard protocol. Data was analysed using the $2^{-\Delta\Delta CT}$ method (*Guide to Performing Relative Quantitation of Gene Expression Using Real-Time Quantitative PCR*, 2004) and compared with controls (i.e. normal B cells, unpolarised monocytes, or untreated cells) for relative expression of genes.

Table 2.5 List of qPCR probes

Gene	ABI assay number	Dye
SPHK1	Hs00184211_m1	FAM
S1PR1	Hs00173499_m1	FAM
S1PR2	Custom assay 5' primer: GTGCTAGGCGTCTTTATCGTC 3' primer: GTAGTGGGCTTTGTAGAGGATC Probe: AGGAGTGGACGGGACAGGCATA	FAM
S1PR3	Hs01019574_m1	FAM
S1PR4	Hs02330084_s1	FAM
S1PR5	Hs00924881_m1	FAM
SGPP1	Hs00229266_m1	FAM
GAPDH	Hs99999905_m1	VIC TAMRA

2.15 RNAscope© fluorescent- *in situ* hybridisation

FFPE (formalin fixed paraffin embedded) samples were incubated in a 60°C oven for 1hr to overnight. Slides were then processed according to RNAscope© Multiplex Fluorescent Assay kit version 2 protocol with the following changes: slides were incubated in boiling antigen retrieval buffer for 20 minutes and incubated with protease plus at 40°C in hybridisation oven for 15 minutes. SPHK1 and IL-10 probes from ACD Bio were used along with Perkin Elmer TSA dye cy3. For multiplex staining by fluorescent-IHC, prior to DAPI step, samples were boiled in citrate buffer pH 6 for 15 minutes on low

and then blocked for 30 minutes with Tris-NaCl blocking buffer (TNB buffer, Perkin Elmer). Primary antibodies were used at the concentrations as shown in Table 2.6. Then stained as for fluorescent-IHC in section 2.17.

2.16 Immunohistochemistry (IHC) and fluorescent-IHC

FFPE sections were mounted on frost free slides by The Royal Orthopaedic Hospital Histology Department. Slides deparaffinised in Histoclear II and IMS (industrial methylated spirits, Fisher) for 10 minutes each.

Following rinse with tap water, exogenous peroxidases were blocked in 0.3% H_2O_2 (Sigma) followed by another rinse in tap water. Citrate buffer was prepared to pH6 and boiled for 10 minutes in microwave. For antigen retrieval, slides were slowly submerged and further heated for 10 minutes on medium power and then 10 minutes on low power. Slides were cooled and a hydrophobic pen used to draw around tissue and then washed in with tris buffered saline with 0.1% tween-20 (TBS-T). Tris-NaCl blocking buffer (TNB) from Perkin Elmer was prepared according to manufacturer's instructions. Slides were blocked in TNB buffer for 30 minutes and then primary antibody diluted in TNB was added for 1hr room temperature or overnight at 4°C (Table 2.6). Primary antibody was then removed and slides washed TBS-T before addition of appropriate secondary antibody either biotinylated or with HRP for 30 minutes (Table 2.6). If biotinylated secondary used, then AVIDIN-D HRP (Vector Labs) was added for a further 30 minutes. DAB HRP (Vector Labs, 3,3'

diaminobenzidine peroxidase substrate kit) was added to each slide for 3-5 minutes and then washed with TBS-T and counter-stained in Mayer's haematoxylin for 5 minutes. Slides were then rinsed in water before mounting with Omnimount (Sigma Aldrich).

For fluorescent IHC, the protocol remained the same as above with the following exceptions: xylene and ethanol were used in place of Histoclear II and IMS for de-paraffinization; after secondary antibody- HRP or biotinylated secondary plus AVIDIN-D HRP, the sections were then incubated with fluorescent dye diluted with assay diluent from Perkin Elmer for 10 minutes; slides were then heated in boiling citrate buffer pH6 for 15 minutes on low; DAPI was added for 5 minutes and then mounted using Prolong Gold (Invitrogen).

Table 2.6 List of antibodies/probes for western, IHC and RNAscope

Antibody	Clone	Host and target specificity	Company and product #	Dilution
β2-M	D8P1H	Human Rabbit IgG HRP conjugated	Cell Signaling 128515	1:1000
CD79a	JCB117	mouse anti-human	Leica PA0599	RTU
CD163	10D6	mouse anti-human	Leica CD163-L-CE	1:200
CD68	PG-M1	mouse anti-human	Dako M087601-2	1:1000
CD11b	M1/70.15	rat anti-mouse	Invitrogen MA1-80091	1:400
cPARP	D64E10	rabbit anti-human	Cell Signaling 5625S	1:50
F4/80	CI:A3-1	rat anti-mouse	BioRad MCA497GA	1:200
S1PR1	H-60	rabbit anti-human	Santa Cruz SC-25489	1:50
S1PR2	6E8.1	rabbit anti-human	Merck MABC96	1:50
Hs-SPHK1	n/a	Human probe (C1)	ACD Bio 416041	RTU
pSPHK1 (Ser225)	12639	rabbit anti-mouse	LSBio C26925	1:1000
tSPHK1	D1H1L	rabbit anti-human	Cell Signaling 12071S	1:000

RTU – ready to use.

2.17 Cytospin of cell lines for immunohistochemistry

Cells were washed in PBS and re-suspended to $2x10^6$ cells/ml. Adhesive frost-free slides (Leica) was placed into Cytospin centrifuge (Thermo Fisher) according to manufacturer's instructions and 100-200 µl of cell suspension was added to Shandon funnel. Slides were centrifuged at 1000 RPM for 5 minutes and then fixed in 10% Neutral Buffered Formalin (10% NBF, Sigma Aldrich) for 5 minutes before storing in -20°C. For IHC of cytospins, de-paraffinisation with Histoclear II was not required. Instead, cytospins were immediately placed in 100% IMS and stained as described for normal IHC.

2.18 Gene expression analysis

Reanalysis of published datasets were performed by Dr Robert Hollows (University of Birmingham). RNAseq data for N=32 ABC-DLBCL and N=54 GCB-DLBCL was downloaded with permission from NCBI dbGaP (Data Base of Genotypes and Phenotypes)at http://www.ncbi.nlm.nih.gov/gap with accession code phs000532.v5p2 (Morin et al., 2013). The dataset for the normal GC-DLBCL (GSE45982) was downloaded from the NCBI Gene Expression Omnibus data repository (http://www.ncbi.nlm.nih.gov/geo) (Beguelin et al., 2013) .

Using Rsubread aligner, Dr Hollows, aligned sequence reads to hg19 reference sequence in order to map the sequencing reads to individual genes with the featureCounts function (Robinson et al., 2010). In order to express gene expression as counts-per-million (CPM), the data was first normalised

using the trimmed mean of M values or TMM method then using edgeR package found in Bioconductor was converted to CPM (Anders et al., 2013). Genes were considered to be differentially expressed between normal vs DLBCL if the $p<0.05$ adjusted for multiple comparisons and there was a fold change of <1.5 (Vockerodt et al., 2019).

2.19 Measurement of S1P in DLBCL cell lines

DLBCL cell lines were prepared by Dr Kate Vrzalikova and S1P was quantified by Professor Sarah Spiegel (University of Virginia, USA) using liquid chromatography-electrospray ionisation-tandem mass spectrometry as previously described (Hait et al., 2009). For measurement of S1P in cell lysates, DLBCL cell lines were counted, washed and snap frozen in liquid nitrogen. For measurement of S1P in conditioned medium, $1x10^6$ SUDHL4 cells/ml were plated in fresh serum free and phenol red free RPMI 1640 (Invitrogen). Conditioned medium was collected at 2 minutes, 5 minutes, 10 minutes and 15 minutes. Cells were centrifuged at 4°C for 10 minutes at 1000RPM and conditioned medium was collected and kept on ice. Samples were then sent to Professor Spiegel for analysis.

2.20 Gene Set enrichment analysis

Gene set enrichment analysis of genes positively correlated with SPHK1 using Gene Ontology (GO) Enrichment Analysis Tool / PANTHER classification system from the Gene Ontology Consortium at http://geneontology.org and http://pantherdb.org (The Gene Ontology, 2017,

Ashburner et al., 2000, Mi et al., 2019a, Mi et al., 2019b) All gene names were converted to standard nomenclature using HGNC (HUGO Genome Nomenclature Committee at https://www.genenames.org/cgi-bin/symbol_checker. Genes were loaded on to GO enrichment analysis tool and resulting biological processes were evaluated. I then calculated p value and odds ratio using chi square method of observed vs expected. Comparisons of gene lists (i.e. genes positively correlated with SPHK1 vs macrophage gene signature) were performed using Venny 2.1 (Oliveros, 2007-2015). Genes associated with GO terms were obtained from the Gene Ontology tool.

2.21 Statistical analysis

GraphPad Prism v8 was used for statistical analysis for all experiments. The Experimental Design Assistant developed by the NC3Rs and available at https://www.nc3rs.org.uk/experimental-design-assistant-eda was used to design *in vivo* experiments. Power calculations and estimation of sample size was determined using the UCSF Sample Size calculator (http://www.sample-size.net/).

P values were calculated using student's t-test when comparing two variables (i.e. treated vs vehicle) and 2-way ANOVA was used when comparing >2 parameters (i.e. vehicle vs treatment A vs treatment B). P values were adjusted for multiple comparisons. The cut off for p value was $< .05$ and for false discovery rate (FDR, q) $< .01$.

CHAPTER 3

SPHK1 expression in DLBCL and its relationship to the expression of macrophage genes

Chapter 3

SPHK1 expression in DLBCL and its relationship to the expression of macrophage genes

3.1 Introduction

Our lab has previously investigated *SPHK1* expression in DLBCL in the context of angiogenesis (Lupino et al., 2019). Using RNAseq, an S1P-response signature in HUVECs (human umbilical vein endothelial cells) was derived. In addition, Lupino *et al* reported genes correlated with *SPHK1* expression in publicly available datasets of DLBCL overlapped significantly with a macrophage gene signature derived from five tumour types including DLBCL (Lupino, 2017).

In this chapter, the relationship between the expression of *SPHK1* and macrophage genes is explored. Specifically to 1) confirm the overexpression of *SPHK1* in primary DLBCL and DLBCL cell lines, 2) survey the biological processes enriched in the genes positively correlated with *SPHK1* using gene set enrichment analysis, and 3) use GO terms to obtain a list of genes associated with macrophage functions to compare with a set of genes differentially expressed in DBLCL.

3.2 *SPHK1* is overexpressed in DLBCL

3.2.1 Evaluating *SPHK1* in primary DLBCL

The expression of *SPHK1* was first examined in primary DLBCL. To do this, published gene expression (RNAseq) datasets were re-analysed by Dr Robert Hollows, these included RNAseq data from four normal germinal centre (GC) B cells, 54 GCB-DLBCL and 32 ABC-DLBCL (Beguelin et al., 2013, Morin et al., 2013, Lupino, 2017). This re-analysis identified a set of genes that were differentially expressed in DLBCL compared to normal GC B cells. Genes with a p value of < .05 and a fold difference of greater than +1.5 or -1.5 were used for analysis and will be referred to as the "Morin" dataset. In the Morin dataset, *SPHK1* was found to be significantly overexpressed in both ABC and GCB type DLBCL compared to normal GC B cells with the expression *SPHK1* in GCB-type tumours appeared to be higher than in ABC-type (Figure 3.1A).

RNAscope© based fluorescent *in situ* hybridisation for *SPHK1* combined with fluorescent IHC for CD79a was performed on 20 cases of primary DLBCL (9 non-GCB type and 11 GCB type) that had confirmed lesions present and three reactive tonsils as controls (Figure 3.1C-D). *SPHK1* expression was independently scored by a pathologist, Dr Matthew Pugh. Three randomly chosen high power fields (HPF; 60x) were examined for each case and a score was given across each field of view. Scoring was as follows: <1 dot per cell=0; 1-5 dots per cell=1; and >5 dots per cell =2 across the field. Average scores across

three HPF was used to calculate an *SPHK1* score (Figure 3.1B and Appendix A1). In 17/20 cases, there was a higher expression of *SPHK1* compared to tonsils. There was no significant difference between non-GCB and GCB types in this cohort.

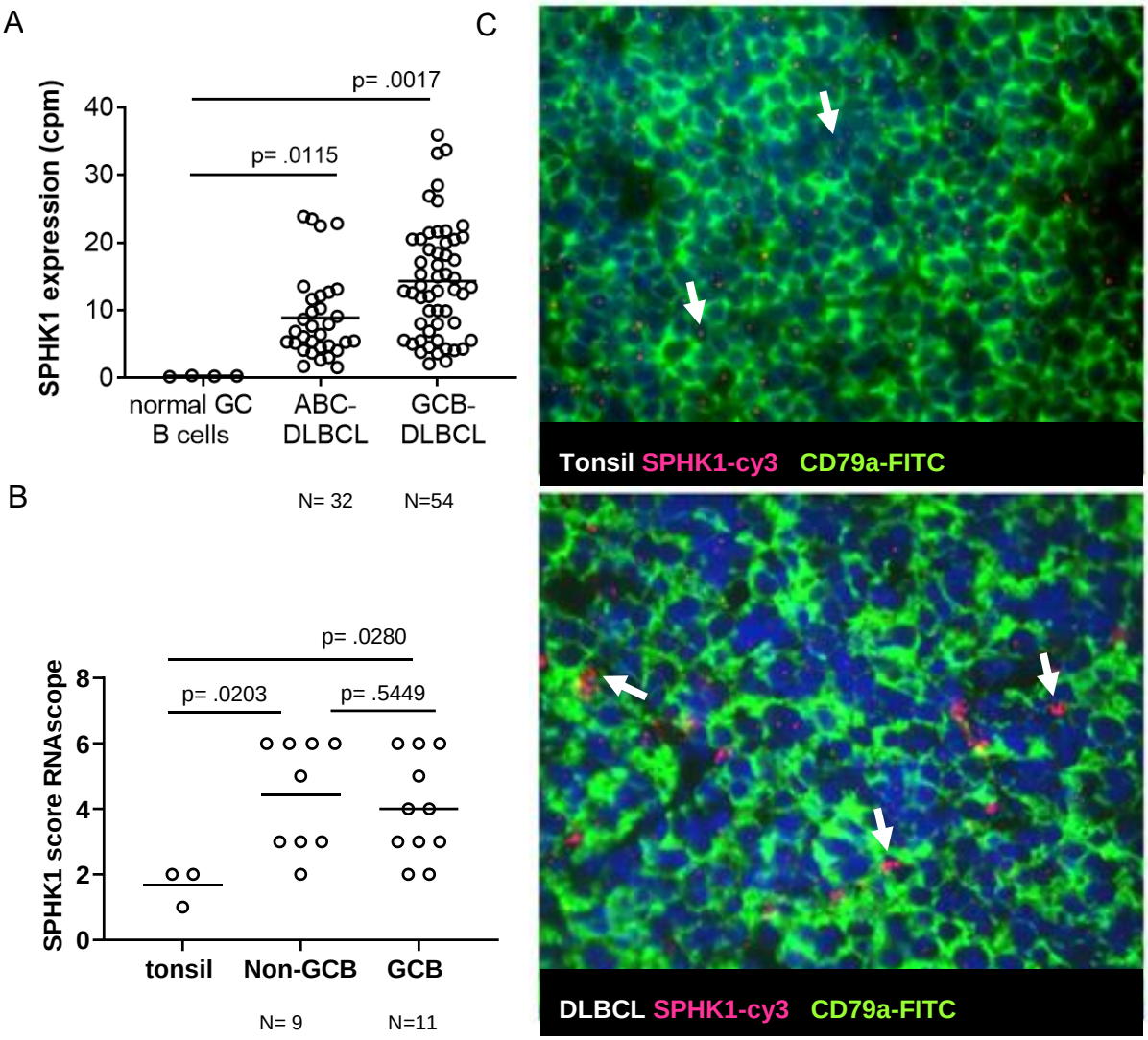

Figure 3.1 *SPHK1* is overexpressed in primary DLBCL. (A) Re-analysis of a primary dataset DLBCL (32 ABC type and 54 GCB type) shows that *SPHK1* mRNA levels were significantly higher in primary DLBCL compared to normal GC B cells (N=4). Student's t-test was performed to test for statistical significance. (B) RNAscope© fluorescent in situ hybridisation for *SPHK1* was performed on N=3 tonsils and N=20 primary DLBCL (9 non-GCB and 11 GCB). 17/20 DLBCL cells had higher SPHK1 score compared to tonsils. There was no significant difference in *SPHK1* expression between non-GCB and GCB. Student's t-test was used to test for statistical significance. Scoring for *SPHK1* expression was independently performed by pathologist, Dr Matthew Pugh. Three high power fields (60x) were assessed for each case. Each total field of view was scored per cell as: no dots =0; 1-5 dots =1; and >5 dots =2 and the average SPHK1 score of three fields was plotted for each case. (C) Representative images from tonsil and DLBCL fluorescent in situ hybridisation for SPHK1-cy3 (pink) and fluorescent IHC for CD79a-FITC (green). White arrows show SPHK1 expressing CD79a+ cells in both tonsil and DLBCL cases. White arrows indicate CD79a+ cells with *SPHK1* expression. Student's t-test was used to calculate p values.

3.2.2 DLBCL cell lines overexpress SPHK1

Cell preps/lysates from a subset of the DLBCL cell lines and conditioned medium from SUDHL4 were sent to Professor Sarah Spiegel, at the University of Virginia, to measure the concentration of S1P. These assays revealed a higher concentration of S1P in DLBCL cell lines compared with normal B cells (Figure 3.2A). Secreted S1P by SUDHL4 was measured by Professor Spiegel appearing within 2 minutes in fresh medium (Figure 3.2B).

Western blotting analysis performed by Dr Kate Vrzalikova verified the protein expression of phospho-SPHK1 and total-SPHK1 in DLBCL cell lines (Figure 3.2C). This includes ABC cell lines: OCI-Ly3 and U2932 and GCB cell lines: HT, Karpas 422, SUDHL4, SUDHL5, OCI-Ly1, OCI-Ly7, BJAB, and the EBV+ Farage cell line. In addition, western blot analysis was used to confirm the SPHK1 expression in the A20 mouse lymphoma cell line using OCI-Ly3 as a positive control (Figure 3.2D). Densitometry analysis using ImageJ software of the western blot was used to calculate the ratio of pSPHK1/tSPHK1 which shows that DLBCL cell lines express varying levels of pSPHK1 with OCI-Ly1 with the lowest relative expression (Figure 3.2E).

Next, the expression of *SPHK1* was examined in DLBCL cell lines by qPCR. These included the ABC DLBCL cell lines: OCI-Ly3 and U2932; and the GCB DLBCL cell lines: HT, SUDHL4, SUDHL5, Farage, OCI-Ly1, OCI-Ly7, and BJAB (Figure 3.2F). All cell lines except for SUDHL4 and OCI-Ly7 had an overexpression of *SPHK1* compared to normal B cells by qPCR.

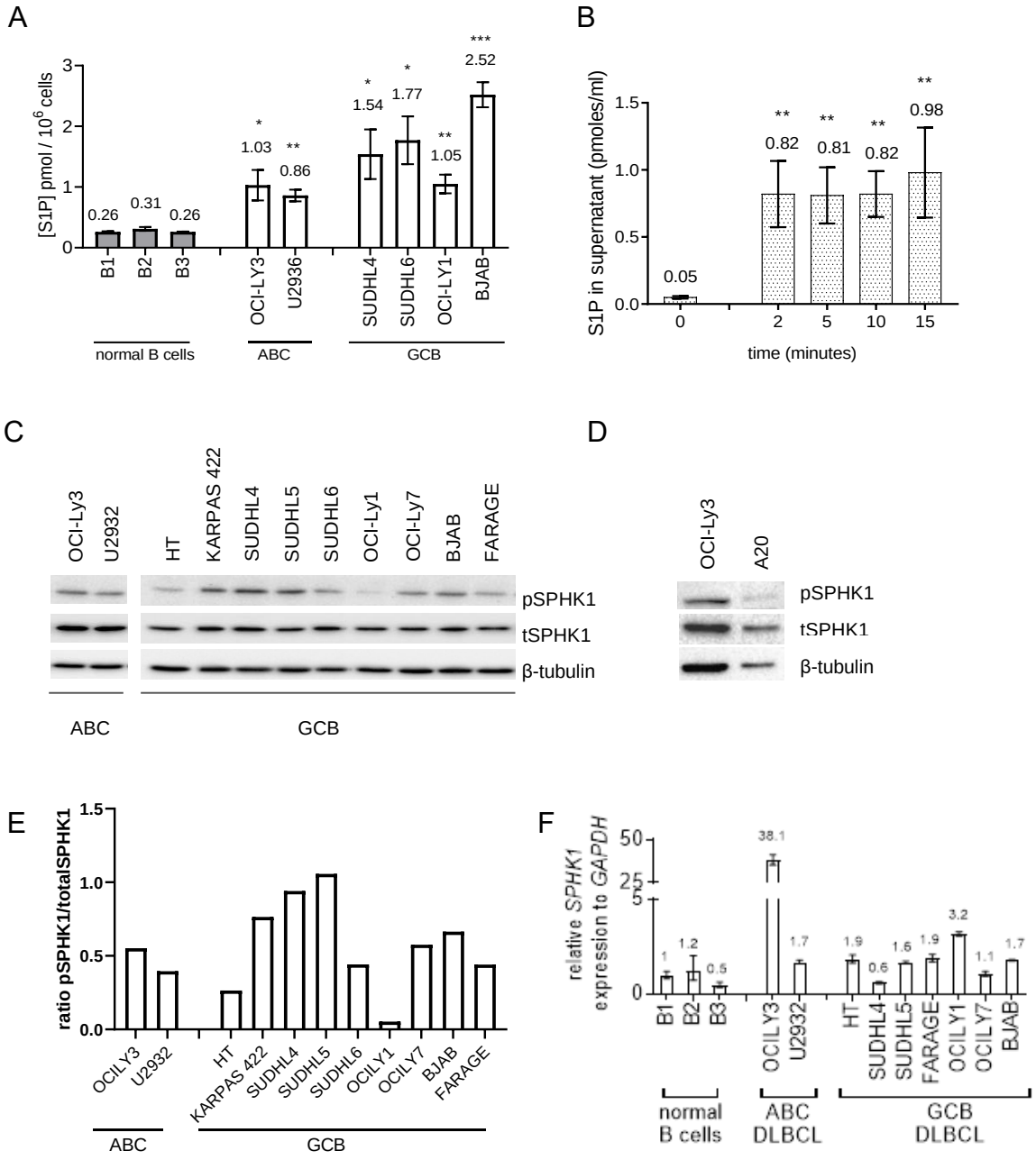

Figure 3.2 DLBCL cell lines express SPHK1 and have higher S1P concentration than B cells. (A) Lysates of DLBCL cell lines have higher levels of S1P than lysates of normal B cell. (B) The concentration of S1P secreted by SUDHL4 over time was measured at 0, 2, 5, 10, 15 min (analysis by Professor Sarah Spiegel at the University of Virginia using mass spectrometry). (C) Western blot analysis performed by Dr Kate Vrzalikova show that DLBCL cell lines express total-SPHK1 and phospho-SPHK1 proteins (D) Western blot analysis of mouse lymphoma cell line, A20, was performed and also showed expression of total and phospho-SPHK1. (E) Densitometry of western blot of the ratio of pSPHK1/tSPHK1 as determined using ImageJ. (F) DLBCL cell lines express *SPHK1* as shown by qPCR. *SPHK1* gene expression is shown relative to OCI-Ly3.

3.3 Evaluating genes correlated with *SPHK1* in DLBCL

3.3.1 *SPHK1* and macrophage genes are positively correlated in primary DLBCL

To confirm the link between *SPHK1* expression and macrophage gene expression in primary DLBCL, two gene expression datasets originally used by a previous post-doctoral researcher was reanalysed (Lupino, 2017). The first was a macrophage gene signature described by Doig *et al* who used a 3-D network analysis to derive a macrophage gene signature from primary tumours including DLBCL, breast, colorectal, glioma, ovarian and testicular tumours (Doig et al., 2013). The second gene set was provided by Professor Rueben Tooze (University of Leeds). Professor Tooze performed a gene expression meta-analysis of publicly available DLBCL datasets (Care et al., 2015), and provided a list of genes that correlated with *SPHK1*. Only genes that correlated with *SPHK1* in at least 6 of the 10 DLBCL datasets with p value < .05 by the Spearman correlation test were used.

Of the 158 genes analysed, there were 90 genes identified that were positively correlated with *SPHK1* and were also present in the macrophage gene signature (Lupino, 2017). This represented a significant enrichment of macrophage genes in the set of genes positively correlated with *SPHK1* (odds ratio (OR) = 30.29; p< .0001) (Figure 3.3A). No macrophage signature genes were negatively correlated with *SPHK1* expression (OR = 0.0; p< .0001) which indicated a significant depletion (Figure 3.3B).

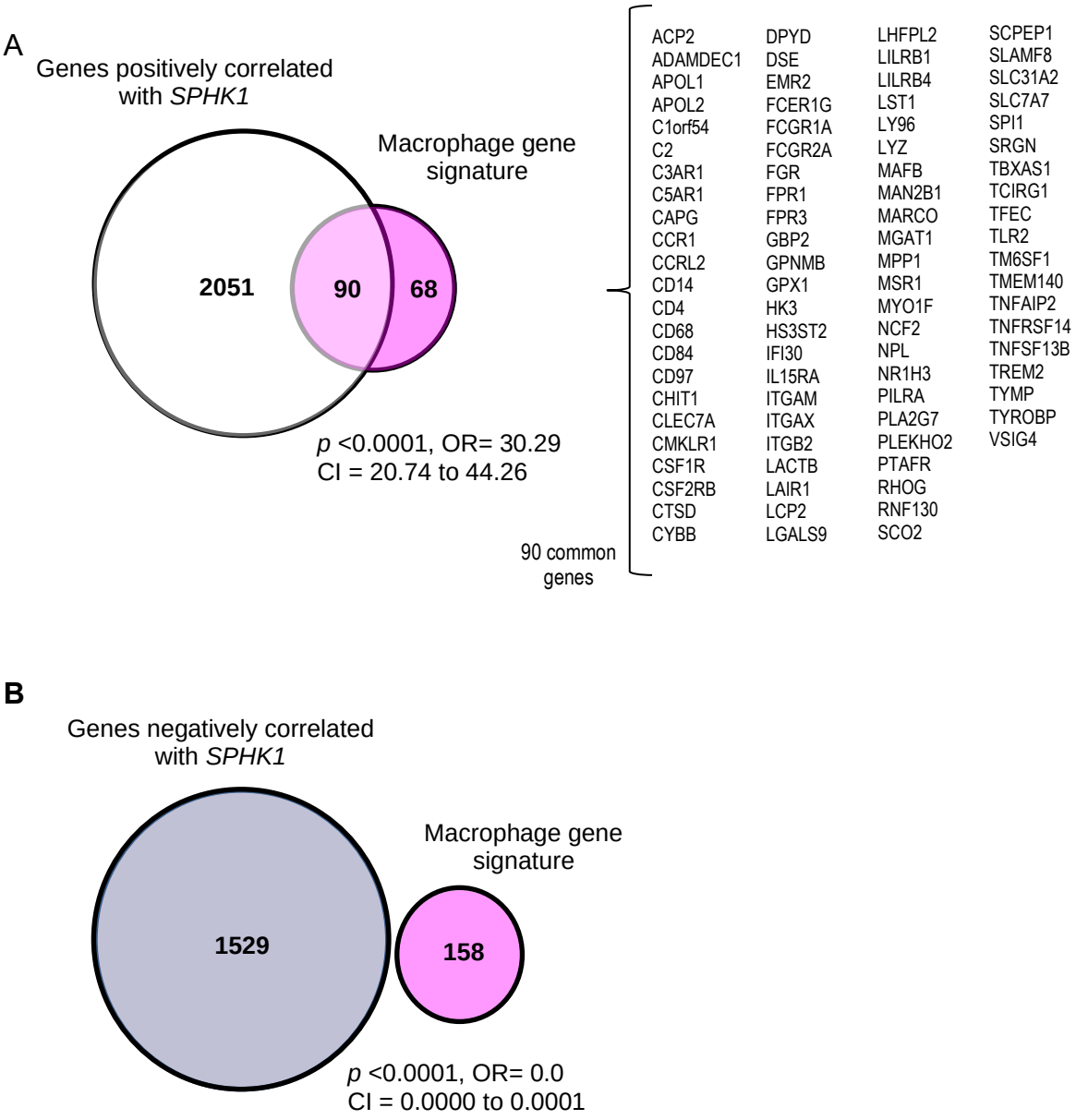

Figure 3.3 Enrichment of genes positively correlated with *SPHK1* in DLBCL among macrophage signature genes. Genes correlated with *SPHK1* expression across >5 out of 10 publicly available datasets from DLBCL patients were compared with a macrophage gene signature derived from DLBCL, breast, colorectal, glioma, ovarian and testicular tumours. The results show (A) an enrichment of macrophage genes in the gene set positively correlated with *SPHK1* and (B) a depletion in the gene set that was negatively correlated with *SPHK1*.

3.3.2 Macrophage signature genes that are also positively correlated with *SPHK1* are upregulated in DLBCL

Taking these 90 macrophage genes that were positively correlated with *SPHK1*, I next explored their differential expression using the Morin dataset of differentially expressed genes in ABC-type and GCB-type DLBCL. In the macrophage signature, there were 72/90 genes positively correlated with *SPHK1* that were also significantly upregulated in ABC-DLBCL. Only 3/90 of these genes were downregulated significantly in ABC-DLBCL. Similarly, in the Morin dataset of differentially expressed genes in GCB-DLBCL, there were 77/90 of the macrophage signature genes positively correlated with *SPHK1* that were upregulated. Only 2/90 macrophage genes were downregulated in GCB-DLBCL (Figure 3.4 A and B).

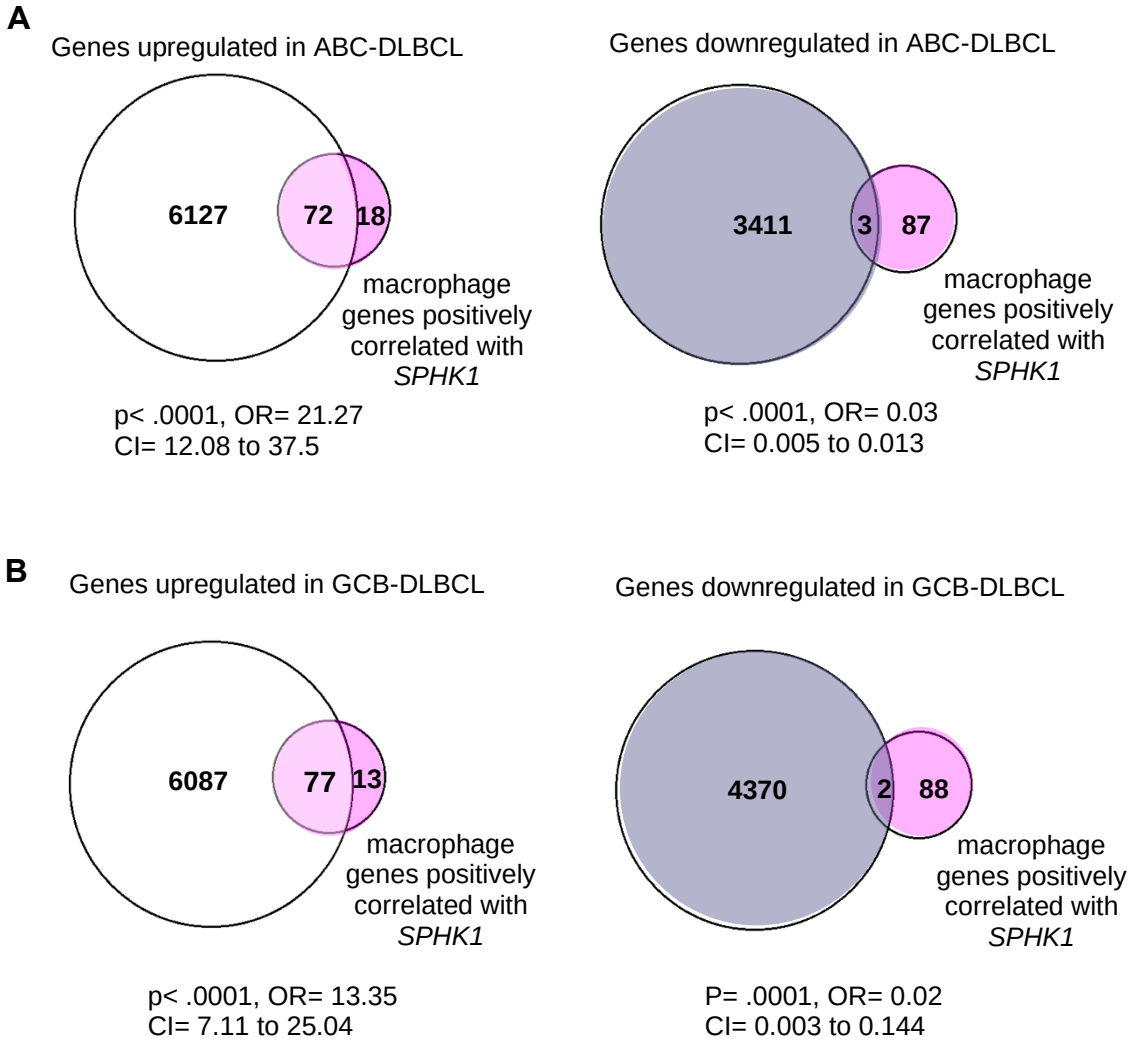

Figure 3.4 Macrophage signature genes positively correlated with *SPHK1* are enriched in genes up-regulated in primary ABC and GCB DLBCL subtypes. (A) Macrophage signature genes positively correlated with *SPHK1* were significantly enriched (72/90) among genes upregulated in primary ABC-DLBCL, but depleted (3/90) among genes downregulated in ABC-DLBCL. (B) Macrophage signature genes positively correlated with *SPHK1* were significantly enriched (77/90) among genes upregulated in GCB-DLBCL and depleted (2/90) among genes downregulated in GCB-DLBCL.

3.3.3 Gene set enrichment analysis of *SPHK1* correlated genes highlights biological processes associated with monocytes/macrophages

So far, I have shown that genes positively correlated with *SPHK1* expression in DLBCL were enriched for macrophage signature genes, and that the majority of genes in the overlap were also upregulated in both subtypes of primary DLBCL. Next, gene set enrichment analysis of genes positively correlated with *SPHK1* was performed using the GO Enrichment Analysis Tool from the Gene Ontology Consortium at http://geneontology.org (Mi et al., 2017, The Gene Ontology, 2017, Ashburner et al., 2000). This analysis revealed the expected enrichment of genes with biological activities including anti-apoptosis, vascular and endothelial cell development, and cytokine regulation, which are functions associated with S1P (Figure 3.5).

However, in keeping with the enrichment of macrophage signature genes described above, there was also an enrichment of genes with functions in the chemotaxis and migration of monocytes/ macrophages, the development and activation of macrophages as well as the regulation of endocytosis and phagocytosis (Figure 3.5). Taken together these data suggest that *SPHK1* expression in DLBCL is associated with macrophage functions.

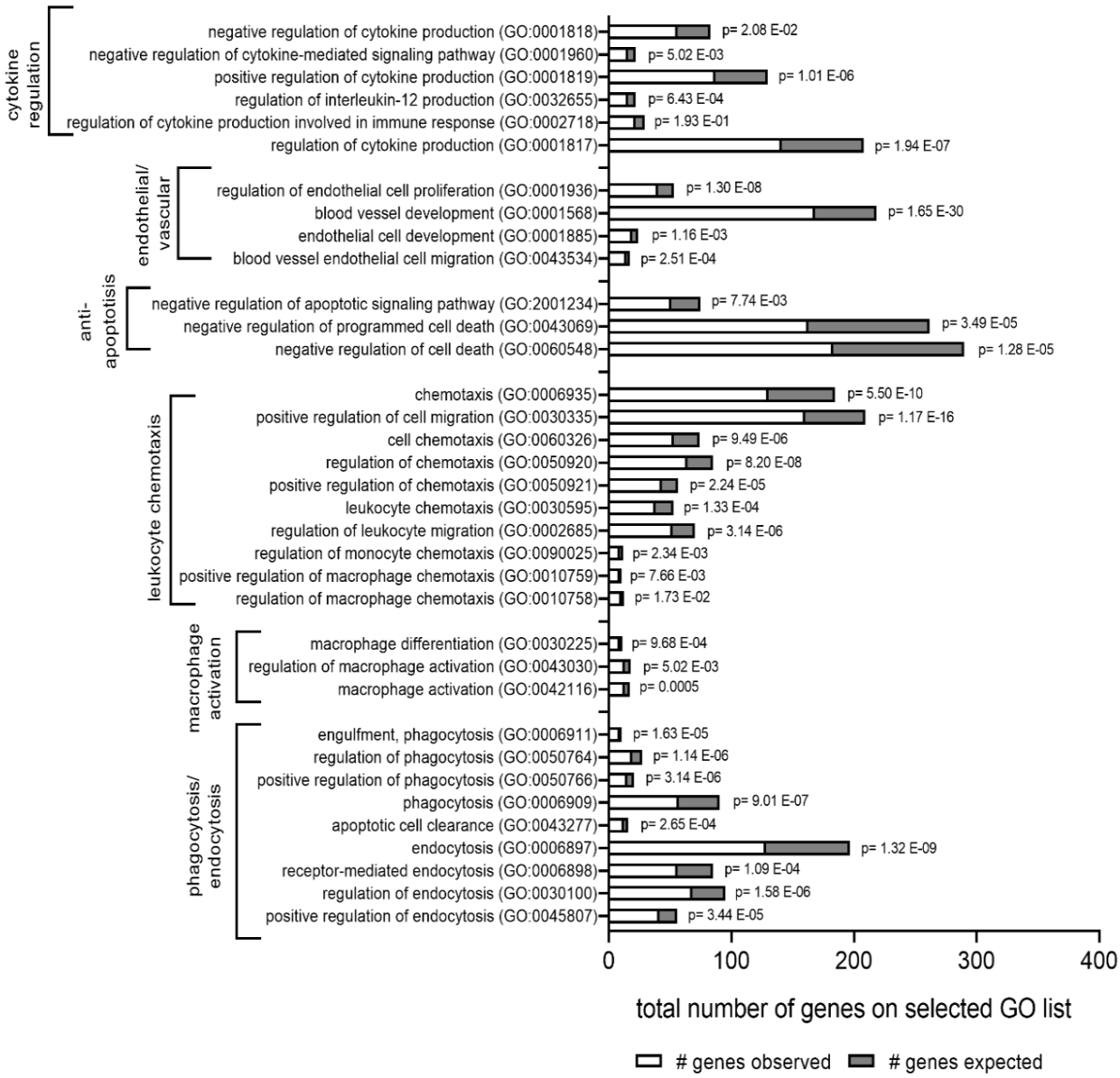

Figure 3.5 Gene set enrichment analysis of genes positively correlated with *SPHK1* in DLBCL. GO Enrichment Analysis Tool from the Gene Ontology Consortium at http://geneontology.org was used to explore the biological processes represented in the *SPHK1* correlated gene set. The gene set enrichment analysis showed an expected enrichment of genes involved in cytokine regulation, endothelial cell proliferation, blood vessel formation and anti-apoptosis genes. Gene set enrichment analysis also showed an enrichment of genes involved in macrophage activation/migration, chemotaxis and phagocytosis, providing justification for the exploration of the role S1P in monocyte/macrophage recruitment and function in DLBCL.

The recruitment of monocytes/macrophages and their function as phagocytes are relevant in DLBCL given the mechanism of action of rituximab previously described. Next, enrichment of the genes involved in the leukocyte /monocyte/ macrophage migration and phagocytosis were determined for genes positively or negatively correlated with *SPHK1*

To do this, a list of genes (N=351) classified under the GO terms leukocyte chemotaxis (GO:0030595); monocyte chemotaxis (GO:0090025); and macrophage migration (GO:0010759) was obtained. Of these genes, 93 were positively correlated with *SPHK1* which represented a significant enrichment (Table 3.1 and Figure 3.6A) and 8/351 were negatively correlated with *SPHK1* (Figure 3.6B) which represented a significant depletion. Using the Morin dataset of differentially expressed genes in ABC and GCB DLBCL, there were 86/93 of the *SPHK1* correlated migration genes were also upregulated in GCB-DLBCL and 69/93 were upregulated in ABC-DLBCL (Appendix A2 and A3).

Table 3.1 Number of genes used for the comparison of *SPHK1* correlated genes and leukocyte/monocyte/macrophage migration genes

	Total number genes	Number of genes overlapping with Migration genes
Genes positively correlated with *SPHK1* in primary DLBCL	2141	93
Genes negatively correlated with *SPHK1* in primary DLBCL	1529	8
Migration genes	351	

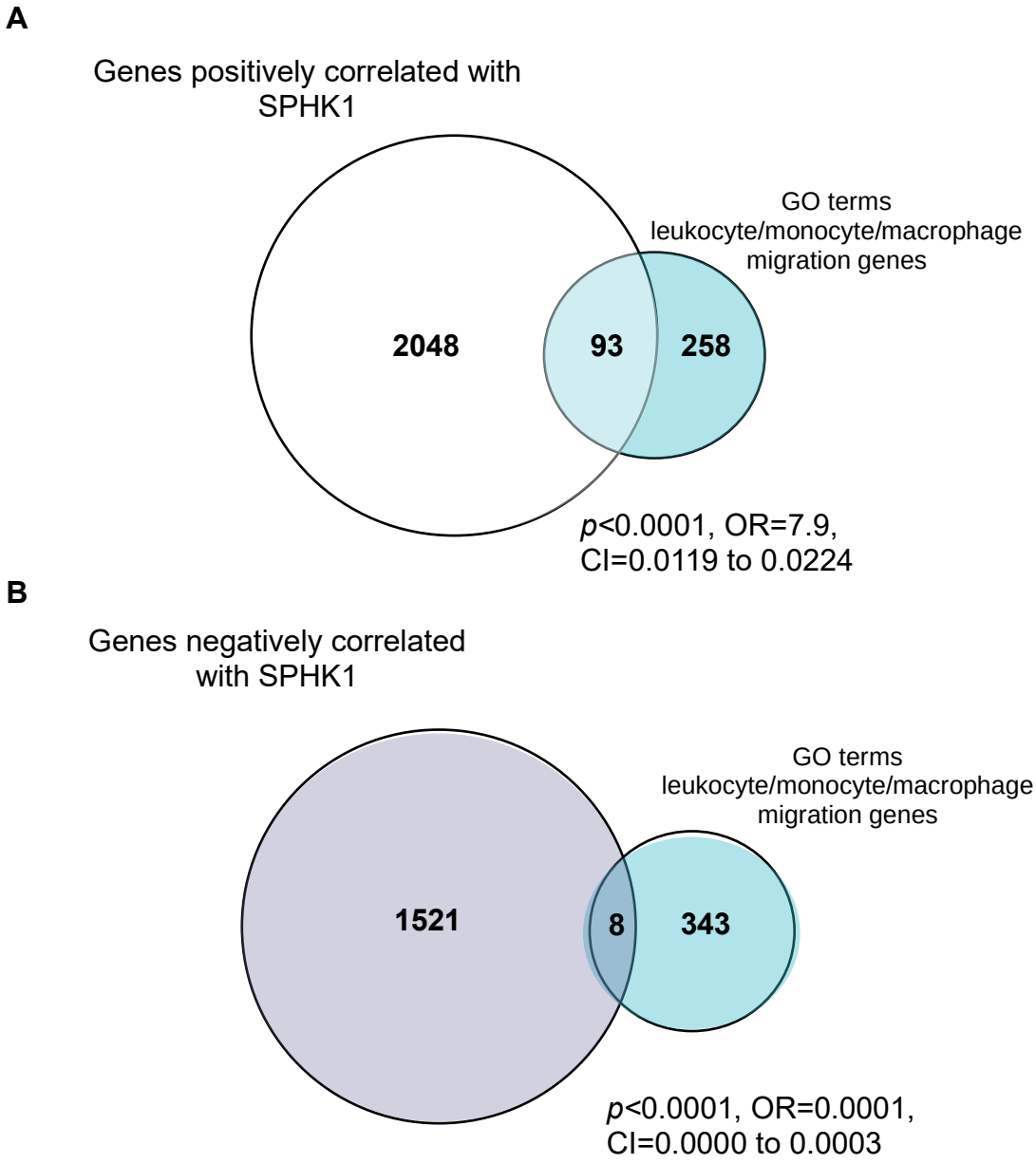

Figure 3.6 Overlap between genes positively correlated with *SPHK1* and genes with a function in migration of leukocytes/ monocytes/ macrophages. (A) Amongst genes positively correlated with *SPHK1,* there was a significant enrichment of leukocyte migration genes including genes involved in monocyte and macrophage migration (93/351). (B) These migration genes were significantly depleted (8/351) among those genes negatively correlated with *SPHK1*. Chi-square test was used to determine p value, odds ratio and confidence intervals.

Next, genes classified under the GO term phagocytosis (GO:0006909) was obtained. A total of 344 phagocytosis genes were compared with the set of genes positively and negatively correlated with *SPHK1*. 66/344 phagocytosis genes positively correlated with *SPHK1* (Table 3.2 and Figure 3.7A). There were 8/344 phagocytosis genes negatively correlated with SPHK1 (Table 3.2 Figure 3.7B). Using the Morin dataset of differentially expressed genes in ABC and GCB DLBCL, there were 56/66 genes in the overlap were upregulated in ABC-type DLBCL 48/66 genes were upregulated in GCB-DLBCL (Appendix A4 and A5).

Table 3.2 Number of genes used for comparison of *SPHK1* correlated genes and phagocytosis gene set

	Total number genes	Number of genes overlapping with Phagocytosis genes
Genes positively correlated with *SPHK1* in primary DLBCL	2141	66
Genes negatively correlated with *SPHK1* in primary DLBCL	1529	8
Phagocytosis genes	344	

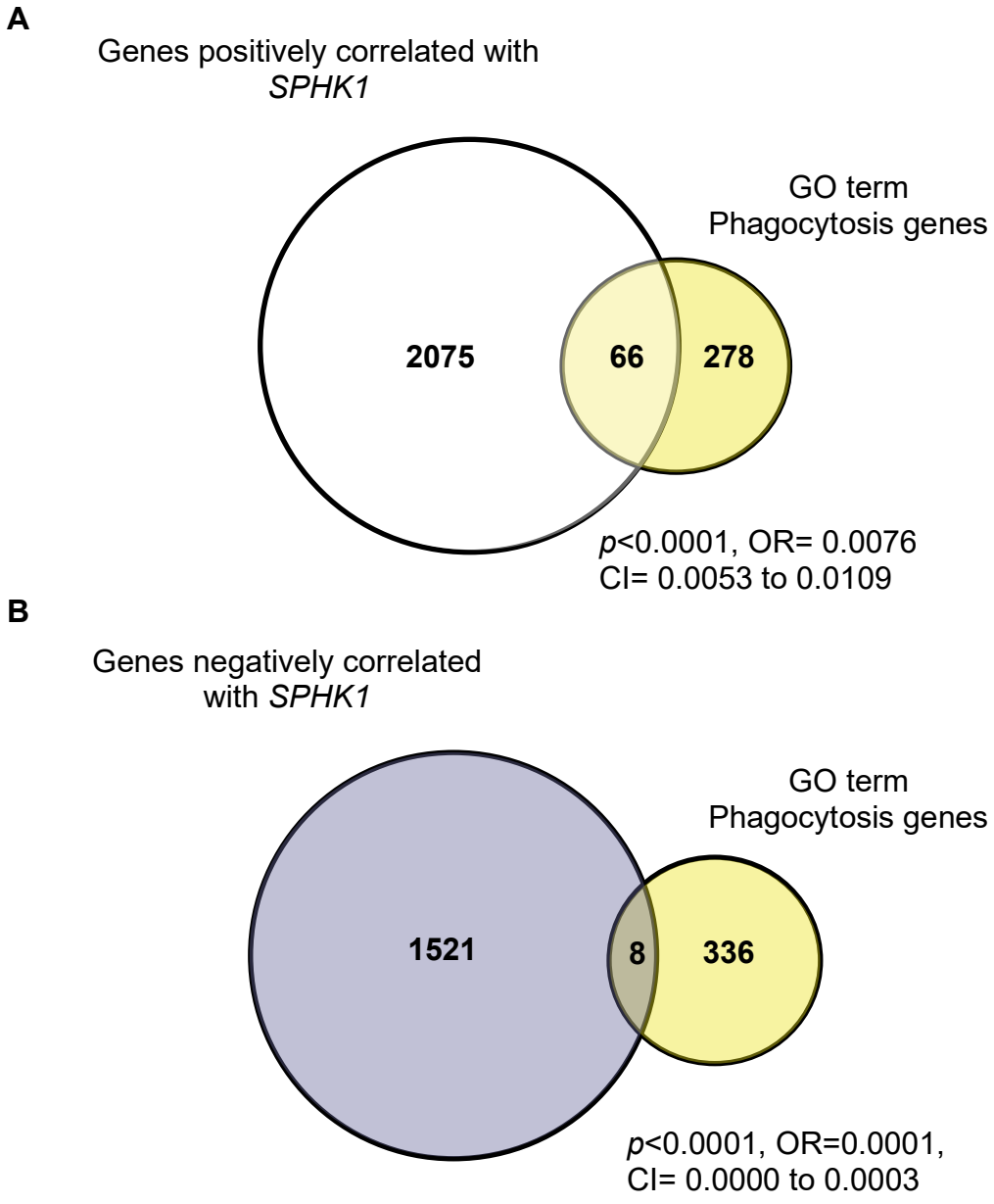

Figure 3.7 Phagocytosis genes were enriched among genes positively correlated with *SPHK1* in DLBCL. (A) Amongst genes positively correlated with *SPHK1*, there was a significant enrichment of phagocytosis genes (66/344). (B) Phagocytosis genes were significantly depleted (8/344) among genes negatively correlated with *SPHK1*. Chi-square test was used to determine p value, odds ratio and confidence intervals.

3.3.4 Macrophages do not regularly express *SPHK1* in DLBCL

The overlap between *SPHK1* and macrophage gene expression may be due to DLBCL-associated macrophages themselves expressing *SPHK1*. To explore this possibility, the same DLBCL cases as examined in section 3.2.1 were stained for CD68 (Figure 3.8 and Appendix A1). CD68 is a pan marker for macrophages (Pham et al., 2018). Five HPFs were counted for CD68+ cells. The frequency of CD68 in the 20 DLBCL cases was an average of 198.6/HPF (Table 3.4).

A subset of these DLBCL cases (N=10) was stained using multiplex fluorescent RNAscope© for *SPHK1* and fluorescent IHC for CD68. Only 12% of the CD68-positive macrophages also expressed *SPHK1* per HPF (Figure 3.9 and Appendix A1). This was confirmed by a pathologist, Dr Matthew Pugh.

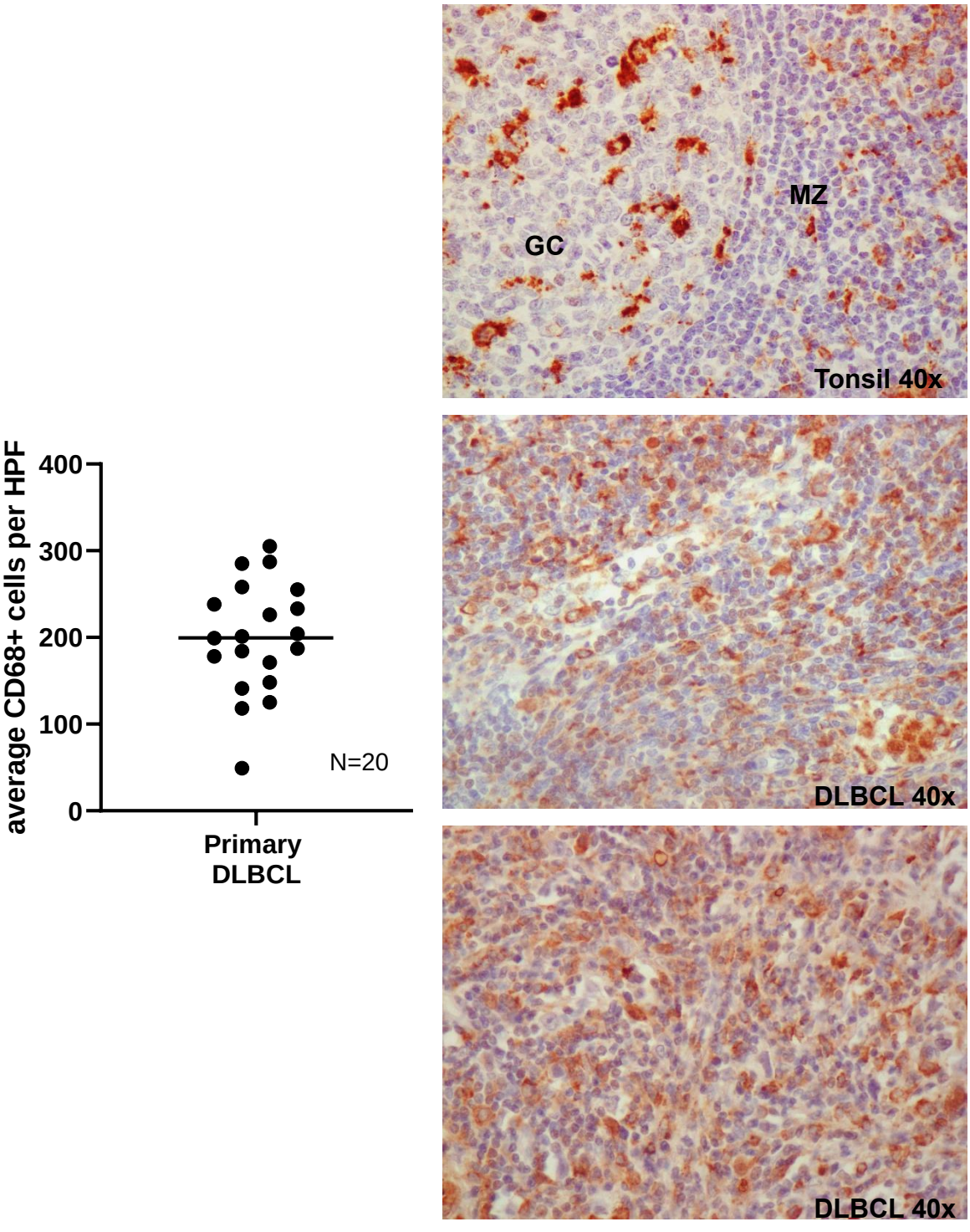

Figure 3.8 CD68+ cells were abundant in primary DLBCL. DLBCL cases (N=20) were stained for CD68 by IHC. The average number of CD68+ cells per five high power fields (HPF) at 40x were counted. There was an abundance of CD68+ cells in DLBCL compared to tonsil controls.

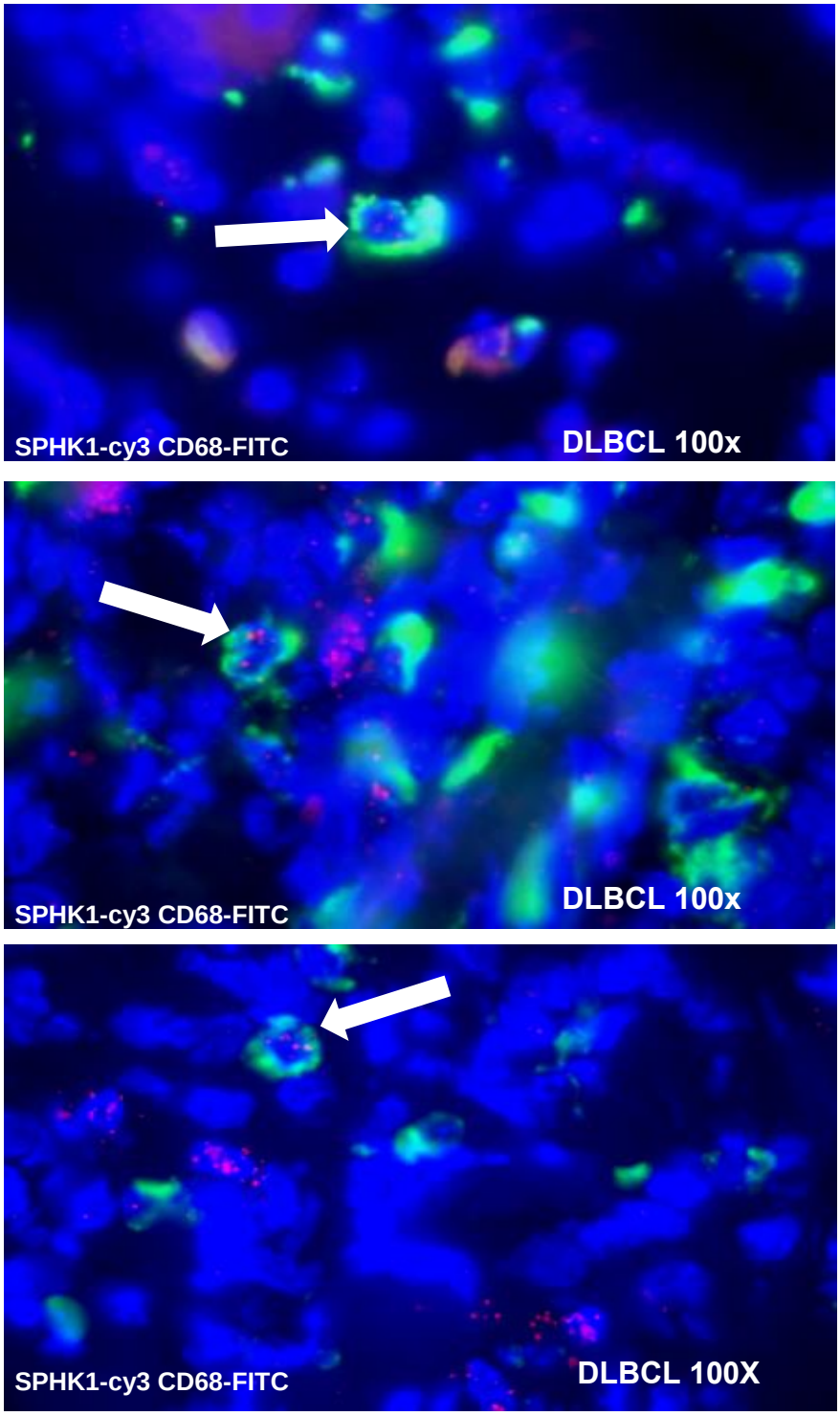

Figure 3.9 Frequency of *SPHK1* expressing macrophages were low in primary DLBCL. *SPHK1* expressing CD68+ cells were found at a frequency of 3/25 CD68+ cells counted per HPF (60x) in N=10 DLBCL cases. This was confirmed by a pathologist, Dr Matthew Pugh. White arrows indicate CD68+ cells that also expresses *SPHK1*.

3.4 Discussion

SPHK1 plays a central role in modulating the proliferation and pro-survival effects of S1P by counter-acting the pro-apoptotic and growth arrest effects of sphingosine and ceramide (Hatoum et al., 2017). This has led to the recognition of S1P as an onco-lipid contributing to the pathogenesis of cancers such as breast and NHL and has sparked the therapeutic targeting of SPHK1, S1P and its receptors (Bayerl et al., 2008, Nagahashi et al., 2012). The role of S1P in the pathogenesis of DLBCL, in particular is strengthened by the observation that disrupting S1PR2 in mice led to the development of DLBCL and the finding that S1PR2 is a tumour suppressor in DLBCL (Cattoretti et al., 2009, Stelling et al., 2018).

From re-analysed published datasets comparing DLBCL and germinal centre B cells, it was determined that *SPHK1* is significantly over-expressed in ABC and GCB subtypes of DLBCL in line with published observations in NHL (Bayerl et al., 2008). The limitation here is that the comparison was made using expression data from whole DLBCL tumours with GC B cells where it would have been more appropriate to have compared gene expression of whole tonsils or isolated various B cells subsets to isolated tumour cells. To address this, RNAscope© was used to probe for *SPHK1* mRNA in primary DLBCL and tonsil co-staining for the B cell marker, CD79A. There were significantly higher levels of *SPHK1* mRNA in B cells of DLBCL also by this appraisal thus supporting the observation that *SPHK1* overexpression was primarily observed within the tumour cell population.

DLBCL cell lines express *SPHK1* in keeping with previous work (Lupino, 2017, Lupino et al., 2019) . Using qPCR, a panel of DLBCL cell lines was shown to have an overexpression of *SPHK1* compared to normal B cells. Measurements of S1P from DLBCL cells also revealed a significantly higher S1P concentration than in normal B cells. Densitometry analysis of SPHK1 protein expression in DLBCL cell lines compared to the gene expression shows that though

Gene set enrichment analysis of the subset of genes that positively correlate with *SPHK1* expression in DLBCL, highlighted processes involved with the promotion of monocyte/ macrophage migration in agreement with publications that describe the recruitment of monocytes/macrophages in inflammatory responses by S1P and its role in the clearance of apoptotic cells (Rodriguez et al., 2016, Weigert et al., 2009, Aoki et al., 2016). *SPHK1* correlated genes associated with macrophage migration was also upregulated in ABC and GCB-DLBCL supporting the hypothesis that recruitment of monocytes/macrophages to DLBCL may be S1P-mediated. This was investigated further in Chapter 4 of this thesis.

Gene set enrichment analysis of genes positively correlated with *SPHK1* also highlighted enrichment of genes with functions in endocytosis and phagocytosis. This is of particular interest due to the proposed mechanisms of action of rituximab. S1P may recruit phagocytes and influence their function. S1P mobilises monocytes/macrophages and the degradation of S1P may also be necessary to prevent further recruitment. In the Morin dataset, I found that

migration and phagocytosis genes correlated with *SPHK1* were upregulated in DLBCL.

The correlation of *SPHK1* and macrophage gene expression may be because macrophages also express *SPHK1*. Macrophages are the dominant non-malignant immune cell type found in DLBCL and in the Morin dataset they analysed samples from whole tumour suspensions of DLBCL cases (Kridel et al., 2015, Gascoyne and Steidl, 2011, Scott and Gascoyne, 2014, Morin et al., 2013). In the RNAscope© analysis for *SPHK1* and CD68 showed that only a small fraction of macrophage in DLBCL express *SPHK1* and none showed the high expression as seen in *SPHK1*/CD79A stained DLBCL samples.

Taken together, these results show that SPHK1 could be important in the formation of the tumour microenvironment of DLBCL, specifically, in the recruitment and retention of monocytes and macrophages. This could be significant due to the current treatment for DLBCL that includes rituximab which works in part to enhance the phagocytosis of B cells by macrophages. While S1P may support the recruitment of macrophages to the tumour site, the aberrant expression of *SPHK1* may also affect the phagocytic function of recruited monocytes and macrophages. This possibility was explored further in Chapter 5.

CHAPTER 4

Evaluating the S1P-mediated migration of monocytes and macrophages

Chapter 4

Evaluating the S1P-mediated migration of monocytes and macrophages

4.1 Introduction

It has been shown that increased macrophage infiltration to the microenvironment of DLBCL had lower progression-free survival (PFS 40%) and lower overall survival (OS 39%) in patients treated with CHOP, however this effect on prognosis reversed in (PFS 74% and OS 90%) patients given R-CHOP (Riihijarvi et al., 2015, Pham et al., 2018). In the previous chapter, *SPHK1* was shown to be over-expressed in DLBCL. Gene set enrichment analysis of genes positively correlated with *SPHK1* revealed an enrichment of genes with functions in monocyte/macrophage migration and phagocytosis. Importantly, the majority of these genes were also upregulated in primary DLBCL.

The specific aims of this chapter are to; 1) confirm the expression of S1P receptors in *in vitro* polarised macrophages; 2) confirm that monocytes and macrophages migrate to S1P; 3) determine if monocyte/macrophage migration to DLBCL conditioned medium (CM) *in vitro* is S1P-mediated; 3) identify which S1P receptor is responsible for migration of monocytes/macrophages to DLBCL conditioned medium; 4) determine if tumours from mouse models of

DLBCL recruit host macrophages and if so, are they reduced with S1P receptor antagonists.

4.2 *In vitro* polarisation of monocytes to M1 and M2 macrophages

4.2.1 Macrophage polarisation with GM-CSF and M-CSF

Having shown that over-expression of *SPHK1* in primary DLBCL is associated with macrophage gene signature, I next studied the effect of S1P on monocyte and macrophage functions. CD14+ monocytes isolated from leukocyte cones from healthy donors were cultured with either GM-CSF or M-CSF for 7 days (Leidi et al., 2009, Lacey et al., 2012). Purity of the CD14 isolation was confirmed and the phenotype of the cells determined by staining for CD14, CD68, CD163, and CD206 (Figure 4.1 A and B).

As mentioned in Chapter 1, there are no definitive markers for M1 and M2 given the spectrum of phenotypic states possible, therefore for this thesis, GM-CSF polarised M1-like macrophages was defined as CD68+CD206+/- and CD163- while M-CSF polarised M2-like macrophages was defined as CD68+CD206+ and CD163+ (Marchesi et al., 2015, Mantovani et al., 2002). The phenotype observed for GM-CSF-M1 was $CD68^{positive}$ $CD14^{positive}$ $CD163^{negative}$ and moderately $CD206^{positive}$ (Figure 4.1C). M-CSF M2-like macrophages were $CD68^{positive}$ $CD14^{positive}$ and largely $CD163^{positive}$ $CD206^{positive}$. There was also a population of cells that were $CD68^{positive}$ $CD14^{positive}$ but $CD163^{negative}$ $CD206^{negative}$ (Figure 4.1C).

M1 is said to secrete IL-12 and M2 is said to secrete IL-10, therefore, GM-CSF M1 and M-CSF M2 polarised macrophages were treated with LPS for 24hrs in order to induce cytokine secretion (Mantovani et al., 2002). ELISA analysis of resulting conditioned media after LPS stimulation indicated that GM-CSF polarised macrophages had characteristic M1 cytokine expression; low IL-10 and high IL-12(p70) secretion. M-CSF polarised macrophages exhibited characteristic M2 macrophage cytokine expression: high IL-10 and low IL-12(p70) secretion (Figure 4.1D). An additional 35 cytokines were tested from a single donor using a cytokine array (Appendix A6). Also, the *SPHK1* expression was evaluated by qPCR in the macrophages from 3 healthy donors where *SPHK1* was found to have variable between donors (Appendix A7).

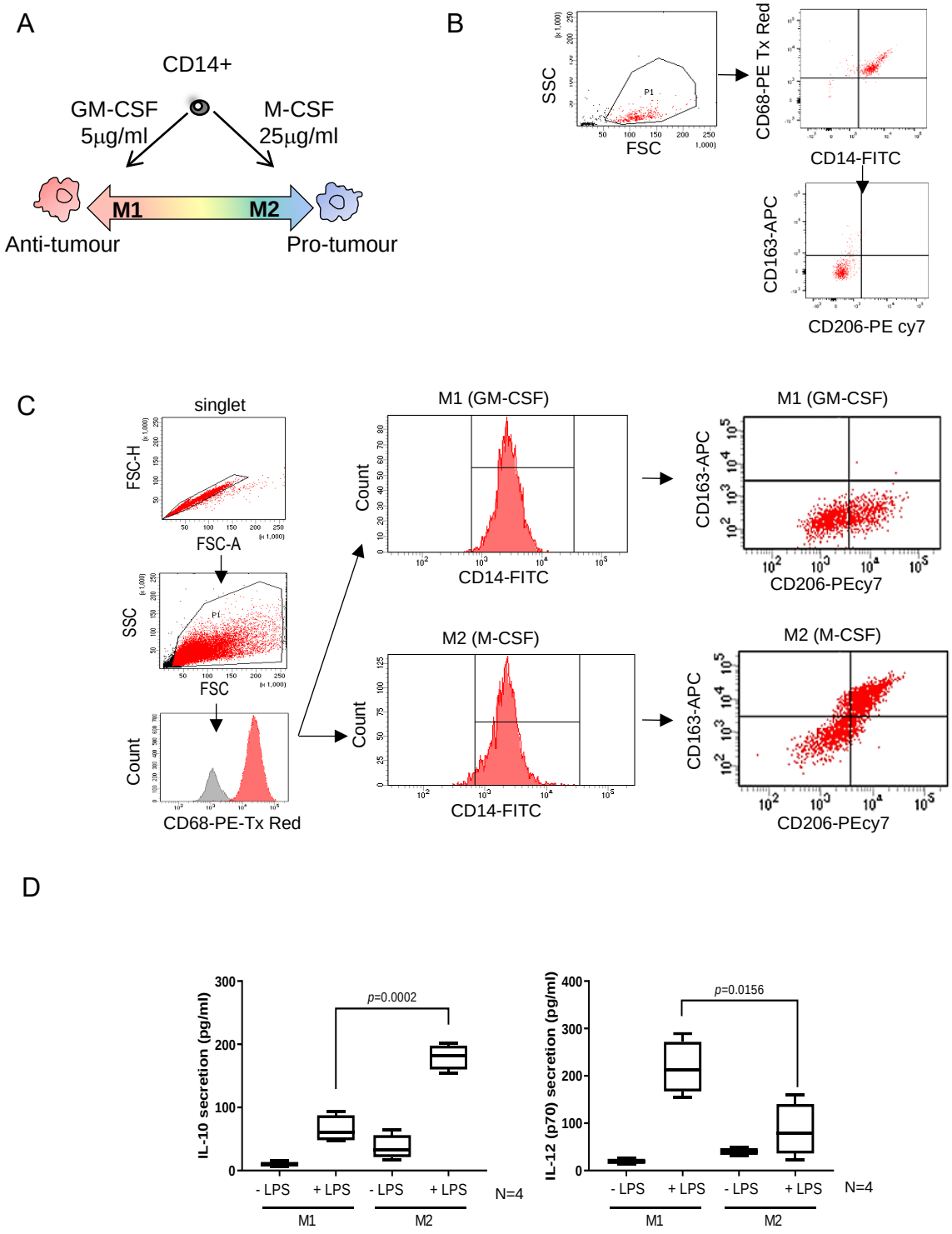

Figure 4.1 Polarisation of CD14+ monocytes to M1 and M2 macrophages. (A) GM-CSF and M-CSF was used to polarise monocytes to M1 and M2 macrophages. (B) Representative dot plots of CD14+ isolated cells on day 0 show 100% purity with CD68 expression and low CD163 and CD206 expression. (C) Representative dot plots of M1 and M2 polarised macrophages for CD163 and CD206. (D) ELISA results from four independent donors for IL-10 and IL-12p70 secretion show that M2 had higher secretion of IL-10 and M1 higher secretion of IL-12p70. The cytokines were measured from the culture medium of M1 and M2 polarised macrophages treated for 24 hr +/- LPS. Student's t-test to calculate p values.

4.2.2 M1 and M2 macrophages express low levels of *S1PR1* and high levels of *S1PR2*

S1P receptor expression in these cells was next measured by qPCR. A total of 34/40 normal CD14+ donors samples showed robust polarisation of M1 and M2 phenotypes and were analysed for S1P receptor expression. There are five S1P receptors (S1PR1-5) and initially the focus of this study was on *S1PR1* and *S1PR2* as these are the most likely to be associated with functional differences in macrophages. Relative expression of these receptors in M1 and M2 macrophages was compared to the donor's own unpolarised monocytes in order to account for differences in base line expression between donors.

The relative expression of *S1PR1* in M1 macrophages was generally lower than in monocytes (Figure 4.2A). In contrast, the relative expression of *S1PR2* was significantly higher in both M1 and M2 macrophages compared to monocytes (Figure 4.2B). Volcano plots were plotted using FDR (false discover rate) < .01 versus the mean difference of the ΔCT for *S1PR1* and *S1PR2* expression between monocytes and M1 and M2 macrophages (Figure 4.3A and B). The green dots signify low expression of S1P receptors and red dots signify high expression. 27/34 donors tested had a significantly negative mean difference in ΔCT for *S1PR1* expression in M1 macrophages compared to monocytes (Figure 4.3A). Three donors showed a significantly higher expression of *S1PR1* in M1 macrophages compared to monocytes. In the M2 macrophages of these donors, 20/34 donors had a significant negative mean ΔCT for S1PR1 expression compared to monocytes (Figure 4.3A). Eight donors

showed a significantly higher expression of *S1PR1* in M2 macrophages compared to monocytes. None of the samples had a high expression of *S1PR1* in both M1 and M2. The 3/34 M1 samples and 2/34 M2 samples had a significantly higher expression of S1PR2 compared to matched monocytes (Figure 4.3B)

A

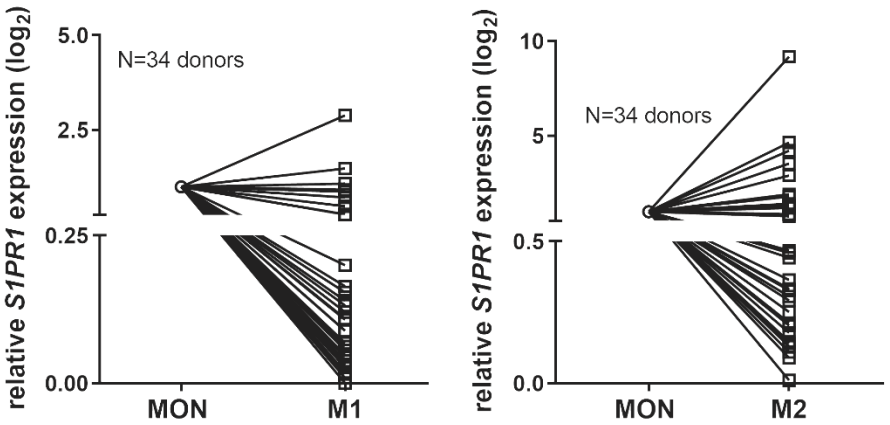

B

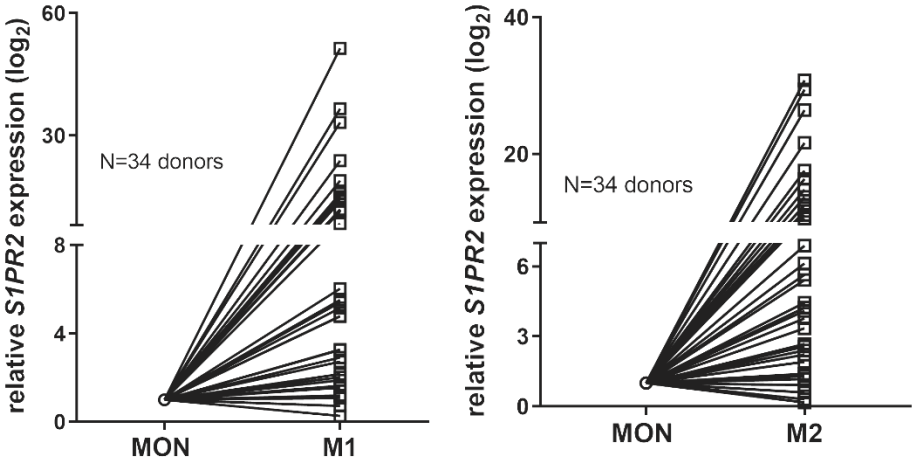

Figure 4.2 Relative *S1PR1* expression was generally lower and relative expression of *S1PR2* was generally higher in M1 and M2 relative to matched monocytes from same donor. (A) There was lower relative *S1PR1* expression in M1 and M2 macrophages compared to matched monocytes in 34 donors. (B) There was a higher relative *S1PR2* expression in M1 and M2 macrophages compared to matched monocytes in 34 donors.

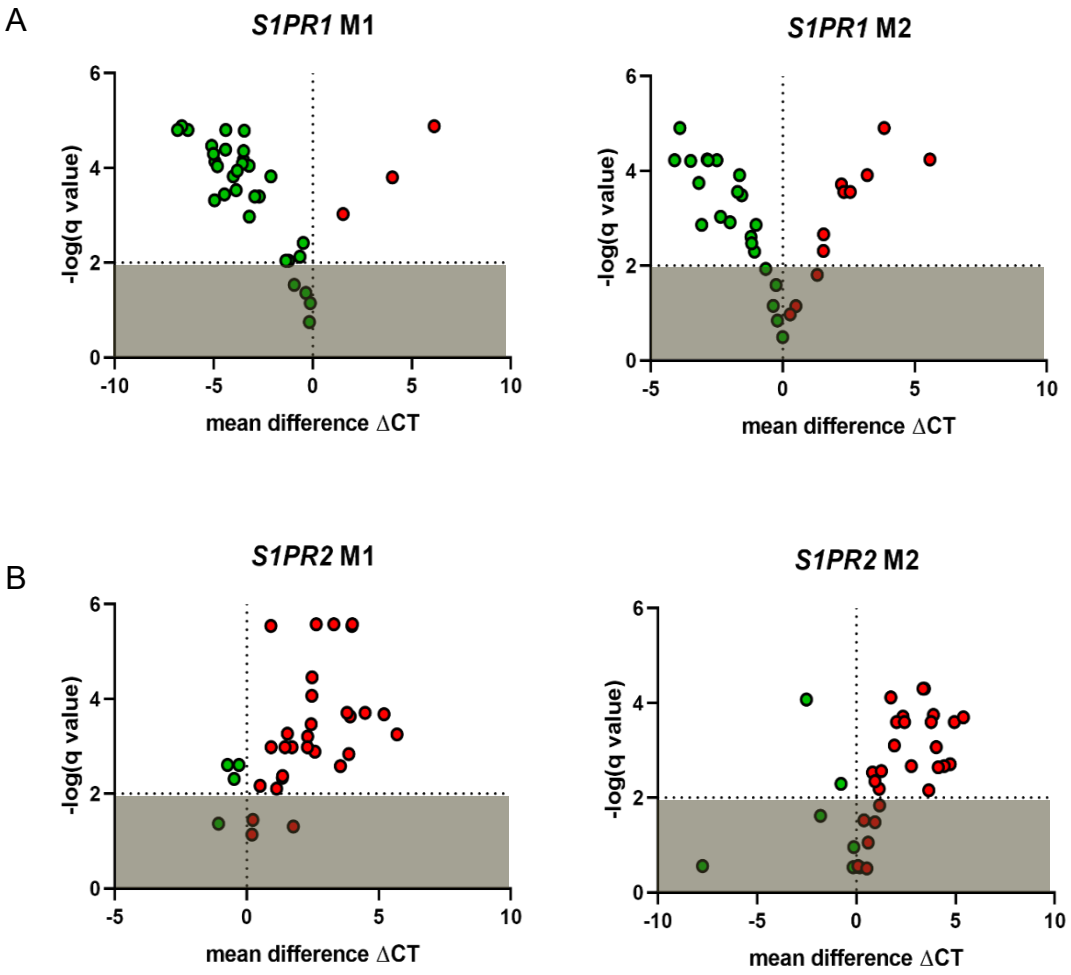

Figure 4.3 Volcano plots of FDR (q< .01) vs mean difference of ΔCT for *S1PR1* and *S1PR2* expression of monocytes and M1 or M2 macrophages. FDR adjusted p-values were calculated by paired t-test adjusted for multiple testing with cut-off for significance set at FDR< .01 using mean and standard error of ΔCT technical triplicates. Red signifies up-regulated and green signifies down-regulated. Greyed out area = not significant. (A) In 27/34 donors, their M1 macrophages had a significant negative mean difference ΔCT compared to monocytes. 3/34 had a significant higher mean difference ΔCT than monocytes. For M2 macrophages, 20/34 donors had a significant negative mean difference ΔCT of *S1PR1* compared to monocytes. (B) Similar analysis for *S1PR2* show a majority of M1 and M2 macrophages with higher expression of *S1PR2* compared to monocytes.

4.2.3 Monocytes, M1 and M2 macrophages express low levels of *S1PR3, S1PR4*, and *S1PR5*

Next, the expression of *S1PR3, S1PR4*, and *S1PR5* in a subset of the same donors previously analysed for *S1PR1* and *S1PR2* was investigated. Results showed that *S1PR3* and *S1PR5* expression was decreased in M1 and M2 macrophages compared to monocytes (Figure 4.4A and B). The expression of *S1PR4* was more variable (Figure 4.4C). Volcano plots of FDR < .01 of the mean difference of ΔCT in monocytes vs M1 or M2 macrophages clearly illustrates these differences (Figure 4.5A-C). A summary of relative expression of *S1PR1-5* for M1 and M2 macrophages relative to matched monocytes from healthy donors (Figure 4.6).

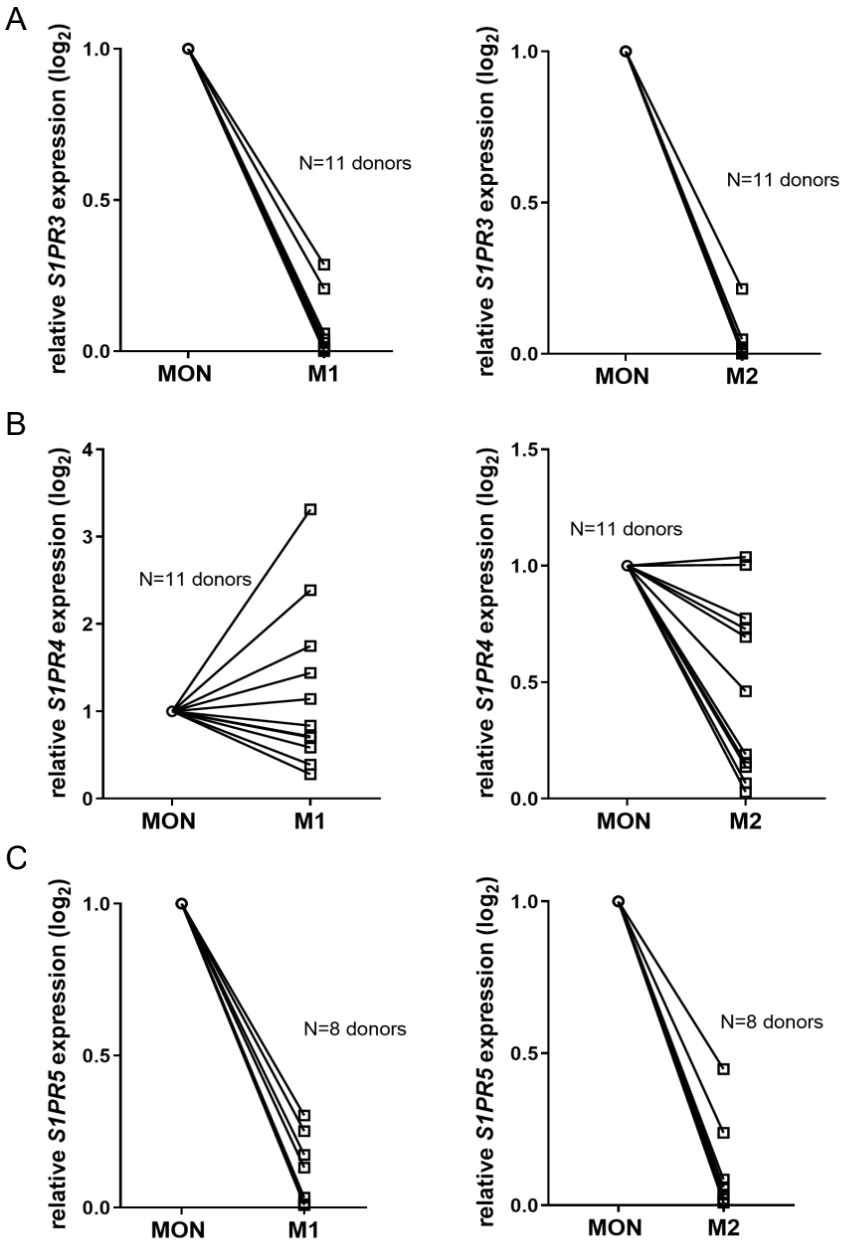

Figure 4.4 Relative expression of *S1PR3* and *S1PR5* was lower in M1 and M2 macrophages compared to monocytes while *S1PR4* was higher in M1 macrophages. Relative expression of (A) *S1PR3* N=11 and (C) *S1PR5* N=8 in M1 and M2 *in vitro* polarised macrophages was significantly lower than their comparative monocytes. (B) *S1PR4* relative expression was higher in M1 than in M2 than their monocytes in N=11 donors.

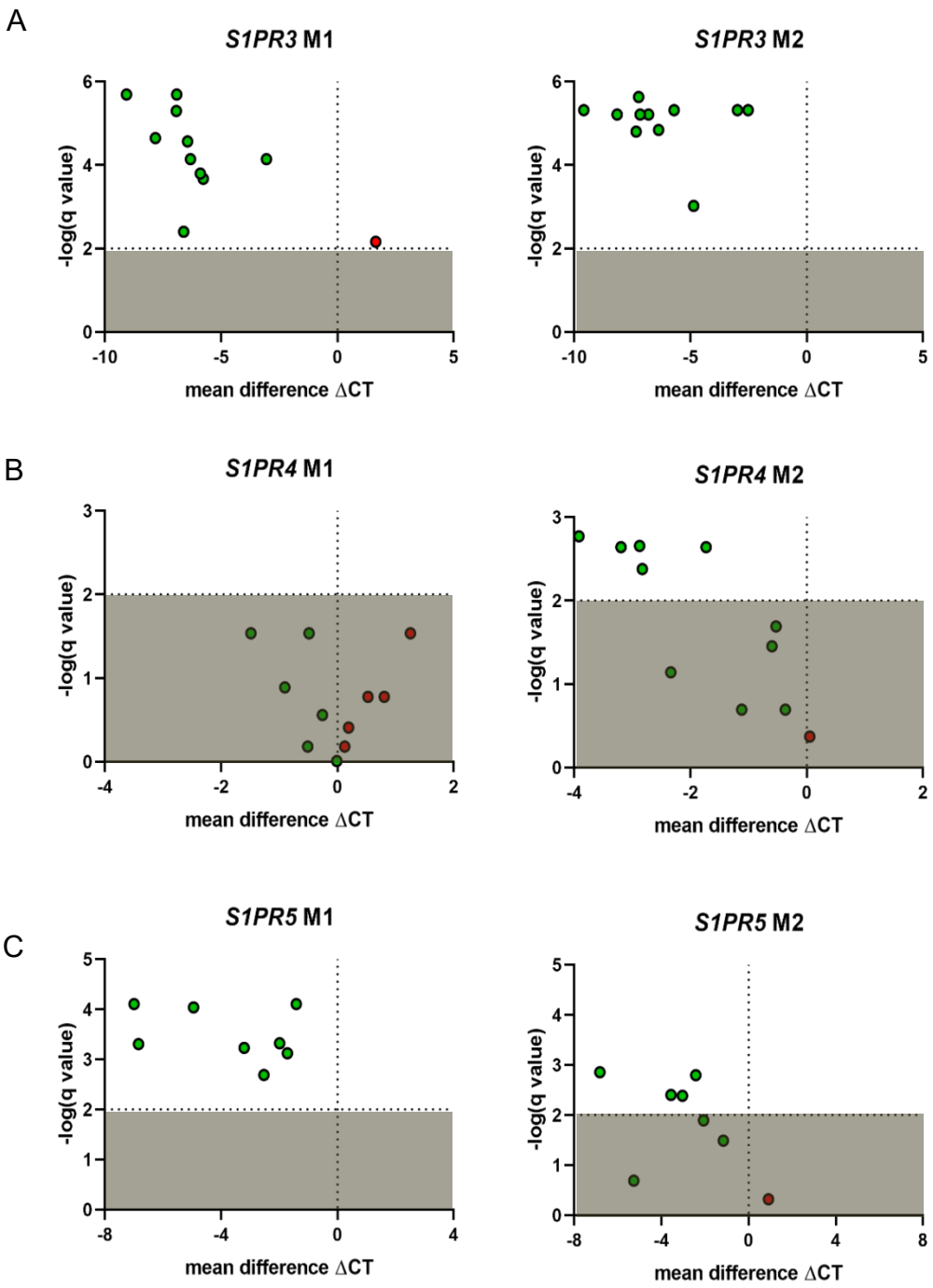

Figure 4.5 Volcano plots of FDR (q< .01) versus mean difference ΔCT for *S1PR3, S1PR4*, and *S1PR5* show that these S1P receptors are generally more lowly expressed in M1 and M2 compared to monocytes. (A) Nearly all of M1 and all of M2 from N=11 donors tested had a negative mean difference ΔCT of *S1PR3* compared to monocytes. (B) *S1PR4* was variable in the N=11 donors tested and the mean difference ΔCT was not significant in the majority of donors. (C) For *S1PR5,* the donors tested (N=8) generally had significantly lower expression than monocytes.

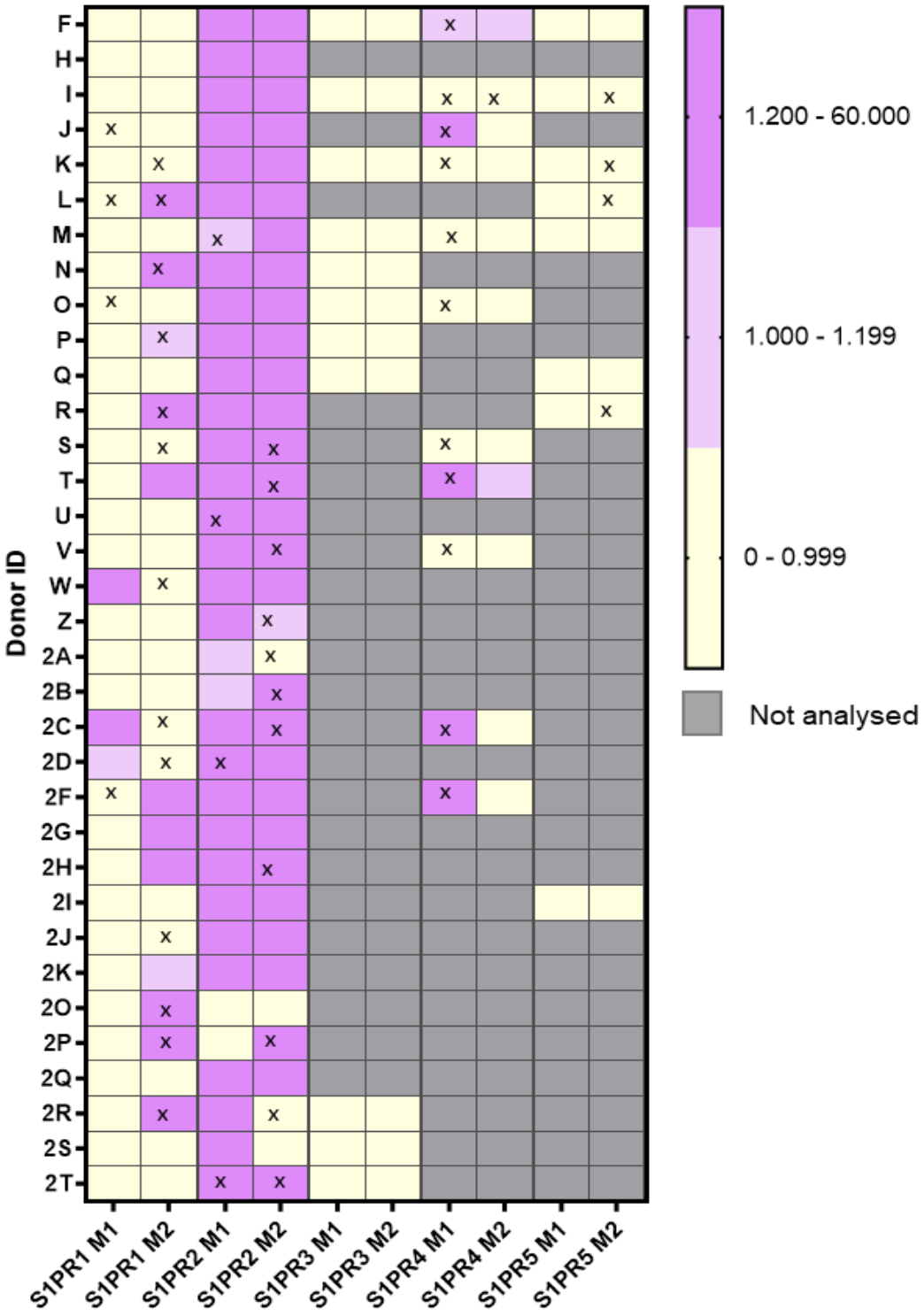

Figure 4.6 Summary of relative S1P receptor expression in M1 and M2 macrophages compared to matched monocytes from healthy donors. The *S1PR1-5* expression of M1 and M2 macrophages from each donor are shown highlighting higher expression compared to monocytes shown in dark pink and lower expression compared to monocytes shown in yellow. Grey denotes donors that were not tested and 'x' insignificant ΔΔCT values. Student's t-test was used to determine p value and $p < 0.05$ was considered significant.

4.2.4 Monocytes, M1 and M2 macrophages express S1PR1 protein

The protein expression of S1PR1 on monocytes and M1/M2 macrophages was next examined by flow cytometry. CD14+ monocytes and M1 and M2 polarised macrophages from three donors were stained with anti-S1PR1-APC. Figure 4.7 shows the decreased but detectable expression of expression of surface S1PR1 in polarised macrophages compared to monocytes (black line) and compared to unstained controls in grey.

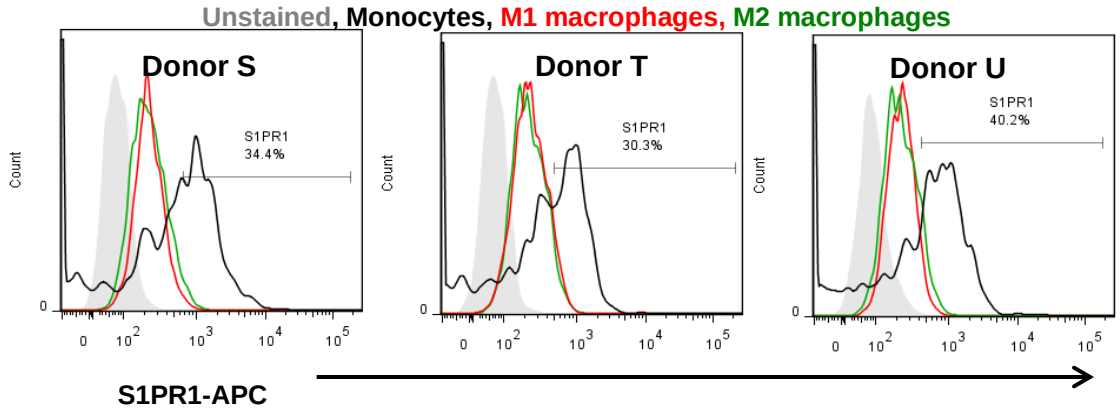

Figure 4.7 S1PR1 is detected in M1 and M2 macrophages. Representative graphs of CD14+ monocytes and M1 and M2 macrophages were stained with S1PR1-APC and analysed by flow cytometry. There were varied levels of expression of S1PR1 observed between donors. Here, three donors are shown with grey curve denoting unstained cells, black curve= monocytes, red curve = M1 and green curve =M2).

4.3 Studying S1P mediated migration of CD14+ monocytes and macrophages

4.3.1 CD14+ monocytes migrate to S1P

Having confirmed the polarisation of M1 and M2 from monocytes with cytokines *in vitro* and their S1P receptor expression, the S1P-mediated migration of monocytes was next examined. Monocytes are already known to readily migrate to sites of infection through the blood stream (Shi and Pamer, 2011). MCP-1 is a known chemoattractant for monocytes during inflammation and therefore, was used as a positive control for transwell migration assays (Yoshimura et al., 1989). Monocytes isolated from three donors showed significant monocyte migration to 50ng/ml MCP-1 over 4 hr (Figure 4.8A). Testing the migration of monocytes to 0.1, 1 and 10 μM S1P showed that monocytes significantly migrated to 0.1μM (Figure 4.8B). Concentrations below 0.1 μM were not tested. This experiment was repeated, this time using 0.1μM S1P +/- Sphingomab (a neutralising antibody to S1P), or isotype control with freshly isolated monocytes from another three donors. Monocytes from all three donors migrated to 0.1μM S1P and this migration was blocked by the addition of Sphingomab (Figure 4.8C). I also treated these monocytes with 0.01% DMSO or 100nM BAF312 for 30 min prior to allowing them to migrate to 0.1μM S1P. Treatment with BAF312 also significantly blocked migration of monocytes to S1P showing that migration was mediated through S1PR1 or S1PR5. In all migration experiments, monocytes were allowed to migrate over 4hrs at 37°C.

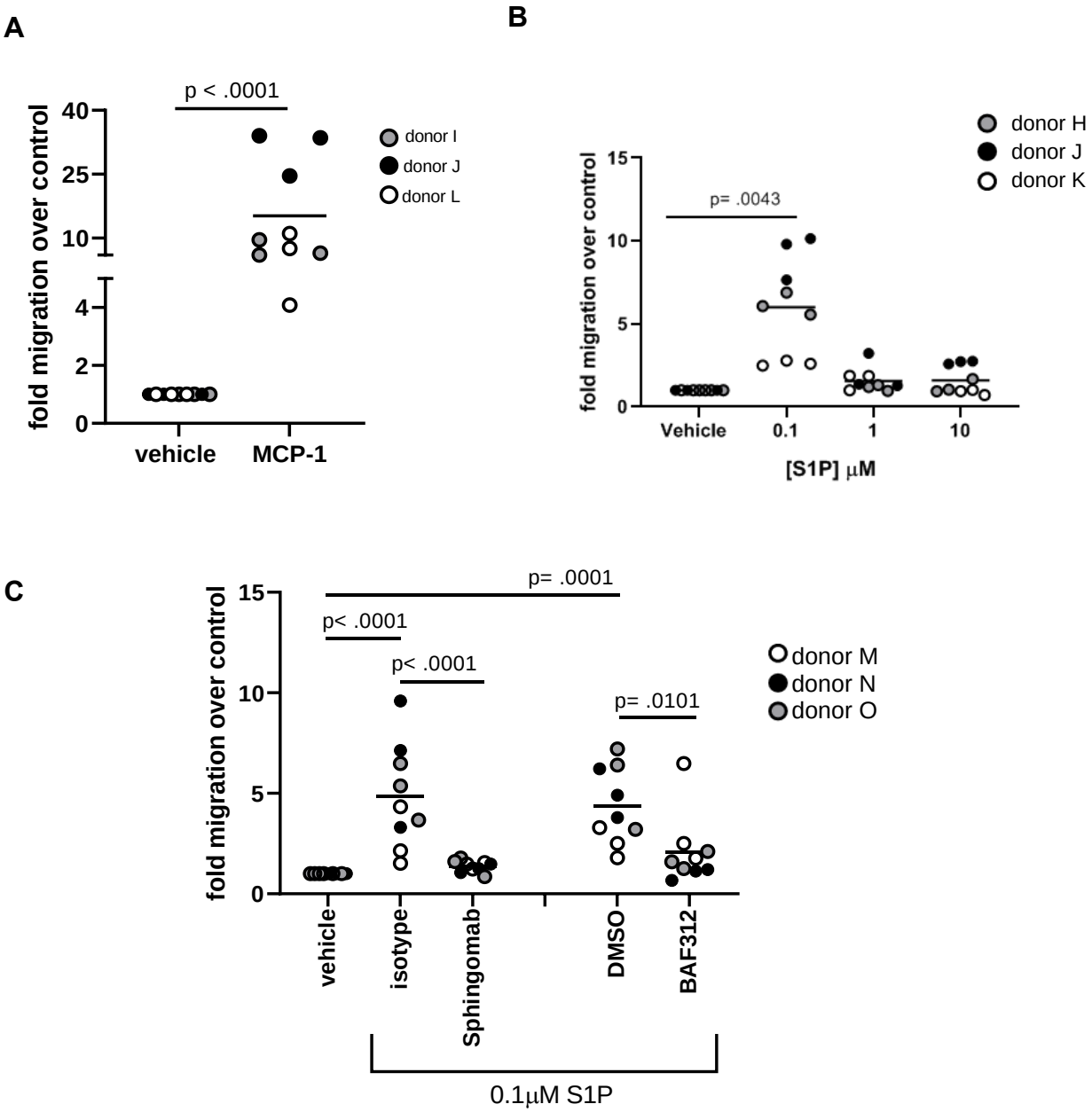

Figure 4.8 Migration of CD14+ monocytes can be mediated by S1P. (A) CD14+ monocytes migrated to MCP-1 50ng/ml in an *in vitro* transwell assay over 4hr. (B) Monocytes significantly migrated to 0.1μM S1P but not to 1μM or 10μM S1P. (C) Monocyte migration to 0.1μM S1P was inhibited with Sphingomab (1μg/ml per 1μM S1P) as well as with 100nM BAF312. Results shown are of 3 different donors in triplicate as indicated by grey, black and white circles. P values were calculated using 2-way ANOVA.

Having demonstrated that monocyte migration to S1P could be blocked with Sphingomab, the monocyte migration to DLBCL conditioned medium was next examined. S1PR1 has the highest binding affinity for S1P and important in leukocyte migration therefore, the antagonism of S1PR1 was the first receptor explored. There are several S1PR1 antagonists commercially available: BAF312 (siponimod) and ponesimod but BAF312 antagonises both S1PR1 and S1PR5.

BAF312 was chosen for these series of experiments because of its proven inhibition of monocyte trafficking *in vivo* and because of its recent FDA approval for the treatment of multiple sclerosis (Kappos et al., 2018). BAF312 was part of a series of compounds developed to be specific for S1PR1 inhibition (Pan et al., 2013). FTY720, the first S1PR inhibitor, antagonised nearly all the S1PRs (except for S1PR4) which lead to off target effects (Gergely et al., 2012). *In vitro*, BAF312 will antagonise S1PR1 and S1PR5 at an EC50 of 0.9nM and an EC80 of 100nM and ponesimod has an EC50 of 5.7nM (Kappos et al., 2018, Lewis et al., 2013, D'Ambrosio et al., 2016). The selective affinity for S1PR1/S1PR5 was reported to be lost at concentrations >700nM where indiscriminate binding to the other S1P receptors was found (Gergely et al., 2012, Lewis et al., 2013). Therefore, 100nM BAF312 was the concentration used in order to achieve maximum antagonism of S1PR1/S1PR5.

Monocytes were treated with 100nM BAF312 for 30 minutes and then allowed to migrate to DLBCL conditioned medium for 4 hr. Monocytes from all three donors tested showed significantly reduced migration after pre-

treatment with BAF312 (Figure 4.9A). The S1PR1 antagonist, ponesimod, was also tested in these experiments to confirm if S1PR1 was the main receptor involved in monocyte migration. Pre-treatment with 100nM ponesimod had the same effect as BAF312, reducing monocyte migration to DLBCL conditioned medium (Figure 4.9B).

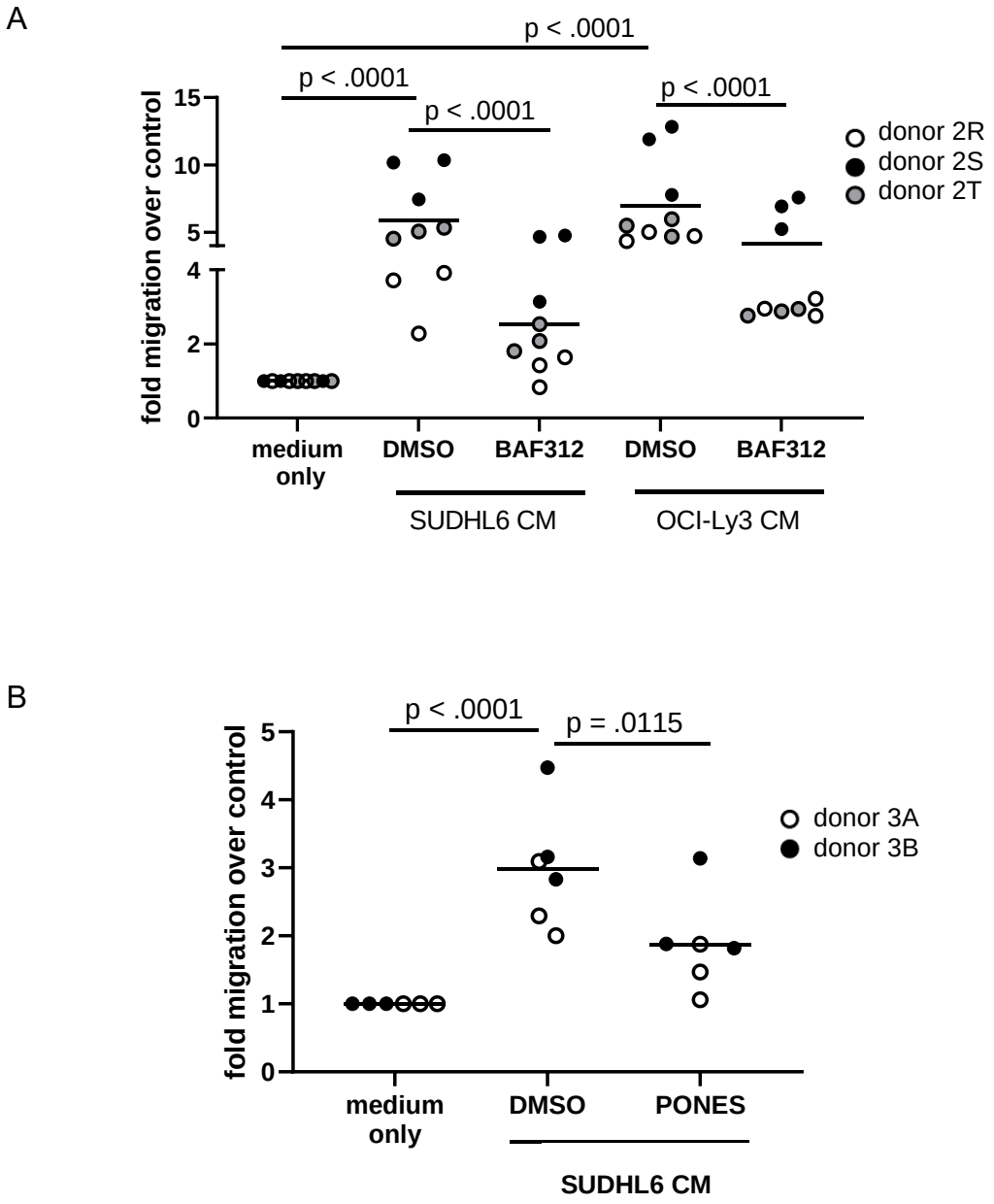

Figure 4.9 Monocyte migration to DLBCL conditioned medium was reduced by S1PR1 inhibitors. (A) SUDHL6 and OCI-Ly3 conditioned medium was used as a chemo-attractant in transwell migration assays with CD14+ monocytes. Monocyte migration to DLBCL conditioned medium was partially blocked by pre-treated with 100nM BAF312 for 30 minutes. Triplicate values of 3 different donors from independent experiments are indicated by grey, black and white circles. P-values were calculated using 2-way ANOVA. (B) The migration of the monocytes from two different donors in triplicate to SUDHL6 conditioned medium was also partially blocked with 100nM ponesimod.

4.3.2 Migration of M1 and M2 is mediated by S1P

Next, the migration of M1 and M2 macrophages S1P was also assessed, on the basis that mature macrophages already resident in surrounding tissues may also be recruited to tumour sites as part of the microenvironment. As with monocytes, the migration of M1 and M2 macrophages to MCP-1 was evaluated. Only 2/4 donors tested showed significantly increased migration to MCP-1 compared to controls (Figure 4.10A). This result was in keeping with previous reports showing that MCP-1 is predominantly a chemoattractant for monocytes (Deshmane et al., 2009).

CXCL12 is a known chemoattractant for macrophages and along with its receptor, CXCR4, also been shown to recruit T-regs creating an immune suppressive environment in DLBCL (Xuan et al., 2015, Durr et al., 2010). To determine if macrophages polarised *in vitro* with GM-CSF and M-CSF would migrate to CXCL12, three donors were tested in triplicate using a transwell migration assay with 100ng/ml CXCL12. All three donors showed significantly increased migration to CXCL12 compared to controls (Figure 4.10B).

A

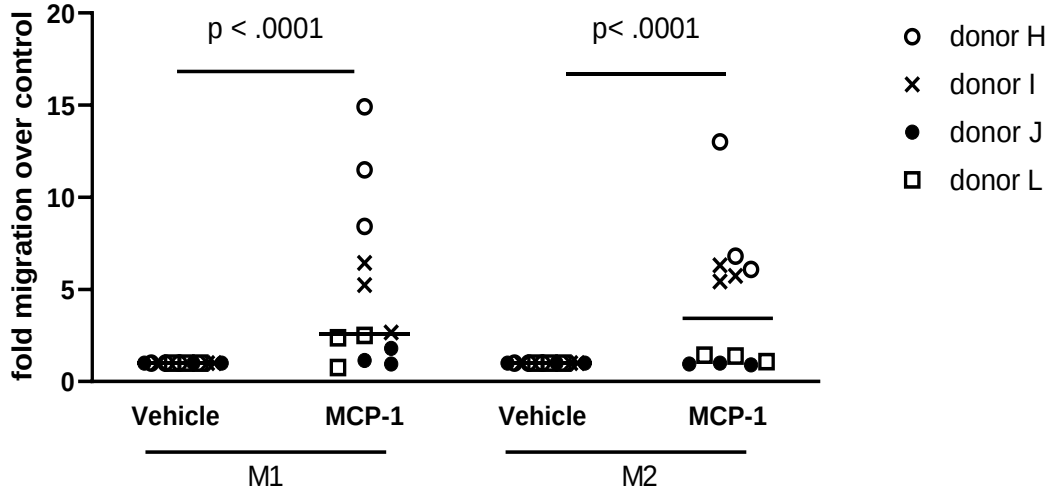

B

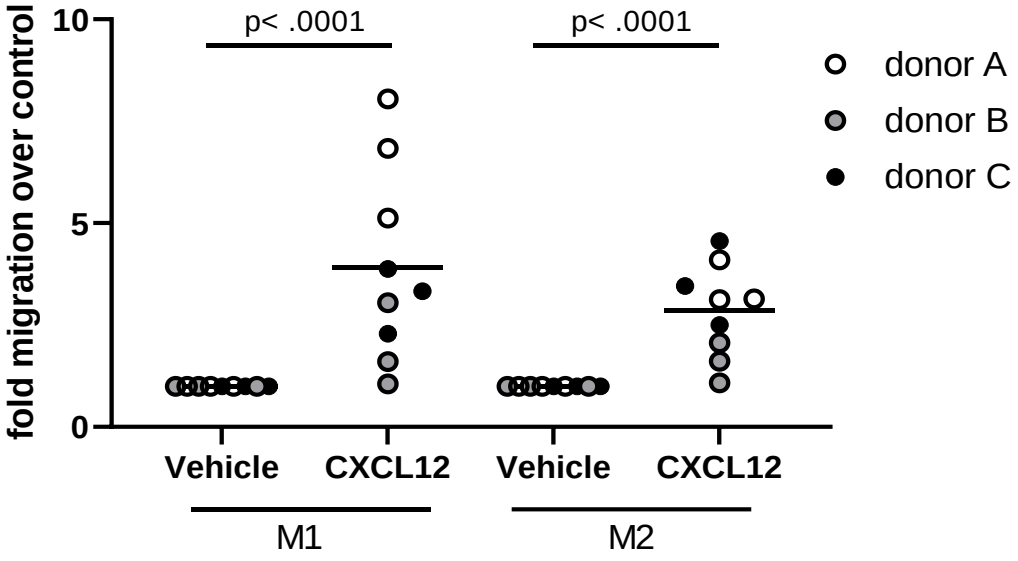

Figure 4.10 M1 and M2 macrophages migrated to CXCL12 but variably to MCP-1. (A) Triplicate M1 and M2 macrophages from each donor are represented on the graph in colour code. There was donor variability of migration to 50ng/ml MCP-1. (B) Another chemoattractant for macrophages, CXCL12, was tested. 3/3 donors tested showed migration to 100ng/ml CXCL12 compared to controls. P values were calculated using 2-way ANOVA.

Having shown that macrophages can migrate to CXCL12 *in vitro*, I next assessed migration to S1P. The M1 and M2 macrophages from three donors showed significantly increased migration to 0.1μM S1P but there was no significant migration to 1μM and 10μM S1P (Figure 4.11A). Next, Sphingomab was used to test for the blocking of macrophage migration to S1P with fresh M1 and M2 macrophages. M1 and M2 macrophages significantly migrated to isotype control + 0.1μM S1P and their migration was significantly blocked with Sphingomab to a level below baseline migration with vehicle (Figure 4.11B).

Migration of M1 and M2 macrophages to DLBCL conditioned medium was evaluated. M1 and M2 macrophages were treated with 100nM BAF312 and 100nM ponesimod and then allowed to migrate to DLBCL conditioned medium. Results showed that migration of M1 and M2 macrophages to SUDHL6 conditioned medium was not significantly different to controls. However, the baseline levels of M1 and M2 macrophage migration was reduced following treatment with either BAF312 or ponesimod (Figure 4.12).

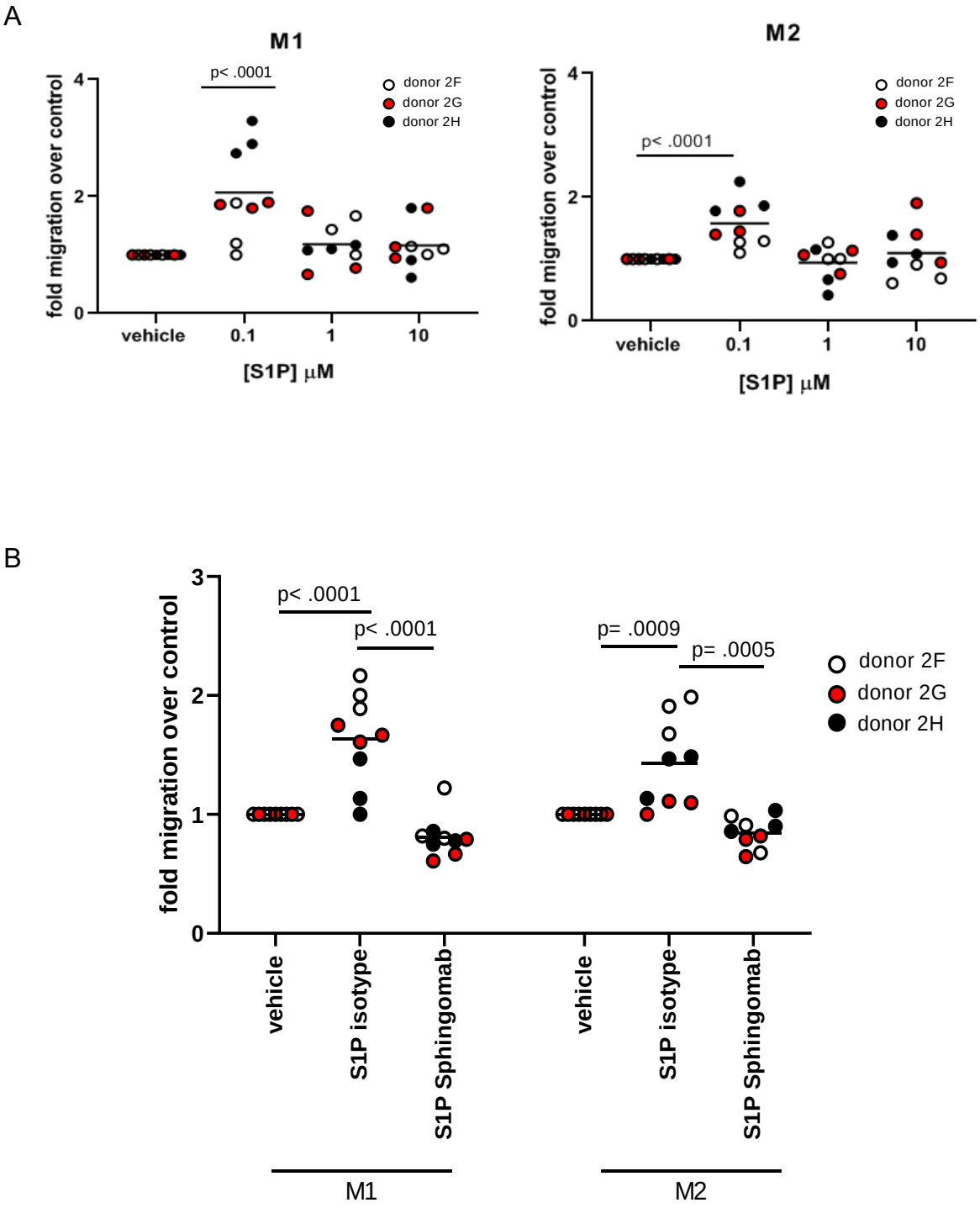

Figure 4.11 M1 and M2 polarised macrophages migrated to 0.1μM S1P. (A) M1 and M2 macrophages migrated to 0.1μM S1P but not to 1 or 10 μM S1P. Three donors tested in triplicate migrated to 0.1μM S1P M1 and M2 macrophages to 0.1μM S1P was blocked with Sphingomab in a transwell migration assay.

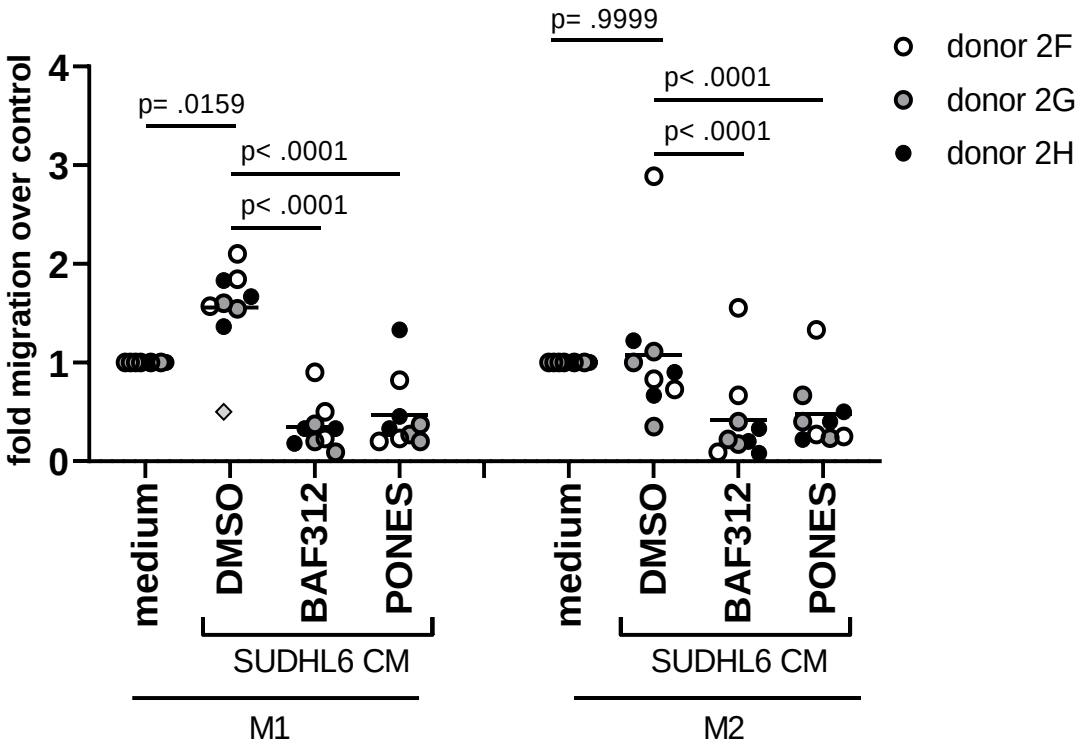

Figure 4.12 Baseline migration of M1 and M2 macrophages is S1PR1-dependent. M1 polarised macrophages showed a significant increase in migration to SUDHL6 conditioned medium and M2 macrophages showed no increase compared to controls. (Outlier ◇ was removed for 2-way ANOVA analysis). However, baseline migration of both M1 and M2 macrophages were blocked with 100nM BAF312 or with 100nM ponesimod (PONES).

4.4 Recruitment of mouse F4/80+CD11b+ cells to mouse DLBCL tumours

4.4.1 Host macrophages are recruited to xenografts tumours of DLBCL

To study the recruitment of host macrophages to tumours, xenograft models of DLBCL using cell lines were optimised. DLBCL cell lines SUDHL6, OCI-Ly1, OCI-Ly3 and U2932 were injected subcutaneously in four NSG mice each to determine engraftment kinetics. Mice injected with GCB-type DLBCL cell lines engrafted within four weeks of injection. All four mice injected with OCI-Ly1 had measurable tumours within 22 days of injection (Figure 4.13A-B). 2/4 mice injected with OCI-Ly1 reached >800mm^3 tumour volume by day 33. In SUDHL6 injected mice, 3/4 mice had measurable tumours within 33 days post injection. 2/4 mice with SUDHL6 tumours reached >800mm^3 tumour volume by day 40 post injection and one mouse never engrafted.

Mice injected with ABC-type DLBCL cell lines did not engraft as robustly compared to GCB-type DLBCL cell lines. One mouse injected with OCI-Ly3 had a measurable tumour by day 35 post injection and the tumour growth plateaued by day 50. A second mouse injected with OCI-Ly3 engrafted by day 50 and reached a tumour volume of >1000mm^3 by day 87. Two mice injected with OCI-Ly3 never engrafted. 3/4 mice injected with U2932 had measurable tumours by day 40 but the tumour growth of two of these mice

plateaued by day 45 with one mouse reaching a tumour volume of >1000mm^3 by day 54. One mouse injected with U2932 never engrafted.

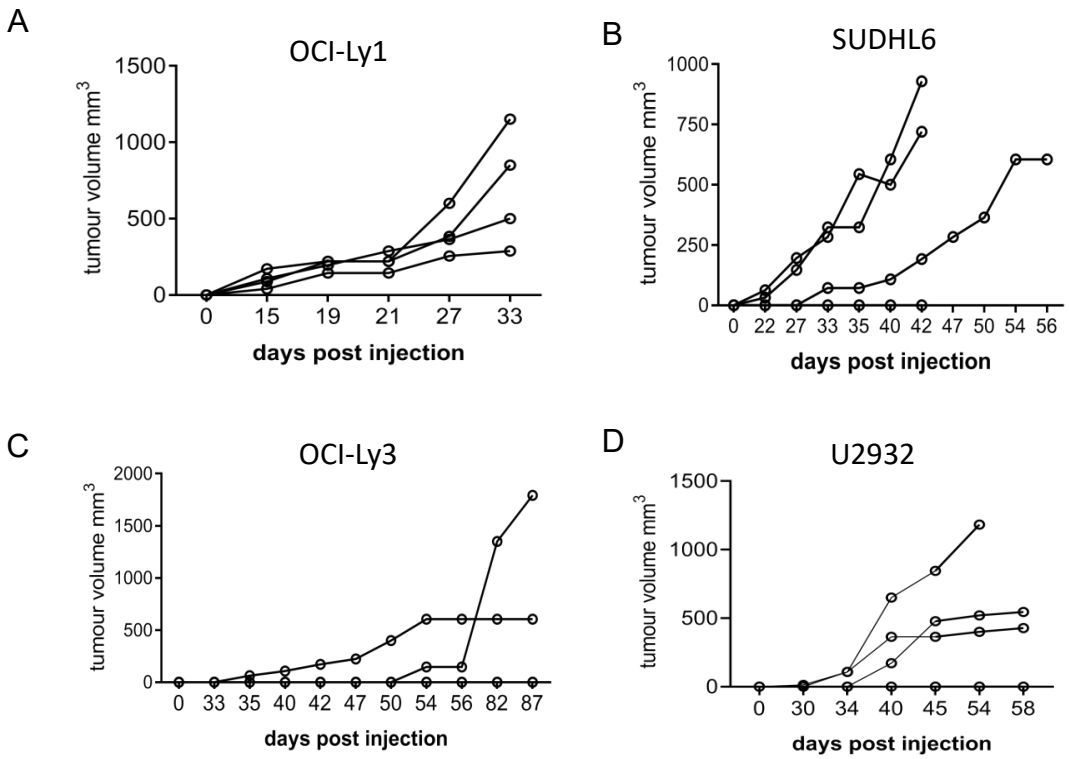

Figure 4.13 Engraftment kinetics of human DLBCL cell lines injected subcutaneously in NSG mice. (A-B) Human GCB-DLBCL cell lines were injected subcutaneously on the flank of NSG mice and monitored weekly for the presence of tumours. N=4 mice were injected for each cell line. Once tumours were palpable, they were measured every 2-3 days. All mice injected with OCI-Ly1 engrafted and 3/4 mice engrafted with SUDHL6. 2/4 mice from each cohort reached >800mm^3 tumour volume <45days post injection. (C-D) Human ABC-DLBCL cell lines were injected into N=4 mice per cell line. 2/4 mice with OCI-Ly3 injection never engrafted and the tumour growth from one mouse plateaued after 54 days post injection. In 2/4 mice injected with U2932, their tumour growth plateaued after 40 days post injection and one never engrafted.

Tumours from engrafted mice were analysed ex vivo for F4/80+CD11b+ cells. By IHC, I found F4/80+CD11b+ mouse macrophages were recruited to subcutaneous xenograft tumours of OCI-Ly1, SUDHL6, OCI-Ly3 and U2932 (Figure 4.14). The presence and F4/80+CD11b+ cells in these xenografts were also confirmed by flow cytometry. Representative dot plots of gating strategy for F4/80+CD11b+ are shown (Figure 4.15A). Mouse CD45+ cells were present in subcutaneous (SC) xenografts at levels around 1-10% of the tumour population (Figure 4.15B). Within the mCD45 populations, about 80-90% were F4/80+CD11b+ (Figure 4.15B). The presence of mouse B220 and mouse CD3 was also assessed. There was a small population of B220+ cells and there was no population of CD3+ cells (Figure 4.15C). Xenografts from OCI-Ly3 and U2932 had a lower percentage of mouse CD45 and F4/80+CD11b+ cells in the tumour than SUDHL6 and OCI-Ly1 xenografts (Figure 4.16).

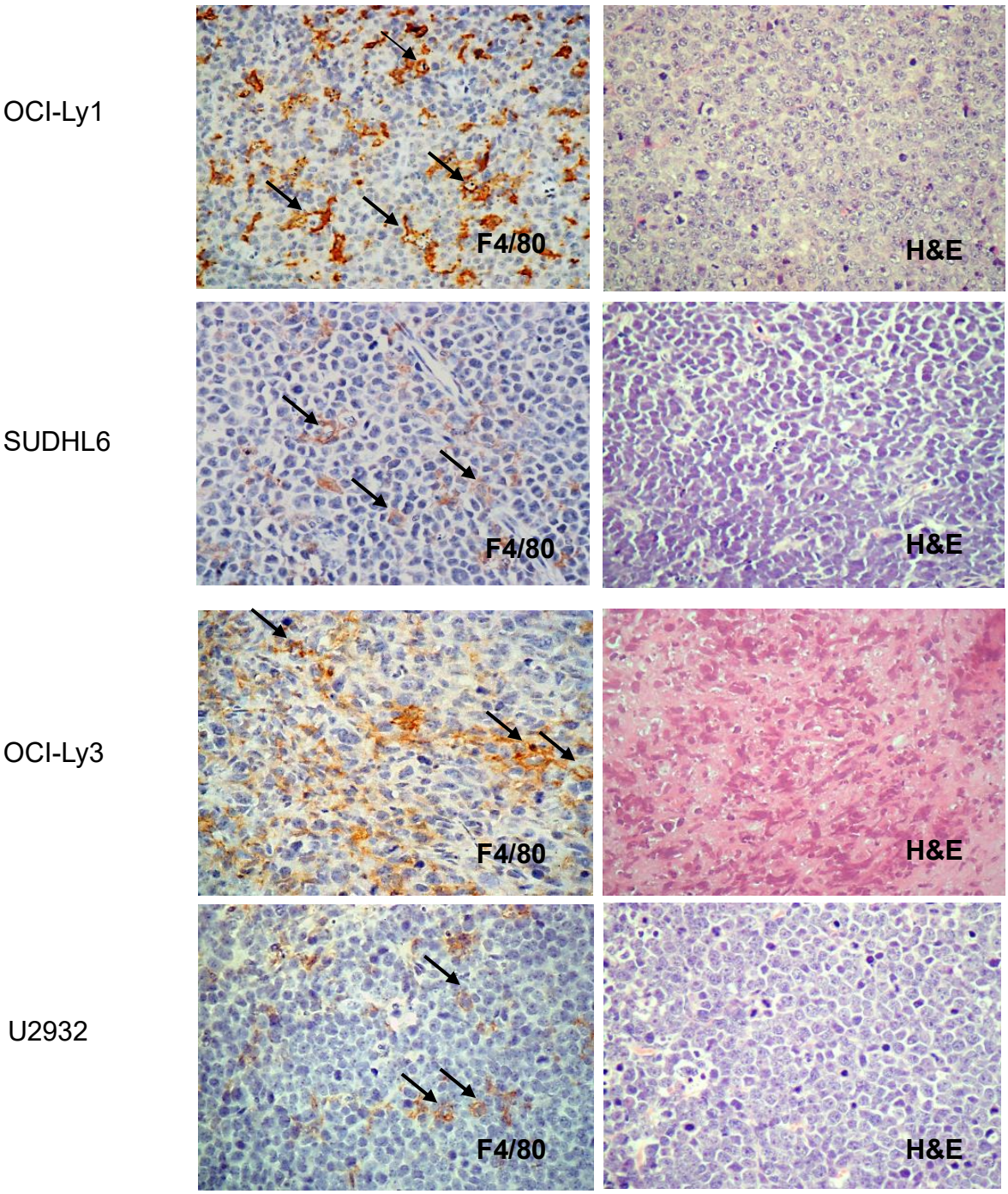

Figure 4.14 IHC analysis of tumours from engrafted mice showed an infiltration of host F4/80+ cells. Representative images of F4/80 staining from each DLBCL cell line grown as xenografts engraftment kinetics study. All tumours had positive staining for F4/80 visible throughout (examples of positive F4/80 cells indicated by black arrows).

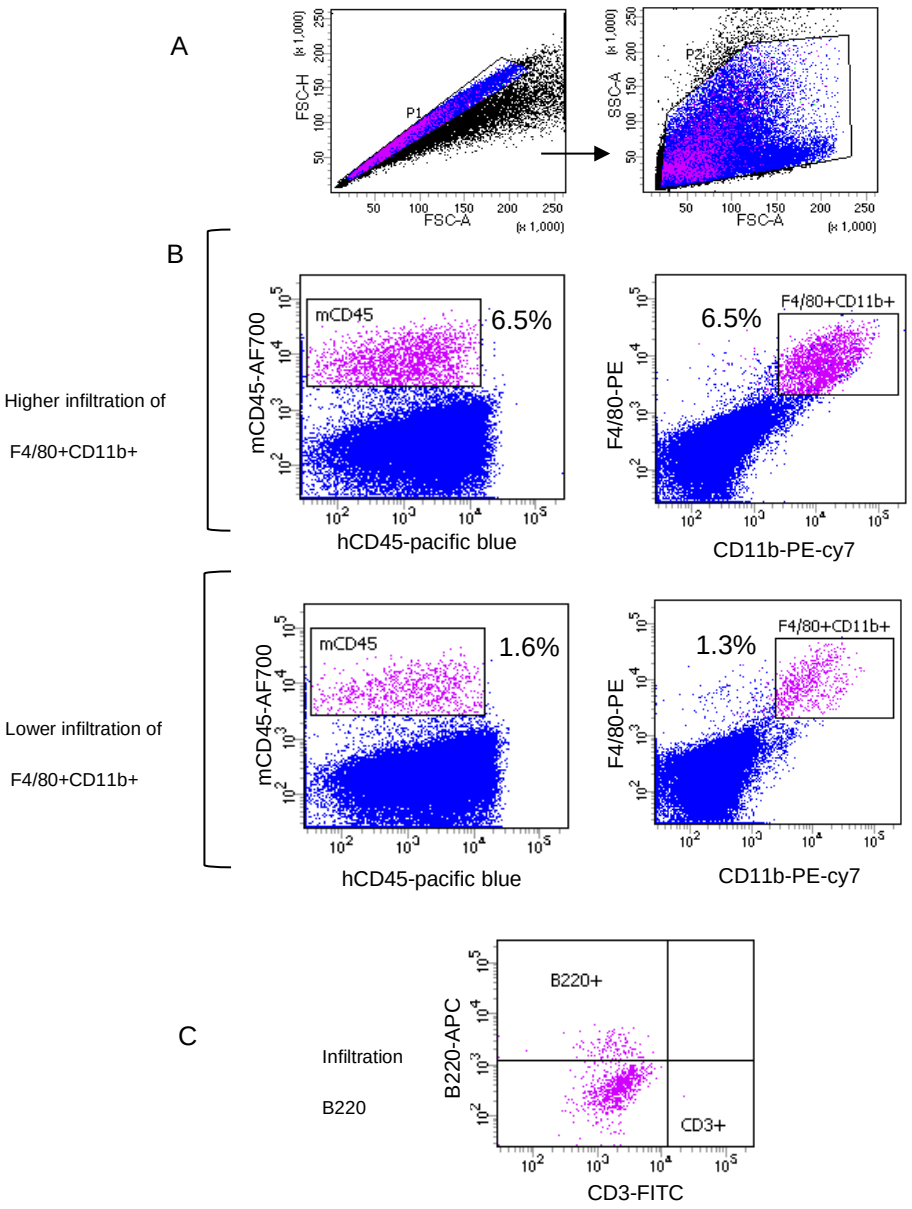

Figure 4.15 Gating strategy for flow cytometry analysis of xenograft tumours. Representative dot plots showing gating strategy for flow cytometry analysis of xenograft tumours. (A) Singlet population was gated. Then from this, cells were gated to exclude debris and dead cells. (B) Tumours from each mouse had variable levels of mouse CD45 ranging from a minimum 0.5% to a maximum of 10% mouse CD45 in tumours. From the mouseCD45 population, I gated for mouse F4/80, CD11b, B220, and CD3 positive populations. Shown are representative dot plots of high and low infiltration of mouse CD45+F4/80+CD11b+ from the same experiment injected with SUDHL6. The majority if not all of the mouse cells found to infiltrate the xenografts were F4/80+CD11b+. (C) There was only a small population of B220+ cells making up <1% of infiltration mouse population as shown by the representative dot plot and no significant staining for CD3.

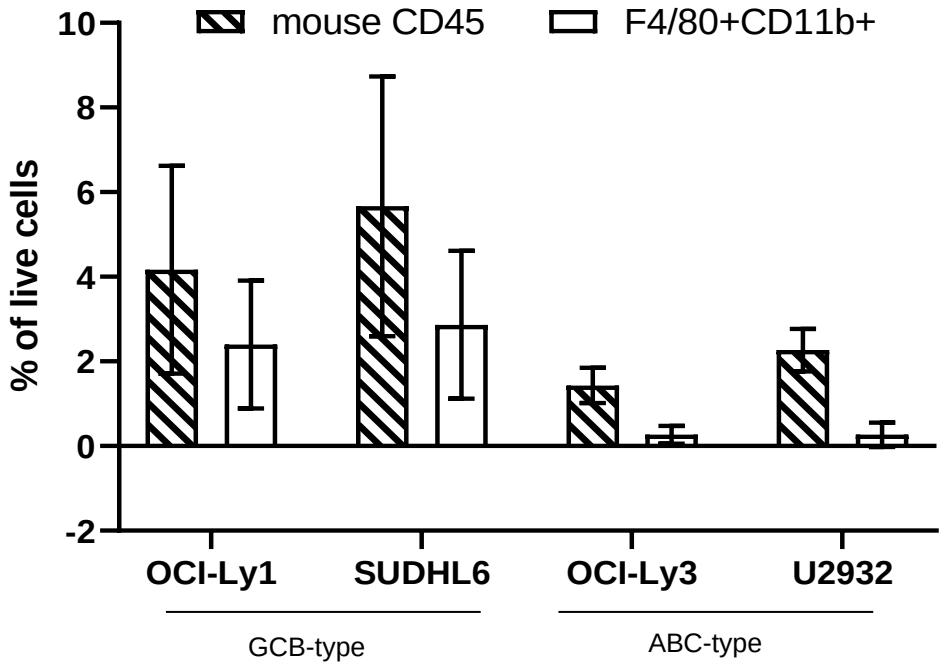

Figure 4.16 Percentage of mouse CD45+ and F4/80+CD11b+ varied between GCB and ABC-type DLBCL cell line xenografts. The percentage of mouse CD45 cells varied between the xenografts derived from DLBCL cell line. The two GCB-type DLBCL xenografts had a higher percentage of mouse macrophage infiltration than the ABC-type DLBCL xenografts.

4.4.2 Reduced infiltration of F4/80+CD11b+ cells in xenograft tumours from mice treated with BAF312

OCI-Ly1 and SUDHL6 xenografts from mice treated with 3mg/kg BAF312 had reduced F4/80+CD11b+ infiltration to their tumours compared to vehicle treated mice. Xenografts were established using OCI-Ly1 and SUDHL6 in NSG mice. OCI-Ly1 engrafted mice were given 3mg/kg BAF312 or vehicle on Monday, Wednesday, and Friday for total of 3 doses. Experiment ended when at least one mouse had a tumour length of 1.1cm, the maximum tumour size under our Home Office project licence. Flow cytometry gating strategy to determine absolute numbers of the F4/80+CD11b+ cells in xenografts (Figure 4.17). There was no significant difference in tumour volume between BAF312 and vehicle treated mice (Figure 4.18A). BAF312 was well tolerated with no weight loss observed (Figure 4.18B). Flow cytometry for F4/80+CD11b+ cells in xenografts were significantly reduced in BAF312 treated tumours (Figure 4.18C).

SUDHL6 engrafted mice were given 3mg/kg BAF312 or vehicle every other day for a total of five doses. There was a significant difference in tumour volume on day 26 (Figure 4.19A). Mice did not lose body weight throughout treatment with BAF312 (Figure 4.19B). Flow cytometry analysis of SUDHL6 xenograft tumours, showed there was a significant decrease in the absolute number of F4/80+CD11b+ cells compared to vehicle treated xenografts (Figure 4.19C).

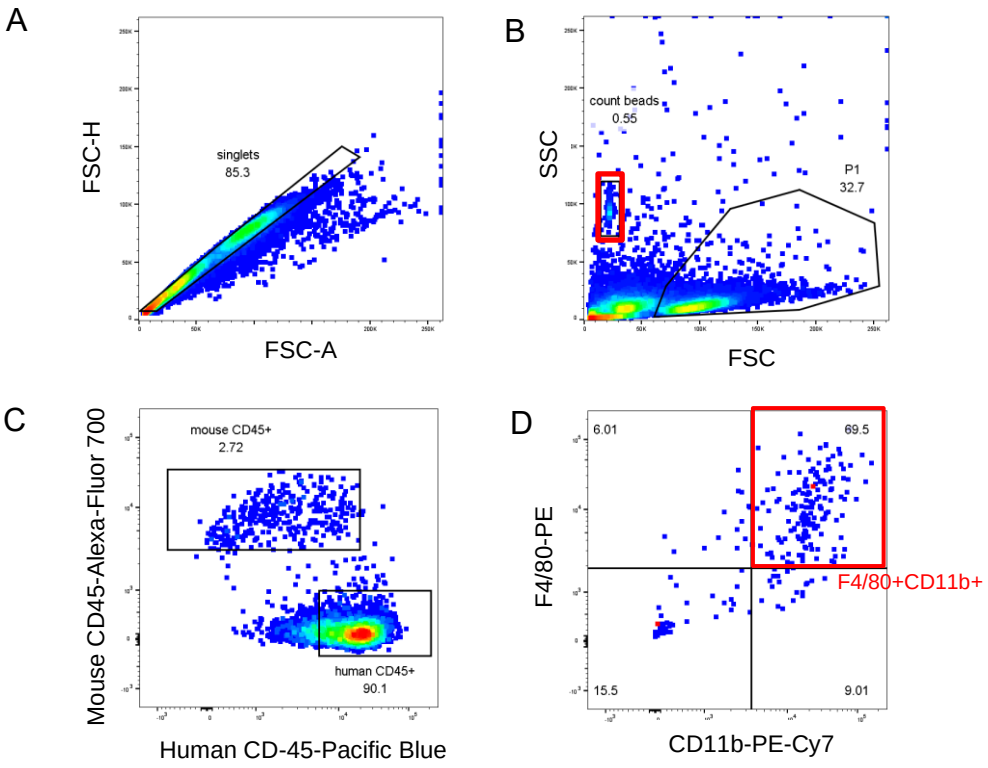

Figure 4.17 Gating strategy for quantitating absolute numbers of F4/80+CD11b+ cells in xenograft tumours. Representative dot plots showing gating strategy for flow cytometry quantitation of xenograft tumours using Count Bright beads. (A) First singlets were gated. (B) Count Bright beads and live cells were gated on FSC/SSC. (C) From this gate, mouse CD45-AlexaFluor 700 vs human CD45-Pacific blue gates were set and (D) from cells in mouse CD45 gate, I gated on F4/80-PE and CD11b-PECy7. See Materials and Methods for method of calculating absolute numbers using Count Bright beads.

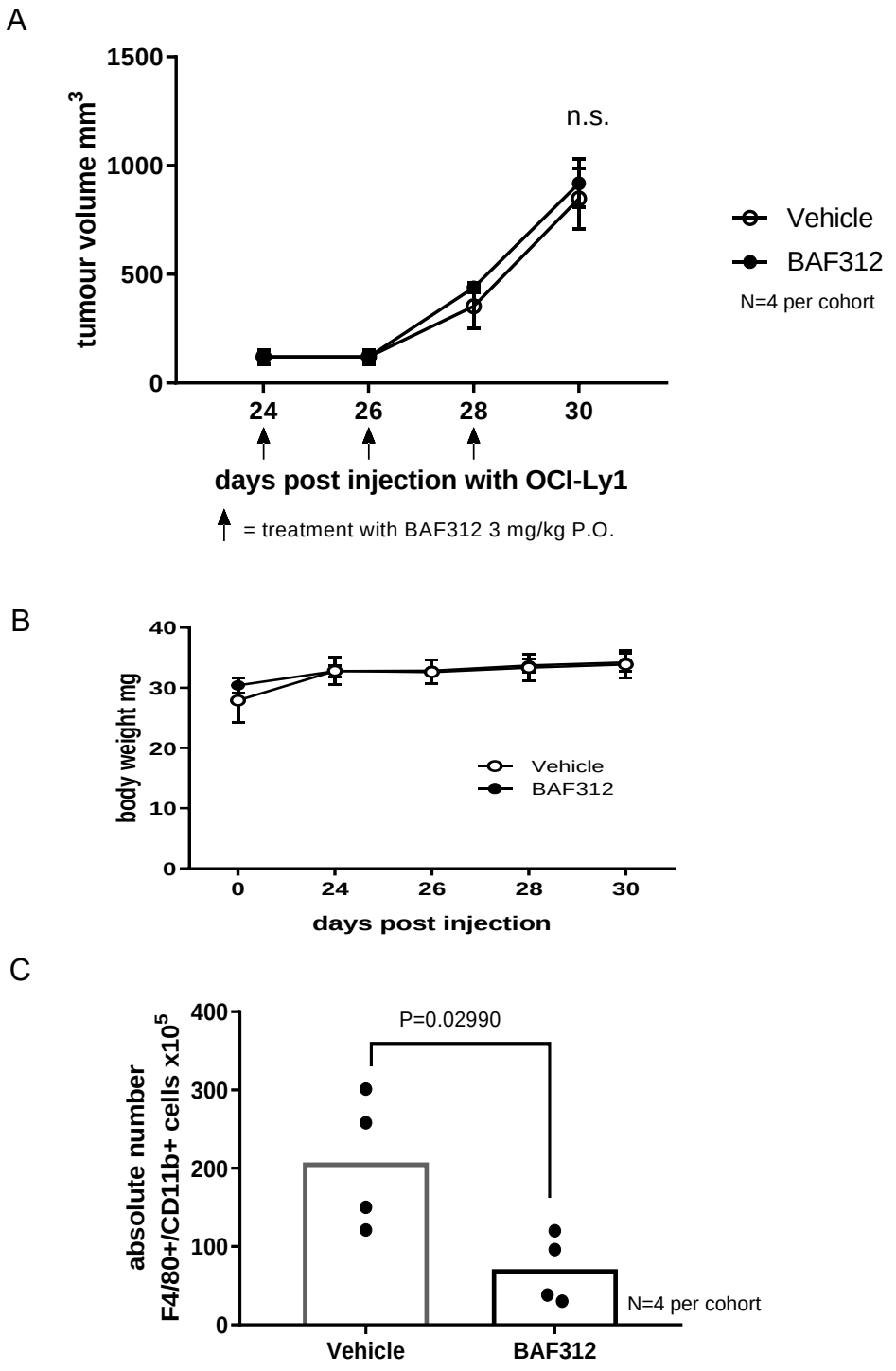

Figure 4.18 BAF312 reduced infiltration of F4/80+CD11b+ cells to OCI-Ly1 xenografts. (A) Tumour measurements show there was no difference in the tumour volumes of vehicle compared to BAF312 treated mice. There were 4 mice per treatment group. I performed these experiments published in Lupino *et al* (2019). (B) 3mg/kg daily treatment with BAF312 was well tolerated and body weight remained steady throughout study. (C) Flow cytometry analysis of tumours did show a significant reduction of F4/80 +CD11b+ mouse cells.

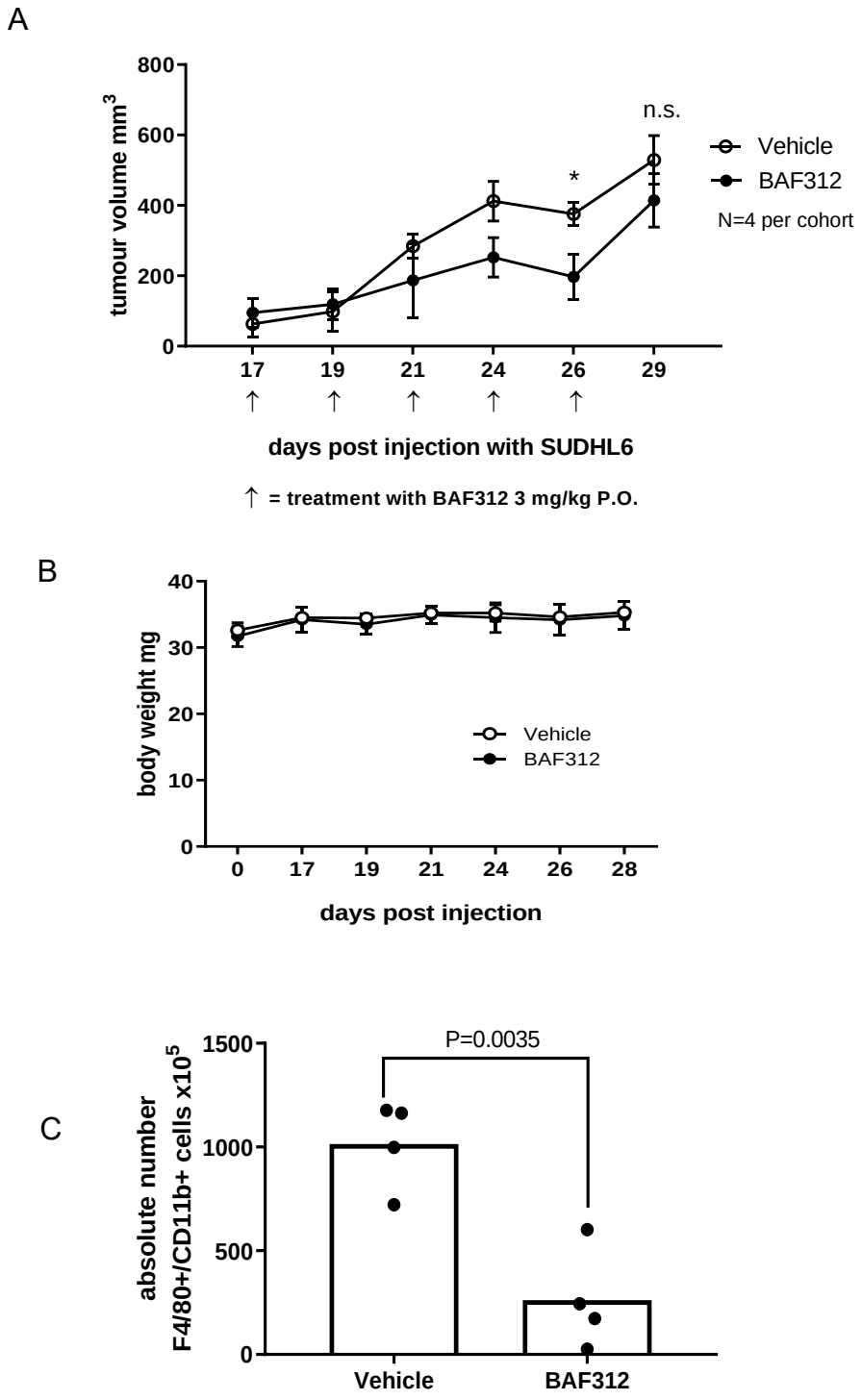

Figure 4.19 BAF312 reduced infiltration of F4/80+CD11b+ cells to SUDHL6 xenografts. (A) Tumour measurements show there was a significant difference in the tumour volumes of vehicle compared to BAF312 treated mice on day 26. There were 4 mice per treatment group. I performed these experiments published in Lupino *et al* (2019) (B) 3mg/kg daily treatment with BAF312 was well tolerated and body weight remained steady throughout study. (C) Flow cytometry analysis of tumours did show a significant reduction of F4/80 +CD11b+ mouse cells.

SUDHL6 xenografts treated with BAF312 were also evaluated for apoptosis marker, cPARP (Lupino et al., 2019). There was an increase in cPARP in the tumours treated with BAF312 compared to vehicle treated tumours (Figure 4.20A). This is in keeping with the anti-apoptotic effect of S1P which was reduced with the inhibition of S1PR1. Total number of CD31+ cells, endothelial cells, was measured by flow cytometry and there was a reduction of endothelial cells in BAF312 treated animals (Figure 4.20B).

A

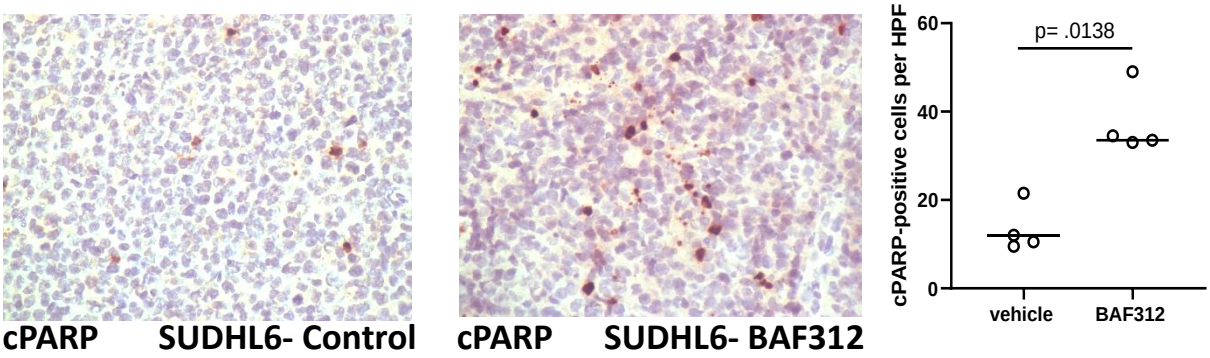

B

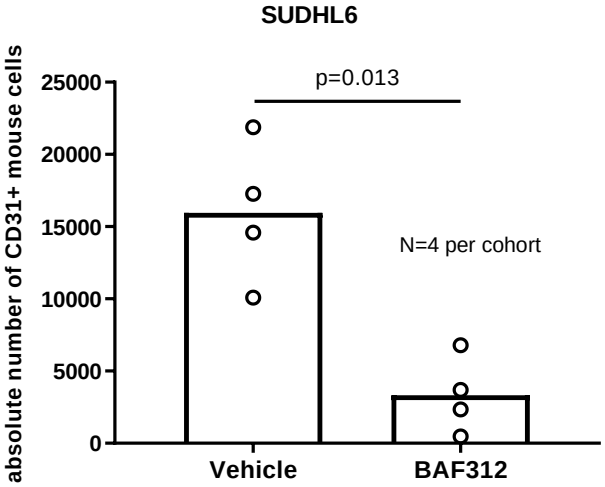

Figure 4.20 cPARP expression was increased and absolute numbers of CD31 was decreased in BAF312 treated SUDHL6. (A) Representative images of SUDHL6 xenografts treated with control or BAF312 3mg/kg were evaluated for presence cPARP as measure of apoptosis. BAF312 treated animals had increased apoptosis compared to control. cPARP counts show a significant increase of cPARP staining in the BAF312 treated tumours compared to control. Staining was performed by Dr Gary Reynolds and counts per 3xHPF (40x) was performed by pathologist, Dr Matt Pugh (Lupino*et al*, 2019). Student's t-test was used to determine value. (B) Mouse CD31 was evaluated in DLBCL xenografts treated with BAF312. There was a significant reduction of CD31 in SUDHL6 BAF312 treated tumours. I analysed tumours for CD31 by flow cytometry published in Lupino *et al* (2019).

4.4.3 Optimising A20, a syngeneic model of DLBCL

A20 mouse lymphoma was derived from an aging BALB/c mouse and therefore, could be engrafted in immune competent BALB/c mice (Donnou et al., 2012, Kim et al., 1979, Palmieri et al., 2010). Engraftment kinetics of A20 cells injected subcutaneously (SC) and intravenously (IV) in BALB/c mice is shown in Figure 4.21. SC will result in solid tumour on flank and IV injection leads to systemic engraftment including spleen and liver involvement.

Three BALB/c mice subcutaneously injected with A20 had measurable tumours on day 13. These tumours reached maximum tumour size by day 27 in 3/3 mice injected (Figure 4.21A). Flow cytometry showed that F4/80+ CD11b+ cells had infiltrated the SC A20 tumours. Using three more BALB/c mice, A20 cells were injected IV in the tail vein and were monitored every other day by palpation of the abdomen, for body condition, and body weight. While the IV injected mice did not lose body weight or show signs of reduced body condition, enlarged organs were detected by palpation of the abdomen. IV injected mice were culled on day 27 where post-mortem revealed significant enlargement of both spleen and liver in A20 engrafted mice compared to controls (Figure 4.21B). H&E staining confirmed the presence of neoplastic lesions in the engrafted spleens and livers (Figure 4.22A-B). The population of F4/80+CD11b+ cells were significantly higher in engrafted mice compared to normal BALB/c spleens and livers. This was confirmed by IHC staining for F4/80 in SC tumours where there was an increased infiltration in engrafted spleens and liver compared to normal liver and spleen (Figure 4.22A-B).

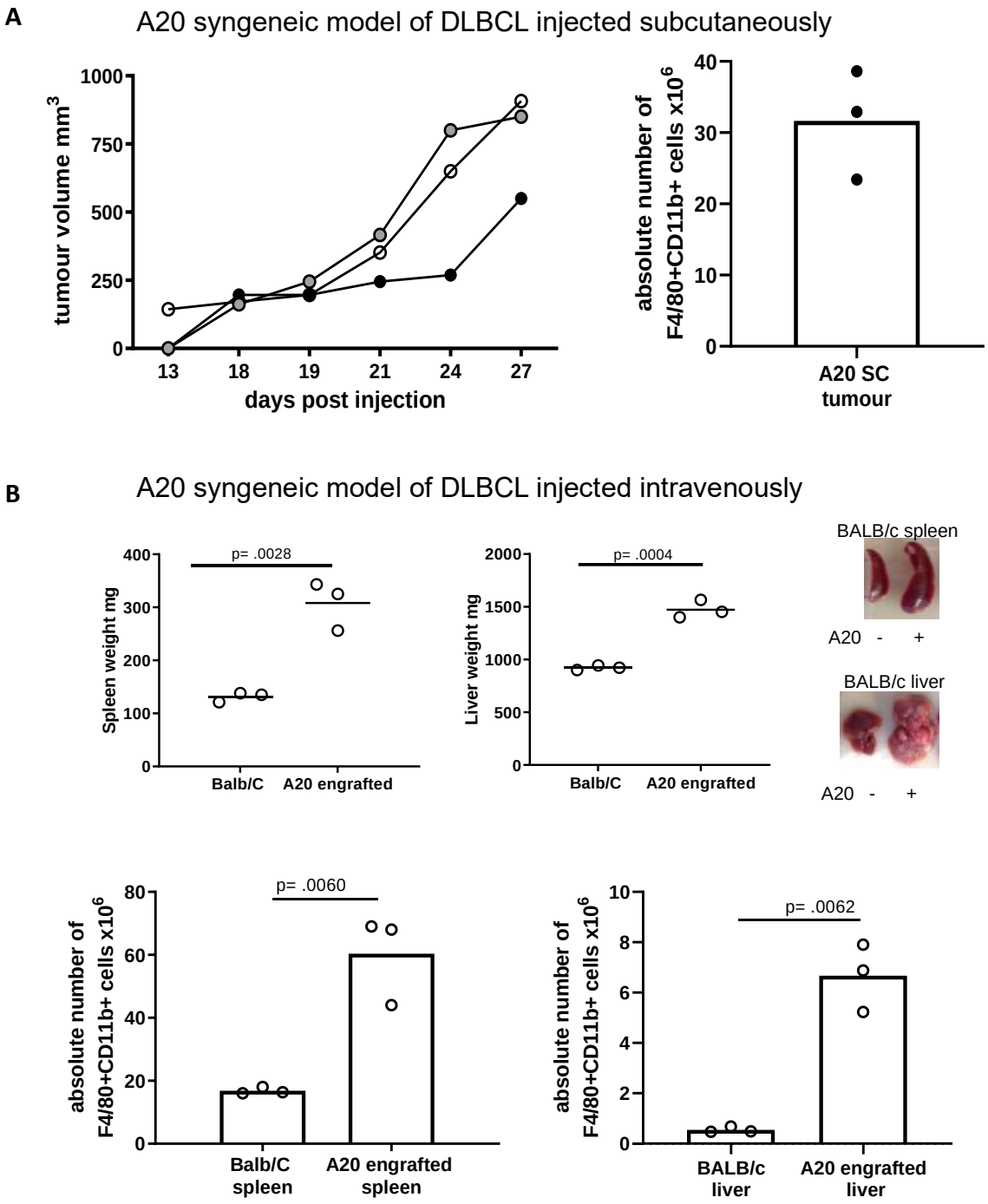

Figure 4.21 Determining engraftment kinetics of mouse DLBCL cell line, A20, injected subcutaneously or intravenously in BALB/c mice. (A) A20 cells were injected subcutaneously on the flank of BALB/c mice. Once tumours were measurable, they were measured every 2-3 days. N=3 mice were injected. By day 27, 3/3 mice engrafted with A20 at maximum tumour length of 1.1cm. SC tumours have an infiltration of F4/80+CD11b+ host mouse cells. (B) A20 cells were injected intravenously in the tail vein of BALB/c mice. Mice were monitored weekly by abdomen palpation. Mice were culled at day 27 as abdomen palpation indicated enlarged spleens compared to control. F4/80+CD11b+ macrophages were increased in the engrafted spleens and livers.

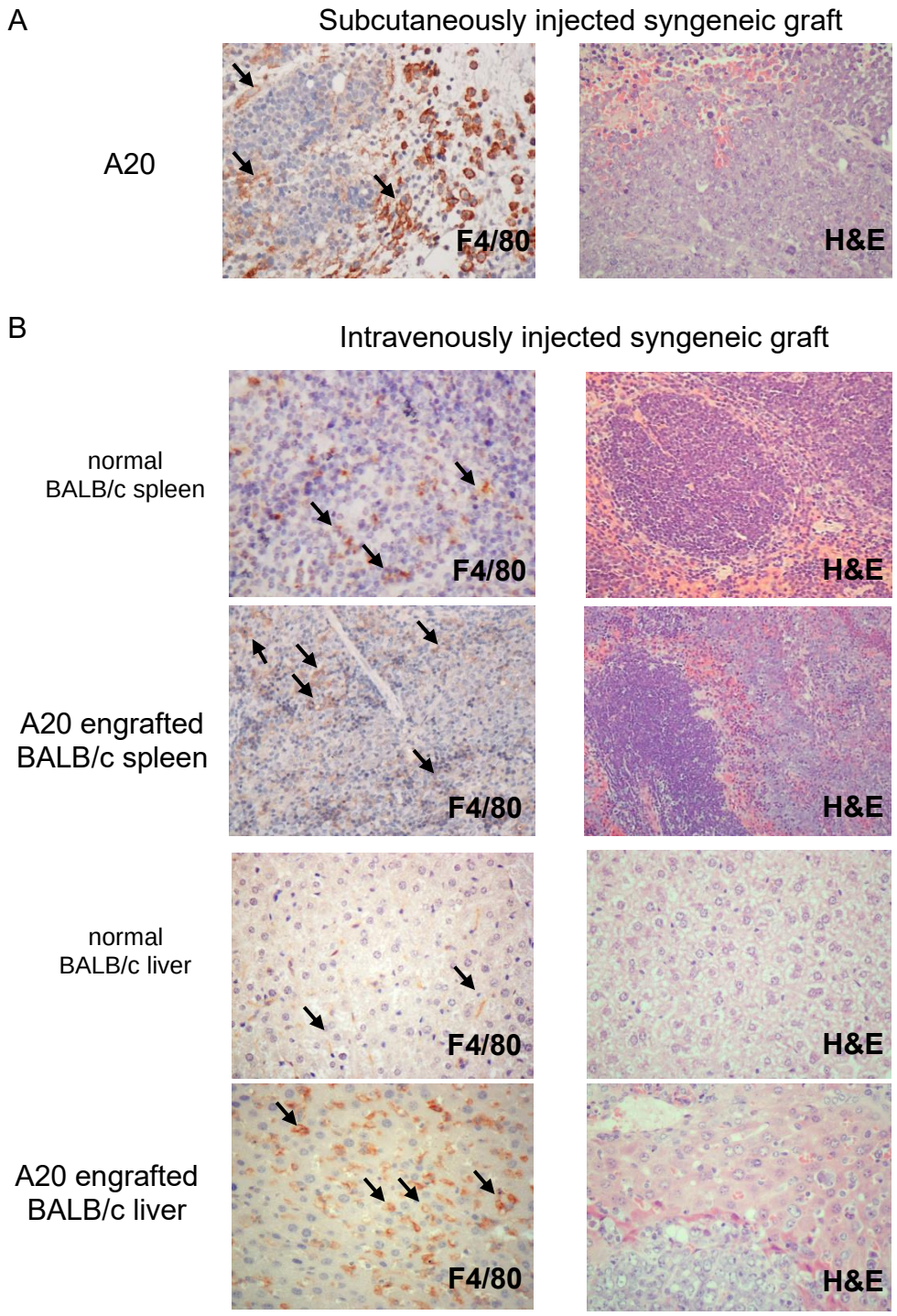

Figure 4.22 F4/80+ cells present in SC tumours, spleen and liver tumours from A20 engrafted mice. Representative images of F4/80 staining A20 engraftment kinetics study. (A) A20 cells injected subcutaneously in BALB/c mice show an infiltration of F4/80+ cells. Black arrows indicate positive F4/80 staining. (B) A20 cells injected IV in BALB/C mice with tumour engraftment to spleen and liver. Resulting tumours had positive staining for F4/80 visible throughout the tumours. H&E staining shows presence of lesions in engrafted spleen and liver compared to controls.

4.4.4 Reduced infiltration of F4/80+CD11b+ cells to spleen and liver from systemically engrafted A20 after BAF312 treatment

A20 engrafted BALB/c mice were treated on day 4 post IV injection with 3mg/kg BAF312. Mice were treated every other day except weekends for three weeks for a total of nine doses with BAF312. On day 25 mice were culled and liver and spleen weights were compared with three normal BALB/c mice. Spleen and liver were significantly enlarged in vehicle treated mice compared to normal mice (Figure 4.23A). Treatment with BAF312 did not significantly reduce spleen or liver weight (Figure 4.23A). Spleens and livers from BALB/c, vehicle or BAF312 treated mice were analysed by flow cytometry for F4/80+CD11b+ cells. There was a significant reduction in F4/80+CD11b+ cells in BAF312 treated mice compared to vehicle (Figure 4.23C). Again BALB/c mice tolerated treatment with BAF312 during three weeks of daily dosing (except weekends) and showed no weight loss throughout experiment (Figure 4.23B).

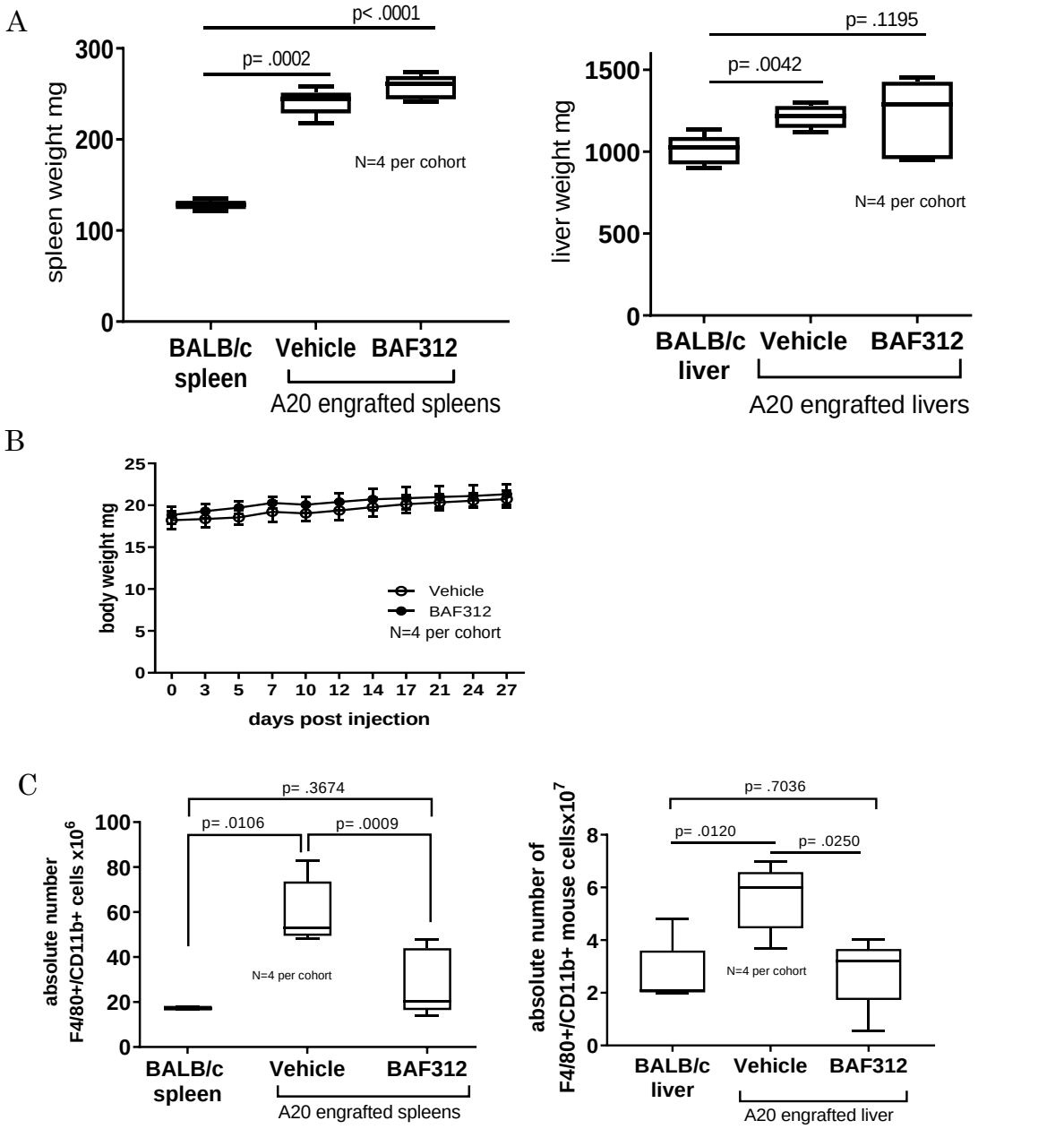

Figure 4.23 In vivo effects of BAF312 in A20 syngeneic grafts. A20 was injected in BALB/c mice by IV injection. On Day 4, mice were randomised into vehicle and BAF312 treatment groups. Mice were given vehicle or 3 mg/kg BAF312 P.O. Three times a week for three weeks. Mice were culled on day 27. (A) Spleen and liver weight of engrafted mice (N=5 per group) was significantly higher than normal BALB/c spleen (N=3). There was no significant difference in spleen or liver weight in BAF312 treated mice compared to vehicle. I performed these experiments published in Lupino *et al* (2019). (B) Body weight of mice remained unchanged throughout treatment. (C) Spleen and liver from BALB/c were analysed by flow cytometry for F4/80 and CD11b. Spleen and liver from mice treated with BAF312 had lower total F4/80CD11b + cells than vehicle treated mice although spleen and liver weight were not significantly different.

4.5 Discussion

TAMs are largely made up of recruited monocytes that have been polarised within the microenvironment but can also include tissue resident macrophages (Franklin and Li, 2016). There is contradicting evidence on the effect of macrophage infiltration on prognosis in DLBCL which may be to the different methods, reagents, and cohorts used to evaluate macrophages in DLBCL (Shen et al., 2016, Wang et al., 2017, Gomez-Gelvez et al., 2016, Hasselblom et al., 2008, Konig et al., 2010). Nonetheless, macrophages are the dominant non-malignant cell type in DLBCL tumours and evidence continues to accumulate showing that macrophages contribute to the pathogenesis of DLBCL (Pham et al., 2018, Li et al., 2019, Scott and Gascoyne, 2014).

Ceramide/sphingosine was shown to induce apoptosis while S1P had an anti-apoptotic effect as discussed in the Introduction section 1.4.5. The S1P secreted by apoptotic cells is said to be primarily formed by SPHK2 and while extracellular S1P, considered to be the onco-lipid, is formed by SPHK1 (Gude et al., 2008, Weigert et al., 2006). Therefore, cell death or apoptosis in monocytes and macrophages after S1P treatment was not evaluated. Apoptosis was evaluated in the xenograft tumours treated with BAF312 which indicated

GM-CSF M1 and M-CSF M2 had different phenotype shown by the absence of CD163+ in GM-CSF polarised M1 macrophages as well as typical IL-10 and IL-12 cytokine profiles for M1 and M2. Despite this, the S1P

receptor expression for M1 and M2 macrophages were similar. Both M1 and M2 had lower *S1PR1* expression and higher *S1PR2* expression compared to matched monocytes. This is in keeping with migration results to S1P.

This inverse expression of *S1PR1* and *S1PR2* has been reported in dendritic cells. In immature dendritic cells, *RAC* signalling by *CCL19/CCR7* binding is limited whilst binding of S1P to *S1PR2* leads to higher *RHO* signalling (Konig et al., 2010). Increased *RHO* results in translocation of *FHL2* to the nucleus inhibiting *S1PR1* expression. As dendritic cells mature, *CCR7* surface expression increases and *S1PR2* expression decreases leading to increased *RAC* and increased expression of *S1PR1* (Konig et al., 2010, Spiegel and Milstien, 2011). *S1PR2* was also shown to antagonise *S1PR1* expression in endothelial cells where the balance of signalling through these receptors regulated their migration (Spiegel and Milstien, 2011).

Previous reports of expression of S1P receptors in monocytes and macrophages have mainly been described in mouse macrophages (Muller et al., 2017, Yang et al., 2018). Expression of *S1PR1, S1PR2* and *S1PR5* were decreased in M1 and M2 macrophages compared to monocytes and *S1PR2* expression was significantly increased. Whilst, expression of *S1PR3* and *S1PR4* was higher in M2 macrophages but lower in M1 macrophages compared with monocytes (Muller et al., 2017). Muller's results with mouse macrophages were similar with the S1P receptor expression profiles reported in this thesis for human macrophages. Discrepancies may be attributed to species differences as well as to the different polarisation methods used.

S1PR1 is important for migration while *S1PR2* is important in cell retention (Wang et al., 1999). With most cells expressing all 5 S1P receptors, the binding of S1P is preferential for *S1PR1* as it has the highest affinity for S1P (Hanson and Peach, 2014). Antagonism of *S1PR1* is an accepted intervention for the treatment of diseases such as multiple sclerosis and there is evidence it may be therapeutic for the treatment of DLBCL (Hanson and Peach, 2014, Liu et al., 2012). Several antagonists to S1PR1 have been developed; ponesimod, ozanimod, and BAF312 that are potent and highly specific (O'Sullivan and Dev, 2013). Both ponesimod and BAF312 blocked migration of monocytes to DLBCL conditioned medium showing that migration to DLBCL was mediated by S1PR1 signalling.

S1PR2 is a tumour suppressor in DLBCL (Stelling et al., 2018). Despite the low expression of *S1PR2* in malignant B cells, a lower *S1PR1/S1PR2* ratio of expression in TAMs may lead to increased recruitment and retention of macrophages. Several studies has found that increased number of macrophages confers a better survival for patients with R-CHOP (Riihijarvi et al., 2015, Wang et al., 2017, Marchesi et al., 2015). S1P attracts monocytes and macrophages in DLBCL where it can contribute to therapeutic responses. BAF312 blocked the migration of monocytes *in vitro* and *in vivo* although reducing the infiltration of monocytes/macrophages may not be sufficient to reduced tumour volume. It remains to be established if this is an appropriate treatment strategy given that S1P could potentially prevent therapeutic responses.

CHAPTER 5

Evaluating the effect of S1P on phagocytosis of rituximab-opsonised DLBCL

Chapter 5

Evaluating the effect of S1P on phagocytosis in rituximab-opsonised DLBCL

5.1 Introduction

Macrophages are vital players in innate immunity providing first-line defence during inflammation and infection (Mills and Ley, 2014). Once monocytes arrive to the site of inflammation, they can be classically activated, secreting inflammatory cytokines to recruit other immune cells. As the inflammation subsides, the switch from an inflammatory state to a wound healing state requires the removal of neutrophils by apoptosis and phagocytosis. S1P acts as a "find me" signal released by apoptotic cells recruiting more monocytes via S1PR1 to phagocytose dying cells. (Martinez and Gordon, 2014, Shi and Pamer, 2011, Mantovani et al., 2010, Wang et al., 1999) Besides recruitment of macrophages, McQuiston *et al* demonstrated that at lower concentrations of S1P there was an increase in phagocytic index while at higher concentrations such as 1μM S1P there was a reduction in the phagocytic index of *Cryptococcus neoformans* by alveolar macrophages (McQuiston et al., 2011).

In the previous chapter, tumours were shown to have elevated S1P levels can mimic this "find me" signal and recruit monocytes/macrophages to the tumour site. Next, high concentrations of S1P in DLBCL were examined

in the context of macrophage function, phagocytosis (Nagahashi et al., 2012, Kunkel et al., 2013). Specifically, *in vitro* polarised macrophages were assessed for their ability to phagocytose latex beads and of rituximab-treated DLBCL cell lines in the presence of S1P.

5.2 Phagocytosis of FITC+ latex beads

5.2.1 Establishing the optimum time point for phagocytosis assays

To establish the optimal timepoint to study phagocytosis, a time course experiment was done using three donors. M1 and M2 macrophages from these donors were stained with eFluor450 dye and resuspended to $1x10^6$ cells /ml. In flow cytometry tubes, 100µl of the macrophage cell suspension was added to 1µl of FITC+ beads (Figure 5.1). Macrophages were incubated with beads for 15, 30, 60, and 90 minutes. Trypan blue was added to quench the signal from FITC+ beads not engulfed by macrophages. Phagocytosis was then assessed by flow cytometry for eFluor450+ macrophages that have engulfed FITC+ beads. Representative dot plots that illustrated the gating for FITC+ eFluor450+ macrophages are shown in Figure 5.2A. The phagocytosis ratio was calculated by dividing the number of FITC+ eFluor450+ macrophages by the total number of macrophages counted. Median fluorescent intensity (MFI) for FITC was also measured for each sample. For some donors, phagocytosis already began to slow at 90 minutes (Figure 5.2B-C). Therefore, this time point was chosen for subsequent assays.

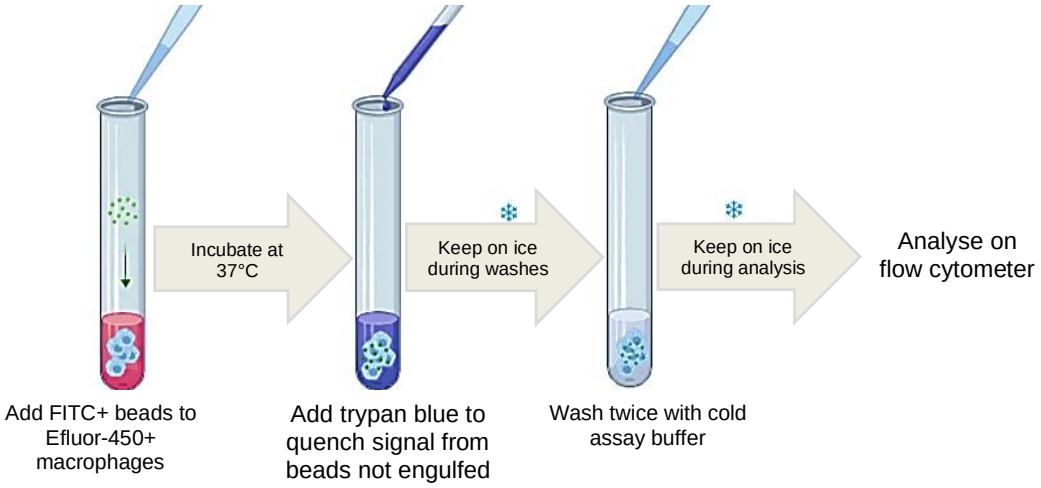

Figure 5.1 Flow diagram of phagocytosis assay using FITC+ beads.
Macrophages were resuspended in 1%FBS/RPMI 1640 and added to FACS tubes. FITC+ beads were then spiked into the FACS tube in 1:100 dilution. FACS tubes were incubated at 37°C for 15, 30, 60, and 90 minutes. At each time point, a FACS tube was removed from the incubator and trypan blue was added to quench beads that had not been phagocytosed. The cells were kept on ice and washed twice with cold assay buffer. Tubes were kept cold until analysed on the flow cytometer.

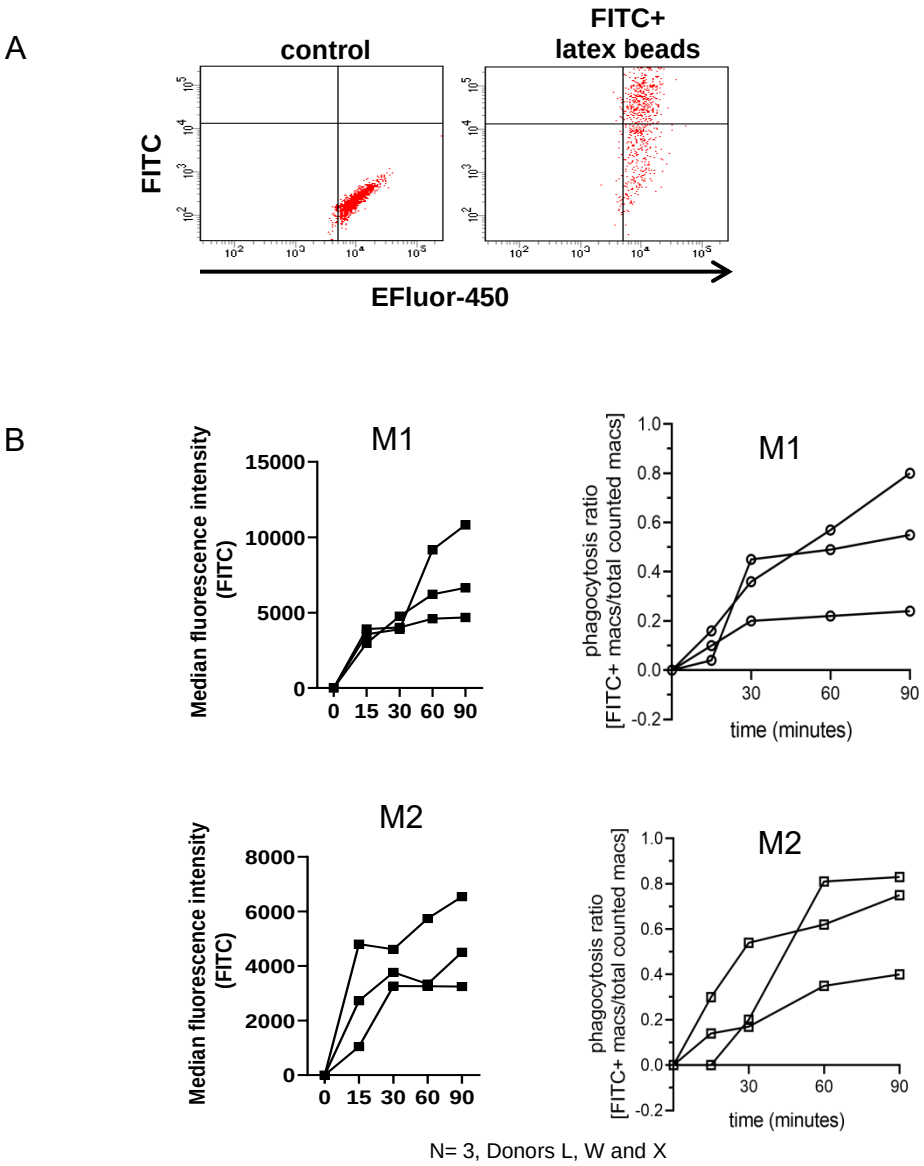

Figure 5.2 Time course to determine optimal time point for phagocytosis *in vitro* (A) Representative graphs of FITC+ rabbit IgG coated latex beads incubated with macrophages and analysed by flow cytometry. Macrophages with no beads were used as controls. (B) $1x10^5$/100µl of macrophages from three donors were incubated with beads in 1:100 ratio at 37°C for 15 min, 30 min, 60 min, and 90 min. The mean fluorescent intensity of FITC was plotted for each time point. In addition, the number of FITC+ macrophages/total number of macrophages counted was used to calculate a phagocytosis ratio. Time point of 90 min was used in subsequent phagocytosis assays.

5.2.2 S1P-treated M1 had reduced phagocytosis of FITC+ beads

Next, the effect of S1P on phagocytosis was examined. To do this, M1 and M2 macrophages from at least two donors in three independent experiments was pre-treated with 1μM S1P for one hour followed by the addition of FITC+ beads. The samples were analysed by flow cytometry as previously described in Figure 5.1. M1 macrophages treated with 1μM S1P had significantly reduced phagocytosis across all seven donors tested. In contrast, S1P had no effect on phagocytosis by M2 macrophages (Figure 5.3A).

To validate the flow assay, microscopy was used to visualise FITC+ macrophages. Macrophages from six donors were plated in duplicate on 8-well chamber slides in two separate experiments. Cells were treated with 1μM S1P or vehicle for one hour before FITC+ beads were added in a ratio of 1:100. Then five high-power fields (40x) from duplicate wells were counted, then the phagocytosis ration was calculated but taking the total number of FITC+ macrophages as a proportion of the total number of macrophages. Using this method, reduced phagocytosis by M1 macrophages in the presence of 1μM S1P compared with vehicle was observed (Figure 5.3B). Overall, there were fewer FITC+ M2 macrophages and no difference between S1P treated and vehicle treated (Figure 5.3B).

Having shown that macrophages can phagocytose FITC+ beads, next phagocytosis of DLBCL cell lines was examined. Flow cytometry was used to assay phagocytosis in order to rapidly assess more samples and conditions in a

single experiment. Analysis by phagocytosis ratio and median fluorescent intensity (MFI) provided similar results, therefore the phagocytosis ratio was used as the measure of phagocytosis of DLBCL cell lines.

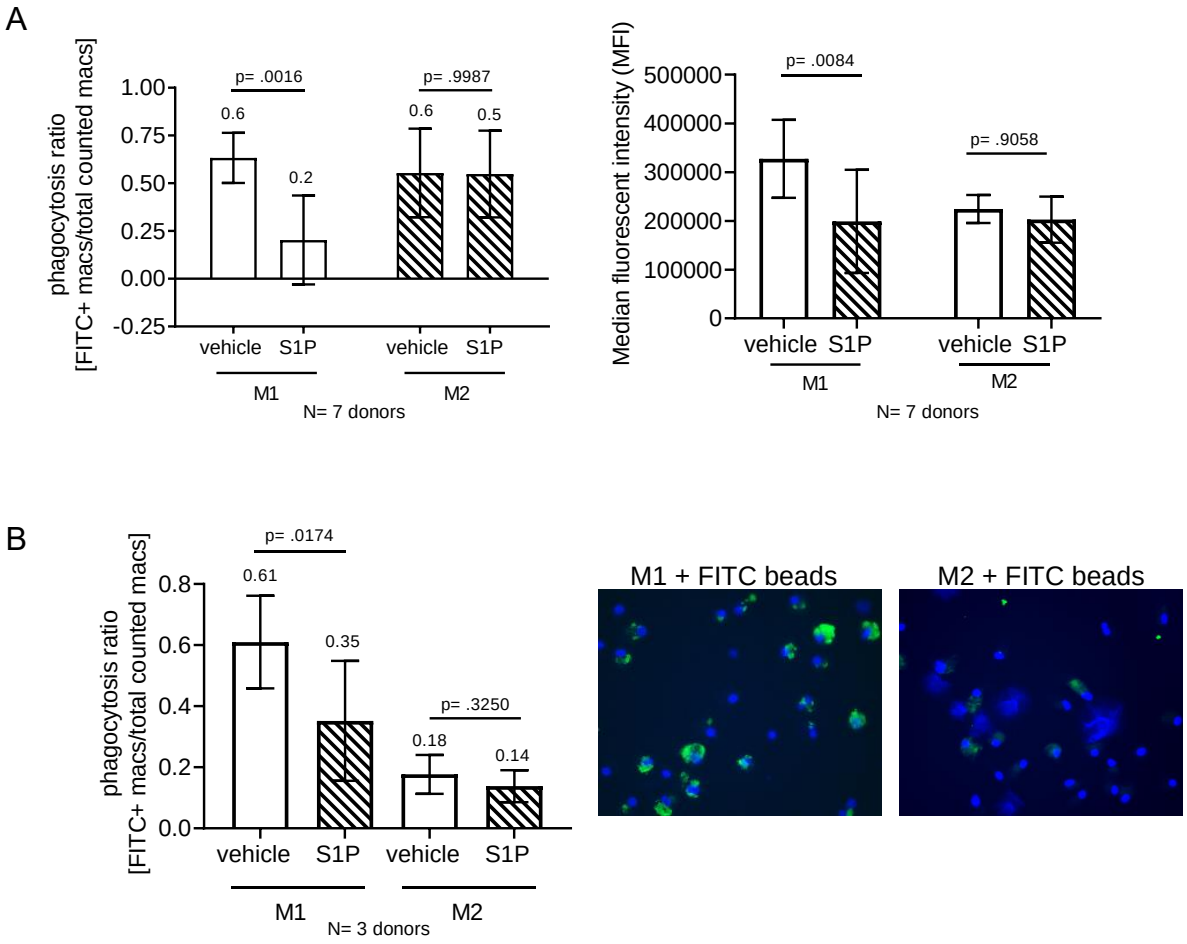

Figure 5.3 M1 macrophages pre-treated with 1 μM S1P showed reduced phagocytosis of FITC+ latex beads. (A) Phagocytosis of FITC+ beads assessed by flow cytometry of a total of 7 donors (donors M, N, O, P, Q, R, S) tested in 3 independent experiments showing an S1P-mediated decrease in phagocytosis M1 compared to control. Median Fluorescent Intensity (MFI) was also calculated and showed reduced MFI in S1P treated M1. P values were calculated using 2-way ANOVA. (B) To validate the phagocytosis assay, three donors in independent experiments (donors 2O, 2P, 2Q and donors 2R,2S, 2T) were plated in duplicate on chamber slides. FITC+ beads were added in 1:100 ratio. Counting at least 5-high power fields (40x), a reduced proportion of FITC+ macrophages in S1P treated M1 and M2 cultures was observed. M2 macrophages overall had a lower level of phagocytosis compared to M1 macrophages in this assay as shown by the representative images of the phagocytosis of FITC+ beads.

5.3 Phagocytosis of rituximab-opsonised DLBCL cell lines

5.3.1 Evaluate surface expression of CD20 in DLBCL cell lines

Flow cytometry was used to study the expression of CD19 and CD20 in DLBCL cell lines with the intention of confirming expression of rituximab target (CD20). OCI-Ly1, SUDHL6, OCI-Ly3, and U2932 all had high expression of CD20 (Figure 5.4). U2932 and OCI-Ly3 expressed low levels of CD19 compared OCI-Ly1 and SUDHL6. It has been reported that U2932 and OCI-Ly3 has lower CD19 surface expression than SUDHL6 (Hojer et al., 2014). All cell lines had high expression of CD20.

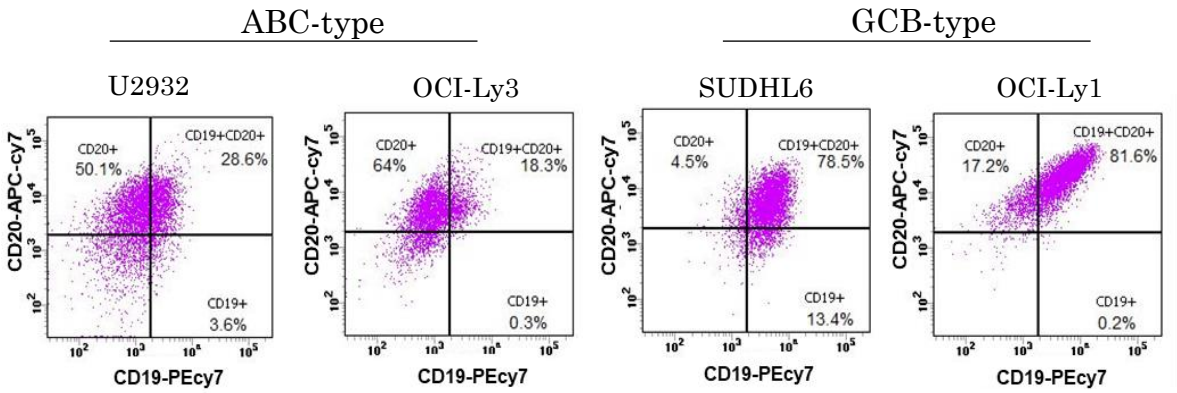

Figure 5.4 DLBCL cell lines expressed CD20. Dot plots for ABC and GCB type DLBCL cell lines assessed for CD19/ CD20 expression using flow cytometry. There was a lower expression of CD19 in the two ABC-type DLBCL cell lines compared to the GCB-type DLBCL cell lines. In all cell lines, >75% of live DLBCL cells expressed CD20.

5.3.2 S1P reduced phagocytosis of DLBCL cell lines by M1/M2 macrophages

The specificity of rituximab-induced phagocytosis was tested by using cells that were not a target for rituximab to evaluate base level phagocytosis of primary macrophages to human cells. Jurkat, a T-lymphoblastic leukaemia cell line, was stained with eFluor450 cell dye and then treated with 10 μg/ml rituximab or with isotype (IgG) control for >2hrs (Figure 5.5). M1and M2 macrophages were stained with CFSE and then co-cultured the tumour cells with macrophages for 90min. Then co-cultures were evaluated for CFSE+ eFluor450+ cells using flow cytometry. Both rituximab and isotype control had similar levels of phagocytosis (<6%) of Jurkat cells. This result reveals that the phagocytosis of rituximab-treated DLBCL cell lines I observed is mediated by rituximab.

S1P concentration is said to be elevated in the tumour microenvironment while circulating levels of S1P remain relatively unchanged and this may point to tumour-associated S1P acting only within the tumour (Ramanathan et al., 2017). The same concentrations used in migration assay were tested in the phagocytosis assay with DLBCL cell lines. CFSE+ M1 and CFSE+ M2 macrophages from three donors were with 0.1, 1, and 10 μM S1P. SUDHL6, a GCB-type DLBCL cell line, was stained with eFluor450 and incubated with 10 μg/ml rituximab for >2hr at 37°C.

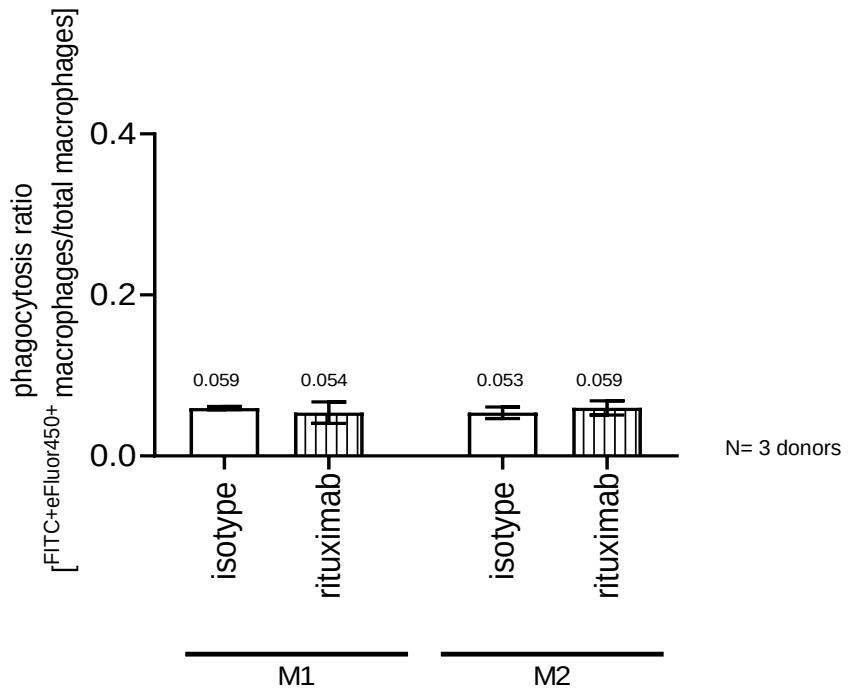

Figure 5.5 No effect of rituximab in the Jurkat cell line. Jurkat, an acute T-cell leukaemia cell line, was treated with 10 µg/ml of rituximab or IgG isotype control as then co-cultured with M1 or M2 for 90 minutes. Phagocytosis was not enhanced after treatment with rituximab. Data is representative of three donors (I2, J2, K2) analysed in triplicate. Phagocytosis ratio was calculated by taking double positive macrophages as a proportion of total macrophages counted.

Rituximab-treated SUDHL6 cells was co-cultured with S1P-treated M1 or M2 for 90 minutes. Co-cultures were analysed by flow cytometry to detect the double positive macrophage population (CFSE+ eFluor450+) indicating phagocytosis. Experimental design and flow cytometry gating is shown in figure (5.6).

I found that 0.1, 1, and 10 μM S1P all significantly reduced the phagocytosis of SUDHL6 by both M1 and M2 macrophages (Figure 5.7A). This experiment was repeated twice with a total of six donors and thus showed that in my experimental system, even low concentrations of S1P were sufficient to reduce phagocytosis of rituximab-treated DLBCL. Having shown that all concentrations of S1P used were effective in inhibiting phagocytosis, I next wanted to confirm the effect of elevated S1P (1μM) on additional donors. I found that M1 and M2 macrophages from 6/9 donors displayed significantly reduced phagocytosis after S1P treatment (Figure 5.7B). There were 2/9 donors (2D and 2E) that had reduced phagocytosis in M1 only. One donor had no reduction of phagocytosis (donor 2C).

To confirm if the effect was rituximab dependent, ofatumumab (gift from Professor Tatjana Stankovic) was also used in similar phagocytosis experiments using 3 donors (C2, D2, E2). I found that there was also a reduction in phagocytosis after S1P treatment in the ofatumumab treated SUDHL6 (Figure 5.8). There was a small reduction though not significant with the M2 macrophages. This experiment should be repeated with more donors.

A

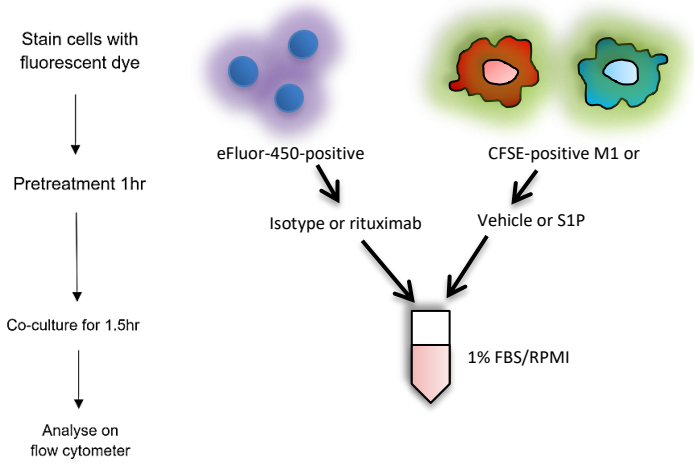

B

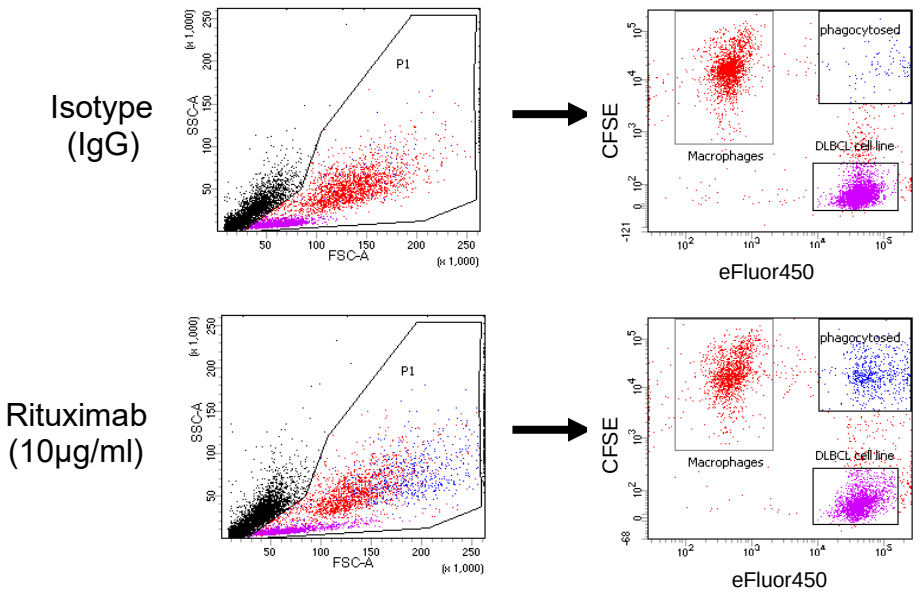

Figure 5.6 Phagocytosis assay: experimental design and flow cytometry gating strategy. (A) Macrophages (CFSE-positive) were pre-treated with 1µM S1P or vehicle and DLBCL cell lines (eFluor450-positive) were pre-treated with 10 µg/ml rituximab or isotype control and then co-cultured for 1.5 hr. (B) Samples were visualised on BD LSRII and analysed with FACS Diva 8.0. Isotype control treated DLBCL cells had a lower level of phagocytosis compared to 1µg/ml rituximab treated DLBCL cells.

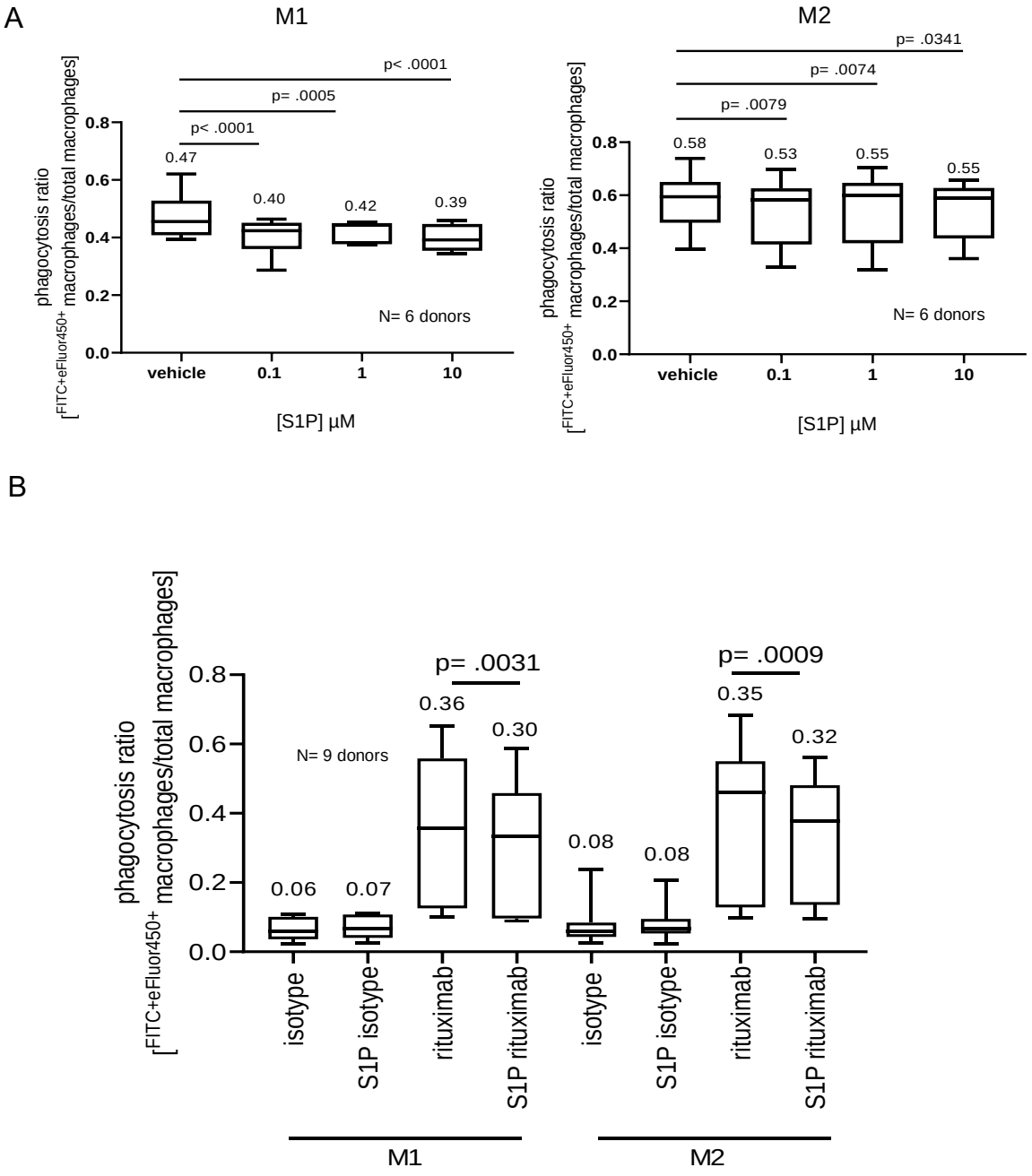

Figure 5.7 Macrophages pre-treated with 1µM S1P had reduced phagocytosis of rituximab treated SUDHL6. (A) Macrophages from six donors in two independent experiments (donors 3A,3B,3C, and donors 2X, 2Y, and 2Z) were treated with vehicle, 0.1,1, or 10 µM S1P and then co-cultured with 10µg/ml rituximab treated SUDHL6 for 90 minutes. There was a significant reduction of phagocytosis in the S1P treated M1 macrophages. There was a smaller yet significant reduction in M2 macrophages. (B) In nine donors tested in three independent experiments (Table 5.1) there was a small but significant reduction in phagocytosis by M1 and M2 macrophages of rituximab-treated SUDHL6. Phagocytosis ratio was calculated by determining the number of double positive macrophages as a proportion of macrophages and p value was calculated using 2-way ANOVA.

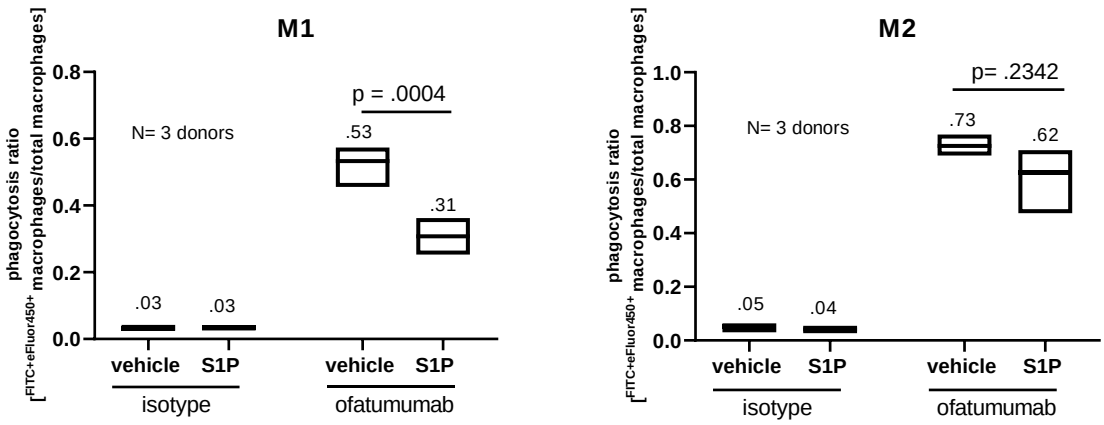

Figure 5.8 M1 and M2 macrophages were pre-treated with 1μM S1P had reduced phagocytosis of ofatumumab treated SUDHL6. (A) Macrophages from three donors in a single experiment were treated with vehicle or 1 μM S1P and then co-cultured with 10μg/ml ofatumumab treated SUDHL6 for 90 minutes. There was a significant reduction of phagocytosis in the S1P treated M1 macrophages. There was a reduction though not significant with M2 macrophages. 2-way ANOVA was used to calculate P values.

To determine if the effect of S1P on phagocytosis could be relevant to other DLBCL cell lines, OCI-Ly1 (GCB-type) and OCI-Ly3 (ABC-type) DLBCL cells were tested. A total of nine donors in triplicate for each cell line over three independent experiments were evaluated in the phagocytosis assay (Table 5.1). There was a significant reduction in phagocytosis by M1 macrophages of both rituximab treated OCI-Ly1 and OCI-Ly3 cells (Figure 5.9A and B). All donors tested had a significant reduction of phagocytosis after S1P treatment when co-cultured with OCI-Ly1. For OCI-Ly3, only 6/9 donors showed a significant reduction in phagocytosis after S1P treatment (there was no significant phagocytosis in donors C2, D2, E2). For both cell lines and all

donors, there was no significant difference in phagocytosis between vehicle treated or S1P treated M2 macrophages.

Taken together, these results reveal that S1P reduced the phagocytosis of rituximab-treated DLBCL cell lines by M1 macrophages and in the case of SUDHL6, also by M2 macrophages. Donor ID of macrophages used in phagocytosis experiments is shown in Table 5.1.

Table 5.1 Donor IDs for samples used in phagocytosis assays

Figure 5.7B SUDHL6	Figure 5.8 SUDHL 6	Figure 5.9A OCI-Ly1	Figure 5.9B OCI-Ly3	Figure 5.10A BAF312 (SUDHL6)	Figure 5.10B JTE013/CYM5220 (SUDHL6)
C2	C2	A2	C2	F2	L2
D2	D2	B2	D2	G2	M2
E2	E2	I2	E2	H2	N2
O2		J2	H2	I2	R2
P2		K2	I2	K2	S2
Q2		O2	Q2	J2	T2
R2		M	M		
S2		U	U		
T2		V	V		

A

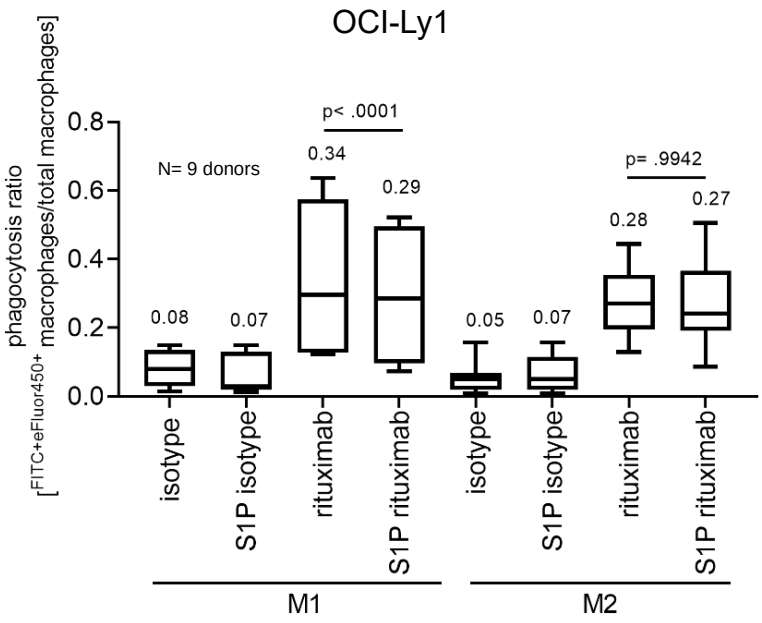

B

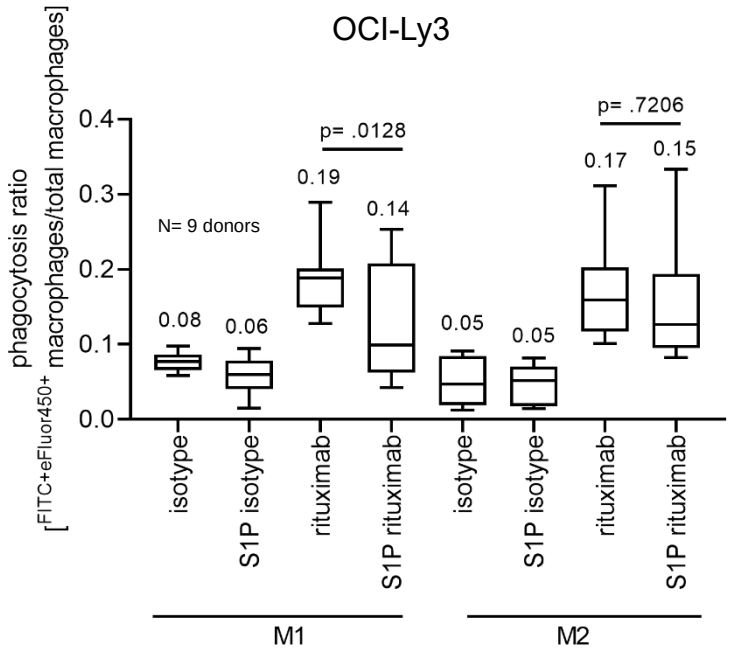

Figure 5.9 S1P reduced the phagocytosis of rituximab-treatment OCI-Ly1 and OCI-Ly3 cells. M1 and M2 macrophages co-cultured with rituximab treated (10 μg/ml) DLBCL cell lines OCI-Ly1 (top panel, A GCB type) and OCI-Ly3 (bottom panel, B; ABC type) were tested for phagocytosis +/- 1μM S1P. A total of nine donors per cell line in three independent experiments were tested (Table 5.1). Despite the variability between donors there was a significant decrease in phagocytosis of both OCI-Ly1 and OCI-Ly3 in S1P treated M1 macrophages. There was no significant difference in phagocytosis in M2 macrophages. There was a lower overall level of phagocytosis of OCI-Ly3 compared to the two GCB-type DLBCL cell lines.

5.3.3 Treatment with S1P receptor antagonist reverses the effect of S1P on phagocytosis

Having shown that S1P reduced the phagocytosis of rituximab-treated DLBCL cell lines, I next explored which S1P receptor was responsible. To do this, CYM5220, an S1PR2 agonist and BAF312, an antagonist to S1PR1 and S1PR5 previously used in the analysis of migration were used (section 4.3.2). Rituximab-treated (10 μg/ml) SUDHL6 was co-cultured with either M1 or M2 macrophages from three donors pre-treated with 1μM CYM5220, 1μM S1P, or 1μM S1P + 100nM BAF312 in two independent experiments. Phagocytosis was not reduced by treatment with CYM5220. In contrast, the addition of BAF312 increased phagocytosis compared to treatment with S1P alone (Figure 5.10A). This indicated that S1PR1 or S1PR5 may be involved in phagocytosis and that S1PR2 was likely not.

To confirm that S1PR2 had no effect on phagocytosis, rituximab-opsonised SUDHL6 was treated with 100nM JTE013, an antagonist of S1PR2. M1 and M2 macrophages from three donors treated with 1μM S1P+JTE013 showed no difference in phagocytosis compared to 1μM S1P alone (Figure 5.10B). From these results, S1PR1, or S1PR5, or both may be responsible for the reduced phagocytosis of rituximab-opsonised SUDHL6 cells observed in the presence of S1P.

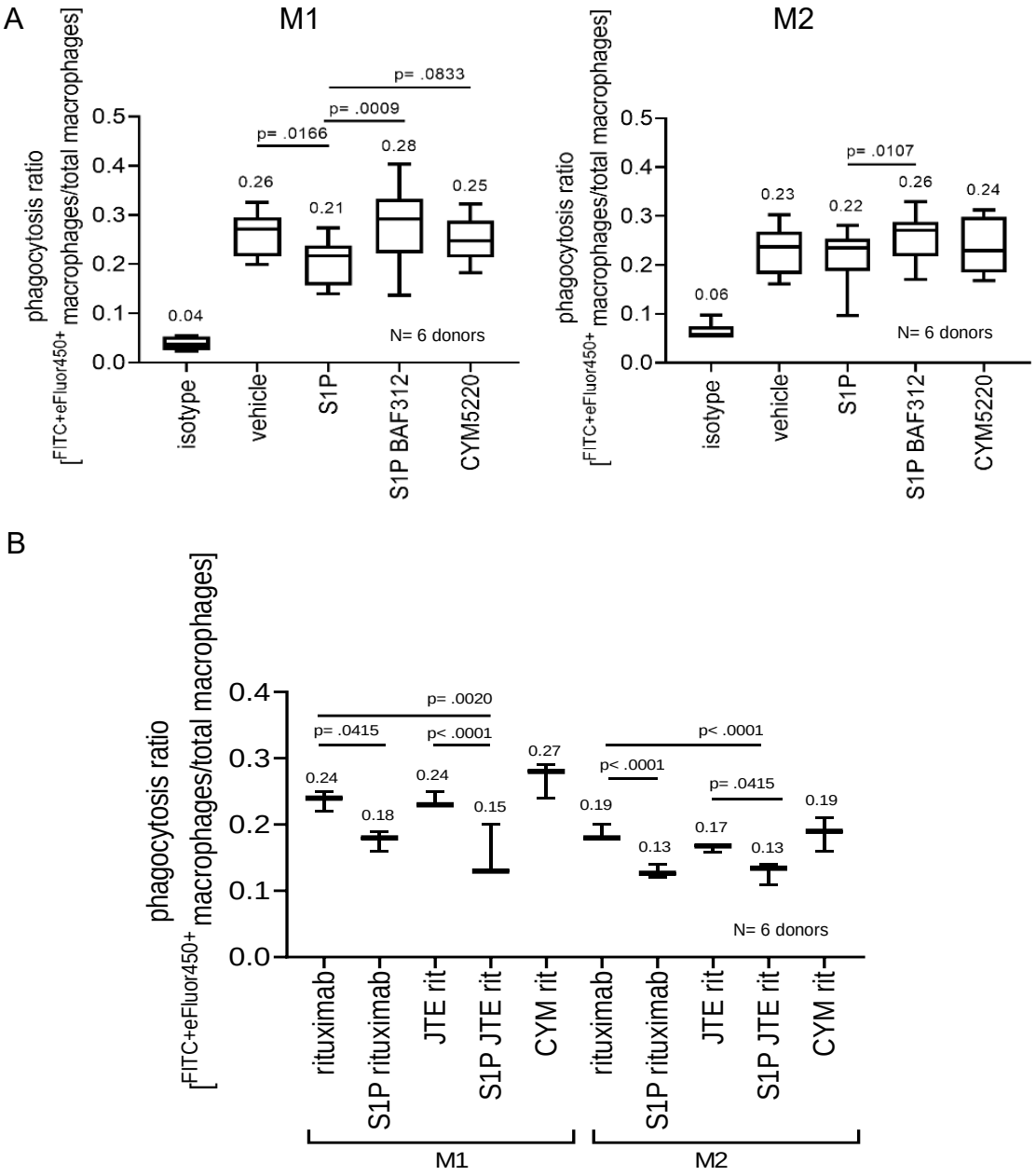

Figure 5.10 S1P receptor antagonist BAF312 blocked the effect of S1P on phagocytosis of SUDHL6 cells. (A) Left panel: M1 and M2 macrophages pre-treated with S1PR1/S1PR5 antagonist, BAF312 and S1PR2 agonist, CYM5220 1μM. There was a decrease in phagocytosis by M1 and M2 after S1P treatment which was reversed with BAF312. There was no effect of CYM5220. Right panel shows no significant decrease with S1P treatment but a significant increase in phagocytosis with BAF312. (B) To confirm that S1PR2 had no effect in reducing phagocytosis, cells were treated with JTE013, an S1PR2 antagonist and was compared to CYM5220 treatment. JTE013 did not reverse the effect of S1P on phagocytosis. Each experiment was performed with three donors in two independent experiments (Table 5.1).

5.3.4 100nm BAF312 and 10 µg/ml rituximab were not cytotoxic to SUDHL6 cells *in vitro*

To confirm that BAF312 did not induce apoptosis of the DLBCL cell lines, SUDHL6 cells were treated with 100nM BAF312 and analysed for apoptosis using Annexin V/PI assay. Assessing apoptosis was essential apoptotic cells are known to release S1P and induce migration and phagocytosis by macrophages. Vincristine (100nM) was used as a positive control. After 24 hrs, cells were stained for Annexin V/PI and analysed on flow cytometer to assess levels of phagocytosis. Only about 20% of the SUDHL6 cells treated with 100nM vincristine survived SUDHL6 cells after 24hr. There was no change in survival of SUDHL6 cell treated with BAF312 compared to untreated/DMSO controls (Figure 5.11).

Given the mechanisms of action of rituximab, I next determined if 10µg/ml rituximab would induce apoptosis in SUDHL6 cells. As with BAF312, SUDHL6 cells were treated with10 µg/ml rituximab for 24hr and for the positive control, 10nM vincristine. A lower dose of vincristine was used in this experiment as 100nM vincristine had killed the majority of SUDHL6 cells after 24hr. With the 10nM vincristine, nearly 40% of the SUDHL6 cells were apoptotic/dead and there was no change in survival of SUDHL6 cells after 24hr treatment with 1µM rituximab (Figure 5.12).

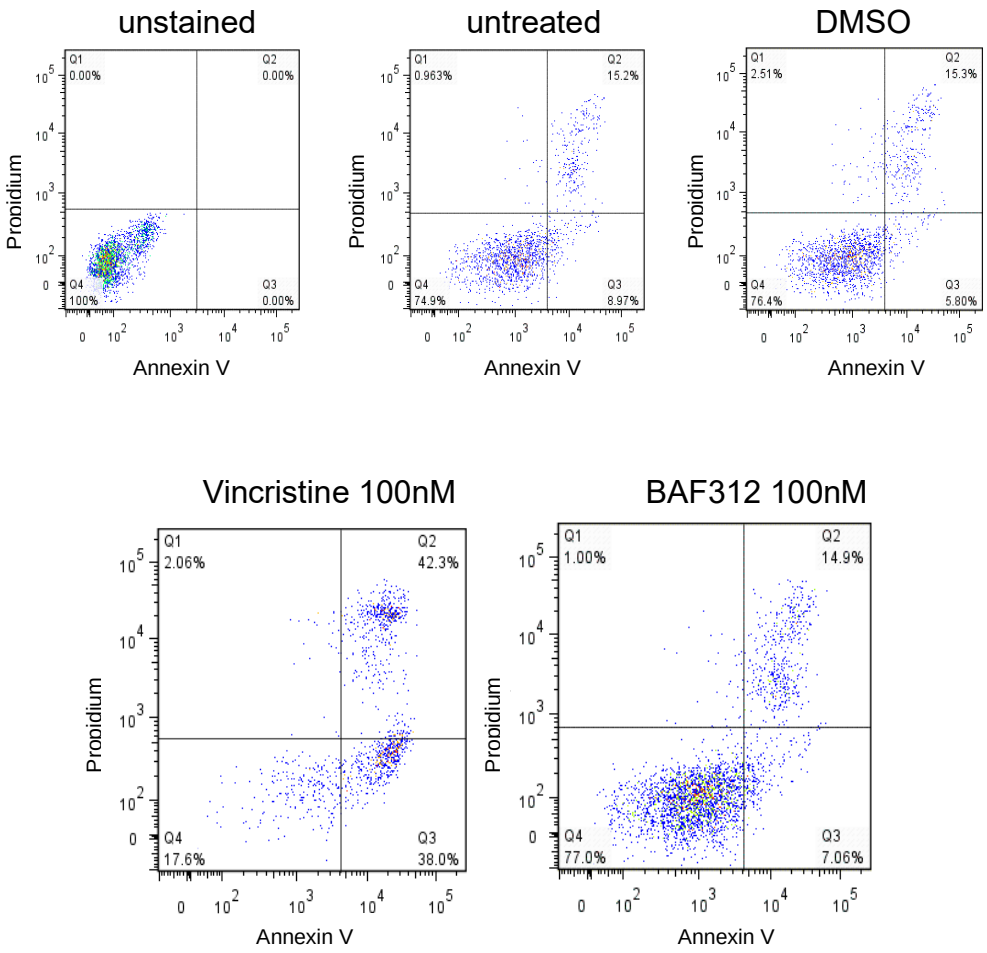

Figure 5.11 BAF312 did not induce apoptosis or cell death SUDHL6 cells after 24 hr. **The** SUDHL6 cell line was treated with DMSO, 100nM vincristine or 100nM BAF312 for 24rs. Cells were assessed for apoptosis using Annexin V/PI. DMSO control and BAF312 treated cells did not differ from untreated cells. As a positive control, cells were also treated with vincristine, which had increased apoptosis.

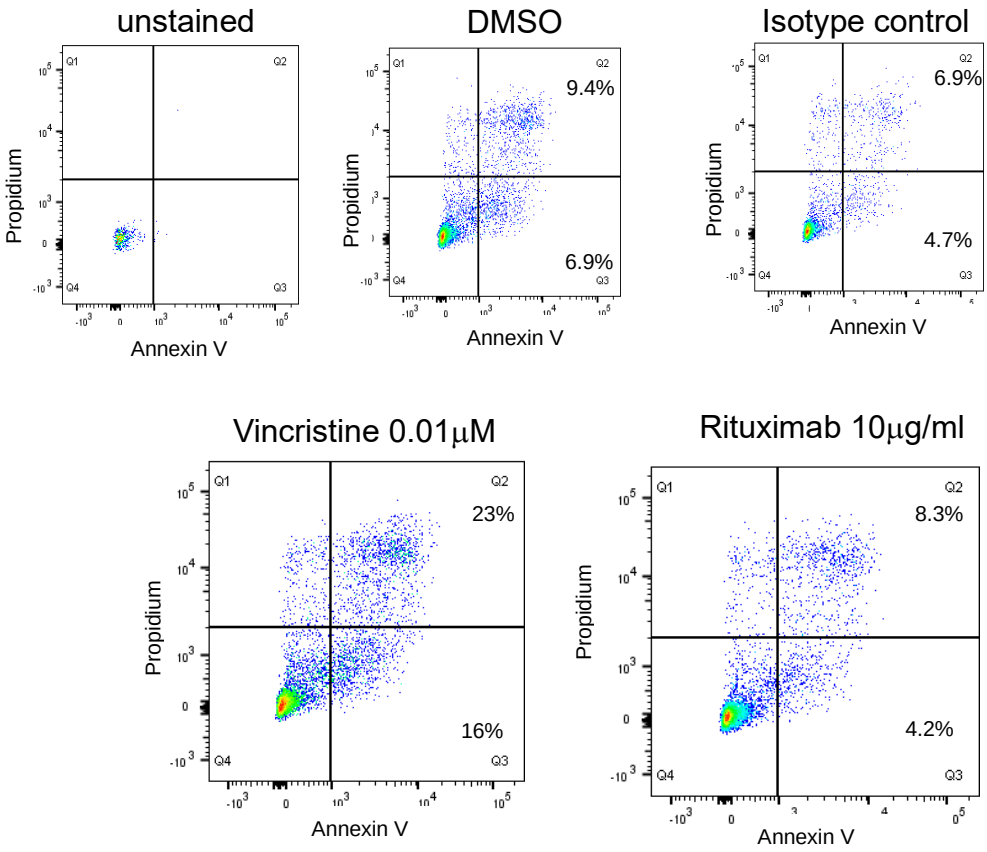

Figure 5.12 Rituximab did not induce apoptosis or cell death SUDHL6 cells after 24hr. SUDHL6 cell line was treated with DMSO, isotype control, 0.01μM vincristine, or 10μg/ml rituximab for 24rs. Cells were assessed for apoptosis using Annexin V/PI. There was no significant difference in apoptosis between rituximab treated cells compared to DMSO or isotype control treated cells. The positive control, vincristine had increased cell death.

5.4 Optimisation of rituximab-chemotherapy for mouse models of DLBCL

5.4.1 Vincristine and doxorubicin are cytotoxic to DLBCL cell lines

Thus far, I have demonstrated that S1P can reduce phagocytosis of rituximab-treated DLBCL cells *in vitro* and that this effect could be ablated in the presence of BAF312. In all cell lines, the effect was mainly in M1 though this decrease could also be seen in M2 with SUDHL6. *In vivo,* mouse macrophages were shown to be recruited to the tumour environment during engraftment of DLBCL and treatment with BAF312 reduced the number of macrophages in the tumour compared to controls with no effect on tumour burden except in the SUDHL6 xenograft. Next, the efficacy of the combination of BAF312 and rituximab-chemotherapy treatment in mouse xenografts was evaluated.

The *in vitro* cytotoxicity of two chemotherapy compounds, vincristine and doxorubicin, routinely used in the treatment of DLBCL patients was determined. Four DLBCL cell lines were tested; OCI-Ly1, SUDHL6, OCI-Ly3 and A20. Cell viability was assessed using the Cell Titre Glo (Promega) luminescent cell viability assay which measures adenosine triphosphate (ATP) release of live cells. Varying concentrations of vincristine or doxorubicin in 96-well plates was added to DLBCL cells and incubated for 96 hr. The surviving fraction was then calculated by taking relative light units (RLU) of luminescence from the treated cells as a proportion of the RLU of vehicle

control cells. The IC50 of vincristine and doxorubicin was then calculated using Graph Pad Prism v8.

All DLBCL cell lines tested were sensitive to vincristine in nanomolar concentrations (Figure 5.13). The IC50 for 96hr treatment with vincristine of these cell lines are as follows: OCI-Ly1 IC50= 5nM; SUDHL6 IC50= 2nM; OCI-Ly3 IC50= 9nM; and for the mouse A20 lymphoma cell line, the IC50= 19nM. The four DLBCL cell lines were also sensitive to doxorubicin but the IC50s were 30-50X higher than for vincristine. The IC50 for 96hr treatment with doxorubicin is as follows: OCI-Ly1 IC50= 178nM; SUDHL6 IC50=106nM; OCI-Ly3 IC50= 444nM; and A20 IC50= 82nM (Figure 5.14).

The IC50 of rituximab was also assessed in two DLBCL cell lines, OCI-Ly1 and OCI-Ly3 using Cell Titre Glo assay after 96 hrs treatment. The IC50 was not reached in the rituximab (1nm – 1000nm) treated cells (Figure 5.15). OCI-Ly1 had a maximum of 20% cell death at 25nM rituximab (Figure 5.15 top panel). Overall there was no difference in viability with rituximab treated and the matching concentrations of IgG isotype treated cells as seen in the apoptosis assay.

Vincristine was chosen for *in vivo* experiments because of its high potency (low IC50s) against the DLBCL cell lines tested. SUDHL6 was the most sensitive DLBCL cell line to vincristine and had a high expression of CD20 shown in the previous chapter. SUDHL6 was also the cell line where reduced phagocytosis was seen by both M1 and M2 S1P treated macrophages

described earlier in this chapter. Therefore, SUDHL6 was chosen for the *in vivo* experiments described in the following sections.

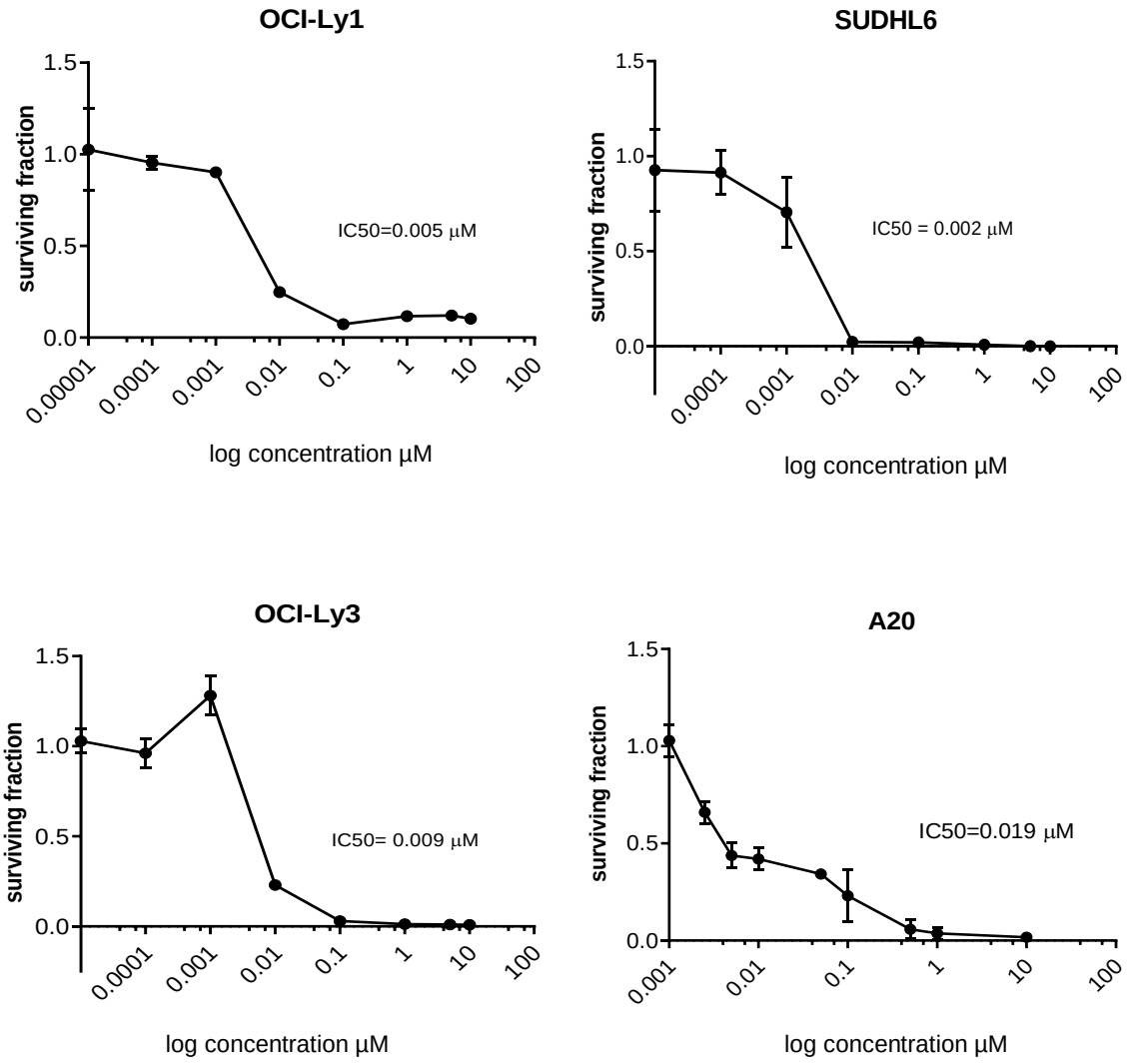

Figure 5.13 DLBCL cell lines were sensitive to vincristine. OCI-Ly1, SUDHL6, OCI-Ly3, and mouse cell line, A20 were treated with vincristine for 96 hours. All three human DLBCL cell lines were highly sensitive to vincristine with IC50s ranging from 2nM – 9nM. The A20 cell line was also sensitive with an IC50 19nM. Each cell line was tested in three independent experiments which is represented on each graph. Error bars represent standard deviation and the IC50 was determined using GraphPad Prism v8.

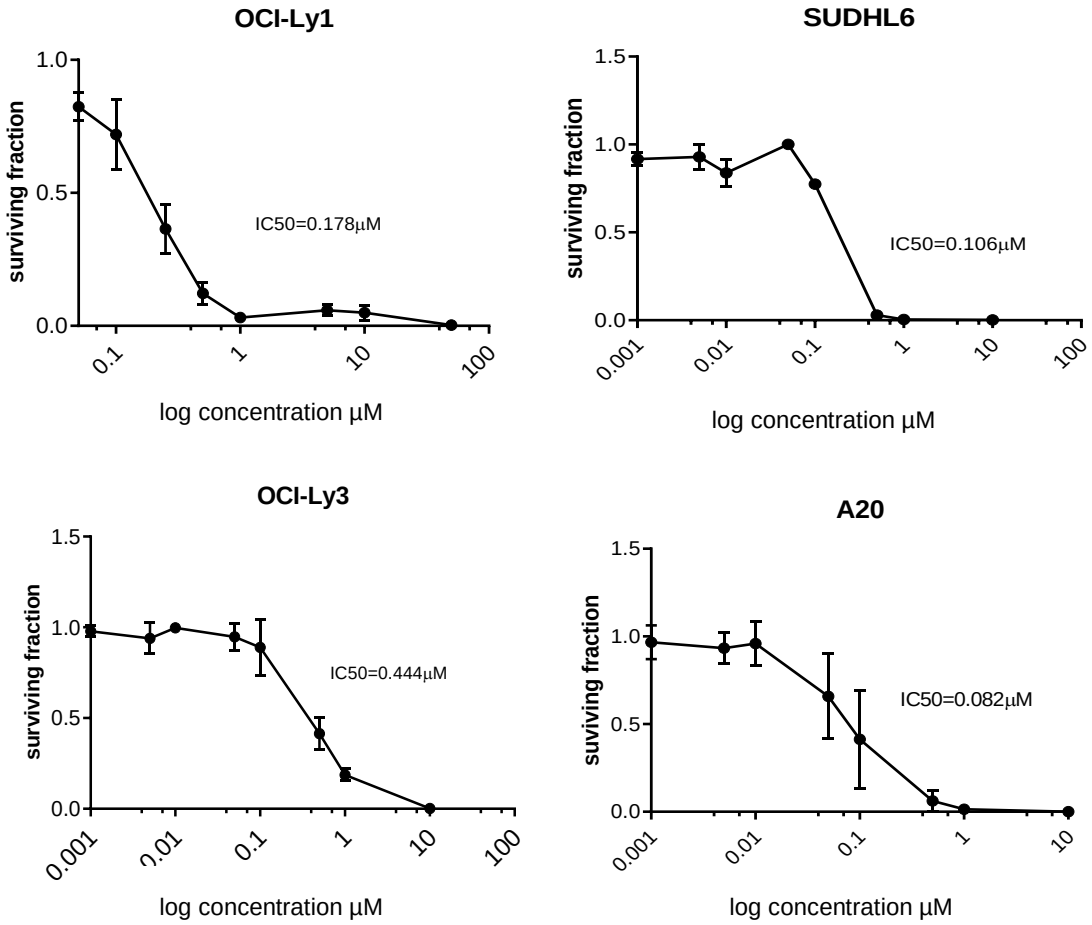

Figure 5.14 DLBCL cell lines are sensitive to doxorubicin. Human DLBCL cell lines; OCI-Ly1, SUDHL6, OCI-Ly3, and the mouse cell line, A20 were treated with doxorubicin for 96 hrs. IC50 was determined for each cell line. OCI-Ly1 and SUDHL6, both GCB-type DLBCL cell lines, were more sensitive to doxorubicin compared to OCI-Ly3, an ABC-type DLBCL cell lines with the IC50>100nM. For the A20 cell line, the IC50 for doxorubicin was 82nM. Each cell line was tested in three independent experiments which is represented on each graph. Error bars represent standard deviation and the IC50 was determined using GraphPad Prism v8.

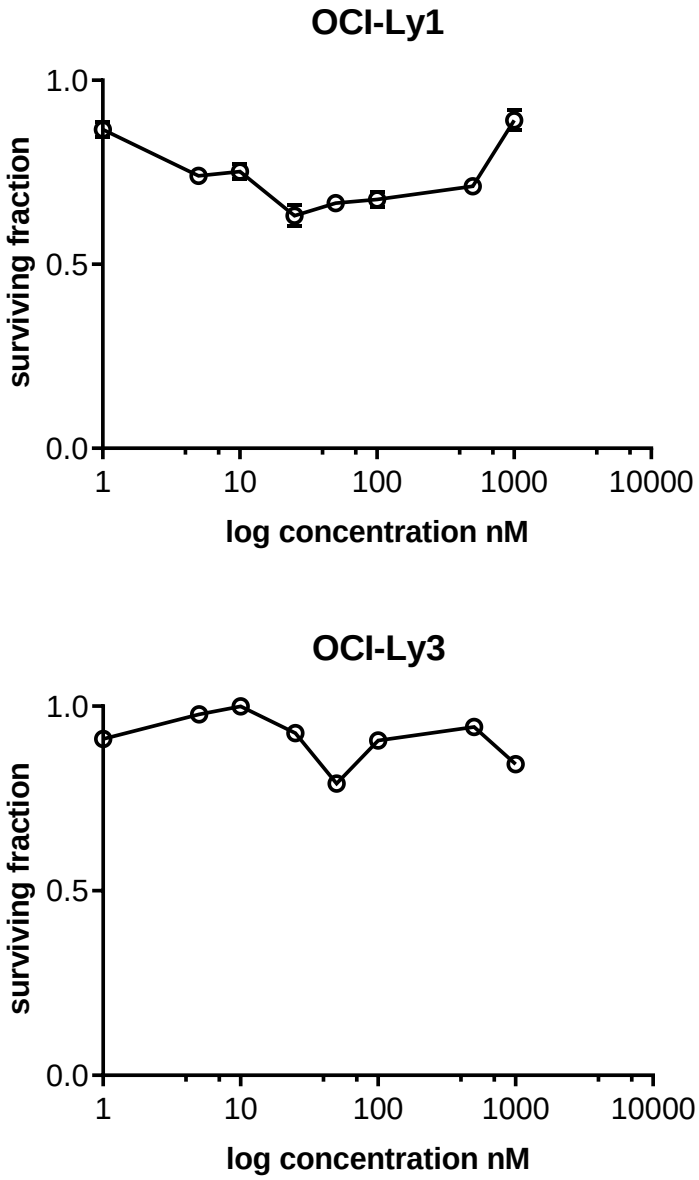

Figure 5.15 Rituximab treated DLBCL cell lines were assessed for cell viability after 96hrs treatment. OCI-Ly1 and OCI-Ly3 were treated with varying concentrations of rituximab for 96 hrs. Cell Titre Glo assay was used to assess surviving fraction as a proportion of control (isotype control) but there was no cell death evident at any concentration. Two independent experiments were done with each point in triplicate. Error bars represent standard deviation and the IC50 was determined using GraphPad Prism v8.

5.4.2 1mg/kg vincristine was sufficient to reduce tumour burden in SUDHL6 xenografts

SUDHL6 was subcutaneously engrafted on the flank of eight NSG mice. Tumours became measurable on day 17 post injection. Mice were then randomised as described in Materials and Methods 2.4.2, into vehicle (N=4) or vincristine (N=4) treatment groups. Vehicle (water for injection) or 1mg/kg vincristine was administered by IV injection and monitored for weight loss and tumour growth every other day. Experiment was ended on day 24 when some of the control mice reached >900mm^3 tumour volume. Vincristine treated mice had significantly delayed tumour growth compared to vehicle treated mice (Figure 5.16A).

Percent change in tumour volume was calculated using the formula: ***((Final tumour volume – Initial tumour volume)/ Initial tumour volume) X 100*** (Gao et al., 2015). Vincristine treated mice had significantly reduced in tumour volume compared to vehicle treated mice (Figure 5.16B). To calculate the percent tumour growth inhibition (TGI), the average tumour volume of the vincristine treated group (483.98 mm^3) was taken and was divided by the average tumour volume of the control group was (1883.23 mm^3) (Blumenthal, 2005). The result was subtracted from 1 and multiplied by 100. Thus, by this calculation, 1mg/kg vincristine reduced tumour growth by 75% and therefore, is a potent therapy against SUDHL6 cells *in vivo* and *in vitro.*

Tumours were analysed by flow cytometry for F4/80+/CD11b+ cells. Despite the 75% reduction of vincristine tumour volumes, the difference in the number of F4/80+CD11b+ cells between vincristine treated tumours and vehicle treated tumours went from 13% down to 8% (Figure 5.16C).

Table 5.2 Summary of average tumour volumes and % tumour growth inhibition

GROUP	Average tumour volume mm^3	% Tumour growth inhibition (TGI)
Vehicle control	1883.23	
Vincristine 1mg/kg	483.98	75%

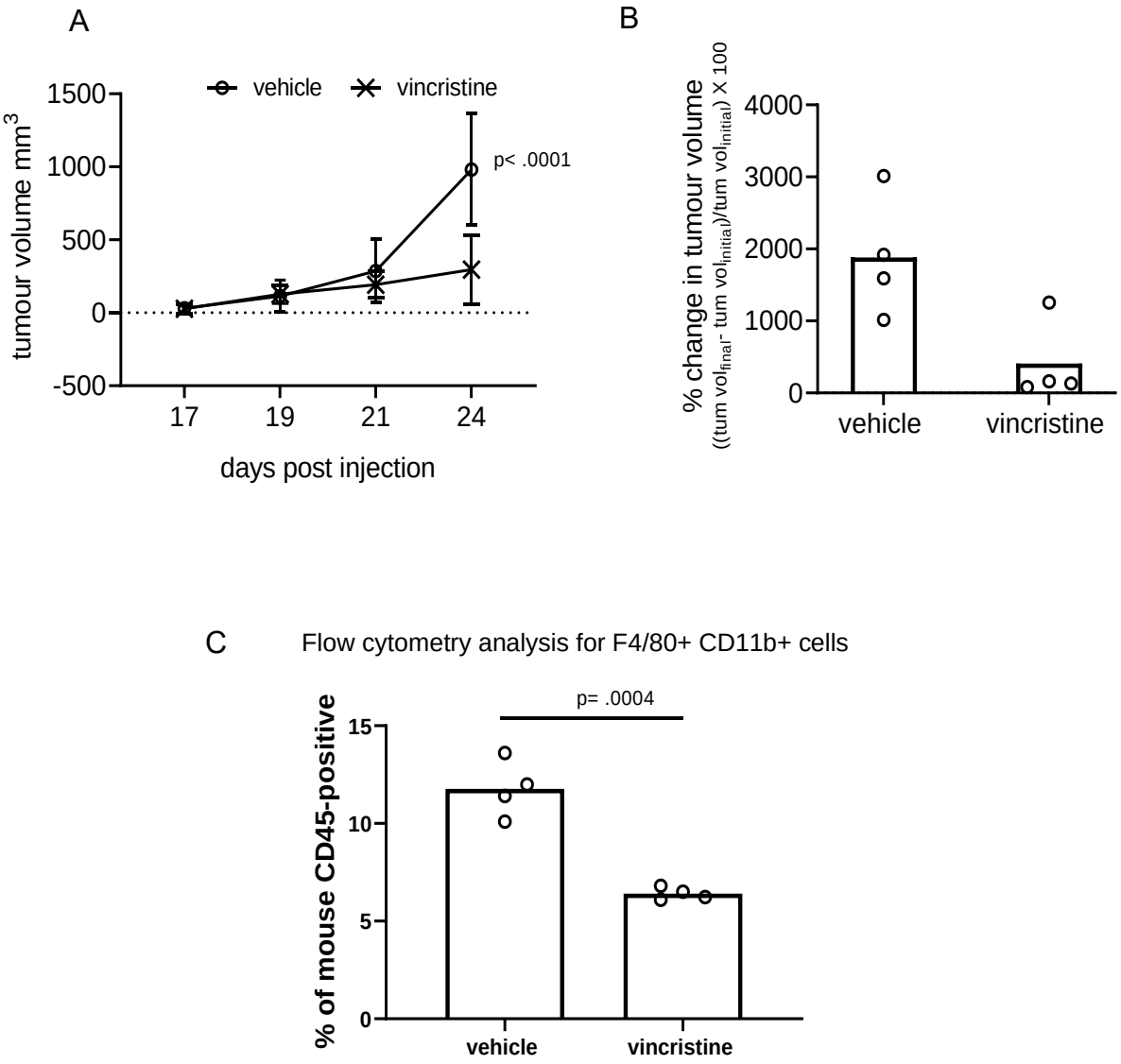

Figure 5.16 1mg/kg vincristine showed potent anti-tumour effect against SUDHL6 xenografts. (A) SUDHL6 engrafted mice were injected with vincristine on day 17 post injection. There was a significant difference in tumour volume between vincristine treated mice vs control treated mice. (B) Percent change in tumour volume calculated using formula: *((tumour volume final – tumour volume initial) / tumour volume initial) X 100* for each mouse indicates that vincristine inhibited tumour growth in 3/4 vincristine treated NSG mice. (C) Tumours were analysed by flow cytometry for the presence of mouse macrophages. There were nearly double the number of F4/80+CD11b+ cells in vehicle treated mice compared to control.

5.4.3 SUDHL6 engrafted mice treated with 0.5mg/kg vincristine combined with 1mg/kg rituximab had a complete response

Having shown that 1mg/kg vincristine was sufficient to reduce tumour volume of SUDHL6 xenografts, next the combination of rituximab with vincristine was tested. A suboptimal dose of vincristine, 0.5mg/kg, was used instead of the full 1mg/kg for two reasons: first, to reduce the risks for adverse effects in mice given drug combination of vincristine and rituximab and second, to determine the efficacy of reduced vincristine dosage combined with rituximab. NSG mice were engrafted subcutaneously with SUDHL6 and then randomised into treatment groups with N=4 mice per group: vehicle, 0.5mg/kg vincristine, 1mg/kg rituximab, 0.5mg/kg vincristine + 1mg/kg rituximab. Vincristine was given on day 19 and rituximab treatment began on day 20 (both by IV injection) (Figure 5.17A).

There was no significant tumour inhibition in the vincristine or rituximab treatment groups compared to control but there was a significant difference in tumour volume observed in the combination treatment group compared to control beginning on day 22 (Figure 5.17A). From the percent change in tumour volume, a complete response in 3/4 mice in the combination treatment group was evident (Figure 5.17B). The TGI was calculated and summarised in Table 5.1, vincristine group had TGI=42.1%, rituximab group had TGI=26.3% and combination group had TGI=93.4%. The absolute number of infiltrating F4/80+CD11b+ cells was lower in the treatment groups compared to vehicle treated mice (Figure 5.18). This experiment was repeated

a second time which confirmed that mice given rituximab+0.5mg/kg vincristine had a complete response to the treatment.

Table 5.3 Summary of average tumour volumes and % tumour growth inhibition

GROUP	Average tumour volume mm^3	% Tumour growth inhibition (TGI)
Vehicle control	869.3	
Vincristine 0.5mg/kg	502.4	42.1
Rituximab 1mg/kg	640.8	26.3
Vincristine→ rituximab	57.2	93.4

% tumour growth inhibition (TGI) calculated using the following formula

TGI= (1-(avg tum vol treated/avg tum vol control)) x 100

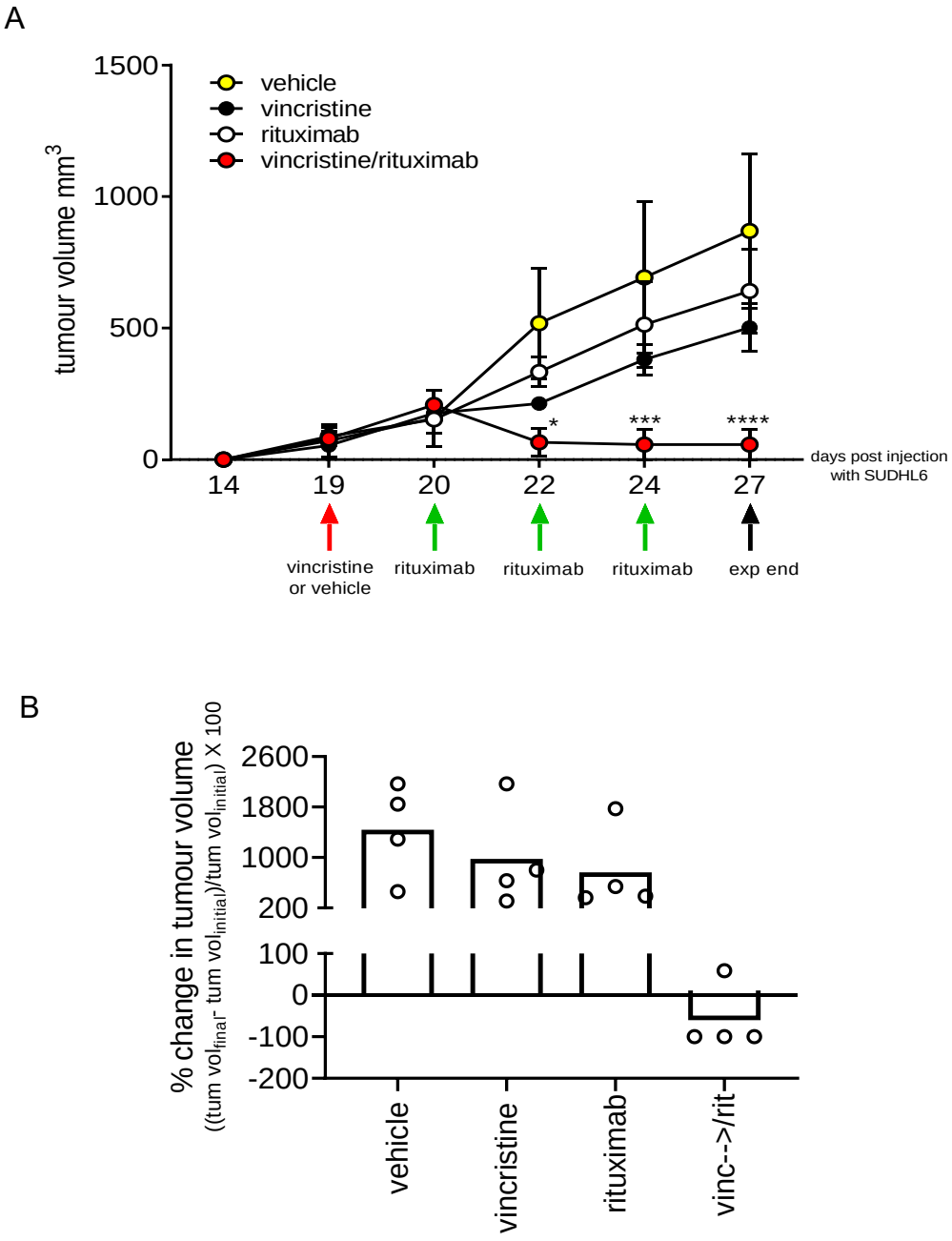

Figure 5.17 Combination treatment with rituximab and 0.5mg/kg vincristine resulted in complete response in SUDHL6 engrafted mice. (A) Average tumour volumes for each group were measured on each treatment day. Randomisation and treatment began on day 19 and experiment ended on day27 due to control mice reaching >900mm^3. There was significant regression of tumour growth in vincristine + rituximab treated mice by day 22 (* p= .0260, *** p= .0008, **** p< .0001). Treating mice with 0.5mg/kg vincristine and 1mg/kg rituximab as single agents did not have significant tumour inhibition compared to control. (B) Percent change in tumour volume indicated that 3/4 mice had complete tumour regression in the combination treatment group.

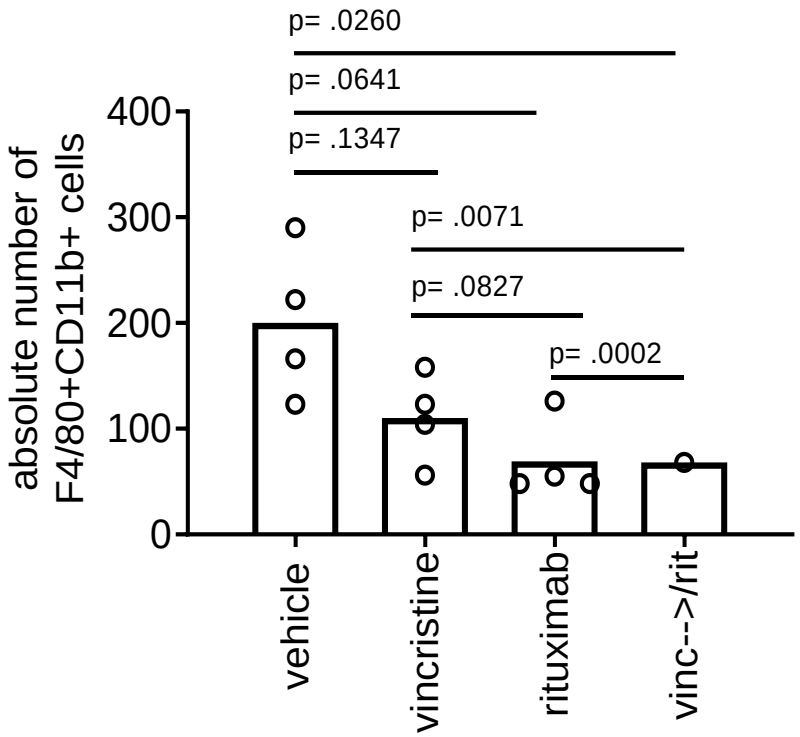

Figure 5.18 Compared to controls, vincristine and rituximab treated mice had reduced absolute numbers of F4/80+ cells compared to control in SUDHL6 xenografts. Rituximab and combination treatment groups had reduced F4/80+/CD11b+ cells compared to control, as assessed by flow cytometry. There was only one mouse left in the combination treatment group to analyse. Student's t-test was used to determine p value.

5.4.4 BAF312 given prior to rituximab reduces the efficacy of rituximab and vincristine treatment *in vivo*

Next, the addition of BAF312 to the combination of vincristine/ rituximab would affect the growth of SUDHL6 tumours was studied. In the previous section, it was demonstrated that the combination of rituximab and vincristine resulted in complete response in 3/4 treated mice. For this experiment, the dose of vincristine was reduced to 25% of the original dose i.e. 0.25mg/kg and the dose of rituximab was reduced to 50% of the original dose i.e. 0.5mg/kg. Several publications reported the testing of 0.03mg/kg, 0.3mg/kg and 3mg/kg BAF312 for therapeutic efficacy using the rat and mouse models for experimental autoimmune encephalomyelitis (EAE) (Gergely et al., 2012, Lewis et al., 2013). BAF312 treatment at 0.3mg/kg and 3mg/kg given daily for >20 days reduced the clinical score in preclinical models. According to the growth kinetics, the window of treatment for SUDHL6 was a maximum of 10 days. Therefore, I opted to use the highest dose employed in these published experiments. This was the same dose used in the previous chapter where treatment with 3mg/kg BAF312 reduced the infiltration of F4/80+ cells in DLBCL xenografts.

Twenty NSG mice were injected with SUDHL6 subcutaneously. On day 18 mice were randomised into four treatment groups: (1) vehicle; (2) vehicle / vincristine / rituximab; (3) BAF312 / vincristine / rituximab; (4) vincristine / rituximab / BAF312. The treatment schedule for this experiment is shown in Table 5.4. Mice given BAF312 prior to vincristine and rituximab treatment

did not have significant tumour inhibition compared to control (Figure 5.19). Vincristine and rituximab without BAF312 showed a significantly reduced tumour volume compared to control. Furthermore, the addition of BAF312 post vincristine and rituximab treatment also led to the significant inhibition of tumour growth compared to control (Figure 5.19). There was no significant difference between tumour volumes in mice treated with BAF312 following vincristine/rituximab and tumour volumes in mice treated with vincristine/rituximab only. The TGI for each group were: Group 2 TGI=36.8%; Group3 TGI=32.1%; Group 4 TGI=54.9% (Table 5.5).

Survival of mice in this experiment was plotted on a Kaplan Meier graph. Mice were censured when their tumours reached 1.1cm, the maximum tumour size allowed under our Home Office licence (Figure 5.20). Mice treated with BAF312 after vincristine and rituximab had better survival than all other groups and this was significant for all groups (p values for group1 vs group 2 p=.0216; group 1 vs group 3 p=.0040; group1 vs group 4 p= .0329).

Table 5.4 Treatment schedule for *in vivo* evaluation of BAF312 with rituximab and vincristine.

Treatment schedule for BAF312, Rituximab, Vincristine								
Group	Day 18	Day 19	Day 20	Day 21	Day 22	Day 25	Day 26	Day 27
1	Vehicle	Vehicle	Vehicle	Vehicle	Vehicle	Vehicle	Vehicle	Experiment Endpoint
2	Vehicle	Vincristine	Rituximab	Vehicle	Rituximab	Rituximab	Rituximab	Experiment Endpoint
3	BAF312	BAF312 Vincristine	BAF312 Rituximab	BAF312	Rituximab	Rituximab	Rituximab	Experiment Endpoint
4	Vehicle	Vincristine	Rituximab	BAF312	BAF312 Rituximab	BAF312 Rituximab	BAF312 Rituximab	Experiment Endpoint

Chart shows the treatment schedule for each group. Group 1: control; Group 2: vehicle/ vincristine followed by rituximab; Group 3: BAF312/vincristine followed by rituximab; Group 4: vincristine followed by rituximab/BAF312

Table 5.5 Summary of average tumour volumes and % tumour growth inhibition

GROUP	Average tumour volume mm^3	%Tumour growth inhibition (TGI)
1 control	777	
2 vehicle/vinc→rituximab	527.5	32.1%
3 BAF312/vinc→rituximab	491.2	36.8%
4 vinc→rituximab/BAF312	350.2	54.9%

Vinc= vincristine, %TGI= (1-(avg tumour volume treated/avg tumour volume control)) x 100

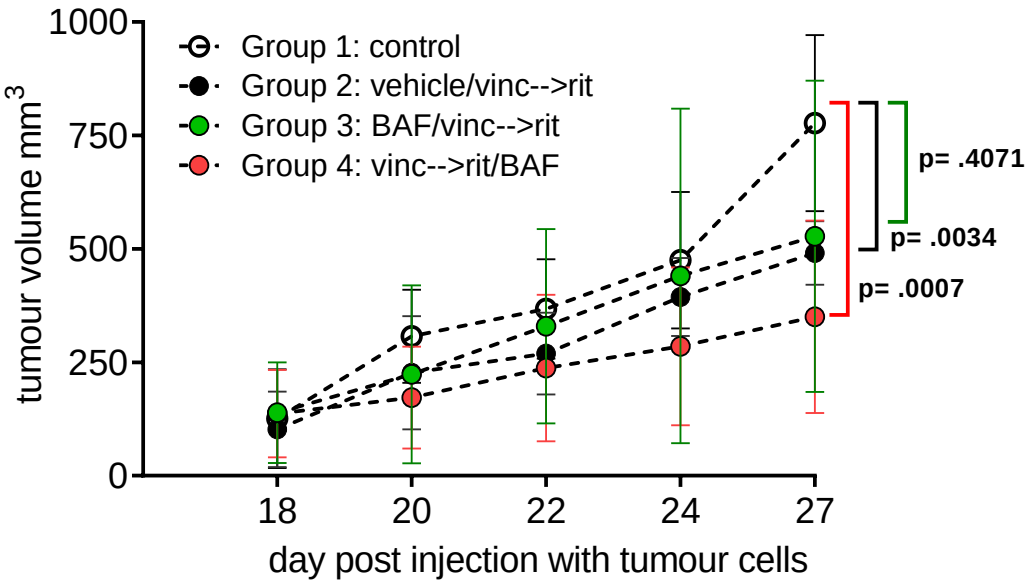

Figure 5.19 BAF312 given prior to vincristine and rituximab had a reduced effect compared to giving BAF312 after vincristine and rituximab. There was a significant difference in average tumour volume when BAF312 was given post vincristine and rituximab treatment. Giving BAF312 prior to vincristine and rituximab did not have a significant effect unlike vincristine and rituximab without BAF312. N=4 per group with student's t-test used to determine p value.

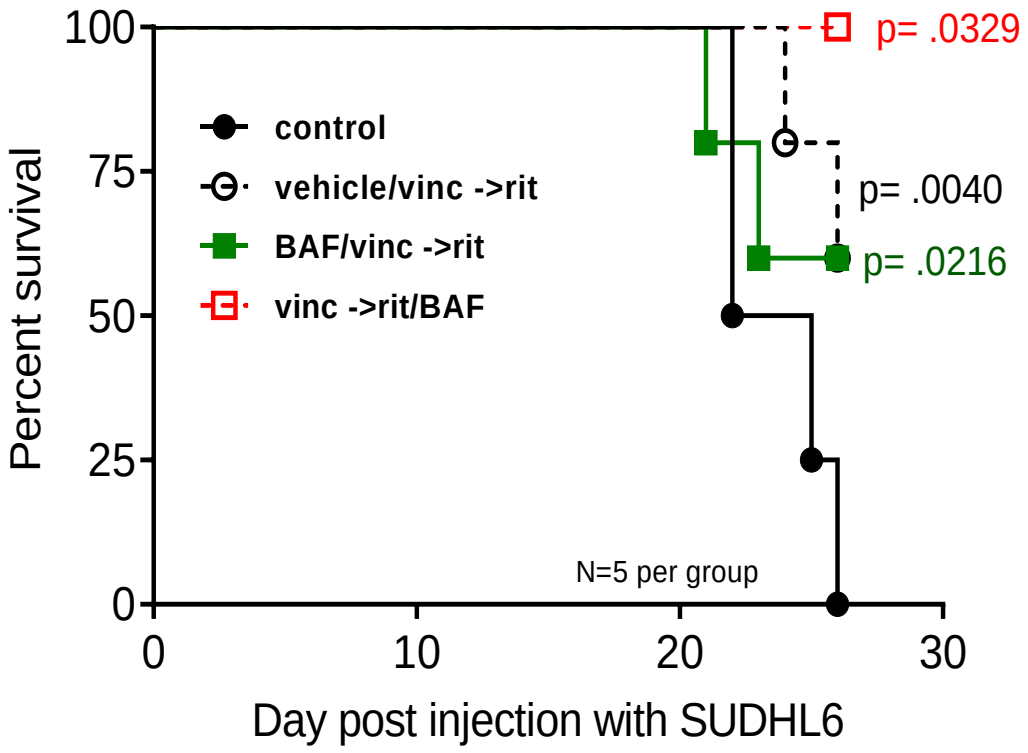

Figure 5.20 Kaplan Meier analysis shows that mice treated with vincristine and rituximab prior to BAF312 had better survival. Mice were censured when tumour size reached 1.1cm in size, the maximum tumour size allowed according to our Home Office licence. All vehicle treated mice reached censure cut-off by day 27. Mice from groups given vincristine and rituximab alone or BAF312 prior to combination treatment also had mice censured. None of the mice treated with vincristine and rituximab combined prior to BAF312 were censured. N=4 per group with student's t-test used to determine p value.

5.5 Discussion

Having shown that monocytes and macrophages migrate in an S1P-dependent manner, I next explored the effect of S1P on phagocytosis and found that S1P reduced the phagocytosis of FITC+ latex beads coated with rabbit IgG by macrophages. Moreover, S1P also was shown to reduce the phagocytosis of rituximab treated DLBCL cell lines. Blocking S1PR1 (and S1PR5) with BAF312 reversed this inhibitory effect reduction and that S1PR2 agonist had no effect. A limitation of my result is that the S1P experimentally added does not mimic the phenotypic effects of S1P produced within tumour cells. Another limitation of my study, is that macrophages are highly adherent and will stick to polystyrene tubes, culture dishes, and glass. M2 macrophages were found to phagocytose at similar ratios but the total macrophages counted were lower than for M1. Perhaps M2 macrophages are stickier than M1 causing them to adhere to the flow cytometry tubes during the phagocytosis assay. This could also be the reason for my results showing M2 macrophages were less likely to migrate as shown in chapter 4. M1 may be less adherent as it is an inflammatory macrophage which should either migrate to appropriate sites or migrate away when no longer needed.

M1 (GM-CSF) macrophages were more phagocytic of rituximab treated DLBCL than M2 (M-CSF) macrophages. My results were in contrast to results shown by Leidi *et al* who examined M1 and M2 phagocytosis of rituximab treated B-CLL (Leidi et al., 2009). Leidi *et al* differentiated primary CD14+ monocytes with GM-CSF and M-CSF for 7 days but also added INFγ and LPS

to the GM-CSF culture for 24hr and added IL-10 and IL-4 for 48hr. Adding cytokines and LPS, a lipoglycan/endotoxin from gram negative bacteria, may have driven their M1 and M2 macrophages polarise to more extreme phenotypes on the spectrum of macrophage polarisation. Also, according to their materials and methods, for each experiment the comparison between M1 and M2 were not always with matched donors (Leidi et al., 2009). Leidi *et al* also do not indicate the number of donors and CLL cases that were evaluated while I have evaluated at least nine different donors in their response to each of the rituximab-opsonised DLBCL cell lines.

The use of cell lines as DLBCL targets in my studies may also account for the disparity with published phagocytosis data as cell lines are considered less representative of primary tumours. Though, I have been careful in the choice of cell lines, using SUDHL6 and OCI-Ly3 which by gene expression were shown to cluster by COO with DLBCL patients (Alizadeh et al., 2000). Another study by Herter *et al* who studied the FC-mediated phagocytosis of different subsets of blood derived macrophages also showed that M1 macrophages has a lower phagocytic index than M2 macrophages (Herter et al., 2014). This discrepancy could be due to the alternative method of polarisation used by Herter whereby monocytes isolated by indirect purification were polarised with M-CSF before a further polarisation with INFγ and LPS for M1 differentiation, and various cytokines such as IL-4 for M2a, LPS + undefined immune complexes for M2b, and IL-10 for M2c differentiation (Herter et al., 2014). Also, in this thesis, phagocytosis assays

were conducted in polystyrene tubes as discussed in Chapter 5 discussion which may also account for the lower phagocytosis of M2 compared to M1.

Modulating the tumour associated macrophages in DLBCL with GM-CSF was in clinical trials but was stopped due to its toxicity in patients (Kahl et al., 2006, Chang et al., 2010). But clinical studies with GM-CSF show that more optimisation should be done as GM-CSF is reported to increase the CD20 expression of B cells and enhance ADCP (Chang et al., 2010). In my studies, I have shown that increased S1P could reduce ADCP in GM-CSF polarised macrophages and taken together with Chang's data could point to a potential stratification of patients with *SPHK1* that may not benefit from GM-CSF treatment. Also, the addition of BAF312 may be beneficial to counter the effects of S1P on ADCP if administered in the appropriate treatment sequence so as to not reduce macrophages but enhance phagocytosis.

From the *in vitro* results, I hypothesised that treating tumour bearing mice with BAF312 would reduce migration of infiltrating monocytes and macrophages which would in turn reduce the availability of macrophages to phagocytose rituximab treated DLBCL cells. Preliminary experiments suggest this is the case. Mice treated with BAF312 prior to the suboptimal dose of vincristine/ rituximab had a small reduction in efficacy. Further work to determine if BAF312 given for at least a week prior optimal treatment would reduce the efficacy of vincristine/rituximab.

CHAPTER 6

Conclusions and future perspectives

Chapter 6

Conclusions and future perspectives

During homeostasis, high levels of ceramide or sphingosine leads to increased apoptosis and senescence. Conversely, high levels of sphingosine-1-phosphate (S1P) will promote cell survival and proliferation. These contradictory functions are modulated by SPHK1, the enzyme responsible for the phosphorylation of sphingosine to S1P. (Spiegel and Milstien, 2003) S1P has also been implicated in angiogenesis and immune responses due to its role in lymphocyte trafficking. As such, S1P is recognised as an onco-lipid which contributes to the pathogenesis of cancers such as DLBCL (Lee et al., 1999, Bayerl et al., 2008, Nagahashi et al., 2018a).

Re-analysis of published gene expression data of primary DLBCL indicate that both GCB and ABC subtypes have a higher *SPHK1* expression than normal germinal centre B cells. Our group has shown that *SPHK1* drives angiogenesis in DLBCL and others have shown that S1PR1 signalling is associated with poor OS in R-CHOP treated patients (Lupino et al., 2019, Paik et al., 2014). Evidence of the role of S1P and S1P receptor signalling in DLBCL continues to mount with the determination of *S1PR2* as a bona fide tumour suppressor in DLBCL (Stelling et al., 2018, Vockerodt et al., 2019, Cattoretti et al., 2009). The cell types involved in the S1P receptor signalling in DLBCL has not been fully elucidated. We showed that HUVECS signal via S1PR1 after stimulation with S1P and we also performed RNAseq of these

cells to obtain a set of differentially expressed genes associated with endothelial cells and S1P (Lupino et al., 2019). From the HUVEC/S1P gene set, we found an enrichment of macrophage signature genes which was taken from Doig *et al* (Doig et al., 2013). This enrichment of macrophage signature genes was confirmed in a set of genes positively correlated with *SPHK1* in DLBCL provided by Professor Reuben Tooze (Care et al., 2015). Gene set enrichment analysis showed that macrophage activation, migration and function were processes over-represented by the *SPHK1* gene set.

Monocytes and macrophages are abundant in the tumour microenvironment of DLBCL. With the primary mechanism of action of rituximab in DLBCL is ADCP, it was relevant to study the role of S1P in the recruitment and function of monocytes and macrophages in the context of DLBCL. It may be that the enrichment of macrophage genes in the *SPHK1* data set is due to macrophages themselves expressing *SPHK1*. The expression of *SPHK1* in macrophages in healthy donors and found that there was variable expression between donors. Examining a small cohort of primary DLBCL cases, macrophages were found to express *SPHK1* at levels similar to tonsillar germinal centre B cells.

To examine the effect of S1P on macrophages in the context of DLBCL, I have used a model of *in vitro* of primary human monocytes and macrophages. THP-1, a myeloid leukaemia cell line, is a widely model for macrophage polarisation for *in vitro* studies but I have opted to use primary human monocytes differentiated with GM-CSF and M-CSF (Schwende et al., 1996,

Lacey et al., 2012). Using primary monocytes will have variability from donor to donor as opposed to using a cell line such as THP-1. Therefore, in order to account for the variability of primary cultures, three healthy donors were used for each experiment performed at least twice with another set of three healthy donors. Indeed, there was heterogeneity amongst the primary macrophages in their response to rituximab treated target cells (DLBCL). Each donor's level of response differed in scale but nearly all donors' macrophages had a level of reduced phagocytosis when treated with S1P.

Careful consideration of the cytokines used for *in vitro* polarisation of monocytes to M1 and M2. Surveying literature using primary monocytes for macrophage polarisation, most used additional cytokines such as INFγ for M1 and for M2, IL-4 and IL-10 (Leidi et al., 2009, Herter et al., 2014, Zhang et al., 2016a, Mendoza-Coronel and Ortega, 2017). In this thesis, the *in vitro* model used by Lacey et al showed that GM-CSF and M-CSF were sufficient to achieve M1 and M2 polarisation and these cytokines have been associated with polarisation of tumour associated macrophages (Lacey et al., 2012, Van Overmeire et al., 2016, Martinez and Gordon, 2014).

I have shown that migration of monocytes and macrophages to DLBCL is mediated through S1PR1. Although S1P induced migration mediated through S1PR1 of monocytes and macrophages is known in the context of apoptosis and inflammation, it has not been described before in DLBCL (Weichand et al., 2013b, Pyne et al., 2016, Pappu et al., 2007). I have shown that monocytes and macrophages migrate to DLBCL conditioned medium and

to DLBCL xenograft tumours in an S1PR1 dependent manner. The observation that changes in S1P receptor expression is associated with macrophage polarisation described in this thesis is the first comprehensive analysis of S1P receptor expression in human monocytes/macrophages. With the panel of 34 healthy donors evaluated, S1PR1 was found to be decreased and S1PR2 increased upon differentiation from monocytes.

In the context of phagocytosis, regardless of the discrepancy in the levels of phagocytosis of M1 and M2 in my studies compared to previously published data, I have shown that the phagocytosis of rituximab-opsonised DLBCL was reduced when macrophages were exposed to high levels of S1P. This reduction was abrogated in the presence of an S1PR1/S1PR5 antagonist. I did not evaluate which S1P receptor was involved in the reduced phagocytosis of FITC+ IgG opsonised latex beads observed after S1P treatment. There has been two reported observations of the reduced phagocytosis in the presence of S1P in a mouse model of chronic obstructive pulmonary disease (COPD) and sepsis (McQuiston et al., 2011, Hou et al., 2015).

In a murine COPD model using C57BL/6 mouse macrophages, they examined phagocytosis of a fungus, *Cryptococcus neoformans* (McQuiston et al., 2011). They found that treatment with JTE013 and S1P reduced phagocytosis which indicates that this reduction may be through another S1P receptor such as S1PR1 or S1PR5 (McQuiston et al., 2011). In the sepsis model, Hou *et al* used C57BL/6 mice that were S1PR2-/- and found that these mice had reduced phagocytosis of bacteria (Hou et al., 2015). This same group

also found that S1PR3 was upregulated in macrophages during sepsis and that S1PR3 was required for bacterial clearing (Hou et al., 2017). These groups along with my results provide evidence of the importance of S1P and its receptors in phagocytosis function of macrophages.

There have not been any reports of S1P and phagocytosis in the context of DLBCL. I have shown that S1P reduces phagocytosis of rituximab treated DLBCL *in vitro*, and have also examined if this observation was relevant *in vivo*. The antagonism of S1PR1 *in vivo* was evaluated using xenograft model of DLBCL. Mice were treated with BAF312 in combination with vincristine and rituximab. The addition of an BAF312 to vincristine/rituximab treatment had reduced efficacy when administered prior to rituximab compared to vehicle control. Mice treated with BAF312 along with rituximab had smaller average tumour volume compared to mice given BAF312 prior to vincristine. The difference in tumour growth may be due to treatment scheduling of BAF312 but data was not statistically significant. Further work to optimise treatment scheduling of BAF312 with vincristine and rituximab is needed.

For future work, I propose the following:

1. To explore the effect of S1P itself on macrophage polarisation. In particular, to investigate if S1P induces macrophages to secrete TGFβ1, known to inhibit inflammatory responses
2. To examine the effect of S1P signalling on DLBCL in the targeted S1PR2 null mouse. S1PR2 null mice develop tumours that are

similar to DLBCL (Cattoretti et al., 2009). It will be of interest to study how S1PR2 impacts the macrophages in these animals.

3. To more broadly explore the impact of S1P on other functions associated with TAMs, use published gene expression data for GM-CSF M1 and M-CSF polarised M2.
4. To do further *in vivo* studies with BAF312 and other S1PR1 antagonists to determine the effect of reducing macrophage infiltration in DLBCL tumours in the context of vincristine/rituximab treatment.

APPENDICES

Appendix A1 DLBCL case IDs summarising SPHK1 score, average CD68 score and average SPHK1+/CD68+ score

CASE ID	SPHK1 score * (60X)	Mean CD68/HPF (40X) **	Mean SPHK1/CD68per HPF (100x) ***	SUBTYPE
DLBCL 4	**5**	**178**	**n/a**	**NON-GCB**
DLBCL 6	**3**	**141**	**5/25**	**NON-GCB**
DLBCL 95	**6**	**171**	**no lesion**	**NON-GCB**
DLBCL 123	**5**	**187**	**no lesion**	**GCB**
DLBCL 126	**4**	**179**	**2/21**	**GCB**
DLBCL 134	**3**	**255**	**n/a**	**NON-GCB**
DLBCL 156	**2**	**49**	**n/a**	**GCB**
DLBCL 159	**3**	**184**	**1/19**	**GCB**
DLBCL 165	**6**	**118**	**3/27**	**GCB**
DLBCL 167	**2**	**287**	**n/a**	**GCB**
DLBCL 175	**3**	**204**	**4/22**	**NON-GCB**
DLBCL 176	**2**	**125**	**5/27**	**NON-GCB**
DLBCL 181	**6**	**237**	**n/a**	**GCB**
DLBCL 185	**6**	**223**	**n/a**	**NON-GCB**
DLBCL 190	**6**	**305**	**3/24**	**NONGCB**
DLBCL 191	**3**	**258**	**6/32**	**GCB**
DLBCL 200	**6**	**226**	**n/a**	**NON-GCB**
DLBCL 208	**4**	**238**	**4/28**	**GCB**
DLBCL 213	**3**	**199**	**n/a**	**GCB**
DLBCL 299	**6**	**287**	**n/a**	**GCB**
tonsil 1	**2**	**48**	**1/37**	
tonsil 2	**2**	**53**	**3/32**	
tonsil 3	**1**	**n/a**	**n/a**	

*SPHK1 score calculated as described in Chapter 3 section 3.2.1 using 60x

**Average CD68+ cells per 5-HPF (high-power field) at 40x

***Average CD68+/SPHK1+ cells per 3-HPF at 100x

Appendix A2 ***SPHK1*-correlated migration genes differentially expressed in ABC-DLBCL from the Morin dataset.** Genes in common with the Tooze gene set and migration gene set were evaluated in the Morin dataset of differentially expressed genes. I found 70//93 *SPHK1*-correlated phagocytosis genes were upregulated in ABC-type DLBCL and 2/93 downregulated (marked as red). Pearson correlation (r) was calculated for each gene versus *SPHK1* within the Morin dataset. Significant genes are marked in blue (p<.05), those that were not significant could be due to the small sample size.

ABC	r	P (two-tailed)
IL6	0.6206	0.0002
ITGA5	0.5575	0.0009
COL1A1	0.5171	0.0024
PIK3R2	0.5123	0.0027
SLC7A11	0.4654	0.0073
COL1A2	0.4646	0.0074
SERPINE1	0.4505	0.0097
ESAM	0.4042	0.0218
ITGAV	0.4017	0.0227
TRPV4	0.4004	0.0232
MYH9 down	0.372	0.036
MMP1	0.3383	0.0582
C5AR1	0.3281	0.0668
PROS1	0.309	0.0853
EPS8	0.3056	0.0889
ITGAM	0.3007	0.0945
CXCL1	0.3004	0.0948
GPC1	0.2884	0.1094
S100A12	0.2572	0.1554
FN1	0.2485	0.1702
TNF down	0.2353	0.1948
ROR2	0.233	0.1994
MERTK	0.2282	0.2091
MMP9	0.2171	0.2327
PDGFB	0.2148	0.2378
SELE	0.2135	0.2408
SDC2	0.2116	0.245
ITGAX	0.2107	0.2471
TRPM2	0.2011	0.2697
LGALS3	0.2005	0.2712
CXCL16	0.2003	0.2718
THBS1	0.1982	0.2768
ANXA1	0.1931	0.2895
CD34	0.1907	0.2958
ANGPT2	0.1896	0.2987
RARRES2	0.1861	0.3078

ABC	r	P (two-tailed)
SLC7A7	0.1859	0.3083
RORA	0.1839	0.3138
ICAM1	0.183	0.316
FPR2	0.1712	0.3489
APP	0.167	0.3609
SLAMF8	0.1523	0.4053
ITGA1	0.1489	0.4162
GAS6	0.1403	0.4439
S100A8	0.1382	0.4507
SRC	0.1329	0.4685
SDC4	0.1314	0.4734
CCR1	0.1229	0.5027
C3AR1	0.09973	0.5871
CSF1	0.09855	0.5915
S100A9	0.06576	0.7207
PECAM1	0.06258	0.7337
SBDS	0.05614	0.7602
FCER1G	0.05076	0.7826
CXCL13	0.04979	0.7867
SELPLG	0.04601	0.8026
PLA2G7	0.03148	0.8642
CCR5	0.02159	0.9066
SLC7A8	0.01857	0.9197
CD44	-0.01511	0.9346
JAM2	-0.02751	0.8812
CMKLR1	-0.05027	0.7847
CCL5	-0.07059	0.701
JAM3	-0.07607	0.679
TNFRSF11A	-0.1135	0.5362
CAV1	-0.1212	0.5086
CCL7	-0.1368	0.4554
YES1	-0.1455	0.4267
ANGPT1	-0.15	0.4124
CCL11	-0.2046	0.2614
F11R	-0.2561	0.1572

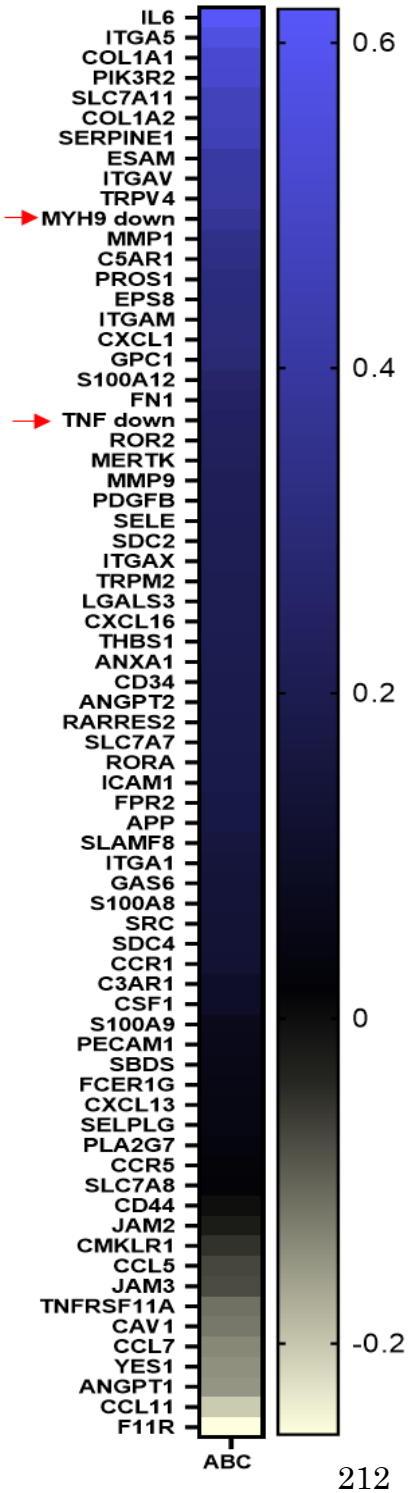

Appendix A3 ***SPHK1*-correlated migration genes differentially expressed in GCB-DLBCL from the Morin dataset.** Genes in common with the Tooze gene set and migration gene set were evaluated in the Morin dataset of differentially expressed genes. I found 86//93 *SPHK1*-correlated phagocytosis genes were upregulated in GCB-type DLBCL and 5/93 downregulated (marked as red). Pearson correlation (r) was calculated for each gene versus *SPHK1* within the Morin dataset. Significant genes are marked in blue (p<.05), those that were not significant could be due to the small sample size.

GCB	r	P (two-tailed)
ITGA5	0.7052	<0.0001
SLC16A3	0.7031	<0.0001
CD44	0.6285	<0.0001
ICAM1	0.6065	<0.0001
SIRPA	0.6022	<0.0001
ITGAM	0.593	<0.0001
SERPINE1	0.5835	<0.0001
SLAMF8	0.5654	<0.0001
TNFRSF11A	0.5383	<0.0001
TRPM2	0.5355	<0.0001
MMP9	0.5308	<0.0001
C5AR1	0.5281	<0.0001
GPC1	0.5203	<0.0001
CSF1	0.5177	<0.0001
RARRES2	0.5147	<0.0001
CMKLR1	0.5116	<0.0001
COL1A1	0.5023	0.0001
ITGB2	0.5008	0.0001
TRPV4	0.5001	0.0001
JAM3	0.4995	0.0001
FN1	0.4909	0.0002
SDC4	0.4905	0.0002
ANXA1	0.4809	0.0002
COL1A2	0.4794	0.0002
CXCL16	0.4675	0.0004
SELPLG	0.4607	0.0005
SLC7A7	0.4406	0.0009
C3AR1	0.4333	0.0011
FCER1G	0.4312	0.0011
THBS1	0.4237	0.0014
IL1B	0.4197	0.0016
ITGAX	0.419	0.0016
OLR1	0.4162	0.0017
SHC1 down	0.4114	0.002
CCL5	0.4075	0.0022
SELE	0.4028	0.0025
SDC2	0.4014	0.0026
APP	0.3935	0.0032
IL6	0.3753	0.0052
TNF down	0.367	0.0063
CCR1	0.3647	0.0067
JAM2	0.3593	0.0076
S100A8	0.3567	0.0081
PDGFB	0.3427	0.0112
ANGPT2	0.342	0.0114
SRC	0.3407	0.0117
ITGAV	0.3386	0.0123
CCL7	0.3139	0.0208
SDC1	0.3138	0.0208
PLA2G7	0.3137	0.0209
CCL20	0.3123	0.0215
MYH9 down	0.3121	0.0216
CCR5	0.311	0.0221
S100A9	0.307	0.024
MAPK3	0.3041	0.0254
FPR2	0.2908	0.0329
F11R	0.2878	0.0348
PIK3R2	0.2834	0.0378
CD84	0.2717	0.0469

GCB	r	P (two-tailed)
CXCL13	0.2633	0.0544
GAS6	0.2567	0.061
PECAM1	0.2563	0.0614
SLC7A11	0.2561	0.0616
MERTK	0.2378	0.0833
CD34	0.2354	0.0867
EPS8	0.2343	0.0881
ESAM	0.2331	0.0898
MSN	0.233	0.09
TREM1	0.206	0.1351
CEACAM3	0.2048	0.1373
ANO6	0.2045	0.1381
PROS1	0.2042	0.1386
ROR2	0.178	0.1979
MMP1	0.1484	0.2841
LGALS3	0.1432	0.3016
ARHGEF5	0.128	0.3562
S100A12	0.1245	0.3696
CD58 down	0.1131	0.4153
YES1	0.1018	0.4637
SLC7A8	0.07681	0.5809
CAV1	0.07608	0.5845
ITGA1	0.06189	0.6566
PDE4D down	0.05892	0.6722
CCL11	0.03567	0.7979
CXCL1	0.01347	0.923
RORA	-0.008628	0.9506
ADD2	-0.05393	0.6986
SBDS	-0.05979	0.6676
CXCR1	-0.07829	0.5736
ANGPT1	-0.1172	0.3988

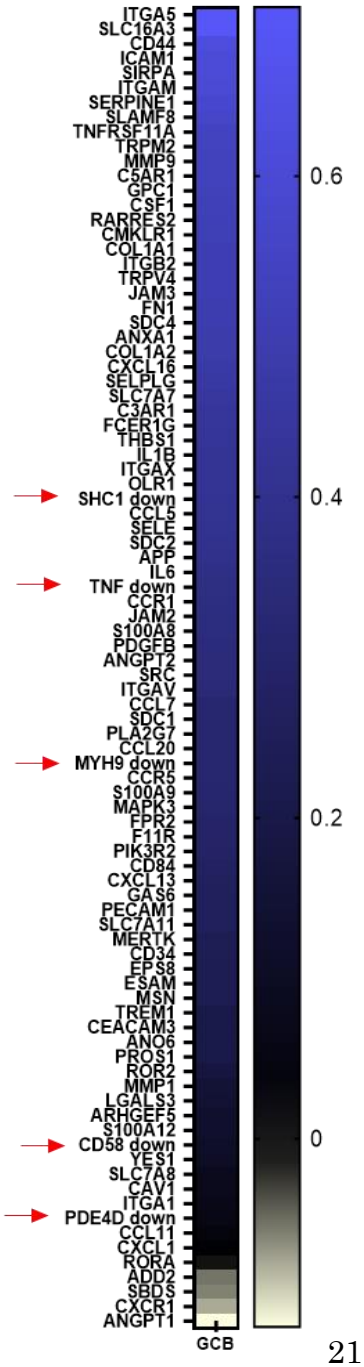

Appendix A4 ***SPHK1*-correlated phagocytosis genes differentially expressed in ABC-DLBCL from the Morin dataset.** Genes in common with the Tooze gene set and phagocytosis gene set were evaluated in the Morin dataset of differentially expressed genes. I found 49/66 *SPHK1*-correlated phagocytosis genes were upregulated in ABC-type DLBCL and 7/66 (red arrows). Pearson correlation (r) was calculated for each gene versus *SPHK1* within the Morin dataset. Significant genes are marked in blue ($p<.05$), those that were not significant could be due to the small sample size.

ABC-DLBCL	r	P (two-tailed)
SPON2	0.5467	0.0012
CD93	0.5279	0.0019
PIK3R2	0.5123	0.0027
SERPINE1	0.4505	0.0097
CYP2S1	0.448	0.0101
SCARB1 down	0.4436	0.011
FGR	0.403	0.0222
ITGAV	0.4017	0.0227
MYH9 down	0.372	0.036
TGM2	0.3225	0.0719
ITGAM	0.3007	0.0945
P2RY6	0.2863	0.1122
LRP1	0.2636	0.145
CD14	0.2552	0.1586
MFGE8	0.2536	0.1613
FCGR2A	0.2531	0.1621
ADORA1	0.2463	0.1742
MARCO	0.2306	0.2041
RHOBTB1	0.23	0.2055
MERTK	0.2282	0.2091
NCF2	0.2139	0.2398
CLIC4 down	0.2087	0.2516
THBS1	0.1982	0.2768
ANXA1	0.1931	0.2895
PLA2G5	0.1905	0.2964
DOCK1	0.1629	0.3731
SLAMF1 down	0.1617	0.3766
PLCG2 down	0.1609	0.3791
GAS6	0.1403	0.4439
SRC	0.1329	0.4685
NR1H3	0.1174	0.5222
TREM2	0.1165	0.5254
P2RX7	0.1101	0.5485
FCGR1A	0.1067	0.561
CSF1	0.09855	0.5915
NCKAP1	0.07649	0.6773
PECAM1	0.06258	0.7337
FCER1G	0.05076	0.7826
SRPX	0.02016	0.9128
AXL	-0.0139	0.9398
CD44	-0.01511	0.9346
LEPR	-0.02162	0.9065
TLR3	-0.02303	0.9004
RAB20	-0.03355	0.8554
CORO1C	-0.05962	0.7458
C3	-0.07998	0.6635
SCARB2	-0.1014	0.5809
CLEC7A	-0.102	0.5786
MSR1	-0.1052	0.5666
GULP1	-0.1241	0.4985
WIPF3	-0.1321	0.471
YES1	-0.1455	0.4267
CYFIP1	-0.1575	0.3892
PRKCE down	-0.2278	0.2099
SYK down	-0.2544	0.1599
CD47	-0.4078	0.0205

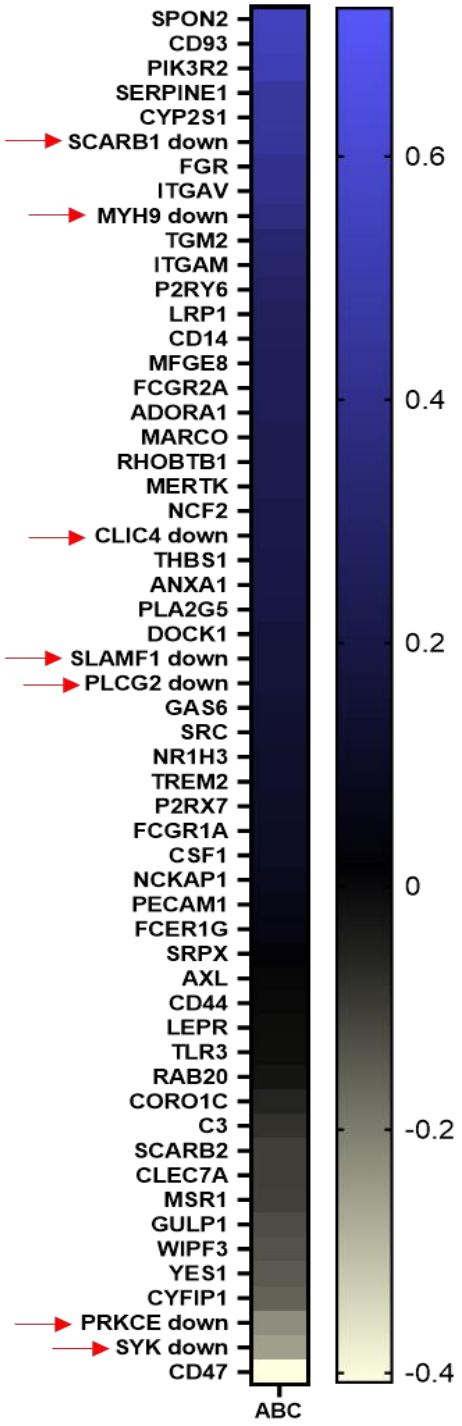

Appendix A5 ***SPHK1*-correlated phagocytosis genes differentially expressed in GCB-DLBCL from the Morin dataset.** Genes in common with the Tooze gene set and phagocytosis gene set were evaluated in the Morin dataset of differentially expressed genes. I found 57/66 *SPHK1*-correlated phagocytosis genes were upregulated in GCB-type DLBCL and 3/66 (red arrows). Pearson correlation (r) was calculated for each gene versus *SPHK1* within the Morin dataset. Significant genes are marked in blue (p<.05) those that were not significant could be due to the small sample size.

GCB-DLBCL	r	p (two-tailed)
CYP2S1	0.7215	<0.0001
MFGE8	0.6748	<0.0001
CD44	0.6285	<0.0001
SLC11A1	0.6067	<0.0001
ITGAM	0.593	<0.0001
SERPINE1	0.5835	<0.0001
RAB34	0.538	<0.0001
LRP1	0.5303	<0.0001
DOCK1	0.5268	<0.0001
CSF1	0.5177	<0.0001
P2RX7	0.5138	<0.0001
ITGB2	0.5008	0.0001
TGM2	0.492	0.0002
CYFIP1	0.4861	0.0002
ANXA1	0.4809	0.0002
GSN	0.4693	0.0003
FGR	0.4525	0.0006
MARCO	0.4421	0.0008
FCER1G	0.4312	0.0011
THBS1	0.4237	0.0014
NR1H3	0.4143	0.0018
CD14	0.4067	0.0023
PLD1	0.4044	0.0024
C3	0.3925	0.0033
ADORA1	0.3851	0.004
WIPF3	0.3829	0.0043
MCF2	0.3807	0.0045
RAB20	0.3759	0.0051
SCARB2	0.3568	0.0081
SRC	0.3407	0.0117
ITGAV	0.3386	0.0123
FCGR2A	0.3318	0.0143
CORO1C	0.3238	0.0169
MYH9 down	0.3121	0.0216
MAPK3	0.3041	0.0254
P2RY6	0.2865	0.0357
PIK3R2	0.2834	0.0378
SRPX	0.2808	0.0397
FCGR1A	0.2711	0.0474
CD93	0.2578	0.0598
GAS6	0.2567	0.061
PECAM1	0.2563	0.0614
MERTK	0.2378	0.0833
FAS	0.2349	0.0873
MSN	0.233	0.09
SPON2	0.2322	0.091
PLA2GS	0.2297	0.0947
NCKAP1	0.2259	0.1005
SCARB1 down	0.2143	0.1196
CEACAM3	0.2048	0.1373
YES1	0.1018	0.4637
RHOBTB1	0.06746	0.6279
GULP1	0.0544	0.696
TLR3	0.04381	0.7531
TREM2	-0.0134	0.9234
SLAMF1	-0.01572	0.9102
CLEC7a	-0.02558	0.8543
MSR1	-0.05629	0.686
MYO10	-0.1767	0.2013
CLIC4 down	-0.1846	0.1814

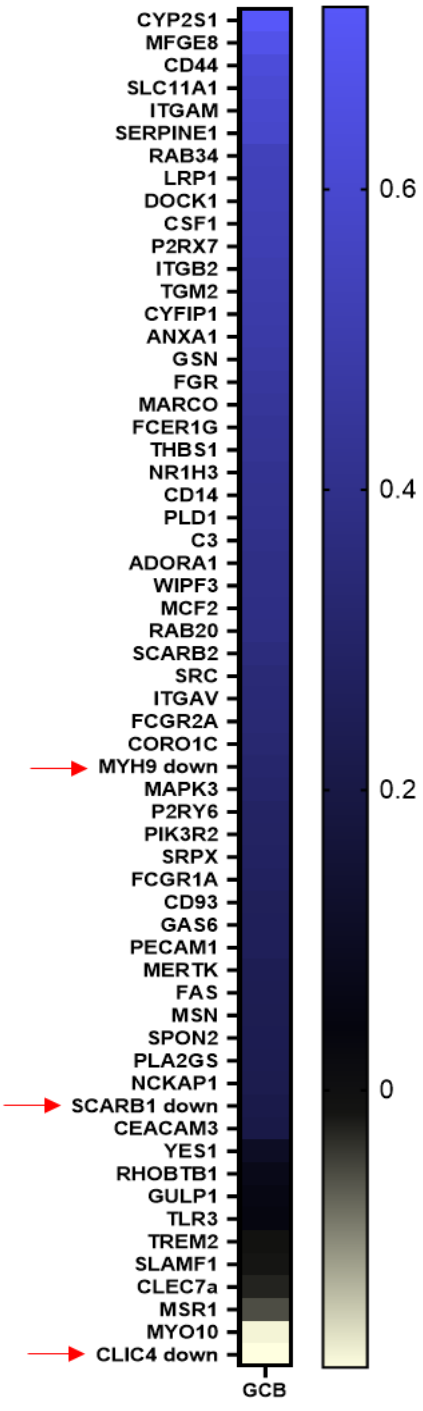

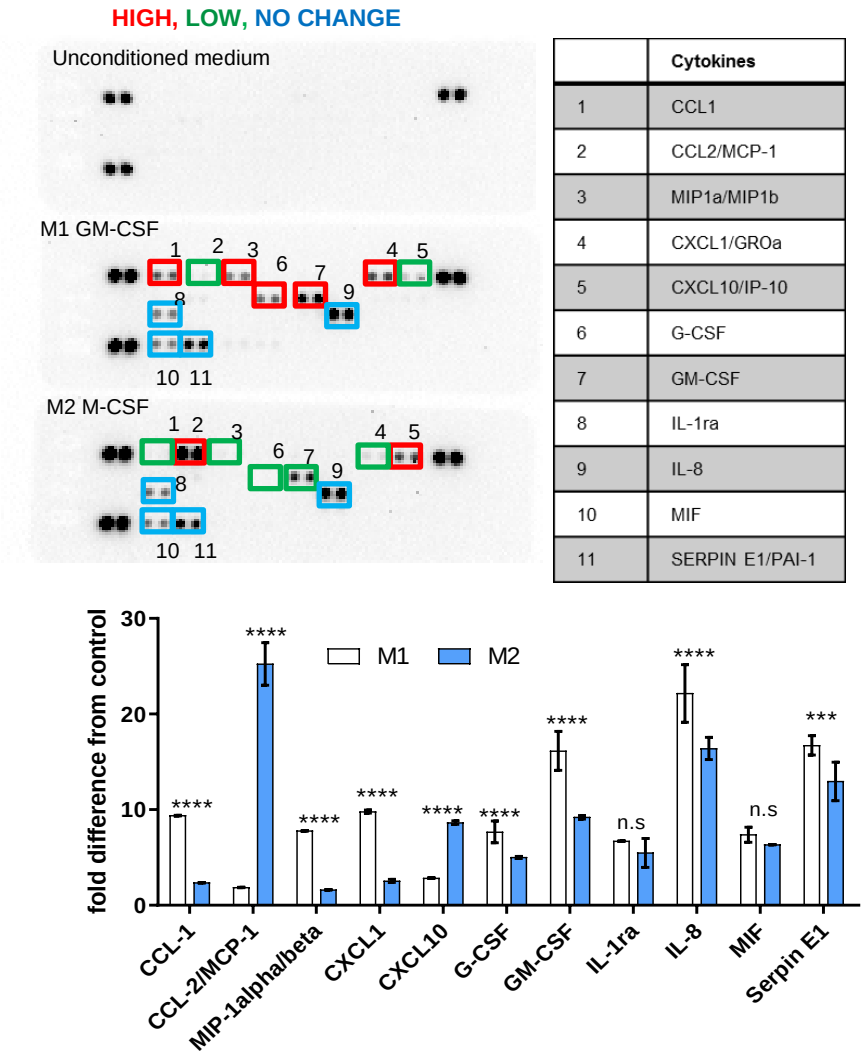

Appendix A6 Cytokine array from M1 and M2 macrophages from donor K. Conditioned medium from day 7 cultures of M1 and M2 macrophages were analysed on a cytokine array with 35 different cytokines. The cytokines are spotted in duplicate and were analysed by densitometry relative to the unconditioned medium blot. There were two cytokines highly secreted by M2; CCL2/MCP-1 and CXCL10. I found seven cytokines more highly secreted by M1 including GM-CSF which acted as an additional control as this cytokine was directly added to the culture medium of M1; CCL1, MIP1a/b, CXCL1, G-CSF, GM-CSF, IL-8 and Serpin EI. There was a high level of GM-CSF secreted by M2.

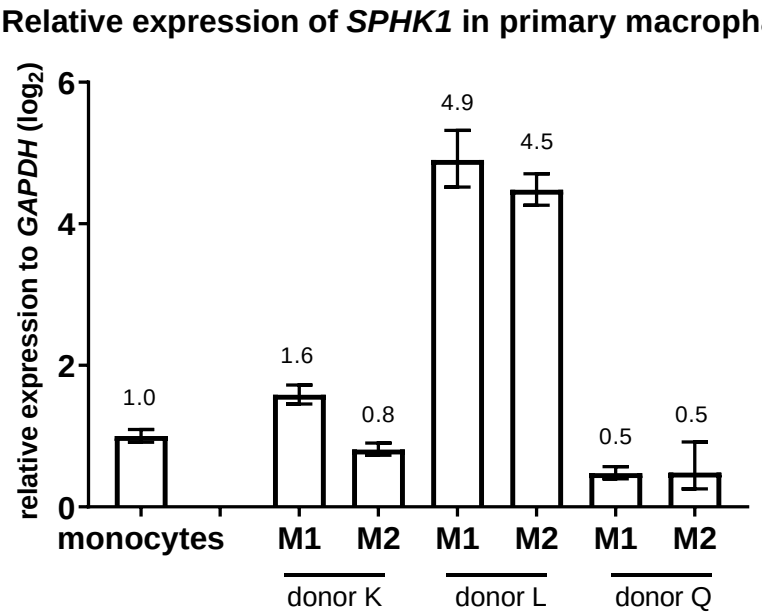

Appendix A7 Expression of *SPHK1* was evaluated in three primary macrophages

The expression of *SPHK1* was evaluated by qPCR in three donors' M1 and M2 macrophages relative to their matched monocytes. Expression between donors varied with donor (L) showing an overexpression of *SPHK1* to donor (Q) showing an under expression of *SPHK1*.

REFERENCES

References

Alizadeh, A. A., Eisen, M. B., Davis, R. E., Ma, C., Lossos, I. S., Rosenwald, A., Boldrick, J. C., Sabet, H., Tran, T., Yu, X., Powell, J. I., Yang, L., Marti, G. E., Moore, T., Hudson, J., Jr., Lu, L., Lewis, D. B., Tibshirani, R., Sherlock, G., Chan, W. C., Greiner, T. C., Weisenburger, D. D., Armitage, J. O., Warnke, R., Levy, R., Wilson, W., Grever, M. R., Byrd, J. C., Botstein, D., Brown, P. O. and Staudt, L. M. (2000) 'Distinct types of diffuse large B-cell lymphoma identified by gene expression profiling', *Nature,* 403(6769), pp. 503-11.

Anders, S., McCarthy, D. J., Chen, Y., Okoniewski, M., Smyth, G. K., Huber, W. and Robinson, M. D. (2013) 'Count-based differential expression analysis of RNA sequencing data using R and Bioconductor', *Nat Protoc,* 8(9), pp. 1765-86.

Aoki, M., Aoki, H., Ramanathan, R., Hait, N. C. and Takabe, K. (2016) 'Sphingosine-1-Phosphate Signaling in Immune Cells and Inflammation: Roles and Therapeutic Potential', *Mediators Inflamm,* 2016, pp. 8606878.

Arandjelovic, S. and Ravichandran, K. S. (2015) 'Phagocytosis of apoptotic cells in homeostasis', *Nat Immunol,* 16(9), pp. 907-17.

Ashburner, M., Ball, C. A., Blake, J. A., Botstein, D., Butler, H., Cherry, J. M., Davis, A. P., Dolinski, K., Dwight, S. S., Eppig, J. T., Harris, M. A., Hill, D. P., Issel-Tarver, L., Kasarskis, A., Lewis, S., Matese, J. C., Richardson, J. E., Ringwald, M., Rubin, G. M. and Sherlock, G. (2000) 'Gene ontology: tool for the unification of biology. The Gene Ontology Consortium', *Nat Genet,* 25(1), pp. 25-9.

Barrans, S., Crouch, S., Smith, A., Turner, K., Owen, R., Patmore, R., Roman, E. and Jack, A. (2010) 'Rearrangement of MYC is associated with poor prognosis in patients with diffuse large B-cell lymphoma treated in the era of rituximab', *J Clin Oncol,* 28(20), pp. 3360-5.

Barrans, S. L., Evans, P. A., O'Connor, S. J., Kendall, S. J., Owen, R. G., Haynes, A. P., Morgan, G. J. and Jack, A. S. (2003) 'The t(14;18) is associated with germinal center-derived diffuse large B-cell lymphoma and is a strong predictor of outcome', *Clin Cancer Res,* 9(6), pp. 2133-9.

Bassing, C. H., Swat, W. and Alt, F. W. (2002) 'The mechanism and regulation of chromosomal V(D)J recombination', *Cell,* 109 Suppl, pp. S45-55.

Bayerl, M. G., Bruggeman, R. D., Conroy, E. J., Hengst, J. A., King, T. S., Jimenez, M., Claxton, D. F. and Yun, J. K. (2008) 'Sphingosine kinase 1 protein and mRNA are overexpressed in non-Hodgkin lymphomas and are attractive targets for novel pharmacological interventions', *Leuk Lymphoma,* 49(5), pp. 948-54.

Beguelin, W., Popovic, R., Teater, M., Jiang, Y., Bunting, K. L., Rosen, M., Shen, H., Yang, S. N., Wang, L., Ezponda, T., Martinez-Garcia, E., Zhang, H., Zheng, Y., Verma, S. K., McCabe, M. T., Ott, H. M., Van Aller, G. S., Kruger, R. G., Liu, Y., McHugh, C. F., Scott, D. W., Chung, Y. R., Kelleher, N., Shaknovich, R., Creasy, C. L., Gascoyne, R. D., Wong, K. K., Cerchietti, L., Levine, R. L., Abdel-Wahab, O., Licht, J. D., Elemento, O. and Melnick, A. M. (2013) 'EZH2 is required for

germinal center formation and somatic EZH2 mutations promote lymphoid transformation', *Cancer Cell,* 23(5), pp. 677-92.

Blaho, V. A. and Hla, T. (2014) 'An update on the biology of sphingosine 1-phosphate receptors', *J Lipid Res,* 55(8), pp. 1596-608.

Blumenthal, R. D. (2005) *Chemosensitivity. Methods in molecular medicine* (2 vols). Totowa, N.J.: Humana Press.

Bolli, M. H., Abele, S., Binkert, C., Bravo, R., Buchmann, S., Bur, D., Gatfield, J., Hess, P., Kohl, C., Mangold, C., Mathys, B., Menyhart, K., Muller, C., Nayler, O., Scherz, M., Schmidt, G., Sippel, V., Steiner, B., Strasser, D., Treiber, A. and Weller, T. (2010) '2-imino-thiazolidin-4-one derivatives as potent, orally active S1P1 receptor agonists', *J Med Chem,* 53(10), pp. 4198-211.

Campo, E., Swerdlow, S. H., Harris, N. L., Pileri, S., Stein, H. and Jaffe, E. S. (2011) 'The 2008 WHO classification of lymphoid neoplasms and beyond: evolving concepts and practical applications', *Blood,* 117(19), pp. 5019-32.

Care, M. A., Westhead, D. R. and Tooze, R. M. (2015) 'Gene expression meta-analysis reveals immune response convergence on the IFNgamma-STAT1-IRF1 axis and adaptive immune resistance mechanisms in lymphoma', *Genome Med,* 7, pp. 96.

Cattoretti, G., Mandelbaum, J., Lee, N., Chaves, A. H., Mahler, A. M., Chadburn, A., Dalla-Favera, R., Pasqualucci, L. and MacLennan, A. J. (2009) 'Targeted disruption of the S1P2 sphingosine 1-phosphate receptor gene leads to diffuse large B-cell lymphoma formation', *Cancer Res,* 69(22), pp. 8686-92.

CBER (2018) *What are "Biologics" Questions and answers*. Rockville, Maryland: U.S. Food & Drug Administration (Accessed: March 30 2019).

Chang, C. L., Ho, M. C., Lee, P. H., Hsu, C. Y., Huang, W. P. and Lee, H. (2009) 'S1P(5) is required for sphingosine 1-phosphate-induced autophagy in human prostate cancer PC-3 cells', *Am J Physiol Cell Physiol,* 297(2), pp. C451-8.

Chang, J. E., Seo, S., Kim, K. M., Werndli, J. E., Bottner, W. A., Rodrigues, G. A., Sanchez, F. A., Saphner, T. J., Longo, W. L. and Kahl, B. S. (2010) 'Rituximab and CHOP chemotherapy plus GM-CSF for previously untreated diffuse large B-cell lymphoma in the elderly: a Wisconsin oncology network study', *Clin Lymphoma Myeloma Leuk,* 10(5), pp. 379-84.

Chapuy, B., Stewart, C., Dunford, A. J., Kim, J., Kamburov, A., Redd, R. A., Lawrence, M. S., Roemer, M. G. M., Li, A. J., Ziepert, M., Staiger, A. M., Wala, J. A., Ducar, M. D., Leshchiner, I., Rheinbay, E., Taylor-Weiner, A., Coughlin, C. A., Hess, J. M., Pedamallu, C. S., Livitz, D., Rosebrock, D., Rosenberg, M., Tracy, A. A., Horn, H., van Hummelen, P., Feldman, A. L., Link, B. K., Novak, A. J., Cerhan, J. R., Habermann, T. M., Siebert, R., Rosenwald, A., Thorner, A. R., Meyerson, M. L., Golub, T. R., Beroukhim, R., Wulf, G. G., Ott, G., Rodig, S. J., Monti, S., Neuberg, D. S., Loeffler, M., Pfreundschuh, M., Trumper, L., Getz, G. and Shipp, M. A. (2018) 'Molecular subtypes of diffuse large B cell lymphoma are associated with distinct pathogenic mechanisms and outcomes', *Nat Med,* 24(5), pp. 679-690.

Chen, J., Xu-Monette, Z. Y., Deng, L., Shen, Q., Manyam, G. C., Martinez-Lopez, A., Zhang, L., Montes-Moreno, S., Visco, C., Tzankov, A., Yin, L., Dybkaer, K., Chiu, A., Orazi, A., Zu, Y., Bhagat, G., Richards, K. L., Hsi, E. D., Choi, W. W., van Krieken, J. H., Huh, J., Ponzoni, M., Ferreri, A. J., Zhao, X., Moller, M. B., Farnen, J. P., Winter, J. N., Piris, M. A., Pham, L. and Young, K. H. (2015) 'Dysregulated CXCR4 expression promotes lymphoma cell survival and independently predicts disease progression in germinal center B-cell-like diffuse large B-cell lymphoma', *Oncotarget,* 6(8), pp. 5597-614.

Chen, W., Lu, H., Yang, J., Xiang, H. and Peng, H. (2016) 'Sphingosine 1-phosphate in metabolic syndrome (Review)', *Int J Mol Med,* 38(4), pp. 1030-8.

Chimen, M., McGettrick, H. M., Apta, B., Kuravi, S. J., Yates, C. M., Kennedy, A., Odedra, A., Alassiri, M., Harrison, M., Martin, A., Barone, F., Nayar, S., Hitchcock, J. R., Cunningham, A. F., Raza, K., Filer, A., Copland, D. A., Dick, A. D., Robinson, J., Kalia, N., Walker, L. S. K., Buckley, C. D., Nash, G. B., Narendran, P. and Rainger, G. E. (2015) 'Homeostatic regulation of T cell trafficking by a B cell-derived peptide is impaired in autoimmune and chronic inflammatory disease', *Nat Med,* 21(5), pp. 467-475.

Choi, W. W., Weisenburger, D. D., Greiner, T. C., Piris, M. A., Banham, A. H., Delabie, J., Braziel, R. M., Geng, H., Iqbal, J., Lenz, G., Vose, J. M., Hans, C. P., Fu, K., Smith, L. M., Li, M., Liu, Z., Gascoyne, R. D., Rosenwald, A., Ott, G., Rimsza, L. M., Campo, E., Jaffe, E. S., Jaye, D. L., Staudt, L. M. and Chan, W. C. (2009) 'A new immunostain algorithm classifies diffuse large B-cell lymphoma into molecular subtypes with high accuracy', *Clin Cancer Res,* 15(17), pp. 5494-502.

Church, A. K., VanDerMeid, K. R., Baig, N. A., Baran, A. M., Witzig, T. E., Nowakowski, G. S. and Zent, C. S. (2016) 'Anti-CD20 monoclonal antibody-dependent phagocytosis of chronic lymphocytic leukaemia cells by autologous macrophages', *Clin Exp Immunol,* 183(1), pp. 90-101.

Coiffier, B., Lepage, E., Briere, J., Herbrecht, R., Tilly, H., Bouabdallah, R., Morel, P., Van Den Neste, E., Salles, G., Gaulard, P., Reyes, F., Lederlin, P. and Gisselbrecht, C. (2002) 'CHOP chemotherapy plus rituximab compared with CHOP alone in elderly patients with diffuse large-B-cell lymphoma', *N Engl J Med,* 346(4), pp. 235-42.

Coiffier, B. and Sarkozy, C. (2016) 'Diffuse large B-cell lymphoma: R-CHOP failure-what to do?', *Hematology Am Soc Hematol Educ Program,* 2016(1), pp. 366-378.

Coutinho, R., Clear, A. J., Mazzola, E., Owen, A., Greaves, P., Wilson, A., Matthews, J., Lee, A., Alvarez, R., da Silva, M. G., Cabecadas, J., Neuberg, D., Calaminici, M. and Gribben, J. G. (2015) 'Revisiting the immune microenvironment of diffuse large B-cell lymphoma using a tissue microarray and immunohistochemistry: robust semi-automated analysis reveals CD3 and FoxP3 as potential predictors of response to R-CHOP', *Haematologica,* 100(3), pp. 363-9.

CRUK (2015) *Non-Hodkgin lymphoma statistics*: Cancer Research UK [website]. Available at: https://www.cancerresearchuk.org/health-professional/cancer-statistics/statistics-by-cancer-type/non-hodgkin-lymphoma#heading-Zero (Accessed: January 2019).

Czabotar, P. E., Lessene, G., Strasser, A. and Adams, J. M. (2014) 'Control of apoptosis by the BCL-2 protein family: implications for physiology and therapy', *Nat Rev Mol Cell Biol,* 15(1), pp. 49-63.

D'Ambrosio, D., Freedman, M. S. and Prinz, J. (2016) 'Ponesimod, a selective S1P1 receptor modulator: a potential treatment for multiple sclerosis and other immune-mediated diseases', *Ther Adv Chronic Dis,* 7(1), pp. 18-33.

Davaille, J., Li, L., Mallat, A. and Lotersztajn, S. (2002) 'Sphingosine 1-phosphate triggers both apoptotic and survival signals for human hepatic myofibroblasts', *J Biol Chem,* 277(40), pp. 37323-30.

Debien, E., Mayol, K., Biajoux, V., Daussy, C., De Aguero, M. G., Taillardet, M., Dagany, N., Brinza, L., Henry, T., Dubois, B., Kaiserlian, D., Marvel, J., Balabanian, K. and Walzer, T. (2013) 'S1PR5 is pivotal for the homeostasis of patrolling monocytes', *Eur J Immunol,* 43(6), pp. 1667-75.

Delage, L., Manzoni, D., Quinquenet, C., Fontaine, J., Maarek, A., Chabane, K., Mosnier, I., Hayette, S., Callet-Bauchu, E., Grange, B., Plesa, A. and Sujobert, P. (2019) 'Molecular analysis of a CD19-negative diffuse large B-cell lymphoma', *Haematologica,* 104(3), pp. e114-e116.

Deshmane, S. L., Kremlev, S., Amini, S. and Sawaya, B. E. (2009) 'Monocyte chemoattractant protein-1 (MCP-1): an overview', *J Interferon Cytokine Res,* 29(6), pp. 313-26.

Doig, T. N., Hume, D. A., Theocharidis, T., Goodlad, J. R., Gregory, C. D. and Freeman, T. C. (2013) 'Coexpression analysis of large cancer datasets provides insight into the cellular phenotypes of the tumour microenvironment', *BMC Genomics,* 14, pp. 469.

Donnou, S., Galand, C., Touitou, V., Sautes-Fridman, C., Fabry, Z. and Fisson, S. (2012) 'Murine models of B-cell lymphomas: promising tools for designing cancer therapies', *Adv Hematol,* 2012, pp. 701704.

Durr, C., Pfeifer, D., Claus, R., Schmitt-Graeff, A., Gerlach, U. V., Graeser, R., Kruger, S., Gerbitz, A., Negrin, R. S., Finke, J. and Zeiser, R. (2010) 'CXCL12 mediates immunosuppression in the lymphoma microenvironment after allogeneic transplantation of hematopoietic cells', *Cancer Res,* 70(24), pp. 10170-81.

Dvorak, H. F. (1986) 'Tumors: wounds that do not heal. Similarities between tumor stroma generation and wound healing', *N Engl J Med,* 315(26), pp. 1650-9.

Eklund, L., Bry, M. and Alitalo, K. (2013) 'Mouse models for studying angiogenesis and lymphangiogenesis in cancer', *Mol Oncol,* 7(2), pp. 259-82.

Ennishi, D., Jiang, A., Boyle, M., Collinge, B., Grande, B. M., Ben-Neriah, S., Rushton, C., Tang, J., Thomas, N., Slack, G. W., Farinha, P., Takata, K., Miyata-Takata, T., Craig, J., Mottok, A., Meissner, B., Saberi, S., Bashashati, A., Villa, D., Savage, K. J., Sehn, L. H., Kridel, R., Mungall, A. J., Marra, M. A., Shah, S. P., Steidl, C., Connors, J. M., Gascoyne, R. D., Morin, R. D. and Scott, D. W. (2019) 'Double-Hit Gene Expression Signature Defines a Distinct Subgroup of Germinal Center B-Cell-Like Diffuse Large B-Cell Lymphoma', *J Clin Oncol,* 37(3), pp. 190-201.

Fast, L. D. (2013) *B and T cell development. Non-Hodgkin Lymphoma; prognostic factors and targets*: Humana Press, p. 11-22.

Fidler, I. J. (2003) 'The pathogenesis of cancer metastasis: the 'seed and soil' hypothesis revisited', *Nat Rev Cancer,* 3(6), pp. 453-8.

Foot, N. J., Dunn, R. G., Geoghegan, H., Wilkins, B. S. and Neat, M. J. (2011) 'Fluorescence in situ hybridisation analysis of formalin-fixed paraffin-embedded tissue sections in the diagnostic work-up of non-Burkitt high grade B-cell non-Hodgkin's lymphoma: a single centre's experience', *J Clin Pathol,* 64(9), pp. 802-8.

Franklin, R. A. and Li, M. O. (2016) 'Ontogeny of Tumor-associated Macrophages and Its Implication in Cancer Regulation', *Trends Cancer,* 2(1), pp. 20-34.

Friedberg, J. W. (2017) 'How I treat double-hit lymphoma', *Blood,* 130(5), pp. 590-596.

Gabay, M., Li, Y. and Felsher, D. W. (2014) 'MYC activation is a hallmark of cancer initiation and maintenance', *Cold Spring Harb Perspect Med,* 4(6).

Gao, H., Korn, J. M., Ferretti, S., Monahan, J. E., Wang, Y., Singh, M., Zhang, C., Schnell, C., Yang, G., Zhang, Y., Balbin, O. A., Barbe, S., Cai, H., Casey, F., Chatterjee, S., Chiang, D. Y., Chuai, S., Cogan, S. M., Collins, S. D., Dammassa, E., Ebel, N., Embry, M., Green, J., Kauffmann, A., Kowal, C., Leary, R. J., Lehar, J., Liang, Y., Loo, A., Lorenzana, E., Robert McDonald, E., 3rd, McLaughlin, M. E., Merkin, J., Meyer, R., Naylor, T. L., Patawaran, M., Reddy, A., Roelli, C., Ruddy, D. A., Salangsang, F., Santacroce, F., Singh, A. P., Tang, Y., Tinetto, W., Tobler, S., Velazquez, R., Venkatesan, K., Von Arx, F., Wang, H. Q., Wang, Z., Wiesmann, M., Wyss, D., Xu, F., Bitter, H., Atadja, P., Lees, E., Hofmann, F., Li, E., Keen, N., Cozens, R., Jensen, M. R., Pryer, N. K., Williams, J. A. and Sellers, W. R. (2015) 'High-throughput screening using patient-derived tumor xenografts to predict clinical trial drug response', *Nat Med,* 21(11), pp. 1318-25.

Gascoyne, R. D. and Steidl, C. (2011) 'The role of the microenvironment in lymphoid cancers', *Annals of Oncology,* 22, pp. 47-50.

Gennero, I., Fauvel, J., Nieto, M., Cariven, C., Gaits, F., Briand-Mesange, F., Chap, H. and Salles, J. P. (2002) 'Apoptotic effect of sphingosine 1-phosphate and increased sphingosine 1-phosphate hydrolysis on mesangial cells cultured at low cell density', *J Biol Chem,* 277(15), pp. 12724-34.

Gergely, P., Nuesslein-Hildesheim, B., Guerini, D., Brinkmann, V., Traebert, M., Bruns, C., Pan, S., Gray, N. S., Hinterding, K., Cooke, N. G., Groenewegen, A., Vitaliti, A., Sing, T., Luttringer, O., Yang, J., Gardin, A., Wang, N., Crumb, W. J., Jr., Saltzman, M., Rosenberg, M. and Wallstrom, E. (2012) 'The selective sphingosine 1-phosphate receptor modulator BAF312 redirects lymphocyte distribution and has species-specific effects on heart rate', *Br J Pharmacol,* 167(5), pp. 1035-47.

Gisselbrecht, C. and Van Den Neste, E. (2018) 'How I manage patients with relapsed/refractory diffuse large B cell lymphoma', *Br J Haematol,* 182(5), pp. 633-643.

Golay, J. and Introna, M. (2012) 'Mechanism of action of therapeutic monoclonal antibodies: promises and pitfalls of in vitro and in vivo assays', *Arch Biochem Biophys,* 526(2), pp. 146-53.

Gomez-Gelvez, J. C., Salama, M. E., Perkins, S. L., Leavitt, M. and Inamdar, K. V. (2016) 'Prognostic Impact of Tumor Microenvironment in Diffuse Large B-Cell Lymphoma Uniformly Treated With R-CHOP Chemotherapy', *Am J Clin Pathol,* 145(4), pp. 514-23.

Gude, D. R., Alvarez, S. E., Paugh, S. W., Mitra, P., Yu, J., Griffiths, R., Barbour, S. E., Milstien, S. and Spiegel, S. (2008) 'Apoptosis induces expression of sphingosine kinase 1 to release sphingosine-1-phosphate as a "come-and-get-me" signal', *FASEB J,* 22(8), pp. 2629-38.

Guide to Performing Relative Quantitation of Gene Expression Using Real-Time Quantitative PCR (2004): Applied Biosystems.

Guillermet-Guibert, J., Davenne, L., Pchejetski, D., Saint-Laurent, N., Brizuela, L., Guilbeau-Frugier, C., Delisle, M. B., Cuvillier, O., Susini, C. and Bousquet, C. (2009) 'Targeting the sphingolipid metabolism to defeat pancreatic cancer cell resistance to the chemotherapeutic gemcitabine drug', *Mol Cancer Ther,* 8(4), pp. 809-20.

Gul, N. and van Egmond, M. (2015) 'Antibody-Dependent Phagocytosis of Tumor Cells by Macrophages: A Potent Effector Mechanism of Monoclonal Antibody Therapy of Cancer', *Cancer Res,* 75(23), pp. 5008-13.

Hait, N. C., Allegood, J., Maceyka, M., Strub, G. M., Harikumar, K. B., Singh, S. K., Luo, C., Marmorstein, R., Kordula, T., Milstien, S. and Spiegel, S. (2009) 'Regulation of histone acetylation in the nucleus by sphingosine-1-phosphate', *Science,* 325(5945), pp. 1254-7.

Hait, N. C. and Maiti, A. (2017) 'The Role of Sphingosine-1-Phosphate and Ceramide-1-Phosphate in Inflammation and Cancer', *Mediators Inflamm,* 2017, pp. 4806541.

Hamilton, J. A. (1997) 'CSF-1 signal transduction', *J Leukoc Biol,* 62(2), pp. 145-55.

Hanahan, D. and Coussens, L. M. (2012) 'Accessories to the crime: functions of cells recruited to the tumor microenvironment', *Cancer Cell,* 21(3), pp. 309-22.

Hans, C. P., Weisenburger, D. D., Greiner, T. C., Gascoyne, R. D., Delabie, J., Ott, G., Muller-Hermelink, H. K., Campo, E., Braziel, R. M., Jaffe, E. S., Pan, Z., Farinha, P., Smith, L. M., Falini, B., Banham, A. H., Rosenwald, A., Staudt, L. M., Connors, J. M., Armitage, J. O. and Chan, W. C. (2004) 'Confirmation of the molecular classification of diffuse large B-cell lymphoma by immunohistochemistry using a tissue microarray', *Blood,* 103(1), pp. 275-82.

Hanson, M. A. and Peach, R. (2014) 'Structural biology of the S1P1 receptor', *Curr Top Microbiol Immunol,* 378, pp. 23-53.

Hashimoto, D., Chow, A., Noizat, C., Teo, P., Beasley, M. B., Leboeuf, M., Becker, C. D., See, P., Price, J., Lucas, D., Greter, M., Mortha, A., Boyer, S. W., Forsberg, E. C., Tanaka, M., van Rooijen, N., Garcia-Sastre, A., Stanley, E. R., Ginhoux, F.,

Frenette, P. S. and Merad, M. (2013) 'Tissue-resident macrophages self-maintain locally throughout adult life with minimal contribution from circulating monocytes', *Immunity,* 38(4), pp. 792-804.

Hasselblom, S., Hansson, U., Sigurdardottir, M., Nilsson-Ehle, H., Ridell, B. and Andersson, P. O. (2008) 'Expression of CD68+ tumor-associated macrophages in patients with diffuse large B-cell lymphoma and its relation to prognosis', *Pathol Int,* 58(8), pp. 529-32.

Hatoum, D., Haddadi, N., Lin, Y., Nassif, N. T. and McGowan, E. M. (2017) 'Mammalian sphingosine kinase (SphK) isoenzymes and isoform expression: challenges for SphK as an oncotarget', *Oncotarget,* 8(22), pp. 36898-36929.

Heckman, C. A., Mehew, J. W. and Boxer, L. M. (2002) 'NF-kappaB activates Bcl-2 expression in t(14;18) lymphoma cells', *Oncogene,* 21(24), pp. 3898-908.

Herbrand, U. (2016) 'Antibody-depending cellular phagocytosis: the mechanism of action that gets no respect', *Bioprocessing Journal,* 15(1), pp. 26-29.

Herter, S., Birk, M. C., Klein, C., Gerdes, C., Umana, P. and Bacac, M. (2014) 'Glycoengineering of therapeutic antibodies enhances monocyte/macrophage-mediated phagocytosis and cytotoxicity', *J Immunol,* 192(5), pp. 2252-60.

Hla, T. and Maciag, T. (1990) 'An abundant transcript induced in differentiating human endothelial cells encodes a polypeptide with structural similarities to G-protein-coupled receptors', *J Biol Chem,* 265(16), pp. 9308-13.

Hojer, C., Frankenberger, S., Strobl, L. J., Feicht, S., Djermanovic, K., Jagdhuber, F., Homig-Holzel, C., Ferch, U., Ruland, J., Rajewsky, K. and Zimber-Strobl, U. (2014) 'B-cell expansion and lymphomagenesis induced by chronic CD40 signaling is strictly dependent on CD19', *Cancer Res,* 74(16), pp. 4318-28.

Hong, G., Baudhuin, L. M. and Xu, Y. (1999) 'Sphingosine-1-phosphate modulates growth and adhesion of ovarian cancer cells', *FEBS Lett,* 460(3), pp. 513-8.

Hou, J., Chen, Q., Wu, X., Zhao, D., Reuveni, H., Licht, T., Xu, M., Hu, H., Hoeft, A., Ben-Sasson, S. A., Shu, Q. and Fang, X. (2017) 'S1PR3 Signaling Drives Bacterial Killing and Is Required for Survival in Bacterial Sepsis', *Am J Respir Crit Care Med,* 196(12), pp. 1559-1570.

Hou, J., Chen, Q., Zhang, K., Cheng, B., Xie, G., Wu, X., Luo, C., Chen, L., Liu, H., Zhao, B., Dai, K. and Fang, X. (2015) 'Sphingosine 1-phosphate Receptor 2 Signaling Suppresses Macrophage Phagocytosis and Impairs Host Defense against Sepsis', *Anesthesiology,* 123(2), pp. 409-22.

Huang, J. Z., Sanger, W. G., Greiner, T. C., Staudt, L. M., Weisenburger, D. D., Pickering, D. L., Lynch, J. C., Armitage, J. O., Warnke, R. A., Alizadeh, A. A., Lossos, I. S., Levy, R. and Chan, W. C. (2002) 'The t(14;18) defines a unique subset of diffuse large B-cell lymphoma with a germinal center B-cell gene expression profile', *Blood,* 99(7), pp. 2285-90.

Italiani, P. and Boraschi, D. (2014) 'From Monocytes to M1/M2 Macrophages: Phenotypical vs. Functional Differentiation', *Front Immunol,* 5, pp. 514.

Jaglowski, S. M., Alinari, L., Lapalombella, R., Muthusamy, N. and Byrd, J. C. (2010) 'The clinical application of monoclonal antibodies in chronic lymphocytic leukemia', *Blood,* 116(19), pp. 3705-14.

Jones, G. E. (2000) 'Cellular signaling in macrophage migration and chemotaxis', *J Leukoc Biol,* 68(5), pp. 593-602.

Jost, P. J. and Ruland, J. (2007) 'Aberrant NF-kappaB signaling in lymphoma: mechanisms, consequences, and therapeutic implications', *Blood,* 109(7), pp. 2700-7.

Kage, F., Winterhoff, M., Dimchev, V., Mueller, J., Thalheim, T., Freise, A., Bruhmann, S., Kollasser, J., Block, J., Dimchev, G., Geyer, M., Schnittler, H. J., Brakebusch, C., Stradal, T. E., Carlier, M. F., Sixt, M., Kas, J., Faix, J. and Rottner, K. (2017) 'FMNL formins boost lamellipodial force generation', *Nat Commun,* 8, pp. 14832.

Kahl, B. S., Go, R. S., Rodrigues, G., Sanchez, F. A., Saphner, T. J., Werndli, J. E., Kirkpatrick, H. M. and Longo, W. L. (2006) 'Phase II study of R-CHOP with GM-CSF cytokine support for elderly patients with untreated diffuse large B-cell lymphoma (DLBCL): A Wisconsin Oncology Network study', *Journal of Clinical Oncology,* 24(18_suppl), pp. 7566-7566.

Kamada, N., Hisamatsu, T., Okamoto, S., Sato, T., Matsuoka, K., Arai, K., Nakai, T., Hasegawa, A., Inoue, N., Watanabe, N., Akagawa, K. S. and Hibi, T. (2005) 'Abnormally differentiated subsets of intestinal macrophage play a key role in Th1-dominant chronic colitis through excess production of IL-12 and IL-23 in response to bacteria', *J Immunol,* 175(10), pp. 6900-8.

Kappos, L., Bar-Or, A., Cree, B. A. C., Fox, R. J., Giovannoni, G., Gold, R., Vermersch, P., Arnold, D. L., Arnould, S., Scherz, T., Wolf, C., Wallstrom, E., Dahlke, F. and Investigators, E. C. (2018) 'Siponimod versus placebo in secondary progressive multiple sclerosis (EXPAND): a double-blind, randomised, phase 3 study', *Lancet,* 391(10127), pp. 1263-1273.

Kenny, P. A., Lee, G. Y. and Bissell, M. J. (2007) 'Targeting the tumor microenvironment', *Front Biosci,* 12, pp. 3468-74.

Kilkenny, C., Browne, W., Cuthill, I. C., Emerson, M., Altman, D. G. and Group, N. C. R. R. G. W. (2010) 'Animal research: reporting in vivo experiments: the ARRIVE guidelines', *Br J Pharmacol,* 160(7), pp. 1577-9.

Kim, K. J., Kanellopoulos-Langevin, C., Merwin, R. M., Sachs, D. H. and Asofsky, R. (1979) 'Establishment and characterization of BALB/c lymphoma lines with B cell properties', *J Immunol,* 122(2), pp. 549-54.

Komohara, Y., Jinushi, M. and Takeya, M. (2014) 'Clinical significance of macrophage heterogeneity in human malignant tumors', *Cancer Sci,* 105(1), pp. 1-8.

Kon, J., Sato, K., Watanabe, T., Tomura, H., Kuwabara, A., Kimura, T., Tamama, K., Ishizuka, T., Murata, N., Kanda, T., Kobayashi, I., Ohta, H., Ui, M. and Okajima, F. (1999) 'Comparison of intrinsic activities of the putative sphingosine 1-phosphate receptor subtypes to regulate several signaling pathways in their cDNA-transfected Chinese hamster ovary cells', *J Biol Chem,* 274(34), pp. 23940-7.

Konig, K., Diehl, L., Rommerscheidt-Fuss, U., Golletz, C., Quast, T., Kahl, P., Kolanus, W., Knolle, P., Buettner, R. and Heukamp, L. C. (2010) 'Four-and-a-half LIM domain protein 2 is a novel regulator of sphingosine 1-phosphate receptor 1 in CCL19-induced dendritic cell migration', *J Immunol,* 185(3), pp. 1466-75.

Kotamraju, S., Williams, C. L. and Kalyanaraman, B. (2007) 'Statin-induced breast cancer cell death: role of inducible nitric oxide and arginase-dependent pathways', *Cancer Res,* 67(15), pp. 7386-94.

Kridel, R., Steidl, C. and Gascoyne, R. D. (2015) 'Tumor-associated macrophages in diffuse large B-cell lymphoma', *Haematologica,* 100(2), pp. 143-5.

Kunkel, G. T., Maceyka, M., Milstien, S. and Spiegel, S. (2013) 'Targeting the sphingosine-1-phosphate axis in cancer, inflammation and beyond', *Nat Rev Drug Discov,* 12(9), pp. 688-702.

Kunkel, L., Wong, A., Maneatis, T., Nickas, J., Brown, T., Grillo-Lopez, A., Benyunes, M., Grobman, B. and Dillman, R. O. (2000) 'Optimizing the use of rituximab for treatment of B-cell non-Hodgkin's lymphoma: a benefit-risk update', *Semin Oncol,* 27(6 Suppl 12), pp. 53-61.

Kuppers, R. (2005) 'Mechanisms of B-cell lymphoma pathogenesis', *Nat Rev Cancer,* 5(4), pp. 251-62.

Kwong, E., Li, Y., Hylemon, P. and Zhou, H. (2015) *Bile acids and sphingosine-1-phosphate receptor 2 in hepatic lipid metabolism.*

Lacey, D. C., Achuthan, A., Fleetwood, A. J., Dinh, H., Roiniotis, J., Scholz, G. M., Chang, M. W., Beckman, S. K., Cook, A. D. and Hamilton, J. A. (2012) 'Defining GM-CSF- and macrophage-CSF-dependent macrophage responses by in vitro models', *J Immunol,* 188(11), pp. 5752-65.

Lawlor, E. R., Soucek, L., Brown-Swigart, L., Shchors, K., Bialucha, C. U. and Evan, G. I. (2006) 'Reversible kinetic analysis of Myc targets in vivo provides novel insights into Myc-mediated tumorigenesis', *Cancer Res,* 66(9), pp. 4591-601.

LeBien, T. W. and Tedder, T. F. (2008) 'B lymphocytes: how they develop and function', *Blood,* 112(5), pp. 1570-80.

Lee, M. J., Van Brocklyn, J. R., Thangada, S., Liu, C. H., Hand, A. R., Menzeleev, R., Spiegel, S. and Hla, T. (1998) 'Sphingosine-1-phosphate as a ligand for the G protein-coupled receptor EDG-1', *Science,* 279(5356), pp. 1552-5.

Lee, O. H., Kim, Y. M., Lee, Y. M., Moon, E. J., Lee, D. J., Kim, J. H., Kim, K. W. and Kwon, Y. G. (1999) 'Sphingosine 1-phosphate induces angiogenesis: its angiogenic action and signaling mechanism in human umbilical vein endothelial cells', *Biochem Biophys Res Commun,* 264(3), pp. 743-50.

Leidi, M., Gotti, E., Bologna, L., Miranda, E., Rimoldi, M., Sica, A., Roncalli, M., Palumbo, G. A., Introna, M. and Golay, J. (2009) 'M2 macrophages phagocytose rituximab-opsonized leukemic targets more efficiently than m1 cells in vitro', *J Immunol,* 182(7), pp. 4415-22.

Lenz, G., Wright, G., Dave, S. S., Xiao, W., Powell, J., Zhao, H., Xu, W., Tan, B., Goldschmidt, N., Iqbal, J., Vose, J., Bast, M., Fu, K., Weisenburger, D. D., Greiner, T. C., Armitage, J. O., Kyle, A., May, L., Gascoyne, R. D., Connors, J. M., Troen, G., Holte, H., Kvaloy, S., Dierickx, D., Verhoef, G., Delabie, J., Smeland, E. B., Jares, P., Martinez, A., Lopez-Guillermo, A., Montserrat, E., Campo, E., Braziel, R. M., Miller, T. P., Rimsza, L. M., Cook, J. R., Pohlman, B., Sweetenham, J., Tubbs, R. R., Fisher, R. I., Hartmann, E., Rosenwald, A., Ott, G., Muller-Hermelink, H. K., Wrench, D., Lister, T. A., Jaffe, E. S., Wilson, W. H., Chan, W. C., Staudt, L. M. and Lymphoma/Leukemia Molecular Profiling, P. (2008) 'Stromal gene signatures in large-B-cell lymphomas', *N Engl J Med,* 359(22), pp. 2313-23.

Lewis, N. D., Haxhinasto, S. A., Anderson, S. M., Stefanopoulos, D. E., Fogal, S. E., Adusumalli, P., Desai, S. N., Patnaude, L. A., Lukas, S. M., Ryan, K. R., Slavin, A. J., Brown, M. L. and Modis, L. K. (2013) 'Circulating monocytes are reduced by sphingosine-1-phosphate receptor modulators independently of S1P3', *J Immunol,* 190(7), pp. 3533-40.

Li, Y. L., Shi, Z. H., Wang, X., Gu, K. S. and Zhai, Z. M. (2019) 'Prognostic significance of monocyte chemoattractant protein-1 and CC chemokine receptor 2 in diffuse large B cell lymphoma', *Ann Hematol,* 98(2), pp. 413-422.

Liu, Y., Deng, J., Wang, L., Lee, H., Armstrong, B., Scuto, A., Kowolik, C., Weiss, L. M., Forman, S. and Yu, H. (2012) 'S1PR1 is an effective target to block STAT3 signaling in activated B cell-like diffuse large B-cell lymphoma', *Blood,* 120(7), pp. 1458-65.

Lunardi, S., Jamieson, N. B., Lim, S. Y., Griffiths, K. L., Carvalho-Gaspar, M., Al-Assar, O., Yameen, S., Carter, R. C., McKay, C. J., Spoletini, G., D'Ugo, S., Silva, M. A., Sansom, O. J., Janssen, K. P., Muschel, R. J. and Brunner, T. B. (2014) 'IP-10/CXCL10 induction in human pancreatic cancer stroma influences lymphocytes recruitment and correlates with poor survival', *Oncotarget,* 5(22), pp. 11064-80.

Lupino, L. (2017) *Investigating the contribution of aberrant sphingosine 1-phosphate signalling to the pathogenesis of diffuse large B-cell lymphoma.* PhD thesis, University of Birmingham, Edgbaston, UK.

Lupino, L., Perry, T., Margielewska, S., Hollows, R., Ibrahim, M., Care, M., Allegood, J., Tooze, R., Sabbadini, R., Reynolds, G., Bicknell, R., Rudzki, Z., Lin Hock, Y., Zanetto, U., Wei, W., Simmons, W., Spiegel, S., Woodman, C. B. J., Rowe, M., Vrzalikova, K. and Murray, P. G. (2019) 'Sphingosine-1-phosphate signalling drives an angiogenic transcriptional programme in diffuse large B cell lymphoma', *Leukemia*.

Maceyka, M., Sankala, H., Hait, N. C., Le Stunff, H., Liu, H., Toman, R., Collier, C., Zhang, M., Satin, L. S., Merrill, A. H., Jr., Milstien, S. and Spiegel, S. (2005) 'SphK1 and SphK2, sphingosine kinase isoenzymes with opposing functions in sphingolipid metabolism', *J Biol Chem,* 280(44), pp. 37118-29.

Maiti, A., Takabe, K. and Hait, N. C. (2017) 'Metastatic triple-negative breast cancer is dependent on SphKs/S1P signaling for growth and survival', *Cell Signal,* 32, pp. 85-92.

Mantovani, A. and Locati, M. (2013) 'Tumor-associated macrophages as a paradigm of macrophage plasticity, diversity, and polarization: lessons and open questions', *Arterioscler Thromb Vasc Biol,* 33(7), pp. 1478-83.

Mantovani, A., Marchesi, F., Malesci, A., Laghi, L. and Allavena, P. (2017) 'Tumour-associated macrophages as treatment targets in oncology', *Nat Rev Clin Oncol*.

Mantovani, A., Savino, B., Locati, M., Zammataro, L., Allavena, P. and Bonecchi, R. (2010) 'The chemokine system in cancer biology and therapy', *Cytokine Growth Factor Rev,* 21(1), pp. 27-39.

Mantovani, A., Sozzani, S., Locati, M., Allavena, P. and Sica, A. (2002) 'Macrophage polarization: tumor-associated macrophages as a paradigm for polarized M2 mononuclear phagocytes', *Trends in Immunology,* 23(11), pp. 549-555.

Marchesi, F., Cirillo, M., Bianchi, A., Gately, M., Olimpieri, O. M., Cerchiara, E., Renzi, D., Micera, A., Balzamino, B. O., Bonini, S., Onetti Muda, A. and Avvisati, G. (2015) 'High density of CD68+/CD163+ tumour-associated macrophages (M2-TAM) at diagnosis is significantly correlated to unfavorable prognostic factors and to poor clinical outcomes in patients with diffuse large B-cell lymphoma', *Hematol Oncol,* 33(2), pp. 110-2.

Martensson, I. L., Almqvist, N., Grimsholm, O. and Bernardi, A. I. (2010) 'The pre-B cell receptor checkpoint', *FEBS Lett,* 584(12), pp. 2572-9.

Martinez, F. O. and Gordon, S. (2014) 'The M1 and M2 paradigm of macrophage activation: time for reassessment', *F1000Prime Rep,* 6, pp. 13.

Mattila, P. K. and Lappalainen, P. (2008) 'Filopodia: molecular architecture and cellular functions', *Nat Rev Mol Cell Biol,* 9(6), pp. 446-54.

Mayer, L. D., Bally, M. B., Cullis, P. R., Wilson, S. L. and Emerman, J. T. (1990) 'Comparison of free and liposome encapsulated doxorubicin tumor drug uptake and antitumor efficacy in the SC115 murine mammary tumor', *Cancer Lett,* 53(2-3), pp. 183-90.

Mbeunkui, F. and Johann, D. J., Jr. (2009) 'Cancer and the tumor microenvironment: a review of an essential relationship', *Cancer Chemother Pharmacol,* 63(4), pp. 571-82.

McQuiston, T., Luberto, C. and Del Poeta, M. (2011) 'Role of sphingosine-1-phosphate (S1P) and S1P receptor 2 in the phagocytosis of Cryptococcus neoformans by alveolar macrophages', *Microbiology,* 157(Pt 5), pp. 1416-27.

McReynolds, L. J., Gupta, S., Figueroa, M. E., Mullins, M. C. and Evans, T. (2007) 'Smad1 and Smad5 differentially regulate embryonic hematopoiesis', *Blood,* 110(12), pp. 3881-90.

Measuring treatment response in Patient Derived Xenograft (PDX) models at The Jackson Laboratory (2017) Jackson Labs tumour response analysis. Bar Harbor, Maine: Jackson Laboratory [web page]. Available at: http://tumor.informatics.jax.org/mtbwi/live/www/html/SOCHelp.html#cohorts (Accessed: March 5 2019).

Mendoza-Coronel, E. and Ortega, E. (2017) 'Macrophage Polarization Modulates FcgammaR- and CD13-Mediated Phagocytosis and Reactive Oxygen Species Production, Independently of Receptor Membrane Expression', *Front Immunol,* 8, pp. 303.

Meyer, P. N., Fu, K., Greiner, T. C., Smith, L. M., Delabie, J., Gascoyne, R. D., Ott, G., Rosenwald, A., Braziel, R. M., Campo, E., Vose, J. M., Lenz, G., Staudt, L. M., Chan, W. C. and Weisenburger, D. D. (2011) 'Immunohistochemical methods for predicting cell of origin and survival in patients with diffuse large B-cell lymphoma treated with rituximab', *J Clin Oncol,* 29(2), pp. 200-7.

Mi, H., Huang, X., Muruganujan, A., Tang, H., Mills, C., Kang, D. and Thomas, P. D. (2017) 'PANTHER version 11: expanded annotation data from Gene Ontology and Reactome pathways, and data analysis tool enhancements', *Nucleic Acids Res,* 45(D1), pp. D183-D189.

Mi, H., Muruganujan, A., Ebert, D., Huang, X. and Thomas, P. D. (2019a) 'PANTHER version 14: more genomes, a new PANTHER GO-slim and improvements in enrichment analysis tools', *Nucleic Acids Res,* 47(D1), pp. D419-D426.

Mi, H., Muruganujan, A., Huang, X., Ebert, D., Mills, C., Guo, X. and Thomas, P. D. (2019b) 'Protocol Update for large-scale genome and gene function analysis with the PANTHER classification system (v.14.0)', *Nat Protoc,* 14(3), pp. 703-721.

Mills, C. D. (2015) 'Anatomy of a discovery: m1 and m2 macrophages', *Front Immunol,* 6, pp. 212.

Mills, C. D., Kincaid, K., Alt, J. M., Heilman, M. J. and Hill, A. M. (2000) 'M-1/M-2 macrophages and the Th1/Th2 paradigm', *J Immunol,* 164(12), pp. 6166-73.

Mills, C. D. and Ley, K. (2014) 'M1 and M2 macrophages: the chicken and the egg of immunity', *J Innate Immun,* 6(6), pp. 716-26.

Minard-Colin, V., Xiu, Y., Poe, J. C., Horikawa, M., Magro, C. M., Hamaguchi, Y., Haas, K. M. and Tedder, T. F. (2008) 'Lymphoma depletion during CD20 immunotherapy in mice is mediated by macrophage FcgammaRI, FcgammaRIII, and FcgammaRIV', *Blood,* 112(4), pp. 1205-13.

Minutti, C. M., Knipper, J. A., Allen, J. E. and Zaiss, D. M. (2017) 'Tissue-specific contribution of macrophages to wound healing', *Semin Cell Dev Biol,* 61, pp. 3-11.

Mitra, P., Oskeritzian, C. A., Payne, S. G., Beaven, M. A., Milstien, S. and Spiegel, S. (2006) 'Role of ABCC1 in export of sphingosine-1-phosphate from mast cells', *Proc Natl Acad Sci U S A,* 103(44), pp. 16394-9.

Morin, R. D., Mungall, K., Pleasance, E., Mungall, A. J., Goya, R., Huff, R. D., Scott, D. W., Ding, J., Roth, A., Chiu, R., Corbett, R. D., Chan, F. C., Mendez-Lago, M., Trinh, D. L., Bolger-Munro, M., Taylor, G., Hadj Khodabakhshi, A., Ben-Neriah, S., Pon, J., Meissner, B., Woolcock, B., Farnoud, N., Rogic, S., Lim, E. L., Johnson, N. A., Shah, S., Jones, S., Steidl, C., Holt, R., Birol, I., Moore, R., Connors, J. M., Gascoyne, R. D. and Marra, M. A. (2013) 'Mutational and structural analysis of diffuse large B-cell lymphoma using whole-genome sequencing', *Blood,* 122(7), pp. 1256-65.

Mueller, K. T., Maude, S. L., Porter, D. L., Frey, N., Wood, P., Han, X., Waldron, E., Chakraborty, A., Awasthi, R., Levine, B. L., Melenhorst, J. J., Grupp, S. A., June, C. H. and Lacey, S. F. (2017) 'Cellular kinetics of CTL019 in relapsed/refractory B-cell acute lymphoblastic leukemia and chronic lymphocytic leukemia', *Blood,* 130(21), pp. 2317-2325.

Muller, J., von Bernstorff, W., Heidecke, C. D. and Schulze, T. (2017) 'Differential S1P Receptor Profiles on M1- and M2-Polarized Macrophages Affect Macrophage Cytokine Production and Migration', *Biomed Res Int,* 2017, pp. 7584621.

Muris, J. J., Meijer, C. J., Vos, W., van Krieken, J. H., Jiwa, N. M., Ossenkoppele, G. J. and Oudejans, J. J. (2006) 'Immunohistochemical profiling based on Bcl-2, CD10 and MUM1 expression improves risk stratification in patients with primary nodal diffuse large B cell lymphoma', *J Pathol,* 208(5), pp. 714-23.

Murray, P. J. and Wynn, T. A. (2011) 'Protective and pathogenic functions of macrophage subsets', *Nat Rev Immunol,* 11(11), pp. 723-37.

Nagahashi, M., Abe, M., Sakimura, K., Takabe, K. and Wakai, T. (2018a) 'The role of sphingosine-1-phosphate in inflammation and cancer progression', *Cancer Sci,* 109(12), pp. 3671-3678.

Nagahashi, M., Ramachandran, S., Kim, E. Y., Allegood, J. C., Rashid, O. M., Yamada, A., Zhao, R., Milstien, S., Zhou, H., Spiegel, S. and Takabe, K. (2012) 'Sphingosine-1-phosphate produced by sphingosine kinase 1 promotes breast cancer progression by stimulating angiogenesis and lymphangiogenesis', *Cancer Res,* 72(3), pp. 726-35.

Nagahashi, M., Yamada, A., Katsuta, E., Aoyagi, T., Huang, W. C., Terracina, K. P., Hait, N. C., Allegood, J. C., Tsuchida, J., Yuza, K., Nakajima, M., Abe, M., Sakimura, K., Milstien, S., Wakai, T., Spiegel, S. and Takabe, K. (2018b) 'Targeting the SphK1/S1P/S1PR1 Axis That Links Obesity, Chronic Inflammation, and Breast Cancer Metastasis', *Cancer Res,* 78(7), pp. 1713-1725.

Nakajima, M., Nagahashi, M., Rashid, O. M., Takabe, K. and Wakai, T. (2017) 'The role of sphingosine-1-phosphate in the tumor microenvironment and its clinical implications', *Tumour Biol,* 39(4), pp. 1010428317699133.

Newton, J., Lima, S., Maceyka, M. and Spiegel, S. (2015) 'Revisiting the sphingolipid rheostat: Evolving concepts in cancer therapy', *Exp Cell Res,* 333(2), pp. 195-200.

Author (2016)*: Non-Hodgkin Lymphoma: Diagnosis and management*. London: National Guideline Alliance (UK). Available at: https://www.ncbi.nlm.nih.gov/books/NBK385282/.

Nishino, S., Yamashita, H., Tamori, M., Mashimo, M., Yamagata, K., Nakamura, H. and Murayama, T. (2019) 'Translocation and activation of sphingosine kinase 1 by ceramide-1-phosphate', *J Cell Biochem,* 120(4), pp. 5396-5408.

Nucera, S., Biziato, D. and De Palma, M. (2011) 'The interplay between macrophages and angiogenesis in development, tissue injury and regeneration', *Int J Dev Biol,* 55(4-5), pp. 495-503.

Nyman, H., Jerkeman, M., Karjalainen-Lindsberg, M. L., Banham, A. H. and Leppa, S. (2009) 'Prognostic impact of activated B-cell focused classification in diffuse large B-cell lymphoma patients treated with R-CHOP', *Mod Pathol,* 22(8), pp. 1094-101.

O'Sullivan, C. and Dev, K. K. (2013) 'The structure and function of the S1P1 receptor', *Trends Pharmacol Sci,* 34(7), pp. 401-12.

Ogretmen, B. (2018) 'Sphingolipid metabolism in cancer signalling and therapy', *Nat Rev Cancer,* 18(1), pp. 33-50.

Olesch, C., Ringel, C., Brune, B. and Weigert, A. (2017) 'Beyond Immune Cell Migration: The Emerging Role of the Sphingosine-1-phosphate Receptor S1PR4 as a Modulator of Innate Immune Cell Activation', *Mediators Inflamm,* 2017, pp. 6059203.

Oliveros, J. C. (2007-2015) *Venny; an interactive tool for comparing lists with Venn diagrams*. Available at: http://bioinfogp.cnb.csic.es/tools/venny/index.htm 2016-2019).

Osawa, Y., Banno, Y., Nagaki, M., Brenner, D. A., Naiki, T., Nozawa, Y., Nakashima, S. and Moriwaki, H. (2001) 'TNF-alpha-induced sphingosine 1-phosphate inhibits apoptosis through a phosphatidylinositol 3-kinase/Akt pathway in human hepatocytes', *J Immunol,* 167(1), pp. 173-80.

Ott, G., Ziepert, M., Klapper, W., Horn, H., Szczepanowski, M., Bernd, H. W., Thorns, C., Feller, A. C., Lenze, D., Hummel, M., Stein, H., Muller-Hermelink, H. K., Frank, M., Hansmann, M. L., Barth, T. F., Moller, P., Cogliatti, S., Pfreundschuh, M., Schmitz, N., Trumper, L., Loeffler, M. and Rosenwald, A. (2010) 'Immunoblastic morphology but not the immunohistochemical GCB/nonGCB classifier predicts outcome in diffuse large B-cell lymphoma in the RICOVER-60 trial of the DSHNHL', *Blood,* 116(23), pp. 4916-25.

Paget, S. (1989) 'The distribution of secondary growths in cancer of the breast. 1889', *Cancer Metastasis Rev,* 8(2), pp. 98-101.

Paik, J. H., Nam, S. J., Kim, T. M., Heo, D. S., Kim, C. W. and Jeon, Y. K. (2014) 'Overexpression of sphingosine-1-phosphate receptor 1 and phospho-signal transducer and activator of transcription 3 is associated with poor prognosis in rituximab-treated diffuse large B-cell lymphomas', *BMC Cancer,* 14, pp. 911.

Palmieri, C., Falcone, C., Iaccino, E., Tuccillo, F. M., Gaspari, M., Trimboli, F., De Laurentiis, A., Luberto, L., Pontoriero, M., Pisano, A., Vecchio, E., Fierro, O., Panico, M. R., Larobina, M., Gargiulo, S., Costa, N., Dal Piaz, F., Schiavone, M., Arra, C., Giudice, A., Palma, G., Barbieri, A., Quinto, I. and Scala, G. (2010) 'In vivo targeting and growth inhibition of the A20 murine B-cell lymphoma by an idiotype-specific peptide binder', *Blood,* 116(2), pp. 226-38.

Pan, S., Gray, N. S., Gao, W., Mi, Y., Fan, Y., Wang, X., Tuntland, T., Che, J., Lefebvre, S., Chen, Y., Chu, A., Hinterding, K., Gardin, A., End, P., Heining, P., Bruns, C., Cooke, N. G. and Nuesslein-Hildesheim, B. (2013) 'Discovery of BAF312 (Siponimod), a Potent and Selective S1P Receptor Modulator', *ACS Med Chem Lett,* 4(3), pp. 333-7.

Pappu, R., Schwab, S. R., Cornelissen, I., Pereira, J. P., Regard, J. B., Xu, Y., Camerer, E., Zheng, Y. W., Huang, Y., Cyster, J. G. and Coughlin, S. R. (2007) 'Promotion of lymphocyte egress into blood and lymph by distinct sources of sphingosine-1-phosphate', *Science,* 316(5822), pp. 295-8.

Pelengaris, S., Abouna, S., Cheung, L., Ifandi, V., Zervou, S. and Khan, M. (2004) 'Brief inactivation of c-Myc is not sufficient for sustained regression of c-Myc-induced tumours of pancreatic islets and skin epidermis', *BMC Biol,* 2, pp. 26.

Perez, D. A., Galvao, I., Athayde, R. M., Rezende, B. M., Vago, J. P., Silva, J. D., Reis, A. C., Ribeiro, L. S., Gomes, J. H. S., Padua, R. M., Braga, F. C., Sousa, L. P., Teixeira, M. M. and Pinho, V. (2019) 'Inhibition of the sphingosine-1-phosphate pathway promotes the resolution of neutrophilic inflammation', *Eur J Immunol,* 49(7), pp. 1038-1051.

Perry, A. M., Alvarado-Bernal, Y., Laurini, J. A., Smith, L. M., Slack, G. W., Tan, K. L., Sehn, L. H., Fu, K., Aoun, P., Greiner, T. C., Chan, W. C., Bierman, P. J., Bociek, R. G., Armitage, J. O., Vose, J. M., Gascoyne, R. D. and Weisenburger, D. D. (2014) 'MYC and BCL2 protein expression predicts survival in patients with diffuse large B-cell lymphoma treated with rituximab', *British Journal of Haematology,* 165(3), pp. 382-391.

Pham, L. V., Pogue, E. and Ford, R. J. (2018) 'The Role of Macrophage/B-Cell Interactions in the Pathophysiology of B-Cell Lymphomas', *Front Oncol,* 8, pp. 147.

Pyne, N. J., El Buri, A., Adams, D. R. and Pyne, S. (2018) 'Sphingosine 1-phosphate and cancer', *Adv Biol Regul,* 68, pp. 97-106.

Pyne, N. J., McNaughton, M., Boomkamp, S., MacRitchie, N., Evangelisti, C., Martelli, A. M., Jiang, H. R., Ubhi, S. and Pyne, S. (2016) 'Role of sphingosine 1-phosphate receptors, sphingosine kinases and sphingosine in cancer and inflammation', *Adv Biol Regul,* 60, pp. 151-159.

Pyne, N. J. and Pyne, S. (2011) 'Selectivity and specificity of sphingosine 1-phosphate receptor ligands: "off-targets" or complex pharmacology?', *Front Pharmacol,* 2, pp. 26.

Pyne, S. and Pyne, N. (2000) 'Sphingosine 1-phosphate signalling via the endothelial differentiation gene family of G-protein-coupled receptors', *Pharmacol Ther,* 88(2), pp. 115-31.

Qian, B. Z., Li, J., Zhang, H., Kitamura, T., Zhang, J., Campion, L. R., Kaiser, E. A., Snyder, L. A. and Pollard, J. W. (2011) 'CCL2 recruits inflammatory monocytes to facilitate breast-tumour metastasis', *Nature,* 475(7355), pp. 222-5.

Qian, B. Z. and Pollard, J. W. (2010) 'Macrophage diversity enhances tumor progression and metastasis', *Cell,* 141(1), pp. 39-51.

Qian, Y., Corum, L., Meng, Q., Blenis, J., Zheng, J. Z., Shi, X., Flynn, D. C. and Jiang, B. H. (2004) 'PI3K induced actin filament remodeling through Akt and p70S6K1: implication of essential role in cell migration', *Am J Physiol Cell Physiol,* 286(1), pp. C153-63.

Quintanilla-Martinez, L. (2015) 'IX. Is it only about MYC? How to approach the diagnosis of diffuse large B-cell lymphomas', *Hematol Oncol,* 33 Suppl S1, pp. 50-55.

Ramanathan, R., Raza, A., Sturgill, J., Lyon, D., Young, J., Hait, N. C. and Takabe, K. (2017) 'Paradoxical Association of Postoperative Plasma Sphingosine-1-Phosphate with Breast Cancer Aggressiveness and Chemotherapy', *Mediators Inflamm,* 2017, pp. 5984819.

Reddy, A., Zhang, J., Davis, N. S., Moffitt, A. B., Love, C. L., Waldrop, A., Leppa, S., Pasanen, A., Meriranta, L., Karjalainen-Lindsberg, M. L., Norgaard, P., Pedersen, M., Gang, A. O., Hogdall, E., Heavican, T. B., Lone, W., Iqbal, J., Qin, Q., Li, G., Kim, S. Y., Healy, J., Richards, K. L., Fedoriw, Y., Bernal-Mizrachi, L., Koff, J. L., Staton, A. D., Flowers, C. R., Paltiel, O., Goldschmidt, N., Calaminici, M., Clear, A., Gribben, J., Nguyen, E., Czader, M. B., Ondrejka, S. L., Collie, A., Hsi, E. D., Tse, E., Au-Yeung, R. K. H., Kwong, Y. L., Srivastava, G., Choi, W. W. L., Evens, A. M., Pilichowska, M., Sengar, M., Reddy, N., Li, S., Chadburn, A., Gordon, L. I., Jaffe, E. S., Levy, S., Rempel, R., Tzeng, T., Happ, L. E., Dave, T., Rajagopalan, D., Datta, J., Dunson, D. B. and Dave, S. S. (2017) 'Genetic and Functional Drivers of Diffuse Large B Cell Lymphoma', *Cell,* 171(2), pp. 481-494 e15.

Riihijarvi, S., Fiskvik, I., Taskinen, M., Vajavaara, H., Tikkala, M., Yri, O., Karjalainen-Lindsberg, M. L., Delabie, J., Smeland, E., Holte, H. and Leppa, S. (2015) 'Prognostic influence of macrophages in patients with diffuse large B-cell lymphoma: a correlative study from a Nordic phase II trial', *Haematologica,* 100(2), pp. 238-45.

Robinson, M. D., McCarthy, D. J. and Smyth, G. K. (2010) 'edgeR: a Bioconductor package for differential expression analysis of digital gene expression data', *Bioinformatics,* 26(1), pp. 139-40.

Rodriguez, Y. I., Campos, L. E., Castro, M. G., Aladhami, A., Oskeritzian, C. A. and Alvarez, S. E. (2016) 'Sphingosine-1 Phosphate: A New Modulator of Immune Plasticity in the Tumor Microenvironment', *Front Oncol,* 6, pp. 218.

Rosenwald, A., Wright, G., Chan, W. C., Connors, J. M., Campo, E., Fisher, R. I., Gascoyne, R. D., Muller-Hermelink, H. K., Smeland, E. B., Staudt, L. M. and Pr, L. L. M. P. (2002) 'The use of molecular profiling to predict survival after chemotherapy for diffuse large-B-cell lymphoma', *New England Journal of Medicine,* 346(25), pp. 1937-1947.

Roszer, T. (2015) 'Understanding the Mysterious M2 Macrophage through Activation Markers and Effector Mechanisms', *Mediators Inflamm,* 2015, pp. 816460.

Ruhl JL, C. C., Hurlbut, A, Ries LAG, Adamo P, Dickie L, Schussler N (2018) *Summary Stage 2018: Codes and Coding Instructions*, Bethsda, Maryland: National Cancer Institute. Available at: https://seer.cancer.gov/tools/ssm/.

Rutherford, C., Childs, S., Ohotski, J., McGlynn, L., Riddick, M., MacFarlane, S., Tasker, D., Pyne, S., Pyne, N. J., Edwards, J. and Palmer, T. M. (2013) 'Regulation of cell survival by sphingosine-1-phosphate receptor S1P1 via reciprocal ERK-dependent suppression of Bim and PI-3-kinase/protein kinase C-mediated upregulation of Mcl-1', *Cell Death Dis,* 4, pp. e927.

Sanchez, T. and Hla, T. (2004) 'Structural and functional characteristics of S1P receptors', *J Cell Biochem,* 92(5), pp. 913-22.

Satsu, H., Schaeffer, M. T., Guerrero, M., Saldana, A., Eberhart, C., Hodder, P., Cayanan, C., Schurer, S., Bhhatarai, B., Roberts, E., Rosen, H. and Brown, S. J. (2013) 'A sphingosine 1-phosphate receptor 2 selective allosteric agonist', *Bioorg Med Chem,* 21(17), pp. 5373-82.

Schlam, D., Bagshaw, R. D., Freeman, S. A., Collins, R. F., Pawson, T., Fairn, G. D. and Grinstein, S. (2015) 'Phosphoinositide 3-kinase enables phagocytosis of large particles by terminating actin assembly through Rac/Cdc42 GTPase-activating proteins', *Nat Commun,* 6, pp. 8623.

Schmitz, R., Wright, G. W., Huang, D. W., Johnson, C. A., Phelan, J. D., Wang, J. Q., Roulland, S., Kasbekar, M., Young, R. M., Shaffer, A. L., Hodson, D. J., Xiao, W., Yu, X., Yang, Y., Zhao, H., Xu, W., Liu, X., Zhou, B., Du, W., Chan, W. C., Jaffe, E. S., Gascoyne, R. D., Connors, J. M., Campo, E., Lopez-Guillermo, A., Rosenwald, A., Ott, G., Delabie, J., Rimsza, L. M., Tay Kuang Wei, K., Zelenetz, A. D., Leonard, J. P., Bartlett, N. L., Tran, B., Shetty, J., Zhao, Y., Soppet, D. R., Pittaluga, S., Wilson, W. H. and Staudt, L. M. (2018) 'Genetics and Pathogenesis of Diffuse Large B-Cell Lymphoma', *N Engl J Med,* 378(15), pp. 1396-1407.

Schuster, S. J., Svoboda, J., Chong, E. A., Nasta, S. D., Mato, A. R., Anak, O., Brogdon, J. L., Pruteanu-Malinici, I., Bhoj, V., Landsburg, D., Wasik, M., Levine, B. L., Lacey, S. F., Melenhorst, J. J., Porter, D. L. and June, C. H. (2017) 'Chimeric Antigen Receptor T Cells in Refractory B-Cell Lymphomas', *N Engl J Med,* 377(26), pp. 2545-2554.

Schwende, H., Fitzke, E., Ambs, P. and Dieter, P. (1996) 'Differences in the state of differentiation of THP-1 cells induced by phorbol ester and 1,25-dihydroxyvitamin D3', *J Leukoc Biol,* 59(4), pp. 555-61.

Scott, D. W. and Gascoyne, R. D. (2014) 'The tumour microenvironment in B cell lymphomas', *Nat Rev Cancer,* 14(8), pp. 517-34.

Sehn, L. H. (2010) 'A decade of R-CHOP', *Blood,* 116(12), pp. 2000-1.

Sehn, L. H. and Gascoyne, R. D. (2015) 'Diffuse large B-cell lymphoma: optimizing outcome in the context of clinical and biologic heterogeneity', *Blood,* 125(1), pp. 22-32.

Seita, J. and Weissman, I. L. (2010) 'Hematopoietic stem cell: self-renewal versus differentiation', *Wiley Interdiscip Rev Syst Biol Med,* 2(6), pp. 640-53.

Sha, C., Barrans, S., Cucco, F., Bentley, M. A., Care, M. A., Cummin, T., Kennedy, H., Thompson, J. S., Uddin, R., Worrillow, L., Chalkley, R., van Hoppe, M., Ahmed, S., Maishman, T., Caddy, J., Schuh, A., Mamot, C., Burton, C., Tooze, R., Davies, A., Du, M. Q., Johnson, P. W. M. and Westhead, D. R. (2019) 'Molecular High-Grade B-Cell Lymphoma: Defining a Poor-Risk Group That Requires Different Approaches to Therapy', *J Clin Oncol,* 37(3), pp. 202-212.

Shaffer, A. L., 3rd, Young, R. M. and Staudt, L. M. (2012) 'Pathogenesis of human B cell lymphomas', *Annu Rev Immunol,* 30, pp. 565-610.

Shain, K. H., Dalton, W. S. and Tao, J. (2015) 'The tumor microenvironment shapes hallmarks of mature B-cell malignancies', *Oncogene*.

Shankland, K. R., Armitage, J. O. and Hancock, B. W. (2012) 'Non-Hodgkin lymphoma', *Lancet,* 380(9844), pp. 848-57.

Shen, L., Li, H., Shi, Y., Wang, D., Gong, J., Xun, J., Zhou, S., Xiang, R. and Tan, X. (2016) 'M2 tumour-associated macrophages contribute to tumour progression via legumain remodelling the extracellular matrix in diffuse large B cell lymphoma', *Sci Rep,* 6, pp. 30347.

Shi, C. and Pamer, E. G. (2011) 'Monocyte recruitment during infection and inflammation', *Nat Rev Immunol,* 11(11), pp. 762-74.

Shroff, E. H., Eberlin, L. S., Dang, V. M., Gouw, A. M., Gabay, M., Adam, S. J., Bellovin, D. I., Tran, P. T., Philbrick, W. M., Garcia-Ocana, A., Casey, S. C., Li, Y., Dang, C. V., Zare, R. N. and Felsher, D. W. (2015) 'MYC oncogene overexpression drives renal cell carcinoma in a mouse model through glutamine metabolism', *Proc Natl Acad Sci U S A,* 112(21), pp. 6539-44.

Spiegel, S. and Milstien, S. (2003) 'Sphingosine-1-phosphate: an enigmatic signalling lipid', *Nat Rev Mol Cell Biol,* 4(5), pp. 397-407.

Spiegel, S. and Milstien, S. (2011) 'The outs and the ins of sphingosine-1-phosphate in immunity', *Nat Rev Immunol,* 11(6), pp. 403-15.

Stelling, A., Hashwah, H., Bertram, K., Manz, M. G., Tzankov, A. and Muller, A. (2018) 'The tumor suppressive TGF-beta/SMAD1/S1PR2 signaling axis is recurrently inactivated in diffuse large B-cell lymphoma', *Blood,* 131(20), pp. 2235-2246.

Swerdlow, S. H., Campo, E., Pileri, S. A., Harris, N. L., Stein, H., Siebert, R., Advani, R., Ghielmini, M., Salles, G. A., Zelenetz, A. D. and Jaffe, E. S. (2016) 'The 2016 revision of the World Health Organization classification of lymphoid neoplasms', *Blood,* 127(20), pp. 2375-90.

Takabe, K. and Spiegel, S. (2014) 'Export of sphingosine-1-phosphate and cancer progression', *J Lipid Res,* 55(9), pp. 1839-46.

The Gene Ontology, C. (2017) 'Expansion of the Gene Ontology knowledgebase and resources', *Nucleic Acids Res,* 45(D1), pp. D331-D338.

Thompson, J., George, E. O., Poquette, C. A., Cheshire, P. J., Richmond, L. B., de Graaf, S. S., Ma, M., Stewart, C. F. and Houghton, P. J. (1999) 'Synergy of topotecan in combination with vincristine for treatment of pediatric solid tumor xenografts', *Clin Cancer Res,* 5(11), pp. 3617-31.

Tilly, H., Gomes da Silva, M., Vitolo, U., Jack, A., Meignan, M., Lopez-Guillermo, A., Walewski, J., Andre, M., Johnson, P. W., Pfreundschuh, M., Ladetto, M. and Committee, E. G. (2015) 'Diffuse large B-cell lymphoma (DLBCL): ESMO Clinical Practice Guidelines for diagnosis, treatment and follow-up', *Ann Oncol,* 26 Suppl 5, pp. v116-25.

Tsai, H. C. and Han, M. H. (2016) 'Sphingosine-1-Phosphate (S1P) and S1P Signaling Pathway: Therapeutic Targets in Autoimmunity and Inflammation', *Drugs,* 76(11), pp. 1067-79.

van Furth, R., Cohn, Z. A., Hirsch, J. G., Humphrey, J. H., Spector, W. G. and Langevoort, H. L. (1972) 'The mononuclear phagocyte system: a new classification of macrophages, monocytes, and their precursor cells', *Bull World Health Organ,* 46(6), pp. 845-52.

Van Overmeire, E., Stijlemans, B., Heymann, F., Keirsse, J., Morias, Y., Elkrim, Y., Brys, L., Abels, C., Lahmar, Q., Ergen, C., Vereecke, L., Tacke, F., De Baetselier, P., Van Ginderachter, J. A. and Laoui, D. (2016) 'M-CSF and GM-CSF Receptor Signaling Differentially Regulate Monocyte Maturation and Macrophage Polarization in the Tumor Microenvironment', *Cancer Res,* 76(1), pp. 35-42.

VanDerMeid, K. R., Elliott, M. R., Baran, A. M., Barr, P. M., Chu, C. C. and Zent, C. S. (2018) 'Cellular Cytotoxicity of Next-Generation CD20 Monoclonal Antibodies', *Cancer Immunol Res,* 6(10), pp. 1150-1160.

Vergadi, E., Ieronymaki, E., Lyroni, K., Vaporidi, K. and Tsatsanis, C. (2017) 'Akt Signaling Pathway in Macrophage Activation and M1/M2 Polarization', *J Immunol,* 198(3), pp. 1006-1014.

Verreck, F. A., de Boer, T., Langenberg, D. M., Hoeve, M. A., Kramer, M., Vaisberg, E., Kastelein, R., Kolk, A., de Waal-Malefyt, R. and Ottenhoff, T. H. (2004) 'Human IL-23-producing type 1 macrophages promote but IL-10-producing type 2 macrophages subvert immunity to (myco)bacteria', *Proc Natl Acad Sci U S A,* 101(13), pp. 4560-5.

Visco, C., Li, Y., Xu-Monette, Z. Y., Miranda, R. N., Green, T. M., Li, Y., Tzankov, A., Wen, W., Liu, W. M., Kahl, B. S., d'Amore, E. S., Montes-Moreno, S., Dybkaer, K., Chiu, A., Tam, W., Orazi, A., Zu, Y., Bhagat, G., Winter, J. N., Wang, H. Y., O'Neill, S., Dunphy, C. H., Hsi, E. D., Zhao, X. F., Go, R. S., Choi, W. W., Zhou, F., Czader, M., Tong, J., Zhao, X., van Krieken, J. H., Huang, Q., Ai, W., Etzell, J., Ponzoni, M., Ferreri, A. J., Piris, M. A., Moller, M. B., Bueso-Ramos, C. E., Medeiros, L. J., Wu, L. and Young, K. H. (2012) 'Comprehensive gene expression profiling and immunohistochemical studies support application of immunophenotypic algorithm for molecular subtype classification in diffuse large B-cell lymphoma: a report from the International DLBCL Rituximab-CHOP Consortium Program Study', *Leukemia,* 26(9), pp. 2103-13.

Vockerodt, M., Vrzalikova, K., Ibrahim, M., Nagy, E., Margielewska, S., Hollows, R., Lupino, L., Tooze, R., Care, M., Simmons, W., Schrader, A., Perry, T., Abdullah, M., Foster, S., Reynolds, G., Dowell, A., Rudski, Z., Krappmann, D., Kube, D., Woodman, C., Wei, W., Taylor, G. and Murray, P. G. (2019) 'Regulation of S1PR2 by the EBV oncogene LMP1 in aggressive ABC subtype diffuse large B cell lymphoma', *J Pathol*.

Wang, F., Van Brocklyn, J. R., Hobson, J. P., Movafagh, S., Zukowska-Grojec, Z., Milstien, S. and Spiegel, S. (1999) 'Sphingosine 1-phosphate stimulates cell migration through a G(i)-coupled cell surface receptor. Potential involvement in angiogenesis', *J Biol Chem,* 274(50), pp. 35343-50.

Wang, J., Gao, K., Lei, W., Dong, L., Xuan, Q., Feng, M., Wang, J., Ye, X., Jin, T., Zhang, Z. and Zhang, Q. (2017) 'Lymphocyte-to-monocyte ratio is associated with prognosis of diffuse large B-cell lymphoma: correlation with CD163 positive M2 type tumor-associated macrophages, not PD-1 positive tumor-infiltrating lymphocytes', *Oncotarget,* 8(3), pp. 5414-5425.

Wang, Q., Xu, J., Li, Y., Huang, J., Jiang, Z., Wang, Y., Liu, L., Leung, E. L. H. and Yao, X. (2018) 'Identification of a Novel Protein Arginine Methyltransferase 5 Inhibitor in Non-small Cell Lung Cancer by Structure-Based Virtual Screening', *Front Pharmacol,* 9, pp. 173.

Wang, W., Hind, T., Lam, B. W. S. and Herr, D. R. (2019) 'Sphingosine 1-phosphate signaling induces SNAI2 expression to promote cell invasion in breast cancer cells', *FASEB J,* 33(6), pp. 7180-7191.

Weichand, B., Popp, R., Dziumbla, S., Mora, J., Strack, E., Elwakeel, E., Frank, A. C., Scholich, K., Pierre, S., Syed, S. N., Olesch, C., Ringleb, J., Oren, B., Doring, C., Savai, R., Jung, M., von Knethen, A., Levkau, B., Fleming, I., Weigert, A. and Brune, B. (2017) 'S1PR1 on tumor-associated macrophages promotes lymphangiogenesis and metastasis via NLRP3/IL-1beta', *J Exp Med,* 214(9), pp. 2695-2713.

Weichand, B., Weis, N., Weigert, A., Grossmann, N., Levkau, B. and Brune, B. (2013a) 'Apoptotic cells enhance sphingosine-1-phosphate receptor 1 dependent macrophage migration', *Eur J Immunol,* 43(12), pp. 3306-13.

Weichand, B., Weis, N., Weigert, A., Grossmann, N., Levkau, B. and Brune, B. (2013b) 'Apoptotic cells enhance sphingosine-1-phosphate receptor 1 dependent macrophage migration', *European Journal of Immunology,* 43(12), pp. 3306-3313.

Weigert, A., Johann, A. M., von Knethen, A., Schmidt, H., Geisslinger, G. and Brune, B. (2006) 'Apoptotic cells promote macrophage survival by releasing the antiapoptotic mediator sphingosine-1-phosphate', *Blood,* 108(5), pp. 1635-42.

Weigert, A., Tzieply, N., von Knethen, A., Johann, A. M., Schmidt, H., Geisslinger, G. and Brune, B. (2007) 'Tumor cell apoptosis polarizes macrophages role of sphingosine-1-phosphate', *Mol Biol Cell,* 18(10), pp. 3810-9.

Weigert, A., Weis, N. and Brune, B. (2009) 'Regulation of macrophage function by sphingosine-1-phosphate', *Immunobiology,* 214(9-10), pp. 748-60.

Weiner, G. J. (2010) 'Rituximab: mechanism of action', *Semin Hematol,* 47(2), pp. 115-23.

Witz, I. P. (2009) 'The tumor microenvironment: the making of a paradigm', *Cancer Microenviron,* 2 Suppl 1, pp. 9-17.

Xiong, Y., Lee, H. J., Mariko, B., Lu, Y. C., Dannenberg, A. J., Haka, A. S., Maxfield, F. R., Camerer, E., Proia, R. L. and Hla, T. (2016) 'Sphingosine kinases are not required for inflammatory responses in macrophages', *J Biol Chem,* 291(21), pp. 11465.

Xiong, Y., Piao, W., Brinkman, C. C., Li, L., Kulinski, J. M., Olivera, A., Cartier, A., Hla, T., Hippen, K. L., Blazar, B. R., Schwab, S. R. and Bromberg, J. S. (2019) 'CD4 T cell

sphingosine 1-phosphate receptor (S1PR)1 and S1PR4 and endothelial S1PR2 regulate afferent lymphatic migration', *Sci Immunol,* 4(33).

Xuan, W., Qu, Q., Zheng, B., Xiong, S. and Fan, G. H. (2015) 'The chemotaxis of M1 and M2 macrophages is regulated by different chemokines', *J Leukoc Biol,* 97(1), pp. 61-9.

Yang, J., Yang, L., Tian, L., Ji, X., Yang, L. and Li, L. (2018) 'Sphingosine 1-Phosphate (S1P)/S1P Receptor2/3 Axis Promotes Inflammatory M1 Polarization of Bone Marrow-Derived Monocyte/Macrophage via G(alpha)i/o/PI3K/JNK Pathway', *Cell Physiol Biochem,* 49(5), pp. 1677-1693.

Yoshimura, T., Robinson, E. A., Tanaka, S., Appella, E. and Leonard, E. J. (1989) 'Purification and amino acid analysis of two human monocyte chemoattractants produced by phytohemagglutinin-stimulated human blood mononuclear leukocytes', *J Immunol,* 142(6), pp. 1956-62.

Zhang, B., Ma, Y., Guo, H., Sun, B., Niu, R., Ying, G. and Zhang, N. (2009) 'Akt2 is required for macrophage chemotaxis', *Eur J Immunol,* 39(3), pp. 894-901.

Zhang, G., Yang, L., Kim, G. S., Ryan, K., Lu, S., O'Donnell, R. K., Spokes, K., Shapiro, N., Aird, W. C., Kluk, M. J., Yano, K. and Sanchez, T. (2013) 'Critical role of sphingosine-1-phosphate receptor 2 (S1PR2) in acute vascular inflammation', *Blood,* 122(3), pp. 443-55.

Zhang, M., Hutter, G., Kahn, S. A., Azad, T. D., Gholamin, S., Xu, C. Y., Liu, J., Achrol, A. S., Richard, C., Sommerkamp, P., Schoen, M. K., McCracken, M. N., Majeti, R., Weissman, I., Mitra, S. S. and Cheshier, S. H. (2016a) 'Anti-CD47 Treatment Stimulates Phagocytosis of Glioblastoma by M1 and M2 Polarized Macrophages and Promotes M1 Polarized Macrophages In Vivo', *PLoS One,* 11(4), pp. e0153550.

Zhang, Y., Garcia-Ibanez, L. and Toellner, K. M. (2016b) 'Regulation of germinal center B-cell differentiation', *Immunol Rev,* 270(1), pp. 8-19.

Zhao, Z., Ma, J., Hu, B., Zhang, Y. and Wang, S. (2018) 'SPHK1 promotes metastasis of thyroid carcinoma through activation of the S1P/S1PR3/Notch signaling pathway', *Exp Ther Med,* 15(6), pp. 5007-5016.